

# **Smart ratiometric ASIC chip for VOC monitoring**

by

**Jesús García Guzmán**

Department of Engineering  
University of Warwick

A thesis submitted to the University of Warwick  
for the degree of Doctor of Philosophy

May 2005

# CONTENTS

|   |      |
|---|------|
| LIST OF FIGURES                                       | vii  |
| LIST OF TABLES  | xi   |
| ACKNOWLEDGEMENTS                                      | xii  |
| DECLARATION   | xiii |
| ABSTRACT  | xiv  |
| ABBREVIATIONS   | xv   |
| <br>  |      |
| <b>Chapter 1. INTRODUCTION</b>                        |      |
| 1.1 SMART SENSORS TECHNOLOGY                          | 1    |
| 1.2 SMART SENSORS FOR GAS SENSING APPLICATIONS        | 7    |
| 1.3 CURRENT STATE OF THE ART IN SMART GAS SENSING     | 13   |
| 1.4 AIMS AND OBJECTIVES OF THE PROJECT                | 19   |
| 1.5 REFERENCES  | 20   |
| <br>  |      |
| <b>Chapter 2. THE RATIOMETRIC PRINCIPLE</b>           |      |
| 2.1 INTRODUCTION                                      | 32   |
| 2.2 THE RATIOMETRIC MEASUREMENT PRINCIPLE             | 33   |
| 2.3 RATIOMETRIC TOPOLOGIES FOR RESISTANCE MEASUREMENT | 35   |
| 2.4 RATIOMETRIC DESIGNS FOR GAS SENSING APPLICATIONS  | 43   |
| 2.5 THE RATIOMETRIC CONFIGURATION USED IN THIS WORK   | 48   |
| 2.6 REFERENCES  | 52   |

## **Chapter 3. SCHEMATIC DESIGN OF THE RATIOMETRIC ASIC CHIP**

|       |   |    |
|-------|---|----|
| 3.1   | INTRODUCTION                            | 54 |
| 3.2   | OVERALL DESCRIPTION OF THE SYSTEM       | 55 |
| 3.3   | SOFTWARE TOOLS AND TECHNOLOGY LIBRARIES | 58 |
| 3.4   | THE GAS SENSOR SECTION                  | 60 |
| 3.4.1 | Voltage reference                       | 63 |
| 3.4.2 | Ratiometric gas sensor circuit          | 64 |
| 3.4.3 | Offset circuit                          | 67 |
| 3.4.4 | Instrumentation amplifier               | 68 |
| 3.4.5 | Bessel low-pass filter                  | 70 |
| 3.5   | THE TEMPERATURE CONTROL CIRCUITRY       | 72 |
| 3.5.1 | The temperature sensors                 | 74 |
| 3.5.2 | The temperature set-point circuit       | 75 |
| 3.5.3 | The compensator amplifier               | 76 |
| 3.5.4 | Current drive circuit                   | 78 |
| 3.5.5 | The resistive heaters                   | 79 |
| 3.6   | ADDITIONAL CIRCUITRY                    | 81 |
| 3.6.1 | The ambient temperature sensor          | 81 |
| 3.6.2 | The bias cells                          | 82 |
| 3.7   | CONCLUSIONS                             | 84 |
| 3.8   | REFERENCES                              | 85 |

## **Chapter 4. RATIOMETRIC ASIC CHIP MODELLING AND SIMULATION**

|       |  |     |
|-------|--|-----|
| 4.1   | INTRODUCTION                           | 87  |
| 4.2   | SIMULATION TOOLS AND ENVIRONMENT       | 88  |
| 4.3   | GAS SENSOR SECTION SIMULATION          | 89  |
| 4.3.1 | Voltage reference signals              | 89  |
| 4.3.2 | Ratiometric circuit                    | 90  |
| 4.3.3 | Instrumentation amplifier              | 96  |
| 4.3.4 | Fourth order Bessel filter             | 98  |
| 4.3.5 | Overall performance                    | 100 |
| 4.4   | TEMPERATURE CONTROL CIRCUIT SIMULATION | 101 |
| 4.4.1 | Temperature sensors                    | 101 |
| 4.4.2 | Heater                                 | 102 |
| 4.4.3 | Overall performance                    | 104 |

|         |  |     |
|---------|--|-----|
| 4.5     | MODELLING AND SIMULATION OF POLYMERIC CHEMORESISTORS | 105 |
| 4.5.1   | Discrete chemoresistor model                         | 108 |
| 4.5.2   | Ratiometric chemoresistor model                      | 109 |
| 4.5.3   | Performance simulation                               | 111 |
| 4.5.3.1 | <i>Gas response simulation</i>                       | 112 |
| 4.5.3.2 | <i>Temperature simulation</i>                        | 112 |
| 4.5.3.3 | <i>Humidity simulation</i>                           | 114 |
| 4.5.3.4 | <i>Noise simulation</i>                              | 115 |
| 4.6     | CONCLUSIONS  | 117 |
| 4.7     | REFERENCES   | 118 |

## **Chapter 5. LAYOUT VIEW DESIGN AND CHECKING**

|         |  |     |
|---------|--|-----|
| 5.1     | INTRODUCTION                               | 119 |
| 5.2     | CAD AND TECHNOLOGY CONSIDERATIONS          | 120 |
| 5.3     | LAYOUT VIEWS                               | 122 |
| 5.3.1   | Standard cells                             | 122 |
| 5.3.1.1 | <i>GBDA_Bandgap</i>                        | 122 |
| 5.3.1.2 | <i>Bias strategy and required cells</i>    | 123 |
| 5.3.1.3 | <i>Operational amplifier</i>               | 126 |
| 5.3.2   | Custom and semi-custom designed cells.     | 126 |
| 5.3.2.1 | <i>Sensor electrodes and heaters</i>       | 126 |
| 5.3.2.2 | <i>Diode</i>                               | 128 |
| 5.3.2.3 | <i>Capacitors</i>                          | 128 |
| 5.3.2.4 | <i>Resistors</i>                           | 129 |
| 5.3.2.5 | <i>NMOSFETs</i>                            | 131 |
| 5.3.3   | Cells distribution and overall layout view | 133 |
| 5.3.4   | Power rails, bondpads and EDS protection   | 135 |
| 5.4     | VERIFICATION AND RULE CHECKING.            | 136 |
| 5.5     | POST LAYOUT TESTING AND VERIFICATION.      | 137 |
| 5.6     | CONCLUSIONS                                | 138 |
| 5.7     | REFERENCES                                 | 139 |

## **Chapter 6. ELECTRICAL CHARACTERISATION OF FABRICATED RATIOMETRIC ASIC CHIP**

|     |                       |     |
|-----|-----------------------|-----|
| 6.1 | INTRODUCTION          | 140 |
| 6.2 | PACKAGING AND BONDING | 142 |

|       |  |     |
|-------|--|-----|
| 6.3   | PRELIMINARY SINGLE-CHIP TESTING BOARD DESIGN | 144 |
| 6.4   | ELECTRICAL CHARACTERISATION AND TESTING      | 146 |
| 6.4.1 | The voltage reference                        | 146 |
| 6.4.2 | The ratiometric gas sensor circuit           | 147 |
| 6.4.3 | Offset circuit                               | 148 |
| 6.4.4 | Amplified and filtered output                | 149 |
| 6.4.5 | Thermodiode characterisation                 | 150 |
| 6.4.6 | Heater characterisation                      | 152 |
| 6.4.7 | Temperature control circuit                  | 154 |
| 6.5   | CONCLUSIONS                                  | 155 |
| 6.6   | REFERENCES                                   | 156 |

## **Chapter 7. SMART SENSORS CHARACTERISATION**

|         |   |     |
|---------|---|-----|
| 7.1     | INTRODUCTION  | 157 |
| 7.2     | POST-CMOS FABRICATION OF CHEMORESISTIVE SENSORS                     | 158 |
| 7.2.1   | <i>Monotype</i> ratiometric devices                                 | 160 |
| 7.2.2   | <i>Duo-type</i> ratiometric devices                                 | 162 |
| 7.3     | AUTOMATED TESTING SYSTEM FOR DEVICE CHARACTERISATION                | 163 |
| 7.3.1   | Dual-chip testing board design                                      | 163 |
| 7.3.2   | FIA test station  | 165 |
| 7.3.2.1 | <i>Hardware</i>   | 165 |
| 7.3.2.2 | <i>Virtual instrumentation</i>                                      | 167 |
| 7.3.3   | Data acquisition system for the control of ASIC devices             | 167 |
| 7.3.3.1 | <i>Hardware</i>   | 167 |
| 7.3.3.2 | <i>Virtual instrumentation</i>                                      | 169 |
| 7.3.4   | I <sup>2</sup> C-bus data control system for digital potentiometers | 171 |
| 7.3.4.1 | <i>Hardware</i>   | 171 |
| 7.3.4.2 | <i>Virtual instrumentation</i>                                      | 172 |
| 7.4     | RESPONSE OF MONOTYPE RATIOMETRIC DEVICES                            | 173 |
| 7.4.1   | Response of monotype devices to ethanol and toluene vapours         | 173 |
| 7.4.1.1 | <i>Response of monotype devices to ethanol concentration</i>        | 173 |
| 7.4.1.2 | <i>Response of monotype devices to toluene concentration</i>        | 174 |
| 7.4.2   | Response of monotype devices to humidity                            | 177 |
| 7.4.2.1 | <i>Response of monotype devices to humidity and ethanol vapours</i> | 178 |
| 7.4.2.2 | <i>Response of monotype devices to humidity and toluene vapours</i> | 178 |

|  |   |     |
|--|---|-----|
| 7.4.3  | Response of monotype devices to temperature                           | 179 |
| 7.4.3.1  | <i>Response of monotype devices to temperature and ethanol vapour</i> | 180 |
| 7.4.3.2  | <i>Response of monotype devices to temperature and toluene vapour</i> | 181 |
| 7.5  | RESPONSE OF DUO TYPE DEVICES  | 183 |
| 7.5.1  | Response of duo-type devices to ethanol and toluene vapours           | 183 |
| 7.5.1.1  | <i>Response of duo-type devices to ethanol concentration</i>          | 183 |
| 7.5.1.2  | <i>Response of duo-type devices to toluene concentration</i>          | 185 |
| 7.5.2  | Response of duo-type devices to humidity                              | 185 |
| 7.5.2.1  | <i>Response of duo-type devices to humidity and ethanol vapours</i>   | 185 |
| 7.5.2.2  | <i>Response of duo-type devices to humidity and toluene vapours</i>   | 187 |
| 7.5.3  | Response of duo-type devices to temperature                           | 188 |
| 7.5.3.1  | <i>Response of duo-type devices to temperature and ethanol vapour</i> | 188 |
| 7.5.3.2  | <i>Response of duo-type devices to temperature and toluene vapour</i> | 189 |
| 7.6  | OVERALL PERFORMANCE   | 191 |
| 7.7  | CONCLUSIONS   | 196 |
| 7.8  | REFERENCES  | 198 |
| <br>   |   |     |
| <b>Chapter 8. CONCLUSIONS AND FURTHER WORK</b> |   |     |
| 8.1  | AIMS REVIEWED   | 199 |
| 8.2  | THE ASIC TOP-DOWN DESIGN  | 204 |
| 8.3  | SMART SENSORS CHARACTERISATION  | 205 |
| 8.4  | ADDITIONAL BENEFITS OF THE RATIOMETRIC DESIGN                         | 207 |
| 8.5  | PROPOSED FURTHER WORK   | 208 |
| 8.5.1  | Application of the ASIC chip with novel nano-materials                | 208 |
| 8.5.2  | Application of the ASIC chip with novel configurations                | 209 |
| 8.5.3  | Characterisation and use of the temperature control circuit           | 210 |
| 8.5.4  | Improving the design: new generations of the ASIC chip                | 212 |
| 8.5.5  | The hand-held instrument  | 213 |
| 8.6  | A FINAL SUMMARY   | 216 |
| 8.7  | REFERENCES  | 219 |
| <br>   |   |     |
| <b>BIBLIOGRAPHY</b>                            |   | 220 |

**Appendix A.** DESIGN AND SIMULATION ENVIRONMENT AND TOOLS

**Appendix B.** AMI SEMICONDUCTOR 0.7 UM CMOS TECHNOLOGY

**Appendix C.** DETAILS AND SPECIFICATIONS OF CIRCUITRY DESIGNED

**Appendix D.** VIRTUAL INSTRUMENTATION

**Appendix E.** SPECIFICATIONS FOR THE MICRO-CONTROLLER UNIT

**Appendix F.** PUBLICATIONS RELATED TO THIS THESIS PROJECT

**Appendix G.** ADDITIONAL DETAILS AND RESULTS (CD-ROM)

# LIST OF FIGURES

| <b>Number and title</b>  | <b>Page</b> |
|--|-------------|
| 2.1 The general ratiometric configuration.   | 33          |
| 2.2 The Wheatstone bridge with a voltage supply.   | 35          |
| 2.3 Quarter-bridge circuit with voltage supply.  | 37          |
| 2.4 Half-bridge circuit with voltage supply.   | 37          |
| 2.5 Linearized bridge circuit with voltage supply.   | 38          |
| 2.6 Current-driven bridge circuit used by Gardner et al. [8].                                | 39          |
| 2.7 Inverting amplifier.   | 40          |
| 2.8 Non-inverting amplifier.   | 41          |
| 2.9 Ratiometric configuration used in this project.  | 49          |
| 3.1 Top representation of the proposed programmable instrument.                              | 56          |
| 3.2 Block diagram of the components inside the ASIC chip.                                    | 60          |
| 3.3 Simplified schematic of the gas sensor section.  | 62          |
| 3.4 Schematic view of the voltage reference cell.  | 63          |
| 3.5 Schematic view of the gas sensor circuit.  | 64          |
| 3.6 Parallel array of FETs for each switch in the gas sensor circuit.                        | 67          |
| 3.7 Offset circuit to be completed with an external resistor.                                | 68          |
| 3.8 Schematic view of the instrumentation amplifier.   | 69          |
| 3.9 Fourth-order Bessel low-pass filter.   | 71          |
| 3.10 (a) Block diagram of the temperature control section; (b) simplified schematic circuit. | 73          |
| 3.11 Temperature sensor.   | 75          |
| 3.12 Temperature set-point circuit.  | 76          |
| 3.13 Schematic view of the temperature compensator circuit.                                  | 77          |
| 3.14 Schematic view of the current drive circuit.  | 79          |
| 3.15 Schematic and layout view of the resistive heater.                                      | 80          |
| 3.16 Non-inverting amplifier for the ambient temperature sensor.                             | 81          |
| 3.17 Schematic views of cells: (a) Bias1, (b) Bias2.   | 82          |
| 4.1 Input and output waveforms in the voltage reference cell.                                | 90          |
| 4.2 Waveforms simulation for 10 k $\Omega$ polymer resistors.                                | 92          |
| 4.3 Waveforms simulation for 1 k $\Omega$ polymer resistors.                                 | 93          |



| Number and title   | Page |
|--|------|
| 4.4 Voltages in the instrumentation amplifier for zero differential input.   | 96   |
| 4.5 Voltage waveforms obtained with $\delta = 0.020$ .   | 97   |
| 4.6 Voltage waveforms obtained with $\delta = 0.200$ .   | 98   |
| 4.7 Bessel filter characteristics obtained with <i>FilterPro</i> <sup>TM</sup> software, showing the gain (green line), phase (red line) and group delay (black line).   | 99   |
| 4.8 Voltages in the gas sensor section obtained with $\delta = 0.200$ .  | 100  |
| 4.9 Simulated voltage-temperature characteristic of the p-n diode.   | 101  |
| 4.10 Heater waveforms when temperature increases from 20°C to 35°C.  | 103  |
| 4.11 Example of overall performance of the temperature control system.   | 104  |
| 4.12 Structure of the polymeric chemoresistor model.   | 105  |
| 4.13 Polymeric chemoresistor cell: (a) schematic view, (b) symbol.   | 106  |
| 4.14 Schematic view of the discrete chemoresistor circuit.   | 108  |
| 4.15 Schematic view of the modelled ratiometric sensor circuit.  | 109  |
| 4.16 Passivation methods tested in the simulations: (a) one inlet, with one uncoated and one coated sensors (b) two separate inlets, with two uncoated sensors.  | 110  |
| 4.17 Gas response of the ratiometric circuit for active and passive baseline resistances of 10 k $\Omega$ at 40°C, gas concentration = 1000 ppm, water vapour mixed to the gas = 5000 ppm. (a) Voltage pulses applied to the sensor cell SCa simulating the humidity and gas concentration (1 V $\leftrightarrow$ 1 ppm); (b) resistance of the active sensor; (c) resistance of the passive sensor; (d) output voltage of the ratiometric circuit; (e) output voltage of the offset circuit; (f) differential input of the instrumentation amplifier; (g) output of the gas sensor section. | 113  |
| 4.18 Simulation of the variation of output voltages with changes in sensor temperature.  | 114  |
| 4.19 Simulation of the effect of water vapour concentration.   | 115  |
| 4.20 Noise power spectral density at the ratiometric circuit output (From d'Amico, University of Torvegata, Rome).   | 116  |
| 5.1 General aspect of cells <i>GBDA_Bandgap</i> and <i>GBDA_BG_bias</i> .  | 123  |
| 5.2 Bias strategy for the AMI Semiconductor 0.7 $\mu\text{m}$ CMOS technology.   | 123  |
| 5.3 General aspect of cells (a) <i>BIAS1</i> and (b) <i>BIAS2</i> .  | 124  |
| 5.4 Layout view of the sensor area.  | 127  |
| 5.5 Layout view of the custom designed thermodiode.  | 128  |
| 5.6 Layout view of a 7.5 pF capacitor.   | 129  |
| 5.7 Layout view of: (a) 10 k $\Omega$ Nwell resistor; (b) 1.05 M $\Omega$ HIPO resistor.   | 131  |

| <b>Number and title</b>   | <b>Page</b> |
|---|-------------|
| 5.8 Layout view of the NMOSFET used in the current drive circuit.   | 132         |
| 5.9 Layout view of the switches array.  | 132         |
| 5.10 Overall layout view of the 0.7 $\mu\text{m}$ CMOS ASIC chip.   | 134         |
| 5.11 Detail of power rails and bondpads.  | 135         |
| 6.1 Photograph of the fabricated ASIC chip, sized 3.30 mm $\times$ 3.75 mm.   | 141         |
| 6.2 The ratiometric ASIC chip, bonded in the PGA 68-pin package.  | 141         |
| 6.3 Diagram showing the bonding guidelines for the ratiometric ASIC chip. Pins labelled with bold typeface are employed (33 out of 68).   | 143         |
| 6.4 The testing PCB for the characterisation of a single ASIC chip.   | 144         |
| 6.5 Response of the instrumentation amplifier for different values of gain.   | 150         |
| 6.6 Photograph of a p-n thermodiode, between the heater and electrodes.   | 151         |
| 6.7 I-V characteristic of the thermodiode.  | 151         |
| 6.8 Temperature characteristic of the thermodiode.  | 152         |
| 6.9 Photograph of the sensor pads and heater area.  | 153         |
| 6.10 Averaged I-V characteristic of the heaters in the ASIC chip.   | 153         |
| 7.1 Cross-section of the general structure of the chemoresistors fabricated onto the ASIC chips.  | 159         |
| 7.2 Aspect of two of the chemoresistors obtained by spray coating carbon black/polymer composite onto the electrode areas. Average resistances at 24°C are: (a) 9.7 k $\Omega$ and (b) 8.9 k $\Omega$ .   | 160         |
| 7.3 Diagram of the testing system for smart sensor characterisation.  | 164         |
| 7.4 Dual-chip test board for the characterisation of smart ratiometric ASIC devices, showing: (a) two packaged chips connected for preliminary testing, and (b) 68-pin and 25-pin PC connectors, and additional electronics for testing.  | 164         |
| 7.5 (a) Photograph of the FIA test station, its interface electronics and the dual-chip test board as they were arranged for the tests. The ratiometric ASIC devices are in the exposure chamber, placed inside the heater block just underneath the dual-chip test board. (b) The front panel of the FIA control software, showing a schematic view of the FIA test station [7]. | 166         |
| 7.6 Front panel of the data acquisition system for characterisation of the smart ratiometric ASIC devices.  | 170         |
| 7.7 Typical response of the poly(ethylene-co-vinyl acetate) ASIC devices to different concentrations of ethanol vapours in air at 35°C. (a) Amplified output voltage. (b) Change in voltage prior to amplification.   | 175         |

| <b>Number and title</b>  | <b>Page</b> |
|--|-------------|
| 7.8 Typical response of the poly(caprolactone) ASIC devices to different concentrations of toluene vapours in air at 35°C. The output shows very small drifting and low humidity dependence. (a) Amplified output voltage. (b) Change in voltage prior to amplification. | 176         |
| 7.9 Typical time response of carbon black/PEVA devices to different concentrations of toluene vapours in air at 35°C.  | 177         |
| 7.10 Humidity dependence of the response of poly(caprolactone) devices at several concentrations of toluene vapour.  | 179         |
| 7.11 Temperature dependence of monotype PEVA-based ASIC devices at several concentrations of ethanol vapour in air.  | 180         |
| 7.12 Temperature dependence of monotype PCL-based ratiometric ASIC devices at several concentrations of toluene vapour in air.   | 181         |
| 7.13 Log plot of temperature dependence of monotype PCL-based ratiometric ASIC devices for several concentrations of toluene vapour in air.  | 182         |
| 7.14 Logarithmic plots showing how increasing temperature produces a decrease on the response of monotype PCL-based ratiometric ASIC devices.  | 182         |
| 7.15 Typical almost null response of the duo-type devices to different concentrations of ethanol vapours in air at 35°C. (a) Output voltage. (b) Change in voltage prior to amplification.   | 184         |
| 7.16 Typical response of the PEVA/PCL duo-type devices to different concentrations of toluene vapours in air at 35°C. (a) Output voltage. (b) Change in voltage prior to amplification.  | 186         |
| 7.17 Typical response of the duo-type ASIC chips to different concentrations of water vapour when exposed to ethanol vapours in air at 35°C.   | 187         |
| 7.18 Typical response of the duo-type ASIC chips to different concentrations of water vapour when exposed to toluene vapours in air at 35°C.   | 188         |
| 7.19 Response of one of the duo-type ASIC chips with the contrasting PEVA-PCL array of sensors to different concentrations of toluene vapours in air at (a) 35°C and (b) 45°C.   | 189         |
| 7.20 Temperature dependence of duo-type ratiometric ASIC devices at several concentrations of toluene vapour in air.   | 190         |
| 7.21 Comparison of voltage sensitivities of duo-type and monotype ratiometric ASIC devices to (a) toluene, and (b) ethanol.  | 192         |
| 8.1 Block diagram of the proposed hand-held VOC monitoring instrument.   | 214         |

# LIST OF TABLES

| <b>Number and title</b>   | <b>Page</b> |
|---|-------------|
| <b>TABLE 1.1</b> A summary of the main categories of monotype sensor arrays used in gas sensing applications, as reviewed by Gardner and Cole [58]. | 8           |
| <b>TABLE 3.1</b> Resistances and capacitances used for the Bessel low-pass filter.  | 71          |
| <b>TABLE 3.2</b> Assignment of the pins for the bias cells.   | 83          |
| <b>TABLE 4.1</b> Parameters obtained for the selection of the FET switches.   | 91          |
| <b>TABLE 4.2</b> Results of simulations for several values of chemosensors resistance.  | 94          |
| <b>TABLE 4.3</b> Model parameters used in the simulations.  | 111         |
| <b>TABLE 5.1</b> Symbols and functions of standard cells in the bias process.   | 125         |
| <b>TABLE 5.2</b> Main characteristics of operational amplifier CFOA23.  | 126         |
| <b>TABLE 5.3</b> Specifications for the layout of capacitors.   | 129         |
| <b>TABLE 5.4</b> Specifications for the layout of resistors.  | 130         |
| <b>TABLE 6.1</b> Complete list of pins of the ASIC chip.  | 142         |
| <b>TABLE 7.1</b> Resistances of several samples of devices based on a single nanomaterial – <i>monotype</i> ratiometric devices.                    | 161         |
| <b>TABLE 7.2</b> Resistances of several samples of devices based on contrasting nanomaterials – <i>duo-type</i> ratiometric devices.                | 162         |
| <b>TABLE 7.3</b> Response coefficients to vapours in air for ratiometric ASIC devices.  | 193         |
| <b>TABLE 7.4</b> Temperature coefficients for ratiometric ASIC devices obtained at different concentrations of ethanol vapour in air.               | 194         |
| <b>TABLE 7.5</b> Temperature coefficients for ratiometric ASIC devices obtained at different concentrations of toluene vapour in air.               | 195         |

# ACKNOWLEDGEMENTS

I would like to express my thankfulness to Dr. Marina Cole and Prof. Julian W. Gardner for their supervision, guidance and continuous support.

My gratitude also for all the people helping me in the realisation of this project. To the staff in the School of Engineering, in particular to Mr. Frank Courtney for his help and friendly support. To Steve Mattheus and Greta Milczanowska, from IMEC, Belgium, and to Dr. Stephen Bell, from Rutherford Appleton Laboratory, for their valuable help and advice.

A very special acknowledgement to my friends and colleagues Irina Ionela Leonte, Forest Tan Su Lim and May Ang for their constant help and encouragement. I simply could not have found better companionship during those difficult days.

Most of all, I would like to thank my family, particularly Rosaura, my wife, and Luz Aurora, Juan Fernando and little Mayin, my children, for their patience, love and inspiration.

# DECLARATION

This thesis is presented according to the regulations for the degree of Doctor of Philosophy.

The work described in this report is original and is the result of the my own work and investigations except where otherwise indicated.

The parametric model for polymer gas sensors presented in Chapter 4 of this work, was developed in collaboration with Mr. Nicola Ulivieri, from the Department of Information Engineering, Università di Siena, Italy.

The thesis has not been submitted in any previous application for a degree at another university.

Parts of this work have been presented at international conferences:

- Cole, M., García Guzmán, J. and Gardner, J.W. (2002). “Smart ratiometric ASIC chip for a palm-top VOC monitor”, *Eurosensors XVI, the 16<sup>th</sup> European Conference on Solid-State Transducers*, Prague, Czech Republic, 509-512.
- Gardner, J.W., García-Guzmán, J. and Cole, M. (2004). “Smart ASIC chip for vapour detection based upon carbon black/polymer composite nanomaterials”, *Proceedings of SPIE*, **5389**, 344-354, in *Smart Structures and Materials 2004: Smart Electronics, MEMS, BioMEMS, and Nanotechnology*, Varadan, V.K., Ed. SPIE, Bellingham, WA.

Parts of the work contained in this thesis have also been published in the scientific literature:

- García-Guzmán, J., Ulivieri, N., Cole, M. and Gardner, J.W. (2003). “Design and simulation of a smart ratiometric ASIC chip for VOC monitoring”, *Sensors and Actuators B*, **95**, 232-243.
- Cole, M., Ulivieri, N., García-Guzmán, J. and Gardner, J.W. (2003). “Parametric model of a polymeric chemoresistor for use in smart sensor design and simulation”, *Microelectronics Journal*, **34**, 865-875.

# ABSTRACT

This thesis reports on the design, modelling, simulation, fabrication and characterisation of a novel smart ratiometric ASIC chip for the monitoring of volatile organic compounds in air.

A ratiometric principle of measurement applied in the design addresses common problems found in the development and performance of polymer-based devices for gas sensing applications. The approach brings about the cancellation of unwanted common mode variations that occur on a pair of chemoresistors arranged in a ratiometric configuration.

Variations in the resistance of fabricated sensors are compensated by the ratiometric array, allowing the use of polymer resistances ranging from 1 k $\Omega$  to 100 k $\Omega$ . Problems such as humidity and temperature dependence of the baseline output voltage are nearly eliminated.

Besides the ratiometric configuration for the chemoresistive sensors, the designed ASIC chip includes relevant smart features such as programmable offset and amplifier gain, low-power pulsed-mode operation, FET-switched alternating voltage driving of the sensors and a temperature control circuit. These features provide extra benefits such as the improvement of measurement sensitivity and the elimination of sensor-related drift problems produced by the use of constant voltage sources.

Cadence software tools were used for the design, modelling, simulation and layout stages. The ASIC chip was fabricated using the standard 0.7  $\mu\text{m}$  CMOS process by AMI Semiconductor, available through the *Europractice IC Service*.

Following the CMOS process fabrication, two types of smart ratiometric ASIC devices were created by depositing carbon black/polymer composite materials across the electrodes of the chip. In the *monotype* devices, the same material was applied on both sensing elements, having one active and one passive sensor. In the *duo-type* devices two different materials were deposited, thus creating two active sensors.

The responses of the ASIC devices to toluene and ethanol vapours in air were characterised in an automated mass flow system. Additional interfacing circuitry and software (*LabView*<sup>TM</sup> virtual instruments) were also designed for the experimental part.

Results of the experiments confirmed the benefits of the ratiometric approach. In particular, the novel *duo-type* ratiometric devices showed how the combined application of two active sensing materials increased the selectivity (average rejection ratio of 127 for toluene/ethanol) of the devices when compared to the *monotype* devices (rejection ratio averaged only 4.53 for the same analytes). Sensitivity to VOC was also improved for the *duo-type* devices, being up to 11.73 times greater than for *monotype* devices.

The design of the ratiometric ASIC chip allows the use of a wide range of resistive gas sensing materials and it is also adaptable to different internal or external configurations of the sensors.

The performance of the ratiometric ASIC chip designed and fabricated exceeded the original expectations and promising further research is already undertaken. It is believed that the circuit offers relevant smart capabilities at a very low cost and hence it can be used as the main component for the mass production of a programmable hand-held instrument for VOC monitoring.

# ABBREVIATIONS

| <b>Abbreviation</b> | <b>Definition</b>   | <b>Introduced in page</b> |
|---------------------|---|---------------------------|
| AC                  | Alternating current   | 11                        |
| AMIS                | AMI Semiconductors  | 54                        |
| ASIC                | Application Specific Integrated Circuit   | 8                         |
| CMOS                | Complementary Metal-Oxide Semiconductor   | 5                         |
| DC                  | Direct current  | 11                        |
| DRC                 | Design rule check   | 136                       |
| ERC                 | Electrical rule check   | 137                       |
| ESD                 | Electrostatic discharge   | 135                       |
| ETH                 | Eidgenössische Technische Hochschule<br>(Swiss Federal Institute of Technology) | 5                         |
| FET                 | Field-Effect Transistor   | 8                         |
| FIA                 | Flow Injection Analysis   | 163                       |
| FPW                 | Flexural plate wave   | 8                         |
| HIPO                | High ohmic polysilicon  | 129                       |
| IC                  | Integrated circuit  | 2                         |
| IMEC                | Interuniversity Micro-Electronics Center  | 120                       |
| LPF                 | Low-pass filter   | 70                        |
| LVS                 | Layout versus schematic   | 136                       |
| MOS                 | Metal-Oxide Semiconductor   | 8                         |
| MOSFET              | Metal-Oxide Semiconductor Field-Effect Transistor                               | 8                         |
| NASA                | National Aeronautics and Space Administration                                   | 14                        |
| NI-DAQ              | National Instruments data acquisition card                                      | 144                       |
| NMOSFET             | N-type Metal-Oxide Semiconductor Field-Effect<br>Transistor                     | 67                        |
| PCB                 | Printed circuit board   | 144                       |
| PCL                 | Poly(caprolactone)  | 159                       |
| PEL                 | Physical Electronics Laboratory   | 5                         |
| PEVA                | Poly(ethylene-co-vinyl acetate)   | 159                       |
| PGA                 | Pin Grid Array  | 142                       |
| <i>rr</i>           | Resistance ratio  | 161                       |
| SAW                 | Surface acoustic wave   | 8                         |
| SDS                 | Sample delivery system  | 105                       |
| SOI                 | Silicon-on-insulator  | 8                         |
| SRL                 | Sensors Research Laboratory   | 15                        |
| VI                  | Virtual instrument  | 145                       |
| VOC                 | Volatile organic compound   | 5                         |



# CHAPTER 1

## INTRODUCTION

### 1.1 SMART SENSORS TECHNOLOGY.

One of the most difficult challenges in microtechnology during the last few years has been the integration of smart circuitry and sensing devices on the same chip. The aim being to produce complete systems capable of measuring and processing in a single unit the measured signals; leading the way to what is called “smart sensor technologies” [1-6].

Many definitions and opinions have arisen about the *smart* ability of sensors and about what is expected from its development in the near future [1, 7-13]. Although the establishment of a final and unique definition of *smart sensors* is still far from being reached, there is already an agreement in some of the basic features.

Most researches agree with the fact that some capabilities beyond basic signal processing circuitry must be included into the same piece as the sensors, in order to be considered smart. The main aims for this are, firstly, the need to deal with unwanted behaviour affecting the sensing response and, secondly, the convenience of providing communication between the sensor system and the host. Whereas for some people this is enough, others argue that further features must be added to the definition. The criteria in the paper by Giachino [9] include the abilities for performing logic functions and for making decisions, apart from the obligated data-communication feature. Other authors add further special requirements in order to delimitate more precisely the boundaries of smart sensors. Van der Horn and Huijsing [14-15], for example, consider that sensors should be fabricated together with smart electronics by using standard *integrated circuit* (IC) processes, and they mention a list of the functions that must be integrated, starting from basic analogue signal processing, analogue to digital conversion, interfacing to processing units, and some programmable calibration. Similar approaches are proposed by other research groups in several fields of microtechnology [2, 3, 16-17].

It is generally accepted that any smart sensor must be capable of processing data at a level in which the outputs of sensing devices are transformed into a form of information that can be handled by programmable devices. From here, feedback can be returned to the system, in a way that self-calibration and self-diagnostic are just a part of the whole set of smart features. Virtual instrumentation has also been evolving during the last few years as a data processing supplement of the sensing systems, which in turn have been evolving in such a way that the ‘intelligence’ has been moving from the ‘virtual’ side, supported by software, to the ‘on-chip’ side of the smart sensor, thus enabling diagnostic and calibration within the sensor itself [14,

18-21]. These and other important aspects related to data processing and communication ability have been considered within the definition of intelligent sensor systems [10, 22].

Nevertheless, the data processing capabilities are not limited to the actual physical location of the sensing elements and embedded circuitry. Recent parallel development on network technologies has altered that concept of a smart sensor in a single piece of silicon or in a clearly defined location. Intelligence can now be distributed along networks where useful information is managed not only through hard-wired interfaces but also through emerging and effective communication protocols. Sensors now range from the simplest digital ‘field-buses’ sensor systems in industrial networks, to the more complex Ethernet-based sensors permitting remote interrogation over the Internet [23-26]. Therefore, smart sensors cannot be defined only in terms of their features on a single-chip and they can rarely be found performing a single-parameter sensing function. Instead, they are often referred to as entire smart microsystems [10, 27].

Smart sensors technology has evolved since the first integrated arrays were developed at the beginning of the eighties and it has been rapidly changing and moving in different directions during these years. However, most of the efforts and advances have concurred towards the fields that at present characterise silicon technologies and microsystems [17, 28]. This has not been due only to a coincidence on the parallel development of related knowledge but it is also derived from the speed at which technical discoveries and information have been spread recently. Early at the beginning of the past decade, for example, a co-operative strategy for the development of smart sensor technologies was proposed [7]. This and other similar

attempts for unification have contributed to the successful growth of smart sensor technology.

Although, as mentioned before, this is not the only aspect to consider in the technological expansion of smart sensors, it is important to take into account how conventional sensors have been linked to, and how their manufacturing methods have been modified to make them compatible with, the fabrication processes developed for integrated circuits.

Putting together signal processing components and sensors has not been an easy task, as different technological approaches have been used for each case. On the one hand, sensing devices have been traditionally fabricated according to the conventional technologies available for the manufacture of each particular type of sensors as they were first produced and applied. On the other hand, however, the development of standard integrated circuit technologies has made available fabrication processes that allow the mass production of complicated circuitry at reasonable costs, small sizes, and being reliable for the implementation of complete systems.

After initial attempts for the design of hybrid systems in which conventional sensors were connected to, or even installed onto the same chip containing the circuits for the signal processing [4, 29-30], there has been a strong tendency for the integration of the sensors within the same process in which the ICs are fabricated. This has led to the adoption of some of these standard processes as the most suitable choice for the fabrication of integrated sensor systems.

As a consequence, some of the original methods for fabrication of sensors have been substantially modified, adapted and even substituted by using silicon

technologies, in order to make them compatible with the standard IC processes [17]. Among these, *Complementary Metal-Oxide Semiconductor* (CMOS) technology has gained a very good reputation as it is a cheap and reliable way to produce integrated smart systems. The low-cost of manufacturing, together with the low power consumption compared to other alternative technologies, make it the ideal choice for on-chip integration. Advantages and characteristics of the use of CMOS processes for the fabrication of on-chip sensor systems have been extensively described by the research group at the Physical Electronics Laboratory (PEL), ETH Zurich, Switzerland [31-33], and a systems approach to the design, verification and testing of CMOS sensors has been also proposed by Hosticka [34].

CMOS technology has been used in a variety of sensing applications, which extend over a broad range of fields. For example, they allow basic interfacing and temperature control [35], high speed communication [36] and other programmable capabilities such as temperature compensation [37], for applications as diverse as biochemical, imaging, and differential pressure sensing, respectively.

The review by Baltes and Brand [38] about the developments in CMOS-based microsensors, describes the post-CMOS approach for the fabrication of microsensors and presents examples of research in different areas: a CMOS thermal imager used for presence detection, a CMOS chemical microsystem for application in detection of gases and *volatile organic compounds* (VOC) in air, and CMOS temperature and stress microsensors used for characterisation of wire bonding processes. All of these are packaged microsensors fabricated by CMOS technology.

Other examples of sensor systems in which post-processing steps were required for the implementation of the sensing elements are the CMOS pressure-

sensor system and the magnetic-field sensor system described by Hosticka [34]. His paper describes how standard CMOS processes were complemented by anisotropic cavity etching, in the case of the pressure sensor, and deposition of a ferromagnetic material, for the magnetic field sensor. Other CMOS magnetic field sensors have been fabricated with the aid of wet etching as a complementary step for the release of the mechanical structures [39].

Certain types of microsensors have been fabricated completely within standard CMOS processes, when the sensing components can be included in the layout without requiring additional steps. This is the case of some optical [40-41] and temperature [42] sensors that have been made available through the implementation of CMOS photodiodes and thermodiodes, respectively. The CMOS temperature sensors reported by Anton Bakker [43-44], the CMOS digital pixel sensor chip developed by the group at Stanford University [45], and the single-chip pH sensor described by Hammond and Cumming [46], are also examples of microsensors fabricated through non-modified CMOS processes.

CMOS process family is at the moment the most representative example of the technology used in the development of smart sensing microsystems. Together with the innovative adaptation of a number of sensing principles, and taking advantage of other recent technological advances in the development of sensing materials and sensor arrays, the fabrication of CMOS-based smart systems is indeed particularly important in the case of gas sensing applications, which are discussed in the next section.

## 1.2 SMART SENSORS FOR GAS SENSING APPLICATIONS

Among the increasing development and research on different types of sensor systems, one of the very interesting and applicative fields is that of the smart systems for gas sensing purposes.

Gas sensing applications, as a research field, has evolved during the last few years by gathering efforts and advances in several related disciplines. Some efforts have been directed towards the implementation of gas sensing systems in the electronic nose instrumentation (“An electronic nose is an instrument, which comprises an array of electronic chemical sensors with partial specificity and an appropriate pattern-recognition system, capable of recognising simple or complex odours” [47]), but also there have been many important improvements and innovations on the original gas sensing devices.

The progress in the field of gas sensors is a consequence of parallel efforts of research work undertaken by several groups around the world. In Europe, some researchers had already pointed out the need of standards for the development of gas sensor systems and their arrangement in the design of electronic-nose instrumentation [48]. Further efforts towards the adoption of standards in the fields of sensors and electronic noses are carried out by the working groups in the Standards Commission of the NOSE II organisation [49]. This early identification of the main issues involved in the development of electronic noses has helped to address technological research in a coordinated way, although the guidelines proposed have not been formally or explicitly adopted.

Modern gas sensing systems can be approached from a more general point of view by considering the performance of the sensor arrays used for each application.

**Table 1.1** A summary of the main categories of monotype sensor arrays used in gas sensing applications, as reviewed by Gardner and Cole [50].

| Type of sensors   | Representative examples  |
|---|--|
| Polymeric sensors   | <p>Neaves and Hatfield [29, 51] Application specific integrated circuit (ASIC) with an array of 32 resistive sensors.</p> <p>Warwick University [52] CMOS micro-bridge with five resistive sensors.</p> <p>Zee and Judy [53] micromachined gas sensor arrays.</p> <p>Polymer gate FET sensor array by Covington et al. [54].</p>   |
| Metal oxide sensors   | <p>Gardner [55] array of six MOS sensors on single silicon substrate.</p> <p>Array of four integrated thick-film tin-oxide gas sensors [56].</p> <p>Array of three micromachined tin oxide gas sensors operating at different temperatures [57].</p> <p>Array of 40 sensors (<math>\text{SnO}_2</math> and <math>\text{WO}_2</math>) with different sensitivities, used for halitosis analysis [58].</p>   |
| Quartz resonator  | <p>Monolithic six-element sensor array on a single quartz crystal for monitoring of agricultural emissions, at resonant frequency of 10 MHz [59].</p>  |
| Flexural plate wave (FPW) and surface acoustic wave (SAW) devices | <p>Baca et al [60] GaAs SAW integrated circuit.</p> <p>Cai et al. [61] integrated array of six polymer-coated FPW.</p> <p>Cunningham et al. [62] integrated FPW sensor array fabricated on silicon-on-insulator (SOI) wafers.</p>  |
| Catalytic FET sensor arrays                                       | <p>Briand et al. [63] MOSFET sensors, in which the gates have been replaced by catalytic materials for detection of gases.</p>   |
| Optical   | <p>Fibre-optic polymer bead-based sensor array designed at Tufts University [64], discriminating odours by the colour pattern.</p> <p>Sensor array of individually addressable polymeric microspheres for the analysis of complex fluids containing various analytes [65].</p> <p>Photomechanical chemical microsensors by Datskos et al. [66] where photo-induced bending of microcantilevers varies with the number of absorbed molecules.</p> <p>Portable homogeneous gas sensor array used to visualize the flow and direction of a target gas, via a real-time image-processing algorithm [67].</p> |
| Silicon-based microelectrode arrays                               | <p>Schoning et al. [68] array of various electrode shapes and sizes, used for study of electrochemical sensing.</p> <p>Warwick University sensor arrays with different electrode geometries for organic crystals, metal oxide and polymer resistive devices [69-70].</p>   |



According to the sensing principles used by the system, an array of sensors can be either *mono-type* or *multi-type*. Traditionally, and being still the preferred choice for most of the applications, gas sensor arrays have relied in using a single type of sensor. Monotype arrays of different kinds have been reported and can be classified upon either the different sensing materials employed or the type of sensor used. An extensive discussion about these, including comments about relevant examples of the most important types, has already been published by Gardner and Cole [50]. Their analysis has been summarised in Table 1.1.

There is also an increasing interest in the use of multi-type arrays for the sensing of gases and vapours. The use of arrays with different types of sensors, also known as hybrid systems, aims to provide better discrimination by including enough materials and transducers combined in such a way that allows the identification of different gases. This approach increases the resolution capability of gas sensing systems, as it has been reported after research work oriented both towards biochemical applications and towards the development of more selective electronic noses [35, 71].

Studies in this field cover different aspects relevant to the development of hybrid or composite systems. The method proposed by Chaudry et al. [72] for the optimisation of a sensor array relies on selecting the group of sensing elements which maximise its overall sensitivity and selectivity.

Interfacing has been also an important issue for the processing of multi-type sensor responses. Dyer and Gardner [73] developed a programmable interface for arrays with both resistive and piezoelectric sensors. Likewise, the interface chip described by Yazdi et al. [27] offers programmability in a multi-parameter

microsystem, although the interfacing function is actually performed over a group of capacitive sensors collecting data from various applications.

An example of the multi-type approach to sensor arrays is the integrated chemical microsensor system reported by the ETH group [74-75], in which a mass-sensitive cantilever, a capacitive sensor and a calorimetric sensor, all of them coated with polymeric sensing layers, are combined in a microsystem for the detection of VOC. The single-chip design includes microelectronic components for signal amplification and conditioning, a Sigma-Delta converter and an interface which transmit the digital data to external units.

A collaborative project between Cambridge and Warwick Universities has also produced an integrated smart sensor composed of chemo-resistive gas sensors combined with micro-calorimeters in a SOI membrane, using active micro-FET heaters and temperature sensors [76].

Many other principles and configurations have been applied in attempts to improve the performance of gas sensing systems. Cardinalli et al. [77], for example, proposed an interface improvement for a multi-sensor architecture, in a standard CMOS process. Bridges, as a classical instrumentation configuration, have been used for several years evolving from the basic discrete arrays to the integrated smart single-chips developed today in CMOS technology [30, 52, 78-79]. In these, resistive sensors have been used and special attention has been devoted to the interfacing aspect.

Regarding the gas sensing materials, conducting polymers are of considerable interest for the present research work. The developments in this field during the last decade have impacted the electronic nose technologies, as it was observed by

Gardner and Bartlett since 1995 [80]. These materials have application in modern microsystems, including those related to biosensors [81-84]. Likewise, the response and acceptance that the scientific community has given to this advances has allowed an increasing growth in the field [85-86]. As a result, conductive polymers and their composites are some of the favourite sensing materials employed in the on-chip implementation of integrated systems for the detection of gases and vapours, being used for the development of modern electronic nose instrumentation for diverse applications [87-91].

Application of conducting polymers to sensors relies in the fact that their resistance changes with absorption or desorption of volatile molecules. These changes are usually measured under direct current (DC) [80, 92-94], although there have been also significant advances in the use of alternating current (AC) techniques for interrogation of conducting polymer gas sensors [95-97].

The electric and chemical properties of carbon black/polymer composites have also been studied [98-102] and the ability of these materials to be incorporated as sensing elements within smart devices has already been successfully tested and characterized [53, 103-104].

Nevertheless, operation of gas sensor systems based on both conducting polymers and carbon black/polymer composites is affected by changes in environmental conditions, variations in power supplies and other interferences. These unwanted variations can be dealt with through the design of smart circuitry that provides automatic calibration and cancellation of undesirable deviations in the output. Conditioning of the signals must be preferably carried out in the same place where the sensors are located, giving this way an increasing need for the design of

ASICs directed both to the incorporation of signal processing and interfacing functions, as well as to the integration of the sensing elements in the same chip. As commented in the previous section, CMOS technology has brought out the opportunity to produce those integrated smart systems at a reasonable cost and with a high reliability.

The consequent growth in the design of ASICs oriented to accomplish these functions is perhaps the most important tendency in the current development towards a smart and reliable sensing and sampling monolithic microsystem.

### **1.3 CURRENT STATE-OF-THE-ART IN SMART GAS SENSING**

Several research groups are currently working on the development of gas sensing systems that are capable of calibrating, testing and diagnosing themselves through the addition of smart circuitry, thus improving their performance and making them more reliable.

The combination of achievements in different areas of microtechnology is producing everyday better devices, and gas sensing systems are rapidly evolving from the conventional and expensive desktop instruments to the smart hand-held prototypes, with the ultimate aim of achieving the optimum system-on-a-chip instrument.

Electronic nose instrumentation, as a whole subject, is a field that involves and requires the rapid development of several disciplines, such as microsensor technologies and nanomaterials, ASIC technologies, microfluidics, and micro-instrumentation. Multidisciplinary research concerning all of these subjects is required, and several groups are making significant progress at present.

Carbon black/polymer composite sensing materials are also under investigation. The research group led by Nathan S. Lewis in the California Institute of Technology has contributed to the formal characterization of the response of such materials for use in vapour detectors [105]. After studies performed with a number of carbon black-polymer composite chemoresistors, exposed during a long period to different analytes, they report on the calibration of the sensors and the analysis of their responses and the inherent drift [106]. This research work has already led to the establishment of the company called Cyrano Sciences, Inc., now Smiths Detection (Pasadena, CA).

In the same research institute, interaction between analytes and carbon black/polymer composites in resistive sensors was also studied and reported by the *Jet Propulsion Laboratory* as part of its work for NASA oriented to air quality monitoring. Efforts were directed towards the development of an electronic nose for the detection of low concentrations of contaminants in air. A model for the composites and their interaction with both inorganic and organic analytes was recently obtained, contributing to a better understanding of this type of resistive sensors [103].

With respect to the current research in the field of CMOS circuits and the development of ASICs for sensing applications, the ETH group in Zurich is continuing its previous work [33, 107]. They have reported on microelectrode arrays integrated with analogue and digital circuitry capable of functions such as signal filtering, analogue and digital conversion, multiplexing, simultaneous recording and stimulation. The most recent example of this is their 4.4 mm × 4.4 mm CMOS chip, containing an array of 4 × 4 electrodes, each measuring 40 μm × 40 μm with a 250 μm pitch [108]. This group is also reporting on a CMOS gas sensor system including, on a single chip, a micro-hotplate and all the required circuitry for control and driving. Temperatures up to 350°C were achieved in the hotplate with a conventional 5 V power supply [109-110].

Considerable amount of work has also been carried out in the field of microfluidics, which is one of the most important areas in the development of on-chip micronose systems. A microfluidic system was reported by Becker et al. [111] for increasing the selectivity in the identification of gases through the arrangement of tin oxide gas sensors into microreactors. Microvalves, micropumps and

microchannels were all fabricated in silicon technology. The smart part of the microfluidic system proposed is its ability to overcome the undesirable signal drift by implementing cycling operation, through constant-flow and no-flow modes, of the sensors with respect to the main functions. Other reports by the same group describe how the changes in the operation modes of the microfluidic system produce information that can be used for the identification of components in a mixture of gases [112-113].

Recent activity in the *Sensors Research Laboratory* (SRL) at Warwick University has been directed towards the development of a smart micronose. An array of 70 gas sensors based on a combined FET/resistive cell has been fabricated under a standard CMOS process and using different carbon black polymer composite materials [114]. The array consists of five rows of 14 sensors each, with integrated circuitry for signal processing. A different polymer coating was deposited onto each row. The design of the combined chemical FET sensor and the resistive element in the same silicon area intends to improve the discriminatory ability of the array, by measuring two different properties with only one sensing material in each sensor cell.

Further work at the SRL has been focused on the velocity at which analytes flow through the surface of polymer based sensors [115]. An array of 5 rows with 16 resistive elements each was fabricated in a matrix configuration, using five different carbon black-polymer composites as sensing materials. The array has been tested with pulses of seven analytes at different pulse widths and flow rates, in order to study its discrimination capability. The response of the system was represented as an olfactory image and distinctive fingerprints were obtained for every analyte. Some ‘stereo’ olfactory images were also obtained.

Olfactory imaging has also been investigated by several groups. Lundström et al. [116-118] have reported on the generation of chemical images for application in electronic noses by using a scanning light pulse technique. Likewise, the so-called ‘olfactory video camera’ reported by Ishida et al. [67, 119] proposes the use of an array of gas sensors combined with a real-time image processing algorithm to visualise the flow of a gas or vapour, estimating from here the direction of the flow and the location of the source.

Electronic nose technology has also been applied in robotics. A robot that can follow odorous trails on the ground was designed by Russell at Monash University, Australia [120-121]. The device uses conductive polymer chemical sensors and a wind vane to locate the source of odours, with the aid of control algorithms. A similar work was previously reported by Tresoldi [122], who used tin-oxide gas sensors and capacitor-charge timing technique for estimating the maximum gas concentration point. The robot here uses the gas sensors information to recursively calculate concentration gradients and then it moves in that direction, controlled through Hall-effect sensors and fuzzy-logic.

A research group at Tufts University has been working on the design of optical sensor arrays for odour recognition [64, 123]. They have reported on high-density arrays of optical fibres with fluorescent dyes incorporated into polymers, which are exposed to brief vapour pulses. The interaction between the dyes light, the vapour molecules and the polymers, results in different temporal responses or fingerprints that are analysed using image software. Recent work of this group has also investigated, using optical vapour sensors, how the flow dynamics affects odour perception and discrimination in vertebrates [124].



In summary, the current development on the field of e-nose instrumentation and gas sensing applications is characterized by the following main features:

- Sensor arrays are being optimised in order to contribute to a better performance of the systems.
- Integration of sensor arrays and signal processing circuits onto the same substrate is an unavoidable target if substantial reductions in sensor deviations, noise, instrument size, power consumption and fabrication costs, are expected; the last being a key point for volume market.
- The use of standard CMOS processes for the fabrication of ASIC chips, allows the integration of complete systems, including sensor arrays together with smart circuitry for signal processing, interfacing and digital data processing.
- Although most of efforts have been directed towards the research on monotype sensor arrays, there are also advances on the design and application of multi-type or hybrid systems.
- Polymeric materials have proved to be a good choice for gas sensing applications, as they can operate at room temperature and can be deposited onto different types of electrodes in the post-fabrication stages. Research work related to conducting polymers and carbon-black polymer composite materials is one of the main areas of interest for the sensing component of e-nose systems.

- There are other materials and technologies that have also found successful e-nose applications, although not all of them have been implemented as integrated arrays. Tin oxide technology, flexural plate wave sensors, SAW devices, bulk acoustic wave sensors and optical sensor arrays are currently under investigation.
- Microfluidics, as the discipline related to the study of fluid dynamics in the micrometer scale, has also emerged as an important area of research and development associated to the field of electronic noses and micro-instrumentation in general.

The work involved in this project has attempted to consider all these basic precepts. Guided on these bases, the project goals defined in the following section are developed with the global aim of contributing to the current research in the novel field of electronic nose instrumentation.

Although significant efforts have been made towards the integration of gas sensors and signal processing circuitry in a single unit [5, 35, 38, 74-75, 125] important problems affecting the performance of the sensing devices have not been completely resolved. It is still necessary to develop smart components that can compensate for typical variations in ambient conditions and other sources of error caused by the power sources and interface electronics associated with the sensors.

This project addresses these issues through the design of a smart ASIC chip in which a ratiometric array of resistive vapour sensors is provided with capabilities that validate its potential application in a micro-power palm-top instrument for the monitoring of VOC. The ratiometric principle, described in chapter 2, allows the smart elimination or reduction of several unwanted variations in the sensors.

## 1.4 AIMS AND OBJECTIVES OF THE PROJECT

The project reported in this thesis aims the design, simulation, fabrication and characterisation of a novel ASIC chip for the monitoring of VOC and gases, which is proposed to be the main component for the further design of a hand-held instrument.

It is expected that the proposed ASIC design will substantially improve the performance of the resulting gas sensing device, providing it with the following features:

- Sensors and basic signal processing circuitry will be integrated in a single chip.
- The circuit will compensate for unwanted variations in the fabrication of the resistive sensors.
- Variations in the baseline of the response produced by changes in temperature will be eliminated.
- Humidity dependence of the output will be substantially reduced through the integrated circuit and sensor configuration.
- The design will allow the testing and characterisation of different resistive sensing materials.

Most of the benefits of the proposed design rely on the characteristics and functional implementation of a particular array of resistive sensors, using the so-called *ratio-metric* measurement principle, which is described in the next chapter.

## 1.5 REFERENCES

1. Gardner, J.W., Varadan, V.K. and Awadelkarim, O.O. (2001). *Microsensors, MEMS, and smart devices*, John Wiley & Sons, Ltd., Chichester, England.
2. Puers, R. (1999). "Sensor, sensor interfacing and front-end data management for stand-alone microsystems", *J. Micromech. Microeng*, **9**, R1-R7.
3. Maloberti, F. and Malcovati, P. (1997). "Microsystems and smart sensor interfaces: a review", *Analog integrated circuits and signal processing*, **15**, 9-26.
4. Gardner, J.W. (1994). *Microsensors: principles and applications*, John Wiley & Sons Ltd., Chichester, U. K.
5. Gardner, J.W., Cole, M. and Udrea, F. (2002). "CMOS gas sensors and smart devices", *Proceedings of the First IEEE International Conference on Sensors*, Orlando, Florida, USA, **1**, 721-726.
6. Brignell, J. and White, N. (1996). *Intelligent sensor systems*, Institute of Physics Publishing, Bristol.
7. Brignell, J.E. (1993). "Quo vadis smart sensors?", *Sensors and Actuators A*, **37-38**, 6-8.
8. Middelhoek, S. and Hoogerwerf, A.C. (1985). "Smart sensors: when and where?", Paper presented at the *Third International Conference on Solid-State Sensors and Actuators (Transducers '85)*, Philadelphia, PA, U.S.A.
9. Giachino, J.M. (1986). "Smart sensors", *Sensors and Actuators*, **10**, 239-248.
10. Frank, R. (1996). *Understanding smart sensors*, Artech House, Inc., Massachusetts, USA.
11. Ko, W.H. (1996). "The future of sensor and actuator systems", *Sensors and Actuators A*, **56**, 193-197.
12. Göpel, W. (1995). "Sensors and 'smart' molecular structures: components for future information technologies" in *Sensors: a comprehensive survey*, **8**, *Micro- and nanosensor technology/ Trends in sensor markets*, Meixner, H. and Jones, R., Ed. Cambridge: VCH, 295-336.

13. Brignell, J.E. (1996). "The future of intelligent sensors: a problem of technology or ethics?", *Sensors and Actuators A*, **56**, 11-15.
14. Van der Horn, G. and Huijsing, J.H. (1997). "Integrated smart sensor calibration", *Analog Integrated Circuits and Signal Processing*, **14**, No. 3, 207-222.
15. Huijsing, J.H., Riedijk, F.R. and van der Horn, G. (1994). "Developments in integrated smart sensors", *Sensors and Actuators A*, **43**, 276-288.
16. De Jong, P.C., Riedijk, F.R. and van der Meer, J. (2002). "Smart silicon sensors - Examples of Hall-effect sensors", *Proceedings of the First IEEE International Conference on Sensors*, Orlando, Florida, USA, **2**, 1440-1444.
17. Hosticka, B.J., Brockherde, W. and Hammerschmidt, D. (1997). "Silicon sensor systems", *Analog Integrated Circuits and Signal Processing*, **14**, 261-273.
18. Taner, A.H. and Brignell, J.E. (1995). "Aspects of intelligent sensor reconfiguration", *Sensors and Actuators A*, **46-47**, 525-529.
19. Brignell, J.E. (1991). "Software techniques for sensor compensation", *Sensors and Actuators A*, **25-27**, 29-35.
20. Taner, A.H. and Brignell, J.E. (1997). "Virtual instrumentation and intelligent sensors", *Sensors and Actuators A*, **61**, 427-430.
21. Van der Horn, G. and Huijsing, J.L. (1998). *Integrated smart sensors: design and calibration*, Kluwer Academic Publishers, The Netherlands.
22. Meijer, G.C.M. (1994). "Concepts and focus point for intelligent sensor systems", *Sensors and Actuators A*, **41-42**, 183-191.
23. Flammini, A., Ferrari, P., Sisinni, E., Marioli, D. and Taroni, A. (2003). "Sensor integration in industrial environment: from field-bus to web sensors", *Computer Standards & Interfaces*, **25**, 183-194.
24. Ferrari, P., Flammini, A., Marioli, D. and Taroni, A. (2002). "A low-cost Internet-enabled smart sensor", *Proceedings of the First IEEE International Conference on Sensors*, Orlando, Florida, USA, **2**, 1549-1554.

25. Flammini, A., Ferrari, P., Sisinni, E., Marioli, D. and Taroni, A. (2002). "Sensor interfaces: from field-bus to Ethernet and Internet", *Sensors and Actuators A*, **101**, 194-202.
26. Rösch, O.J., Schilling, K. and Roth, H. (2002). "Haptic interfaces for the remote control of mobile robots", *Control Engineering Practice*, **10**, 1309-1313.
27. Yazdi, N., Mason, A., Najafi, K. and Wise, K.D. (2000). "A generic interface chip for capacitive sensors in low-power multi-parameter microsystems", *Sensors and Actuators A*, **84**, 351-361.
28. Hurley, R.E. and Gamble, H.S. (1995). "Some recent advances in silicon microtechnology and their dependence on processing technique", *Vacuum*, **46**(3), 287-293.
29. Neaves, P. I. and Hatfield, J. V. (1994). "Current-mode multiplexer for interrogating resistive sensor arrays", *Electronic letters*, **30**, No. 12, 942-943.
30. Cole, M., Gardner, J.W., Lim, A.W.Y., Scivier, P.K. and Brignell, J.E. (1999). "Polymeric resistive bridge gas sensor array driven by a standard cell CMOS current drive chip", *Sensors and Actuators B*, **58**, 518-525.
31. Baltes, H. (1993). "CMOS as sensor technology", *Sensors and Actuators A*, **37-38**, 51-56.
32. Müller, T., Brandl, M., Brand, O. and Baltes, H. (2000). "An industrial CMOS process family adapted for the fabrication of smart silicon sensors", *Sensors and Actuators A*, **84**, 126-133.
33. Hierlemann, A. and Baltes, H. (2003). "CMOS-based chemical microsensors", *Analyst*, **128**(1), 15-28.
34. Hosticka, B.J. (1998). "CMOS sensor systems", *Sensors and Actuators A*, **66**, 335-341.
35. Lauwers, E., Suls, J., Gumbrecht, W., Maes, D., Gielen, G. and Sansen, W. (2001). "A CMOS multiparameter biochemical microsensor with temperature control and signal interfacing", *IEEE Journal of Solid-State Circuits*, **36**, No. 12, 2030-2038.

36. Ercan, A.O., Xiao, F., Liu, X., Lim, S.H., El Gamal, A. and Wandell, B. (2002). "Experimental high speed CMOS image sensor system and applications", *Proceedings of the First IEEE International Conference on Sensors*, Orlando, Florida, USA, **1**, 15-20.
37. Trieu, H.K., Kordas, N. and Mokwa, W. (2002). "Fully CMOS compatible capacitive differential pressure sensors with on-chip programmabilities and temperature compensation", *Proceedings of the First IEEE International Conference on Sensors*, Orlando, Florida, USA, **2**, 1451-1455.
38. Baltès, H. and Brand, O. (2000). "CMOS-based microsensors", *EuroSensors XIV.*, Copenhagen, Denmark, 1-8.
39. Beroulle, V., Bertrand, Y., Latorre, L. and Nouet, P. (2003). "Monolithic piezoresistive CMOS magnetic field sensors", *Sensors and Actuators A*, **103**, 23-32.
40. Pui, B.H., Hayes-Gill, B., Clark, M., Somekh, M., See, C., Morgan, S. and Ng, A. (2002). "The design of a real time VLSI optical centroid processor", *Proceedings of the First IEEE International Conference on Sensors*, Orlando, Florida, USA, **1**, 5-10.
41. Viarani, L., Stoppa, D., Gonzo, L., Gottardi, M. and Simoni, A. (2002). "A CMOS smart pixel for active 3D vision applications", *Proceedings of the First IEEE International Conference on Sensors*, Orlando, Florida, USA, 11-14.
42. Valente, A., Morais, R., Couto, C. and Correia, J.H. (2004). "Modeling, simulation and testing of a silicon soil moisture sensor based on the dual-probe heat-pulse method", *Sensors and Actuators A*, **115**, 434-439.
43. Bakker, A. (2000). "High-accuracy CMOS smart temperature sensors", Thesis, Delft University of Technology, Delft, The Netherlands.
44. Bakker, A. (2002). "CMOS smart temperature sensors – An overview", *Proceedings of the First IEEE International Conference on Sensors*, Orlando, Florida, USA, **2**, 1423-1427.
45. Kleinfelder, S., Lim, S.H., Liu, X. and El Gamal, A. (2001). "A 10,000 frames/s CMOS digital pixel sensor", *IEEE Journal of Solid-State Circuits*, **36**, 2049-2059.

46. Hammond, P.A., Cumming, D.R.S. and Ali, D. (2002). "A single-ship pH sensor fabricated by a conventional CMOS process", *Proceedings of the First IEEE International Conference on Sensors*, Orlando, Florida, USA, **1**, 350-355.
47. Gardner, J.W. and Bartlett, P.N. (1994). "A brief history of electronic noses", *Sensors and Actuators B*, **18-19**, 211-220.
48. Gardner, J.W. and Bartlett, P.N. (1996). "Performance definition and standardization of electronic noses", *Sensors and Actuators B*, **33**, 60-67.
49. NOSE, "Standards Commission of NOSE II", Information available at <http://www.nose-network.org/members/wg/default.asp>.
50. Gardner, J.W. and Cole, M. (2003). "Integrated electronic noses and microsystems for chemical analysis", Chapter 10 in *Handbook of machine olfaction.*, Pearce, T.C., Schiffman, S.S., Nagle, H.T. and Gardner, J.W., Ed. Weinheim, Germany: Wiley-VCH.
51. Neaves, P. I. and Hatfield, J. V. (1995). "A new generation of integrated electronic noses". *Sensors and Actuators B*, **26-27**, 223-231.
52. Cole, M., Gardner, J.W., Covington, J.A., Fife, D., Kwok, C.Y., Brignell, J.E. and Bartlett, P.N. (2000). "Active bridge polymeric resistive device for vapour sensing", *Euroensors XIV.*, Copenhagen, Denmark, 895-898.
53. Zee, F. and Judy, J.W. (2001). "Micromachined polymer-based chemical gas sensor array", *Sensors and Actuators B*, **72**, 120-128.
54. Covington, J.A., Gardner, J.W., Briand, D. and de Rooij, N.F. (2001). "A polymer gate FET sensor array for detecting organic vapours", *Sensors and Actuators B*, **77**, 155-162.
55. Gardner, J.W., Pike, A., de Rooij, N.F., Koudelka-Hep, M., Clerc, P.A., Hierlemann, A. and Göpel, W. (1995). "Integrated array sensor for detecting organic solvents", *Sensors and Actuators B*, **26-27**, 135-139.
56. Das, R.R., Shukla, K.K., Dwivedi, R. and Srivastava, A.R. (1999). "Discrimination of individual gas/odor using responses of integrated thick film tin oxide sensor array and fuzzy-neuro concept", *Microelectronics Journal*, **30**, 793-800.



57. Cané, C., Gràcia, I., Götz, A., Fonseca, L., Lora-Tamayo, E., Horrillo, M.C., Sayago, I., Robla, J.I., Rodrigo, J. and Gutiérrez, J. (2000). "Detection of gases with arrays of micromachined tin oxide gas sensors", *Sensors and Actuators B*, **65**, 244-246.
58. Ehrmann, S., Jüngst, J., Goschnick, J. and Everhard, D. (2000). "Application of a gas sensor microarray to human breath analysis", *Sensors and Actuators B*, **65**, 247-249.
59. Boeker, P., Horner, G. and Rösler, S. (2000). "Monolithic sensor array based on a quartz microbalance transducer with enhanced sensitivity for monitoring agricultural emissions", *Sensors and Actuators B*, **70**, 37-42.
60. Baca, A.G., Heller, E.J., Hietala, V.M., Casalnuovo, S.A., Frye-Mason, G.C., Klern, J.F. and Drummond, T.J. (1999). "Development of a GaAs monolithic surface acoustic wave integrated circuit", *IEEE Journal of Solid-State Circuits*, **43**, 1254-1258.
61. Cai, Q.Y., Park, J., Heldsinger, D., Hsieh, M.D. and Zellers, E.T. (2000). "Vapor recognition with an integrated array of polymer-coated flexural plate wave sensors", *Sensors and Actuators B*, **62**, 121-130.
62. Cunningham, B., Weinberg, M., Pepper, J., Clapp, C., Bousquet, R., Hugh, B., Kant, R., Daly, C. and Hauser, E. (2001). "Design, fabrication and vapor characterization of a microfabricated flexural plate resonator sensor and application to integrated sensor arrays", *Sensors and Actuators B*, **73**, 112-123.
63. Briand, D., van der Schoot, B., de Rooij, N.F., Sundgren, H. and Lundström, I. (2000). "A low-power micromachined MOSFET gas sensor", *Journal of Microelectromechanical Systems*, **9**, No. 3, 303-308.
64. Albert, K.J., Walt, D.R., Gill, D.S. and Pearce, T.C. (2001). "Optical multibead arrays for simple and complex odor discrimination", *Analytical Chemistry*, **73**, No. 11, 2501-2508.
65. Goodey, A., Lavigne, J.J., Savoy, S.M., Rodriguez, M.D., Curey, T., Tsao, A., Simmons, G., Wright, J., Yoo, S.J., Sohn, Y., Anslyn, E.V., Shear, J.B., Neikirk, D.P. and McDevitt, J.T. (2001). "Development of multianalyte sensor arrays composed of chemically derivatized polymeric microspheres localized

- in micromachined cavities”, *Journal of the American Chemical Society*, **123**, 2559-2570.
66. Datskos, P.G., Sepaniak, M.J., Tipple, C.A. and Lavrik, N. (2001). “Photomechanical chemical microsensors”, *Sensors and Actuators B*, **76**, 393-402.
  67. Ishida, H., Yamanaka, T., Cusida, N., Nakamoto, T. and Moriizumi, T. (2000). “Study of real-time visualization of gas / odor flow image using gas sensor array”, *Sensors and Actuators B*, **65**, 14-16.
  68. Schöning, M.J., Buß, G., Faßbender, F., Glück, O., Emons, H., Schmitt, G., Schultze, J.W. and Lüth, H. (2000). “A silicon-based microelectrode array for chemical analysis”, *Sensors and Actuators B*, **65**, 284-287.
  69. Gardner, J.W., Iskandarani, M.Z. and Bott, B. (1992). “Effect of electrode geometry on gas sensitivity of lead phthalocyanine thin films”, *Sensors and Actuators B*, **9**, 133-142.
  70. Gardner, J. W. (1995). "Intelligent gas sensing using an integrated sensor pair", *Sensors and actuators B*, **26-27**, 261-266.
  71. Ulmer, H., Mitrovics, J., Weimar, U. and Göpel, W. (2000). “Sensor arrays with only one or several transducer principles? The advantage of hybrid modular systems”, *Sensors and Actuators B*, **65**, 79-81.
  72. Chaudry, A.N., Hawkins, T.M. and Travers, P.J. (2000). “A method for selecting an optimum sensor array”, *Sensors and Actuators B*, **69**, 236-242.
  73. Dyer, D.C. and Gardner, J.W. (1997). “High precision intelligent interface for a hybrid electronic nose”, *Sensors and Actuators A*, **62**, 724-728.
  74. Hagleitner, C., Hierlemann, A., Lange, D., Kummer, A., Kerness, N., Brand, O. and Baltes, H. (2001). “Smart single-chip gas sensor microsystem”, *Nature*, **414**, 293-296.
  75. Hierlemann, A., Lange, D., Hagleitner, C., Kerness, N., Koll, A., Brand, O. and Baltes, H. (2000). "Application-specific sensor systems based on CMOS chemical microsensors", *Sensors and actuators B*, **70**, 2-11.

76. Udrea, F., Gardner, J.W., Setiadi, D., Covington, J.A., Dogaru, T., Lu, C.C. and Milne, W.I. (2001). "Design and simulations of SOI CMOS micro-hotplate gas sensors", *Sensors and Actuators B*, **78**, 180-190.
77. Cardinalli, G.C., Dori, L., Fiorini, M., Sayago, I., Faglia, G., Perego, C., Sberveglieri, G., Liberali, V., Maloberti, F. and Tonietto, D. (1997). "A smart sensor system for carbon monoxide detection", *Analog integrated circuits and signal processing*, **14**, No. 3, 275-296.
78. Bruschi, P., Nannini, A. and Neri, B. (1995). "Vapour and gas sensing by noise measurements on polymeric balanced bridge microstructures", *Sensors and actuators B*, **24-25**, 429-432.
79. Gardner, J.W., Vidic, M., Ingleby, P., Pike, A.C., Brignell, J.E., Scivier, P., Bartlett, P.N., Duke, A.J., Elliot, J.M. (1998). "Response of a poly(pyrrole) resistive micro-bridge to ethanol vapour", *Sensors and Actuators B*, **48**, 289-295.
80. Gardner, J.W. and Bartlett, P.N. (1995). "Application of conducting polymer technology in mycosystems", *Sensors and Actuators A*, **51**, 57-66.
81. Clark, D.T. (1994). "Surface, transforms and interfaces; the SMART direction for polymer science", *Synthetic Metals*, **67**, 63-70.
82. Hirano, S. and Kishimoto, A. (1998). "Effect of heating rate on positive-temperature-coefficient-of-resistivity behaviour of conductive composite thin films", *Appl. Phys. Lett.*, **73**(25), 3742-3744.
83. Ingleby, P., Gardner, J.W. and Bartlett, P.N. (1999). "Effect of micro-electrode geometry on response of thin-film poly(pyrrole) and poly(aniline) chemoresistive sensors", *Sensors and Actuators B*, **57**, 17-27.
84. Gerard, M., Chaubey, A. and Malhotra, B.D. (2002). "Application of conducting polymers to biosensors", *Biosensors & Bioelectronics*, **17**, 345-359.
85. The Royal Swedish Academy of Sciences (2000). "The 2000 Nobel Prize in Chemistry", Information for the public available at <http://www.nobel.se>.
86. The Royal Swedish Academy of Sciences. (2000). "The 2000 Nobel Prize in Chemistry, 2000: Conductive polymers", Information available at <http://www.nobel.se>.

87. Hatfield, J. V., Neaves, P., Hicks, P. J., Persaud, K. and Travers, P. (1994). "Towards an integrated electronic nose using conducting polymer sensors", *Sensors and Actuators B*, **18-19**, 221-228.
88. Sohn, J.H., Smith, R., Yoong, E., Leis, J. and Galvin, G. (2003). "Quantification of odours from piggery effluent ponds using an electronic nose and an artificial neural network", *Biosystems Engineering*, **86**, 399-410.
89. Stuetz, R.M., Engin, G. and Fenner, R.A. (1998). "Sewage odour measurements using a sensory panel and an electronic nose", *Water Science and Technology*, **38**, 331-335.
90. Costa Freitas, A.M., Parreira, C., and Vilas-Boas, L. (2001). "The use of an electronic aroma-sensing device to assess coffee differentiation—Comparison with SPME gas chromatography-mass spectrometry aroma patterns", *Journal of Food Composition and Analysis*, **14**, 513-522.
91. Misselbrook, T.H., Hobbs, P.J. and Persaud, K.C. (1997). "Use of an electronic nose to measure odour concentration following application of cattle slurry to grassland", *Journal of Agricultural Engineering Research*, **66**, 213-220.
92. Palmqvist, E., Kriz, C.B., Svanberg, K., Khayyami, M. and Kriz, D. (1995). "DC-resistometric urea sensitive device utilizing a conducting polymer film for the gas-phase detection of ammonia", *Biosensors and Bioelectronics*, **10**, 283-287.
93. Ahlskog, M. and Reghu, M. (1999). "The localization-interaction model for the DC-conductivity of metallic conducting polymers", *Synthetic Metals*, **101**(1-3), 367-368.
94. Lankinen, E., Sundholm, G., Talonen, P., Laitinen, T. and Saario, T. (1998). "Characterization of a poly(3-methyl thiophene) film by an in-situ dc resistance measurement technique and in-situ FTIR spectroelectrochemistry", *Journal of Electroanalytical Chemistry*, **447**, 135-145.
95. Amrani, M.E.H. and Payne, P.A. (1999). "Multi-frequency interrogation technique applied to conducting polymer gas and odour sensors", *IEE Proceedings - Science, Measurement and Technology*, **146**, No. 2, 95-101.

96. Musio, F., Amrani, M.E.H. and Persaud, K.C. (1995). "High-frequency a.c. investigation of conducting polymer gas sensors", *Sensors and Actuators B*, **23**, 223-226.
97. Amrani, M.E.H., Payne, P.A. and Persaud, K.C. (1996). "Multi-frequency measurements of organic conducting polymers for sensing of gases and vapours", *Sensors and Actuators B*, **33**, 137-141.
98. McLachlan, D.S. and Heaney, M.B. (1999). "Complex ac conductivity of a carbon black composite as a function of frequency, composition, and temperature", *Physical Review B*, **60**, No. 18, 12 746-12 751.
99. Carmona, F. and Ravier, J. (2002). "Electrical properties and mesostructure of carbon black-filled polymers", *Carbon*, **40**, 151-156.
100. Heaney, M.B. (1996). "Resistance-expansion-temperature behaviour of a disordered conductor-insulator composite", *Appl. Phys. Lett.*, **69**(17), 2602-2604.
101. Wycisk, R., Poźniak, R. and Pasternak, A. (2002). "Conductive polymer materials with low filler content", *Journal of Electrostatics*, **56**, 55-66.
102. Heaney, M.B. (1995). "Measurement and interpretation of nonuniversal critical exponents in disordered conductor-insulator composites", *Physical Review B*, **52**, No. 17, 12 477-12 480.
103. Shevade, A.V., Ryan, M.A., Homer, M.L., Manfreda, A.M., Zhou, H. and Manatt, K.S. (2003). "Molecular modeling of polymer composite-analyte interactions in electronic nose sensors", *Sensors and Actuators B*, **93**, 84-91.
104. Burl, M.C., Sisk, B.C., Vaid, T.P. and Lewis, N.S. (2002). "Classification performance of carbon black-polymer composite vapor detector arrays as a function of array size and detector composition", *Sensors and Actuators B*, **87**, 130-149.
105. Sisk, B.C. and Lewis, N.S. (2003). "Estimation of chemical and physical characteristics of analyte vapors through analysis of the response data of arrays of polymer-carbon black composite vapor detectors", *Sensors and Actuators B*, **96**, 268-282.

106. Sisk, B.C. and Lewis, N.S. (2005). "Comparison of analytical methods and calibration methods for correction of detector response drift in arrays of carbon black-polymer composite vapor detectors", *Sensors and Actuators B*, **104**, 249-268.
107. Hierlemann, A., Brand, O., Hagleitner, C. and Baltes, H. (2003). "Microfabrication techniques for chemical/biosensors", *Proceedings of the IEEE*, **91**, No. 6, 839-863.
108. Heer, F., Franks, W., Blau, A., Tachini, S., Ziegler, C., Hierlemann, A. and Baltes, H. (2004). "CMOS microelectrode array for the monitoring of electrogenic cells", *Biosensors and Bioelectronics*, **20**, 358-366.
109. Barrentino, D., Graf, M., Song, W.H., Kirstein, K.U., Hierlemann, A. and Baltes, H. (2004). "Hotplate-based monolithic CMOS microsystems for gas detection and material characterization for operating temperatures up to 500 °C", *IEEE Journal of Solid-State Circuits*, **39**, No. 7, 1202-1207.
110. Graf, M., Barrentino, D., Zimmermann, M., Hierlemann, A., Baltes, H. and Hahn, S. (2004). "CMOS monolithic metal-oxide sensor system comprising a microhotplate and associated circuitry", *IEEE Sensors Journal*, **4**, No. 1, 9-16.
111. Becker, T., Mühlberger, S., Bosch-v.Braunmühl, C., Müller, G., Meckes, A. and Benecke, W. (2001). "Microreactors and microfluidic systems: an innovative approach to gas sensing using tin oxide-based gas sensors", *Sensors and Actuators B*, **77**, 48-54.
112. Becker, T., Mühlberger, S., Bosch-v.Braunmühl, C., Müller, G., Meckes, A. and Benecke, W. (2000). "Gas mixture analysis using silicon micro-reactor systems", *Journal of Microelectromechanical Systems*, **9**, No. 4, 478-484.
113. Benecke, W., Meckes, A. (1998). "A smart gas sensing microsystem", *Proceedings of the IEEE International Symposium on Industrial Electronics*, **1**, 263-266.
114. Covington, J.A., Tan, S.L., Gardner, J.W., Hamilton, A., Koickal, T.J. and Pearce, T.C. (2003). "Combined smart chemFET/resistive sensor array", *Proceedings of the IEEE International Conference on Sensors*, Toronto, Canada, **2**, 1120-1123.

115. Tan, S.L., Covington, J.A. and Gardner, J.W. (2004). "Ultra-fast chemical sensing microsystem employing resistive nanomaterials", *SPIE 11<sup>th</sup> International Symposium on Smart Structures and Materials*, San Diego, **5389**, 366-376.
116. Lundström, I., Erlandsson, R., Frykman, U., Hedborg, E., Spetz, A., Sundgren, H., Welin, S. and Winquist, F. (1991). "Artificial 'olfactory' images from a chemical sensor using a light-pulse technique", *Nature*, **352**, 47-50.
117. Lundström, I. (2000). "Artificial noses: picture the smell", *Nature*, **406**, 682-683.
118. Uchida, H., Filippini, D. and Lundström, I. (2004). "Unsupervised scanning light pulse technique for chemical sensing", *Sensors and Actuators B*, **103**, 225-232.
119. Ishida, H., Tokuhiko, T., Nakamoto, T. and Moriizumi, T. (2002). "Improvement of olfactory video camera: gas/odour visualization system", *Sensors and Actuators B*, **83**, 256-261.
120. Russell, R.A. and Purnamadajaja, A.H. (2002). "Odour and airflow complementary senses for a humanoid robot", *Proceedings of the IEEE International Conference on Robotics and Automation*, Washington DC, 1842-1847.
121. Russell, R.A. (2004). "Robotic location of underground chemical sources", *Robotica*, **22**(1), 109-115.
122. Tresoldi, S. (1999). "Sniffing robot: robotic odor perception", *Circuit Cellar Magazine*, **108**, 12-16.
123. Albert, K.J. and Walt, D.R. (2003). "Information coding in artificial olfaction multisensor arrays", *Anal. Chem.*, **75**, 4161-4167.
124. Stitzel, S.E., Stein, D. R. and Walt, D.R. (2003). "Enhancing vapor sensor discrimination by mimicking a canine nasal cavity flow environment", *Journal of the American Chemical Society*, **125**, 3684-3685.
125. Seguire, D. (2002). "Just add sensor -- Integrating analog and digital signal conditioning in a programmable system on chip", *Proceedings of the First IEEE International Conference on Sensors*, Orlando, Florida, USA, **1**, 665-668.

## **CHAPTER 2**

# **THE RATIOMETRIC PRINCIPLE**

### **2.1 INTRODUCTION**

This chapter describes the basic measurement principle used in this project for the design of a ratiometric ASIC chip. The description starts with a general overview of the operating principle and the depiction of its most commonly used configurations, and is followed by details of the specific design employed here.

A brief analysis is presented of the topologies based on the ratiometric measurement principle, together with a summary of previous ratiometric designs used for gas sensing applications.



## 2.2 THE RATIOMETRIC MEASUREMENT PRINCIPLE

The *ratiometric* approach is used in measurement and instrumentation because of its benefits when small variations in a signal need to be detected and recorded. In its most general definition, the ratiometric principle consists in the comparison of ratios from a common supply [1]. When these ratios are equal, the system is in its balanced condition. Any change in one of the ratios can be detected through the differential output produced by the unbalanced condition derived from these changes.

In the case of standard analogue electronic circuits, a common practice for the implementation of this measurement principle is the use of voltage supplies that are applied to voltage dividers. In particular, resistive voltage dividers are of interest for this project, given that resistive sensors are used for the detection of changes in the concentrations of gases or VOC.

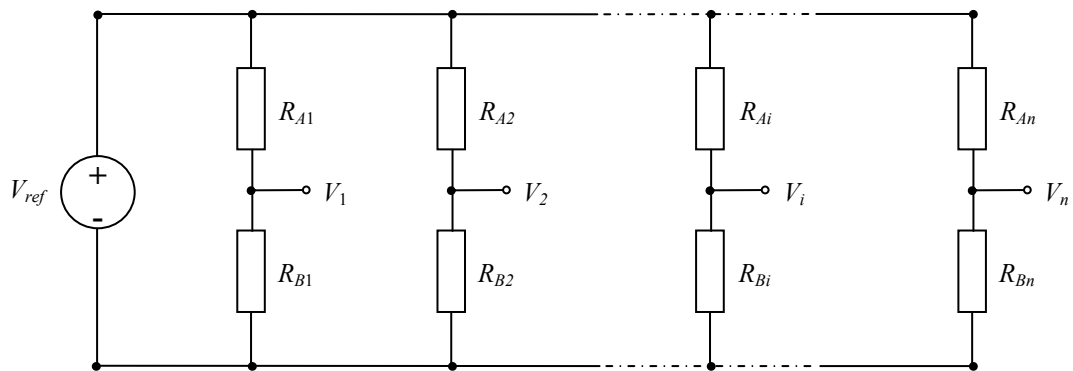


**Figure 2.1** The general ratiometric configuration.

Figure 2.1 illustrates the ratiometric principle simplified for the case of resistive measurements and a voltage source. A reference voltage  $V_{ref}$  is applied to a set of  $n$  resistive dividers. In the *balanced condition*, the resistance ratio  $R_{Ai}/R_{Bi}$  is the same for each arm of the circuit, i.e.

$$\frac{R_{A1}}{R_{B1}} = \frac{R_{A2}}{R_{B2}} = \dots = \frac{R_{Ai}}{R_{Bi}} \dots = \frac{R_{An}}{R_{Bn}} \quad (2.1)$$

Under this condition, the potential at every partial output  $V_i$  ( $i = 1, 2, \dots, n$ ) is the same for every arm of the circuit and there is no difference in voltage between the points at the middle of each arm; i.e. the differential output taken between any pair of partial outputs will be zero.

As a consequence of this configuration, any change in the reference voltage will not have an effect on the measurements, as the ratios make the circuit insensitive to supply variations [1]. Moreover, it makes possible to obtain greater accuracy in control and measurement than the inherent stability of the voltage reference, permitting the measuring of small variations produced by changes in any of the resistive elements in the arms. Only those variations that are originated by the response of some resistor to a particular phenomenon will lead to measurable variations in the corresponding differential output voltage.

Ratiometric circuits compensate for common problems that appear in discrete resistive sensors, where the values of the output obtained are affected by the magnitude and duration of the applied voltage, and the effects of temperature and humidity must also be considered, particularly for high resistances [2].

The ratiometric principle is most commonly used in its simplest form in the classic bridge circuits that are described in the next section.

## 2.3 RATIOMETRIC TOPOLOGIES FOR RESISTANCE MEASUREMENT

Measurement of changes in electrical resistance has been successfully dealt with for many years by using different methods and by applying basic principles, which have been implemented in successively updated versions of modern instrumentation.

In particular, symmetric topologies have been an appropriate tool due to the ability for compensation of variations from temperature and other external interferences that such structures offer and the fact that they allow a way of measuring small changes in resistance that would be very difficult to detect by direct measurement [3-5].

Bridges are perhaps the most representative of these circuit topologies, the Wheatstone bridge being the classical example and most common of these structures found in measurement and instrumentation.

A general schematic circuit for the Wheatstone bridge is represented in Figure 2.2. Four resistive elements are arranged in a symmetrical polygonal configuration, obtained by using only two arms of the general ratiometric structure described in section 2.1.

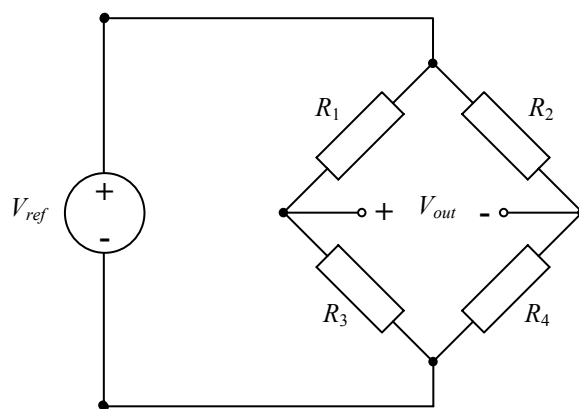


**Figure 2.2** The Wheatstone bridge with a voltage supply.

The differential output voltage  $V_{out}$  is taken between the halfway points of the arms, being zero under the balanced condition.

$$V_{out} = \left( \frac{R_3}{R_1 + R_3} - \frac{R_4}{R_2 + R_4} \right) V_{ref} \quad (2.2)$$

This is also the voltage for the Thévenin equivalent of the bridge, i.e. the open-circuit output voltage. The Thévenin impedance  $Z_{Th}$  is given by:

$$Z_{Th} = \frac{R_1 R_3}{R_1 + R_3} + \frac{R_2 R_4}{R_2 + R_4} \quad (2.3)$$

This configuration allows compensation of changes in resistances, because it is not necessary that any of the resistances are identical or that they have particular individual values in order to maintain the balance; the only requirement for a balanced condition is that the resistance ratios are the same:

$$\frac{R_1}{R_3} = \frac{R_2}{R_4} \quad (2.4)$$

In order to use the bridge as a measurement system, at least one of the resistive elements must be exposed to variations, while the others remain fixed. If all the elements have the same resistance  $R$  and only one of them, say  $R_3$ , changes by a quantity  $\Delta R$ , then the output of the resulting *quarter-bridge* circuit [3] is given by:

$$V_{out} = \left( \frac{R + \Delta R}{R + R + \Delta R} - \frac{R}{R + R} \right) V_{ref} = \frac{\Delta R}{2(2R + \Delta R)} V_{ref} \quad (2.5)$$

Likewise, the output of a *half-bridge*, i.e. an unbalanced bridge with two active arms  $R_2$  and  $R_3$ , is given by:

$$V_{out} = \left( \frac{R + \Delta R}{R + R + \Delta R} - \frac{R}{R + \Delta R + R} \right) V_{ref} = \frac{\Delta R}{2R + \Delta R} V_{ref} \quad (2.6)$$

which is the double of the quarter-bridge output.

Quarter-bridge circuit and half-bridge circuit are represented in Figure 2.3 and Figure 2.4, respectively.

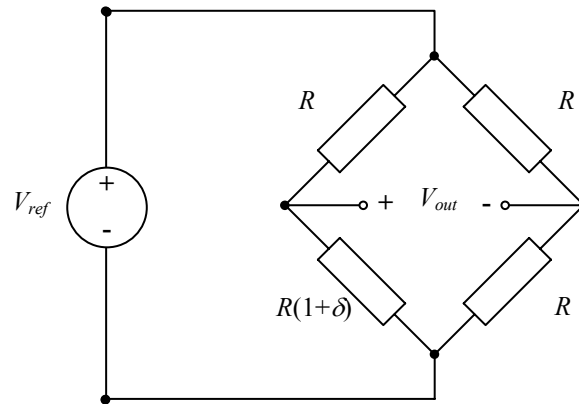


**Figure 2.3** Quarter-bridge circuit with voltage supply.

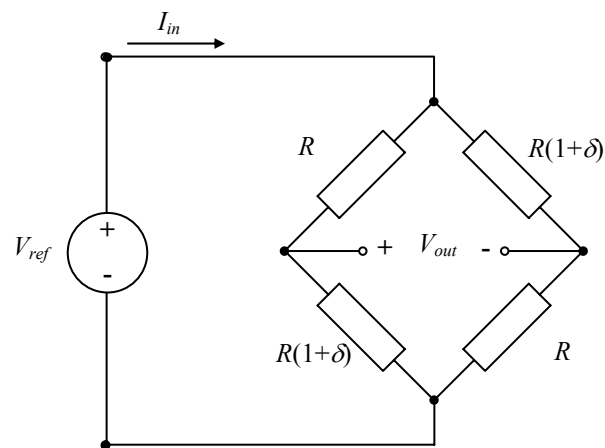


**Figure 2.4** Half-bridge circuit with voltage supply.

It can be observed that the output is not linear in  $\Delta R$ . However, when the change in resistance is small, i.e.  $\Delta R \ll R$ , it is possible to obtain an approximately linear response from these circuits [2].

The *relative resistance variation*  $\delta$ , also known as *bridge deflection*, expresses the ratio of the change in resistance to the baseline resistance:

$$\delta = \frac{\Delta R}{R} \quad (2.7)$$

Using  $\delta$ , Equations 2.5 and 2.6 can be rewritten as follows:

$$V_{out} = \frac{\delta}{2(2+\delta)} V_{ref} \approx \frac{\delta}{4} V_{ref} - \frac{\delta^2}{8} V_{ref} \quad (2.8)$$

$$V_{out} = \frac{\delta}{2+\delta} V_{ref} \approx \frac{\delta}{2} V_{ref} - \frac{\delta^2}{4} V_{ref} \quad (2.9)$$

In most cases, the output of bridge circuits is non linear with respect to the change in resistance. However, there is a linear relationship between voltage at the output of the half-bridge circuit and the current applied to the input:

$$V_{out} = \frac{\delta}{2+\delta} \frac{R(2+\delta)}{2} I_{in} = \frac{R\delta}{2} I_{in} \quad (2.10)$$

Linearity obtained in this way, makes current driven bridges a suitable option for many sensor circuits, given that they have the additional advantages of being less susceptible to lead resistance and, in some cases, they may be easier to implement in practice [6-7].

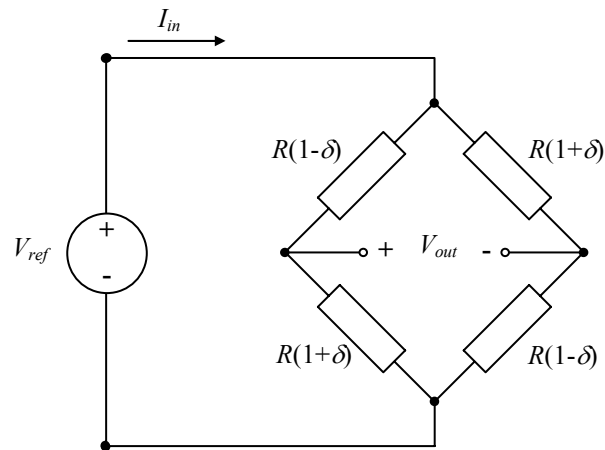


**Figure 2.5** Linearized bridge circuit with voltage supply.

A linearized bridge for both voltage and current can also be obtained when compensation in variations of resistances maintain the bridge under balance, as

shown in Figure 2.5. The output can be expressed as a linear function of either the voltage or the current at the input, according to the following equations:

$$V_{out} = \delta V_{ref} \quad (2.11)$$

$$V_{out} = \delta R I_{in} \quad (2.12)$$

In general, sensors produce a small signal when exposed to measurands. Therefore, the output signal from bridges and other sensor circuits must be normally amplified using operational amplifiers. This allows the selection of the desired impedance levels, the conversion of the balanced output to a single ended output, and, in some cases, the linearization of the output.

Different configurations are available for the amplification of the signals. In the simplest form, the differential output of the bridge could be connected to the inputs of a single operational amplifier, with an additional resistor in the feedback path for the control of gain and impedance levels. As an example, the current drive bridge used by Gardner et al. [8], shown in Figure 2.6, uses an operational amplifier and a feedback resistor in order to adjust the gain of the output of the bridge, and another operational amplifier is employed to set the offset or bias voltage.

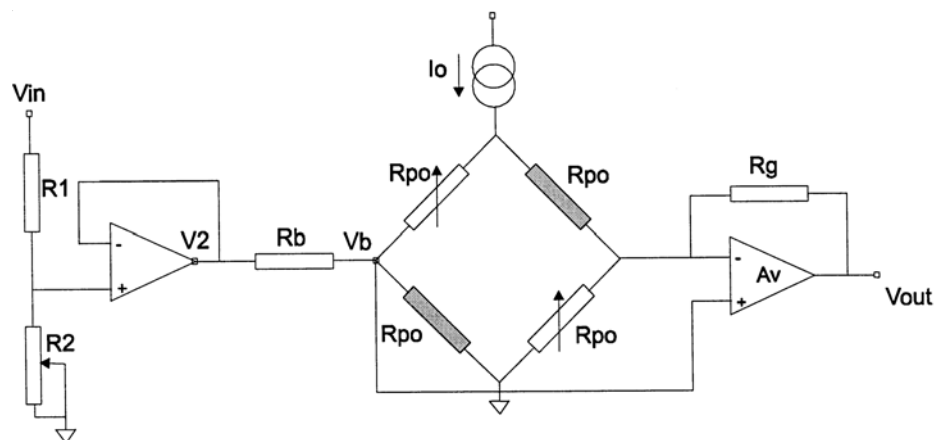


**Figure 2.6** Current-driven bridge circuit used by Gardner et al. [8].

Operational amplifier configurations for linear amplification and for the conditioning of sensor signals are extensively described in literature [1, 6, 9-10].

Two special cases of ratiometric circuits based on operational amplifiers are the inverting and the non-inverting amplifiers. These circuits are commonly used in instrumentation for the processing of sensor signals.

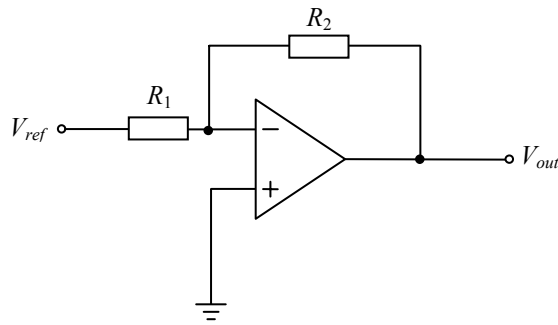


**Figure 2.7** Inverting amplifier.

The inverting amplifier, shown in Figure 2.7, amplifies a voltage reference according to the ratio of the two resistors in the circuit. In general, the voltages are related by the basic equation:

$$V_{out} = -\frac{R_2}{R_1} V_{ref} \quad (2.13)$$

When the resistances are the same, the output voltage equals the reference input with an inversion in sign. If one of the resistors, say  $R_2$ , is a sensor exposed to variations in the measurand, then the ratio changes and the magnitude of the output voltage will be different from the reference, as given by:

$$V_{out} = -\frac{R + \Delta R}{R} V_{ref} \quad (\text{for } R_1 = R_2 = R) \quad (2.14)$$

In terms of the relative resistance variation, the output voltage is related to the input reference as follows:



$$V_{out} = -(1 + \delta) V_{ref} \quad (2.15)$$

If the resistor  $R_1$  is the sensor exposed to changes, then the circuit measures conductance and the output voltage is given by:

$$V_{out} = -\frac{G_1}{G_2} V_{ref} = -(1 + \delta_G) V_{ref} \quad (2.16)$$

In the non-inverting configuration, shown in Figure 2.8, the voltage reference is passed through an operational amplifier to a resistive divider which defines the level of amplification applied to the signal. The output of the circuit is the voltage  $V_{out}$  taken directly from the output of the operational amplifier.

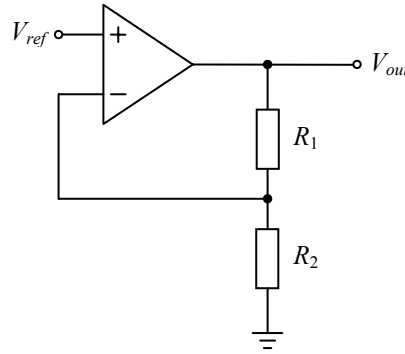


**Figure 2.8** Non-inverting amplifier.

The output voltage of the non-inverting amplifier is given by the equation:

$$V_{out} = \left(1 + \frac{R_1}{R_2}\right) V_{ref} \quad (2.17)$$

In a balanced condition,  $R_1$  equals  $R_2$  and the magnitude of the output is exactly the double of the input. If, starting from this balanced condition, the resistance  $R_1$  is affected by variations, the output of the non-inverting circuit is given by:

$$V_{out} = \left(1 + \frac{R + \Delta R}{R}\right) V_{ref} \quad (\text{for } R_1 = R_2 = R) \quad (2.18)$$

The same relationship can be expressed as follows in terms of the relative resistance variation:

$$V_{out} = (2 + \delta) V_{ref} \quad (2.19)$$

Conductance measurement can also be achieved if the resistor  $R_2$  is the sensor exposed to changes. The output voltage is given in this case by:

$$V_{out} = \left(1 + \frac{G_2}{G_1}\right) V_{ref} = (2 + \delta_G) V_{ref} \quad (2.20)$$

Different and more complex relationships between the input and output voltages are obtained when even both resistors are exposed to variations. A more detailed analysis of these relationships is presented in section 2.5, along with the description of the ratiometric configuration adopted for the present work.

## 2.4 RATIOMETRIC DESIGNS FOR GAS SENSING APPLICATIONS

Ratiometric designs for gas sensing purposes have been developed by several research groups relying on diverse mechanisms and oriented to many different applications. Early sonar instruments, for example, were designed based on a ratiometric comparison of velocity of sound in different gases, in order to determine the concentration of components in binary mixtures of gases [11].

Ratiometric bridges have been used with gas sensing systems because of its ability for temperature compensation and also for an easier conversion of the measurands into voltage signals. Commercial pellistors by City Technology Ltd. use a half-bridge circuit for temperature compensation. Also, the micro-calorimeter bridge arrays developed at the SRL for methane detection make use of the ratiometric properties for compensation of temperature in the measurements [12].

Likewise, the resonating cantilever reported by the PEL ETH group, uses embedded piezoresistors in a Wheatstone configuration to obtain the voltage signal to be amplified [13].

The research group at the SRL in the University of Warwick has been working for years on the design of ratiometric devices based on conducting polymer chemoresistors for the sensing of gases and vapours. The use of this type of gas sensors offers several particular advantages that make them suitable for electronic nose applications. First, deposition of polymers is relatively easy, either by electrochemical processes or by direct injection or spraying. A large variety of conducting polymers can be obtained and they can be used for the identification of a large range of gases or odours. Secondly, conducting polymers can operate at or near ambient temperature, contrasting with the high temperature required by the classical

tin oxide resistors (e.g. Taguchi gas sensor) which therefore demand the use of heaters that are highly power consuming (200-800 mW). Moreover, polymer chemoresistors can be grown on the same chip containing the interfacing and signal conditioning circuitry, fulfilling this way the basic requirements for the development of an integrated hand-held instrument for gas sensing.

However, there are some drawbacks in the performance of conducting polymers. Environmental conditions, such as temperature and humidity, affect their resistance and compensation is required to eliminate these unwanted variations. Also, applied voltage and ageing are potential causes of drift in the resistance value, which makes necessary a method of calibration within the instrument itself. The ratiometric approach has been attempted through several designs at SRL in order to cancel most of these effects.

Early research work was carried out in collaboration with the University of Southampton [7-8, 14]. Four arm half-bridge microcircuits were designed using *Tanner Tools L-Edit™* software, and fabricated with conducting polymer (poly(pyrrole) and poly(aniline)) chemoresistors on all arms in a CMOS-compatible process. Two of the arms opposite were coated with an epoxy resin to make them inert to the effect of gas exposure, obtaining this way a half-bridge configuration with only two active arms. The poly(pyrrole) bridges were tested using a discrete measurement system and the responses to ethanol vapour in air were obtained in an automated mass flow system under different values of humidity and temperature. It was reported that the response followed the Langmuir isotherm in concentration and showed competitive binding hence, falling with both increasing temperature and humidity [7-8, 14].

Further investigation on these bridges was performed with the aid of a standard cell CMOS current drive chip, designed to supply currents to an array of six polymeric resistive micro-bridges. The chip was designed at the University of Southampton and fabricated using a CMOS process [7]. This joint Warwick-Southampton work was an important step towards the integration of sensors and smart circuitry.

The four arm half-bridge design was improved by adding a fifth element in the operational amplifier feedback path, as previously shown in Figure 2.6 [8, 15-16]. The purpose of this additional polymer resistor was to set the gain of the circuit matching the temperature dependence with the bridge elements. In addition to the constant gain obtained, the five-element bridge improves compensation for variations in polymer resistance and temperature sensitivity. Temperature and humidity sensitivity were reduced with respect to the previous four-element design, but most of all with respect to the single chemoresistor performance.

The five-element bridges were designed using again L-Edit software, and they were fabricated in two versions: a discrete CMOS-compatible and a fully standard CMOS. For the discrete one, conducting polymers films were grown by the Chemistry Department at the University of Southampton. For the CMOS version, three types of carbon black/polymer composite were deposited at the Cyrano Sciences, California, USA.

Both types of devices were characterised after deposition; their response to ethanol vapour, as well as their sensitivity, temperature and humidity dependence, were obtained. It was observed that the use of the feedback polymer resistor helped to reduce the batch-to-batch variations in the resistors, reduced the high temperature

coefficient, and nearly eliminated the long term drift produced by the applied DC voltage when a dual voltage supply was used [15].

Looking for further improvement in the response of the sensors, and as an alternative and more direct method to compensate for both the wide range in the values of polymer resistances, and their temperature and humidity dependence, several ratiometric devices using the inverting configuration were proposed.

Discrete devices were designed with arrays of polymeric resistors either in series or parallel for the feedback and forward elements. The discrete devices were fabricated at the Institute of Microtechnology in the University of Neuchâtel, Switzerland, and conducting polymers were grown at Southampton University [17]. The forward resistor was coated using epoxy resin, while the feedback element was left uncovered as the active sensing element for the presence of gases or vapours. The use of the inverting configuration has the additional advantage that it directly cancels those variations that are common to both resistors, like those produced by temperature changes, applied voltage or ageing. The reference coated resistor is not affected by changes in ambient humidity.

The devices were exposed to different concentrations of ethanol vapour in air, under controlled temperature and humidity conditions. The results showed a reduction in the temperature dependence of the baseline signal (approximate linear coefficient of  $1.2 \times 10^{-3}/^{\circ}\text{C}$ ), and negligible humidity dependence.

A CMOS integrated version of these circuits was fabricated via the *Europractice* scheme using an AMS 0.8  $\mu\text{m}$  standard CMOS process. Electrodes were obtained in two different ways, namely aluminium electrodes and P-type

electrodes. The chip contained an operational amplifier and also a heater and a temperature sensor [17-19].

Based on those previous experiences, a much more ambitious project is attempted here, oriented to the design of a complete ASIC chip in which a ratiometric array of carbon black-polymer composite chemoresistors is integrated with signal processing circuitry.

The following section describes the features of the ratiometric configuration selected for the current thesis work.

## 2.5 THE RATIOMETRIC CONFIGURATION USED IN THIS WORK

Previous experience in the design of ratiometric devices suggested that the use of an appropriate array of chemoresistive sensors could help to both reduce most of the unwanted variations in the response, by removing the common mode effects, and to improve the sensitivity of the response to vapours, while reducing the sensitivity to temperature and humidity. The benefits of the ratiometric devices could also be improved with the aid of signal processing circuitry.

Therefore, a ratiometric approach was selected for the design of the ASIC chip which would serve as the main building block in the design of a complete smart hand-held system for the monitoring of gases and vapours. Following the basic principle, two ratios of the same supply are compared. A voltage reference is applied to a pair of non-inverting circuits, in which the resistance ratios are measured through the built-in voltage dividers. This configuration results in a ratiometric bridge with an amplified differential output. The basic arrangement is shown in Figure 2.9.

In the first of the non-inverting circuits, labelled “*Gas sensor circuit*”, the two resistors are actual chemoresistive sensors used for the detection of gas or VOC. The second circuit, labelled “*Offset circuit*”, acts as a reference, providing the offset signal required for the comparison of the resistance ratios. One of the resistors in this circuit is digitally programmable, so the offset signal can be adjusted as required. The pre-amplified differential output is taken between the individual outputs of the two non-inverting circuits.

This configuration combines the major advantages of previous ratiometric devices. According to Equation 2.17, the ratio of the sensor resistances  $R_1/R_2$  will



cancel undesirable effects that are common to both sensors in the same way that it was explained for the inverting devices described in section 2.4. However, the use of only one pair of resistors in the inverting array had still the drawback of a high sensitivity to the applied voltage, which could be significant when compared to the relatively low response of the polymer resistors. Also, it was not easy to control in practice the required matching in the resistance values of the actual sensors.

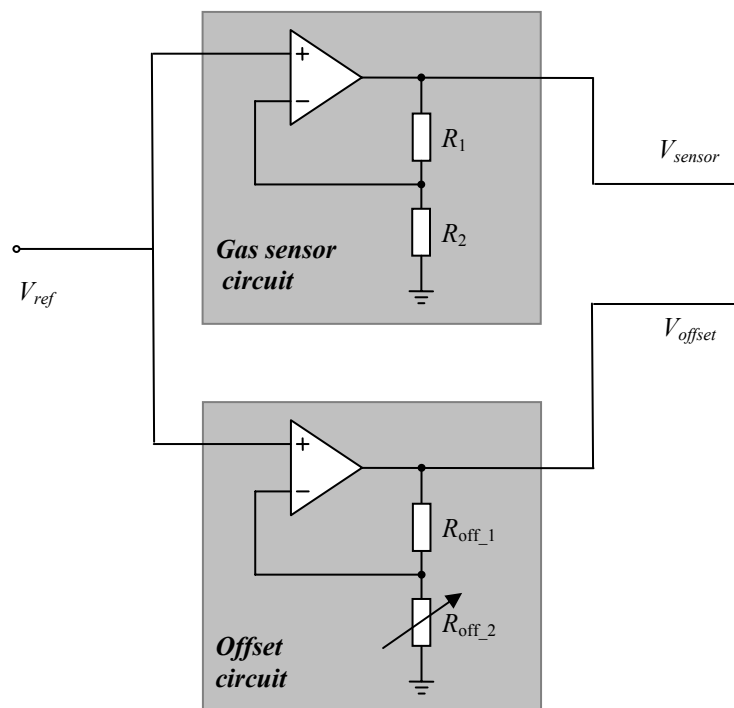


**Figure 2.9** Ratiometric configuration used in this project.

These disadvantages are tackled through the use of the offset circuit, which mimics in parallel the behaviour of the sensor circuit and produces an output that is calibrated as required by the resistance ratio of the chemoresistors. As a result, variations in the supply voltage are common to both circuits and therefore they are cancelled in the differential output. Differences in the resistances of the fabricated sensors are also compensated through the programmable resistor in the offset circuit.

The use of the non-inverting configuration also contributes to an improvement in the performance of the sensing system and facilitates its implementation. Recalling Equation 2.15, the output of the inverting configuration affects the reference input by a factor  $-(1+\delta)$  that barely can be detected in the output because of both the required low level of the reference voltage and the typical small response of the conducting polymer sensors (0.1-1%). In the non-inverting array, however, there is an implicit pre-amplification by a  $2+\delta$  factor (Equation 2.19) which makes voltage levels more accessible for the subsequent analogue signal processing. The use of a non-inverted signal is also an advantage because this allows a higher amplitude variation when using a single-supply CMOS technology like the one selected for the fabrication of the ASIC chip in this project.

All of these features are still more important when dealing with practical application of the chemoresistors, in which the ideal balanced condition of the bridge is not easy to maintain and environmental disturbances modify the overall performance of sensors and related circuitry.

The configuration shown in Figure 2.9 was used in this project in two different modes for the measurement of gas or vapour concentrations. In the first case, only one of the chemoresistors acts as an active gas sensor, while the other remains passive or inert to gas effects. In the ideal case that  $R_2$  remains constant and  $R_1$  is exposed to changes, the corresponding change in the sensor output voltage is given by:

$$\frac{\partial V_{sensor}}{\partial R_1} = V_{ref} \frac{\partial}{\partial R_1} \left( 1 + \frac{R_1}{R_2} \right) = \frac{1}{R_2} V_{ref} \quad (2.21)$$

Hence, under ideal conditions, the sensitivity is a constant and the response linear in concentration ( $R_1 \propto C$ ).

If  $R_2$  is exposed to variations while  $R_1$  stays constant, the change in the output voltage is given by:

$$\frac{\partial V_{sensor}}{\partial R_2} = V_{ref} \frac{\partial}{\partial R_2} \left( 1 + \frac{R_1}{R_2} \right) = -\frac{R_1}{R_2^2} V_{ref} \quad (2.22)$$

which corresponds to a non-linear and more complicated response in terms of resistance, although it would be linear in terms of conductance.

In a second mode of operation, which is attempted for the first time in this project, both chemoresistors are exposed to changes in gas concentration. For this case, the overall change in the sensor output voltage is expressed by:

$$dV_{sensor} = \frac{V_{ref}}{R_2^2} (R_2 dR_1 - R_1 dR_2) \quad (2.23)$$

where again  $R_2$  produces a non-linear component in the response. The use of this mode would make no sense in the ideal case where resistances are matched and both sensors respond in the same way, which would lead to a null change in the output. However, relevant results are obtained when two different types of chemoresistors are used and the differences in their responses are applied for the identification of gases or vapours, as it will be described in depth in the experimental part of this work.

The next chapter describes every component of the entire smart ASIC chip designed around the ratiometric configuration explained in this section.

## 2.6 REFERENCES

1. Horowitz, P. and Hill, W. (1989). *The art of electronics*, 2nd ed., Cambridge University Press. New York, USA.
2. Gregory, B.A. (1981). *An introduction to electrical instrumentation and measurement systems*, 2nd ed., The Macmillan Press Ltd., London.
3. Brignell, J. and White, N. (1996). *Intelligent sensor systems*, Institute of Physics Publishing, Bristol.
4. Pallàs-Areny, R. and Webster, J.G. (2001). *Sensors and signal conditioning*, 2nd ed., John Wiley & Sons, Inc., New York.
5. Ramsay, D.C. (1996). *Principles of engineering instrumentation*, Arnold, London.
6. Ismail, M. and Fiez, T. (1994). *Analog VLSI: signal and information processing*, McGraw-Hill, Inc. New York.
7. Cole, M., Gardner, J.W., Lim, A.W.Y., Scivier, P.K. and Brignell, J.E. (1999). "Polymeric resistive bridge gas sensor array driven by a standard cell CMOS current drive chip", *Sensors and Actuators B*, **58**, 518-525.
8. Gardner, J.W., Vidic, M., Ingleby, P., Pike, A.C., Brignell, J.E., Scivier, P. Bartlett, P.N., Duke, A.J. and Elliot, J.M. (1998). "Response of a poly(pyrrole) resistive micro-bridge to ethanol vapour", *Sensors and Actuators B*, **48**, 289-295.
9. Floyd, T.L. and Buchla, D. (1999). *Fundamentals of analog circuits*, Prentice-Hall, Inc., Upper Saddle River, New Jersey.
10. Sedra, A.S. and Smith, K.C. (1998). *Microelectronic circuits*, 4th. ed., Oxford University Press, New York, USA.
11. Hallewell, G., Crawford, G., McShurley, D., Oxoby, G. and Reif, R. (1988). "A sonar-based technique for the ratiometric determination of binary gas mixtures", *Nuclear Instruments and Methods in Physics Research*, **A264**, 219-234.

12. Lee, S.M. (2002). "Low-power silicon planar micro-calorimeter employing nanostructured catalyst", PhD Thesis, University of Warwick, Coventry, UK.
13. Hagleitner, C., Hierlemann, A., Lange, D., Kummer, A., Kerness, N., Brand, O. and Baltes, H. (2001). "Smart single-chip gas sensor microsystem", *Nature*, **414**, 293-296.
14. Vidic, M. and Gardner, J.W. (1997). "ASIC Project: progress report", University of Warwick, Coventry, UK.
15. Cole, M., Gardner, J.W., Covington, J.A., Fife, D., Kwok, C.Y., Brignell, J.E. and Bartlett, P.H. (2000). "Active bridge polymeric resistive device for vapour sensing", Eurosenors XIV, Copenhagen, Denmark, 895-898.
16. Fife, D. (2000). "The design, analysis and implementation of two analogue CMOS chips for incorporation in hand-held gas sensing equipment", BEng final report, University of Warwick, Coventry, UK.
17. Cole, M., Gardner, J.W. and Bartlett, P.N. (2001). "Low-drift odour and vapour ratiometric resistive elements for analogue CMOS smart sensors", *Electrochemical Society Proceedings*, **15**, 117-120.
18. Gardner, J.W., Cole, M. and Udrea, F. (2002). "CMOS gas sensors and smart devices", *Proceedings of the First IEEE International Conference on Sensors*, Orlando, Florida, USA, **1**, 721-726.
19. West, C. (2001). "Design of an ASIC chip for a hand held gas detector", BEng Final Report, University of Warwick, Coventry, UK.

## **CHAPTER 3**

# **SCHEMATIC DESIGN OF THE RATIOMETRIC ASIC CHIP**

### **3.1 INTRODUCTION**

This chapter describes the schematic design of a novel ASIC chip that has been created following the ratiometric measurement principle explained in the previous chapter. The design of the ratiometric ASIC chip is presented starting from a top block-diagram level and then the description goes down to the details of the components in every section.

An overview of the system is given first, followed by information about the software employed for the design process. Next, the explanation is divided in two sections corresponding to the main circuit components of the ASIC chip, namely the gas sensor section and the temperature control circuitry.

### 3.2 OVERALL DESCRIPTION OF THE SYSTEM

The ratiometric ASIC chip is designed for use in a hand-held instrument for the monitoring of volatile organic compounds. It facilitates the integration of a ratiometric array of chemoresistors together with smart circuitry into a single chip fabricated through a standard silicon CMOS process. The integrated circuit provides automatic compensation of variation in both supply voltage and ambient temperature, and permits control of sensor temperature. The ratiometric design principle also compensates for a large range in values of polymer resistance. It is believed that the circuit offers relevant smart capabilities at a very low cost and hence it can be used as the main component for the mass production of a self-calibrating programmable instrument.

The overall structure of the system is shown in Figure 3.1. The main components of the proposed programmable instrument are:

- i) The ratiometric ASIC chip, which integrates the gas sensors and the necessary circuitry for the conditioning of signals.
- ii) A programmable unit for the control of the whole system. This may be a micro-controller unit or any equivalent programmable device.
- iii) A set of programmable digital potentiometers, as an auxiliary device for the automatic setting of the signals required for the ASIC chip.

The ratiometric ASIC chip has been designed to perform two basic functions: (a) sensing the gas presence and concentration, and (b) controlling the operating temperature of the gas sensors.

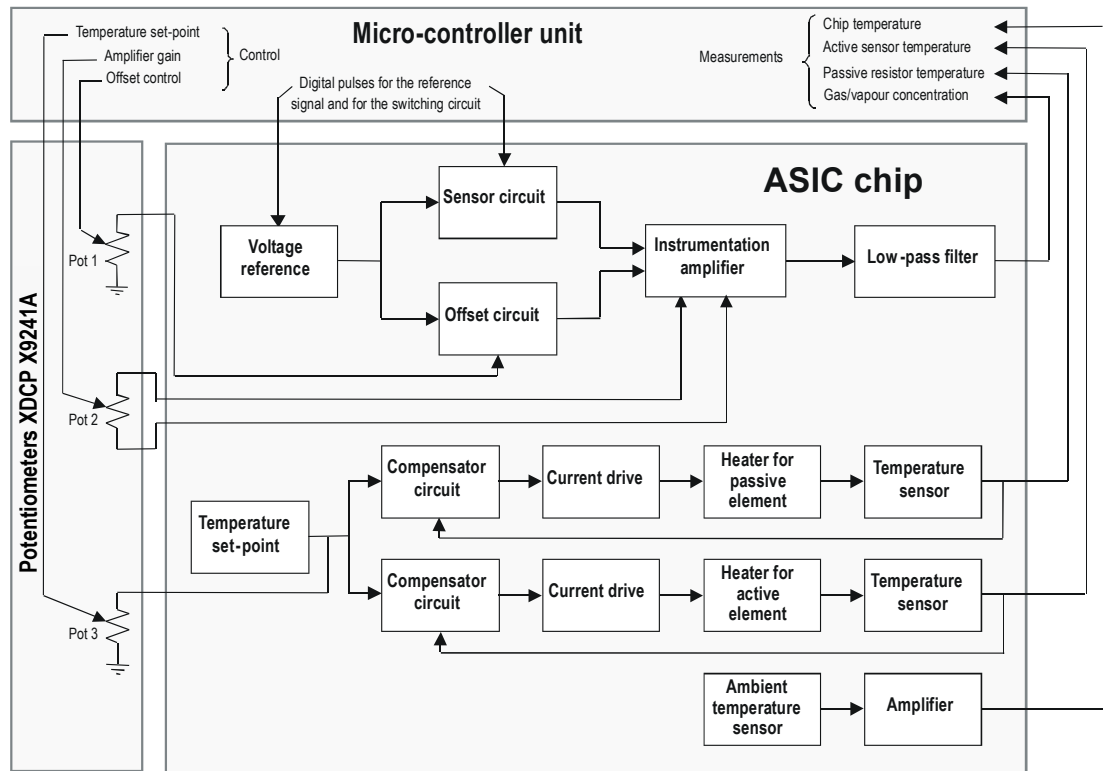


**Figure 3.1** Top representation of the proposed programmable instrument.

The ASIC chip includes therefore both a *gas sensor section* and a *temperature control section*, performing the main functions of the system, as it will be explained in this chapter.

The gas sensor section consists of the five blocks shown on the top part of the ASIC diagram. A *voltage reference* cell feeds a constant voltage to the *sensor circuit* and to the *offset circuit* as it was described in section 2.5. The differential output is amplified and then filtered in the two following blocks, before sending the final output to the controlling unit.

The temperature control section, shown on the lower half of the ASIC block diagram, contains two identical circuits that are intended to regulate the operating temperature of two gas sensors, by using a heater and a temperature sensor associated with each one of them.



A microcontroller unit is proposed for digital signal processing of the outputs obtained from the chip, as well as for the control of required inputs and feedback. Additionally, the set of digitally controlled potentiometers, included in a separate interface circuit, is to accomplish some control functions for the ASIC. The three digital potentiometers are shown in the corresponding block at the left side of Figure 3.1. The first one of them will be acting as the offset regulator described in section 2.5, within the ratiometric array with the gas sensors. A second one will be used to adjust the gain for the amplification of the signals and the third one is used to set the temperature on the heaters.

To complete the system, further interfacing circuitry and a power source are also required.

This chapter includes the description of the schematic views of every section and component of the designed ASIC chip.

### 3.3 SOFTWARE TOOLS AND TECHNOLOGY LIBRARIES

The process of design of the ASIC chip depends directly on the characteristics of the technology used for the actual fabrication of the devices. Availability of standard cells, limitations on the power supply, and special requirements for interconnection and operation of selected cells, defined several important aspects in the final structure of the overall circuit design.

Cadence™ IC software tools version 4.4.3 were used for the design. The schematic views were constructed using *Composer-Schematic* tool and the behaviour of the circuits was simulated using the *Analog Artist* tool with the *Spectre* simulator. The layout of the devices was designed using the *Virtuoso* tool.

Together with the Cadence software tools, the AMI Semiconductor (formerly Alcatel Microelectronics) 0.7  $\mu\text{m}$  CMOS analogue process was selected for the fabrication. This software-technology combination is supported under the *Europractice* scheme, through which the ASIC chip was produced.

A preliminary schematic design was obtained with the aid of *Composer-Schematic* and using only the generic analogue cells available in the Cadence libraries. This theoretical design also enabled the simulation, via the *Analog Artist* tools, of the responses of the circuit, although no practical considerations, such as the actual type or size of resistors, capacitors, and other components, could be included at this stage. Nevertheless, this preliminary work served as the foundation for the development of the final design of the ASIC, which is based in the use of the AMI Semiconductor CMOS process selected.

The schematic views of the circuit that are described in this chapter were obtained after adapting the original preliminary design to the particular specifications and characteristics of the AMI Semiconductor 0.7  $\mu\text{m}$  technology. Diagrams included here are the ones originally created with Cadence software for the final design.

A more detailed reference to the software and technology libraries used for the design can be found in appendices A and B.

### 3.4 THE GAS SENSOR SECTION

Figure 3.2 shows the *Composer* schematic view of the block diagram for the ASIC chip. The five blocks at the top represent the components of the gas sensor section whereas the other blocks correspond to the temperature control components. *Bias\_1* and *Bias\_2* are required standard cells providing the bias current for the operational amplifiers and they also supply the current for the excitation of the temperature sensors.

The gas sensor section is the circuit that includes the resistive polymeric sensors for the monitoring of VOC in a ratiometric configuration, as shown in Figure 2.9. As described in chapter 2, each sensor can be either exposed to vapours or it may remain passive by being coated with an inert material. When exposed to the presence

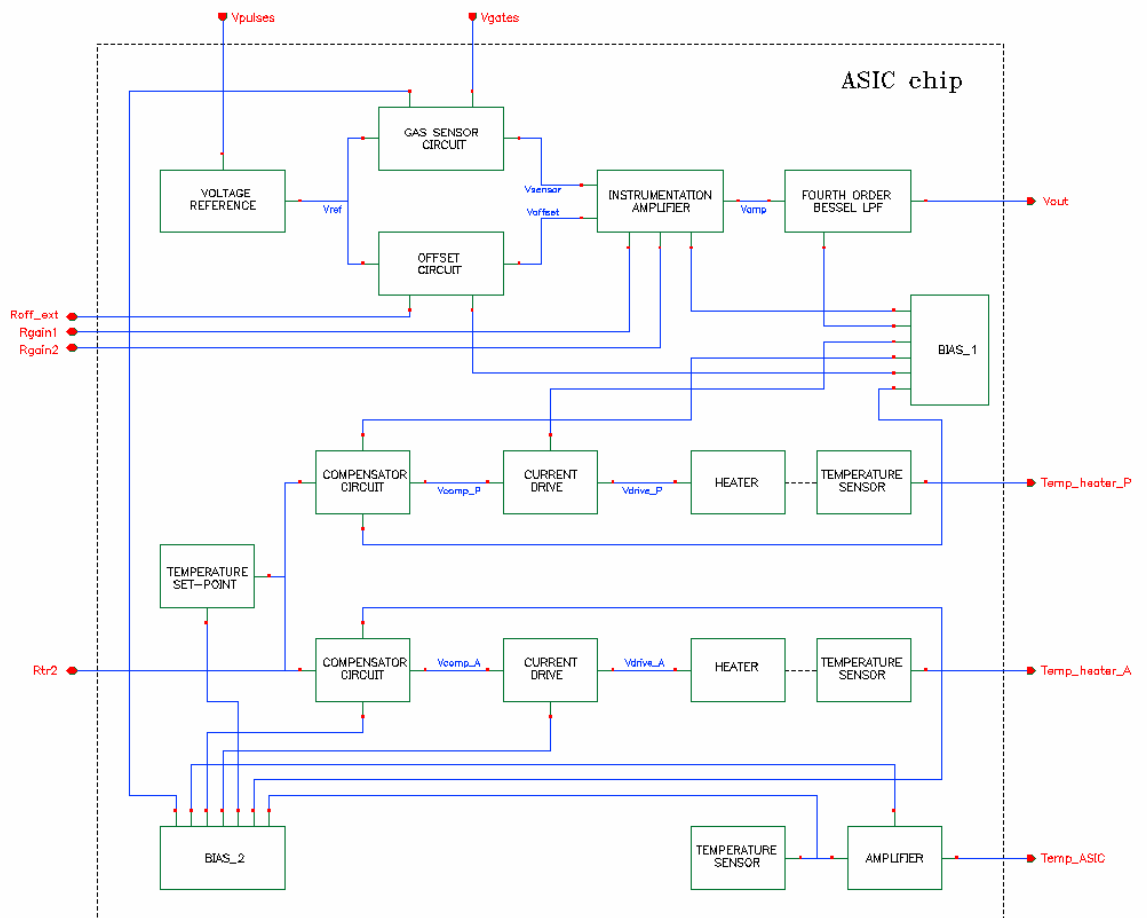


**Figure 3.2** Block diagram of the components inside the ASIC chip.

of VOC, the electrical resistance of the active polymer elements changes, giving an indication of the concentration of the VOC. Only the metal electrodes used for the gas sensors are fabricated through the AMI Semiconductor 0.7  $\mu\text{m}$  CMOS process. The gas microsensors are constructed by depositing a carbon black-polymer composite onto the electrodes, in a post-CMOS fabrication step that will be described in Chapter 7. Passive coating, as required, completes the fabrication of the passive chemoresistors.

The actual behaviour of these chemoresistors cannot be precisely predicted. It is known from previous research [1-5] that the polymer resistance will vary in the presence of VOC, but there are several factors which affect these variations, e.g. temperature, humidity, ageing and applied voltage. Even the actual resistance value of the devices is not easily controllable during the deposition process and significant differences appear between resistors fabricated through apparently identical steps.

Therefore, the structure of the gas sensor circuit was designed with the aim to overcome these problems. Firstly, a ratiometric array of polymer resistors is used in order to provide at least partial cancellation of variations that affect the resistance of both sensors. Secondly, the polymeric sensors are excited through the use of circuitry that also reduces effects such as the drift induced by a constant voltage source. Finally, smart circuitry is added for the self-cancellation of some unwanted effects such as the differences in the fabrication of the resistors as well as for the calibration of the device.

The gas sensor section, simplified in Figure 3.3, works as follows. A voltage reference signal is sent to the pair of non-inverting circuits described in section 2.5. The first one of these, shown at the top of Figure 3.3, is the *gas sensor circuit*, which

contains the resistive gas sensors. The second one is the *offset circuit*, used to calibrate the baseline for the comparison of the outputs, by adjusting a programmable resistor that is not included inside the ASIC chip; this is the external potentiometer *Pot 1* shown in Figure 3.1.

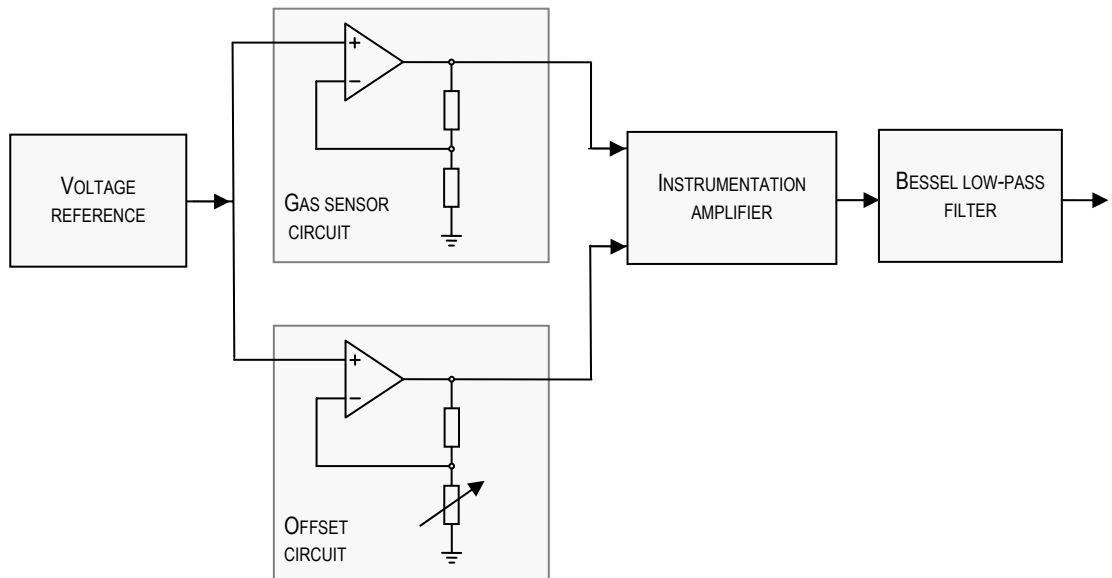


**Figure 3.3** Simplified schematic of the gas sensor section.

The outputs of both the gas sensor circuit and the offset circuit are connected to the inputs of an instrumentation amplifier in which any difference will cause an output related to the response of the gas sensors to the variations in the concentration of the VOC applied. The output signal is adjusted with the aid of the external potentiometer *Pot 2*, which sets the gain of the amplifier. Finally, high-frequency components are removed from the amplified signal via a fourth-order Bessel low-pass filter.

Every component of the gas sensor section is described below.



### 3.4.2 Ratiometric gas sensor circuit

The schematic of the ratiometric gas sensor circuit is shown in Figure 3.5. The polymeric resistors  $R_p$  and  $R_{po}$  are connected to an operational amplifier in a non-inverting configuration, following basically the same ratiometric configuration described in section 2.5. The main difference is that a set of FET-based switches was added in order to eliminate a common problem produced by the use of DC voltage sources.

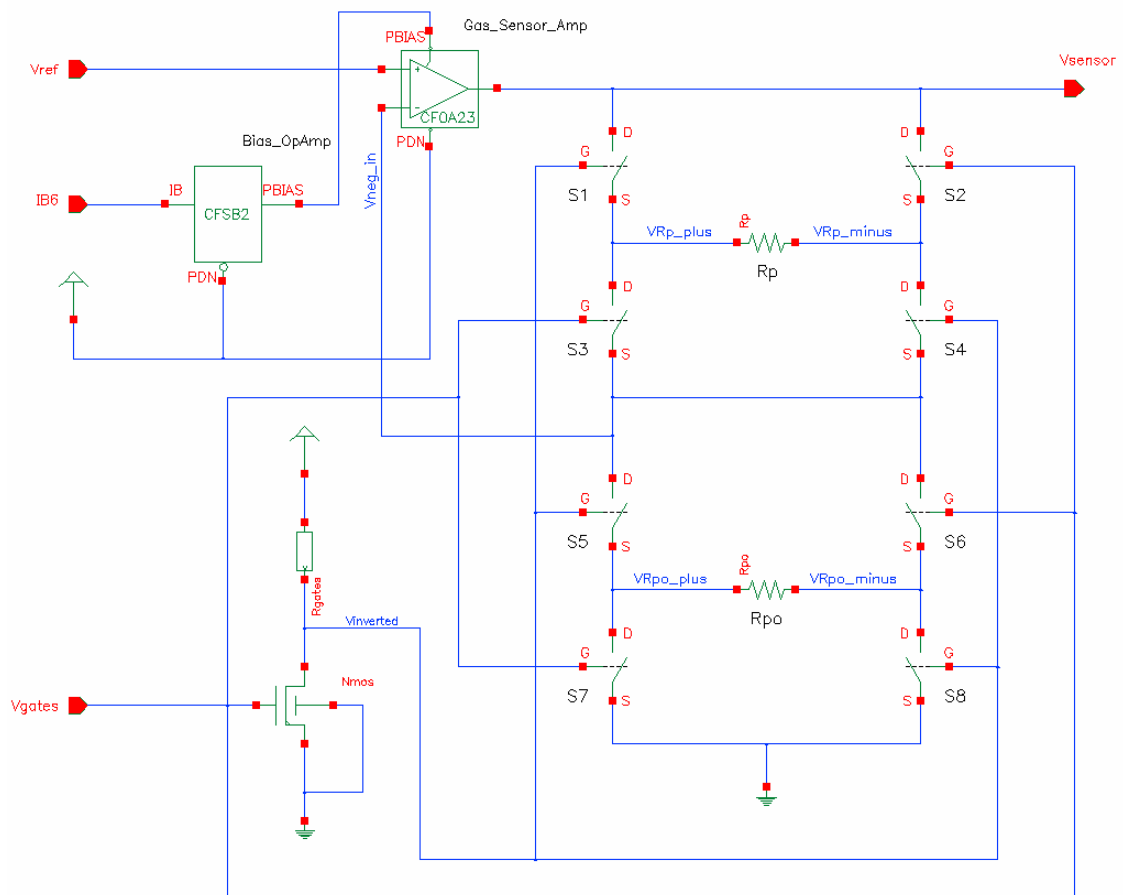


**Figure 3.5** Schematic view of the gas sensor circuit.

In effect, given that the use of constant voltage for prolonged periods induces drifting in the signals and polarises the sensing materials, the natural choice was to apply a square voltage to the sensors, alternatively changing signs between positive



and negative. This solution, however, was not possible due to the limitation of the AMI Semiconductors 0.7  $\mu\text{m}$  technology, which allows operation with only positive voltages between 0 and +5V.

The problem was solved with the FET-based switches  $S1$  to  $S8$ , controlled through pulses applied to the input  $V_{gates}$ , which invert alternatively the voltage at the terminals of  $R_p$  and  $R_{po}$ , providing compensation against any polarisation effect and drifting associated with a constant DC voltage.

The voltage  $V_{ref}$ , obtained from the voltage reference cell, is applied to the input, and the output voltage  $V_{sensor}$  is ideally given by the basic relationship:

$$V_{sensor} = \left(1 + \frac{R_p}{R_{po}}\right) V_{ref} \quad (3.1)$$

In ideal conditions, the two resistors should be identical and the output voltage should be the double of the voltage at the input. According to the ratiometric principle, any variation in the resistance of the active element that is also present in the passive resistor, e.g. temperature or ageing, will be cancelled from the output voltage. The circuit will respond only to variations that affect in different ways to both chemoresistors, like the changes in VOC concentration or the humidity effect.

However, considering the characteristics of the polymeric resistors and the FET switches, that ideal behaviour of the circuit is not easy to obtain under practical conditions due to the following factors:

- It is very difficult to obtain identical polymeric resistors during the fabrication process.

- The values of the resistance obtained when depositing the polymers cannot easily be controlled.
- The forward resistance of individual FETs has a relatively high value when compared to the expected resistance of the polymer resistors.
- The voltage scope from 0 to +5 V that is allowed by the AMI Semiconductor 0.7  $\mu\text{m}$  technology is not wide enough to permit an easy operation of the FET switches, because their on-resistance can be as high as 10% of the polymer sensors resistance, leading easily to unwanted saturation problems.
- The combination of the pulses applied to the gates of the FETs together with the pulsed voltage reference originates some spikes at the switching edges, as it was shown by the simulations reported in Chapter 4.

Consequently, special considerations are made for the design, considering the fabrication process and the post-processing steps. First of all, it is required to control the process of polymer deposition, monitoring the actual value of the resistance in order to make it as close to 10 k $\Omega$  as possible, which was found to be the optimal value compared to the forward resistance of the FETs, according to the simulations described in the next chapter. In addition, parallel arrays of FETs (Figure 3.6) are used to override the problems originated by the high forward resistance value of individual FETs, which causes an important voltage drop when compared with the relatively low voltage of the supply. Finally, the period, width and delay of the digital pulses applied to the gates are adjusted to values (200 ms, 100 ms and 50 ms, respectively) that help to minimise the glitch at the switching edges by avoiding interaction with the pulses applied to the voltage reference cell.

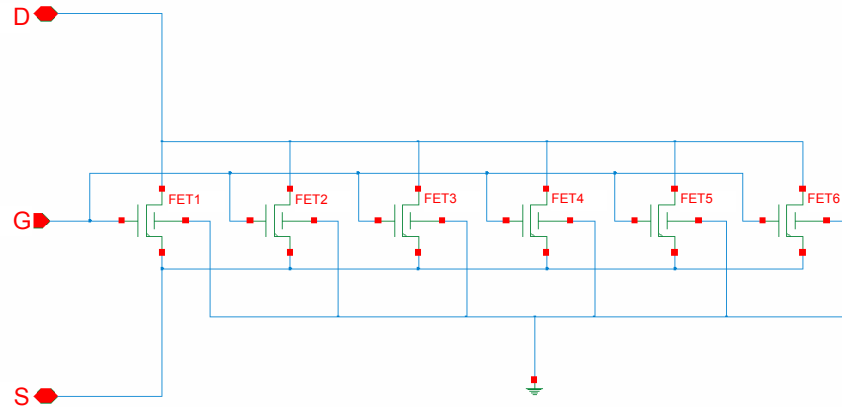


**Figure 3.6** Parallel array of FETs for each switch in the gas sensor circuit.

Each switch from  $S1$  to  $S8$  in the circuit of Figure 3.5 is an instance of the cell shown in Figure 3.6. This cell consists of six NMOSFETs in a parallel array in order to reduce the equivalent resistance that otherwise would significantly affect the performance of the circuit when added in series to the resistance of the polymer sensors. As explained above, the function of the switches is to invert alternatively the voltage applied to the terminals of the resistors  $R_p$  and  $R_{po}$  avoiding in this way the drifting and polarisation problems associated with the use of a constant voltage source in some types of polymers. To make the switches alternate between the *on* and *off* states, the pulsed voltage  $V_{gates}$  is directly applied to the gate of a basic FET inverter and to the gates of the switches  $S2$ ,  $S3$ ,  $S6$  and  $S7$ . The inverted signal, taken from the output of the FET inverter, is applied to the remaining switches  $S1$ ,  $S4$ ,  $S5$  and  $S8$ .

### 3.4.3 Offset circuit

The offset circuit, represented in Figure 3.7, has the same non-inverting configuration as the gas sensor circuit. The operational amplifier and one of the resistors are included inside the chip, whereas the second resistor is the external programmable potentiometer *Pot 1* shown in Figure 3.1.

The same 1.2V reference voltage  $V_{ref}$  applied to the gas sensor circuit is applied to the offset circuit. By taking the output of the gas sensor circuit under non-exposing conditions as a reference, the output of the offset circuit is digitally adjusted through the external potentiometer connected to the pin  $R_{off\_ext}$ , so that the ratio of resistances in the offset circuit equals to that of the gas sensor circuit. Once the circuit is calibrated, the offset signal is fixed, compensating the differences in the resistances of the polymer sensors and setting a baseline, leaving the circuit ready for further tests.

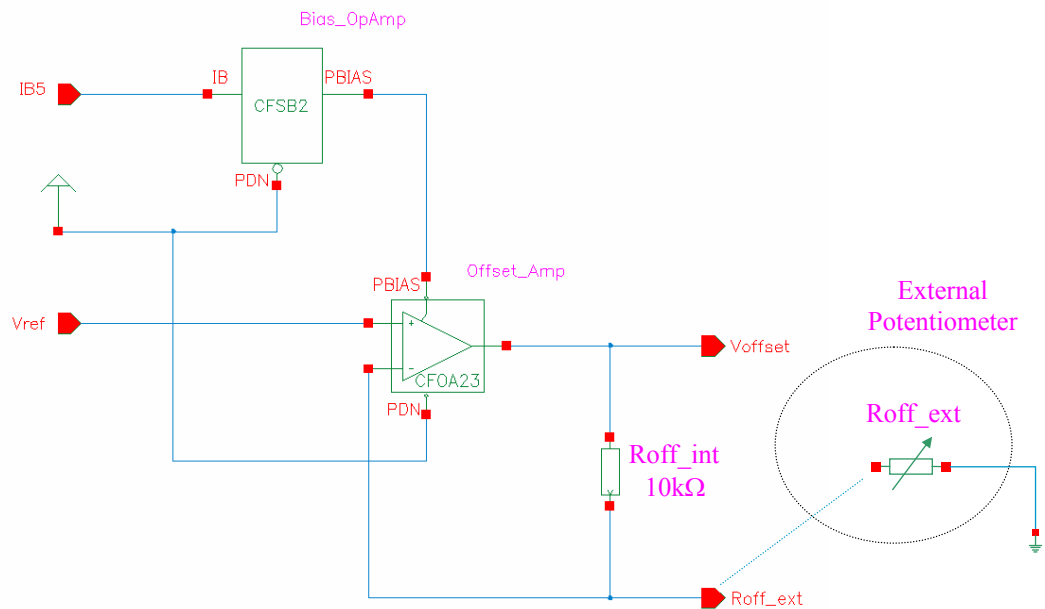


**Figure 3.7** Offset circuit to be completed with an external resistor.

### 3.4.4 Instrumentation amplifier

Both the gas sensor circuit and the offset circuit outputs are fed to the inputs of the next stage, where any difference between the signals is amplified. Figure 3.8 shows the schematic view of the instrumentation amplifier whose gain is adjustable through the external potentiometer *Pot 2* (Figure 3.1) connected between the terminals  $R_{gain1}$  and  $R_{gain2}$ .

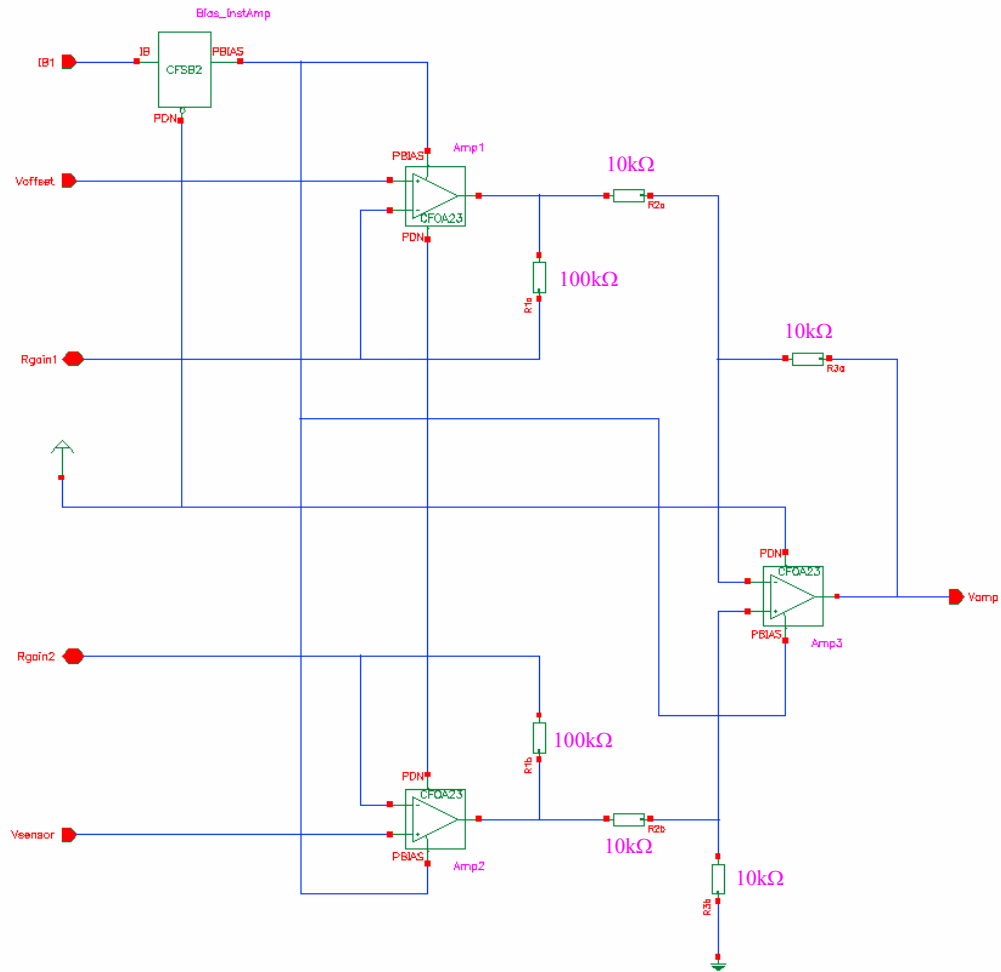


**Figure 3.8** Schematic view of the instrumentation amplifier.

The resistance values selected for the differential amplifier stage were 100 k $\Omega$  for the feedback resistors and 10 k $\Omega$  for the forward paths. These values were successfully tested during the simulations and are used in the final design.

The amplifier gain  $G$  is given [8] by:

$$G = 1 + \frac{2R_1}{R_{gain}} \quad (3.2)$$

where  $R_{gain}$  is the resistance of the potentiometer *Pot 2* and  $R_1$  is 100 k $\Omega$ . Varying  $R_{gain}$  between 0 and 50 k $\Omega$ , the gain of the amplifier can in theory be adjusted to any value starting from 5 and above. However, variations in the actual values of the components in the fabricated devices can slightly modify this minimum value.

The AMI Semiconductor cell CFSB2 is used in this and every circuit that includes operational amplifiers in order to provide the required bias voltage. However, only one of these cells was necessary for the instrumentation amplifier, as the row distribution in the layout (to be described in Chapter 5) allowed placing the three operational amplifiers close to each other, saving space and reducing the cost of the fabricated chip.

### 3.4.5 Bessel low-pass filter

A low-pass filter (LPF) is required in order to eliminate any high frequency noise in the output of the amplifier. In particular, given that the circuit can be driven by pulsed signals, it is important to consider the differences in time delay between the frequency components of the raising and falling edges, which produce effects such as overshoot when conventional Butterworth filters are used [9].

For this reason, a Bessel filter was included in the design, given that it has the maximally flat delay characteristic [10]. It results the most suitable type of filter for pulsed signals, although its attenuation is rather poor near the cut-off frequency when compared to Butterworth or Chebyshev filters. The response of a Bessel filter to step or pulses is free from overshoot.

The circuit in Figure 3.9 is a Bessel LPF with cut-off frequency  $f_c = 10\text{kHz}$ . The final design was obtained after considering several choices [9-11], such as conventional Butterworth filters and low order circuits, and after trying a number of changes in order to select the proper sizes for resistors and capacitors when using the cells available within the AMI Semiconductor libraries. The response of the circuit was also tested with the aid of software by *Texas Instruments* [12]. A fourth order

filter was chosen because of the poor attenuation slope near the cut-off frequency typical of the Bessel characteristic.

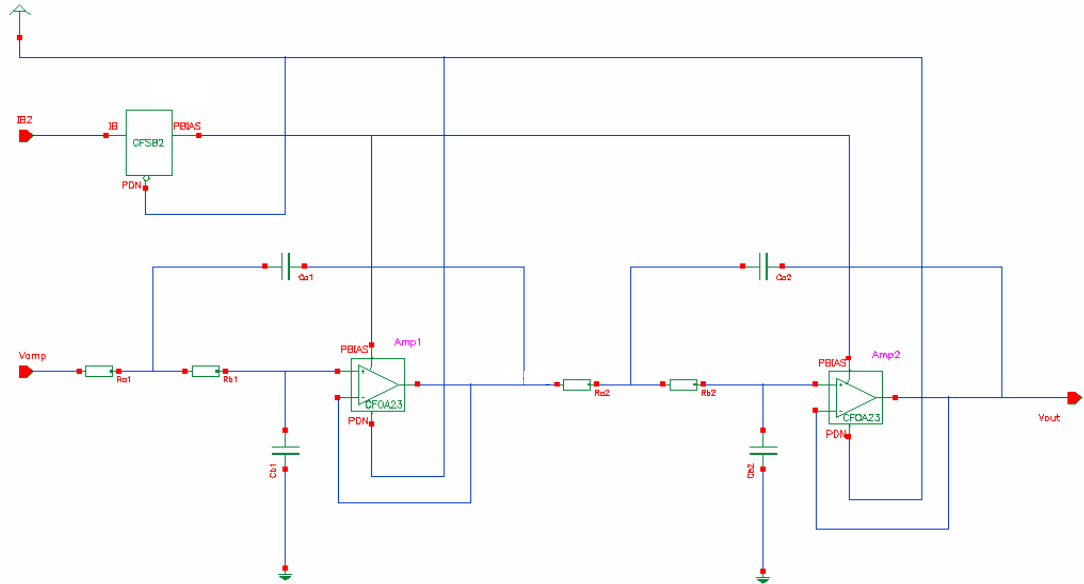


**Figure 3.9** Fourth-order Bessel low-pass filter.

After simulations of the frequency response (refer to Figure 4.7 in section 4.3.4) and several considerations about the actual size of resistors and capacitors, the set of values shown in Table 3.1 was obtained for the components of the filter.

**Table 3.1** Resistances and capacitances used for the Bessel low-pass filter.

| Component | Capacitance (pF) | Component | Resistance ( $\Omega$ ) |
|-----------|------------------|-----------|-------------------------|
| Ca1       | 20.0pF           | Ra1       | 402 K                   |
| Cb1       | 14.7pF           | Rb1       | 1.05 M                  |
| Ca2       | 20.0pF           | Ra2       | 687 K                   |
| Cb2       | 7.5pF            | Rb2       | 956 K                   |

### 3.5 TEMPERATURE CONTROL CIRCUITRY

The second major task to be performed by the ASIC chip is the control of temperature for the operation of the polymer sensors, which are designed to operate at a constant temperature above ambient. To this aim, a heater is placed underneath the electrodes of each polymer resistor, with temperature sensors used in a control loop.

The circuit for the control of temperature has particular importance within the design of this ASIC chip. Previous research work [1-2, 5] has reported how temperature affects the response of gas sensors and on-chip compensation of temperature variations is considered to be an important feature on the development of hand-held instruments.

The availability of circuitry for temperature control adds versatility to the chip, because it makes it capable to compensate for ambient temperature, which affects the chemical reactions in polymer-based chemoresistors [13]. Common-mode effects are inherently removed by the ratiometric configuration when the two chemoresistors are fabricated with the same material.

However, there is the possibility for the use of the chip with combinations of different sensing materials, as will be shown in Chapter 7. In this case, temperature dependence will be different for each sensor and variations can strongly affect the response of the ASIC chip. It will be useful, hence, to have the possibility for operation at a controlled temperature.

Also, given that the ASIC chip is theoretically suitable for the use of any type of chemoresistive nanomaterials, having the choice of a temperature control within the chip expands the possibilities for the operation at different temperatures.



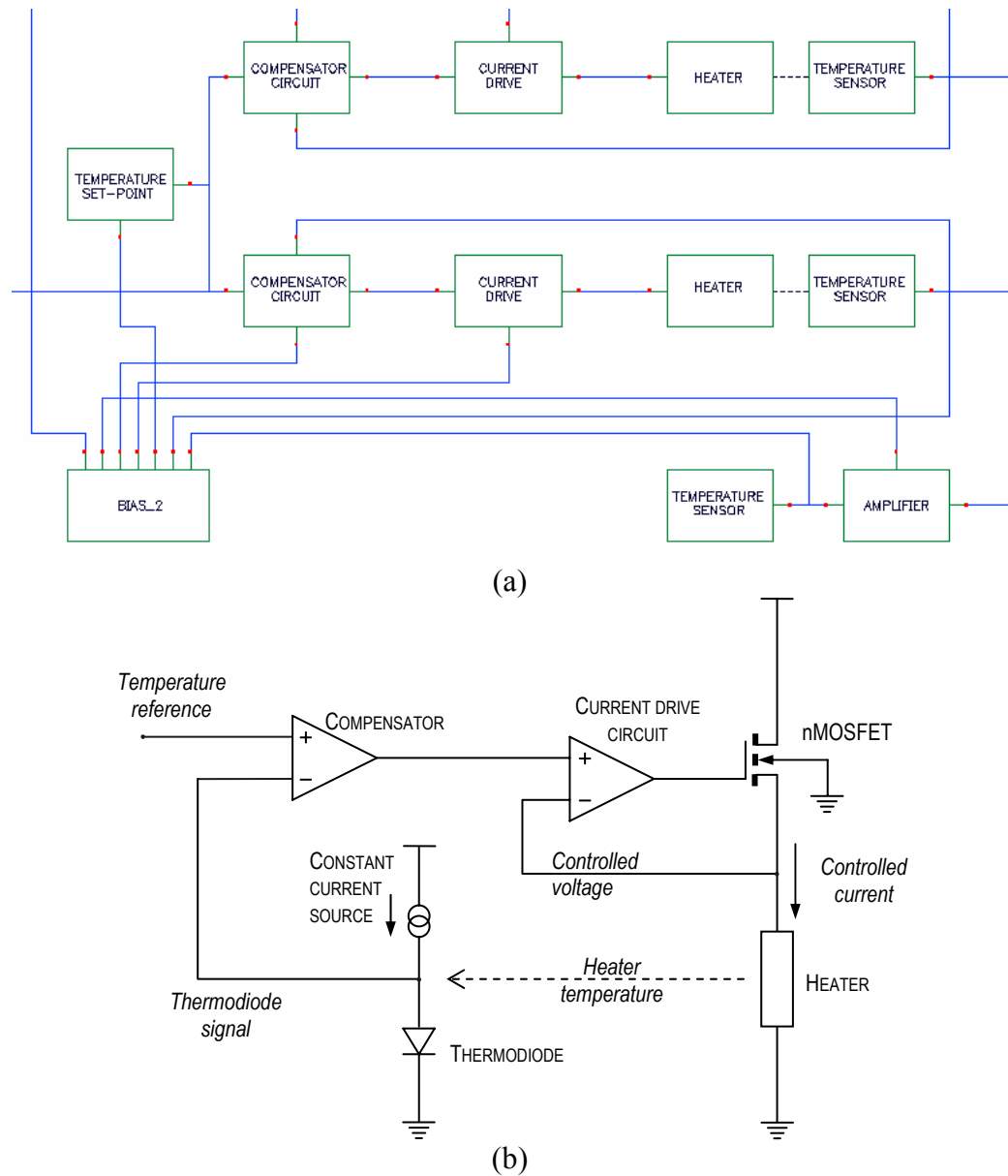


**Figure 3.10** (a) Block diagram of the temperature control section; (b) simplified schematic circuit.

A block diagram of the temperature control system is shown in Figure 3.10(a), and a simplified schematic circuit is given in Figure 3.10(b). The temperature of the heaters, which is the function to be controlled, is measured through temperature sensors. With the aid of the external potentiometer *Pot 3* (Figure 3.1), the *temperature set-point* block provides a reference signal that is fed to the *compensator circuits* controlling the signals required by the heaters. This reference signal is compared with the feedback signals obtained from the outputs of the

*temperature sensor* blocks. In each compensator block, a differential amplifier produces a compensation signal proportional to the difference of temperatures between the respective heater and the set-point. The compensation signal is sent to the circuit that drives the current for the heater.

An additional temperature sensor, whose output is amplified, is included for the monitoring of the operating temperature of the chip. The outputs of the temperature sensors are made externally available for further processing.

Each of the components of the temperature control system is briefly described in the following sections.

### 3.5.1 The temperature sensors

As mentioned above, the temperature of the polymer resistors is controlled by the action of the heaters and the feedback signal is obtained through temperature sensors placed near the heaters and sensor pads.

A forward-biased diode is used as the temperature-sensing element. The reference current obtained from one of the outputs of the *Bias* cells is passed across the diode and the voltage is measured as an indication of the temperature. In the diagram of Figure 3.11, the constant reference current flows through the terminal  $V_{ts}$  towards the diode, and the output voltage at the same terminal corresponds to the measured temperature. The output of each thermodiode is connected to one of the inputs of the differential amplifier in the compensator circuit of the next stage.

The thermodiodes used in the ASIC were specifically designed for this project, as it will be described in Chapter 5. However, schematic design and simulations were performed using the standard cells and data that were available

before fabricating the ASIC. Characterisation of the fabricated diodes, as it is reported in Chapter 6, showed that the actual thermosensors have a linear response to temperature with an average slope of  $-2.36 \text{ mV}/^\circ\text{C}$ .

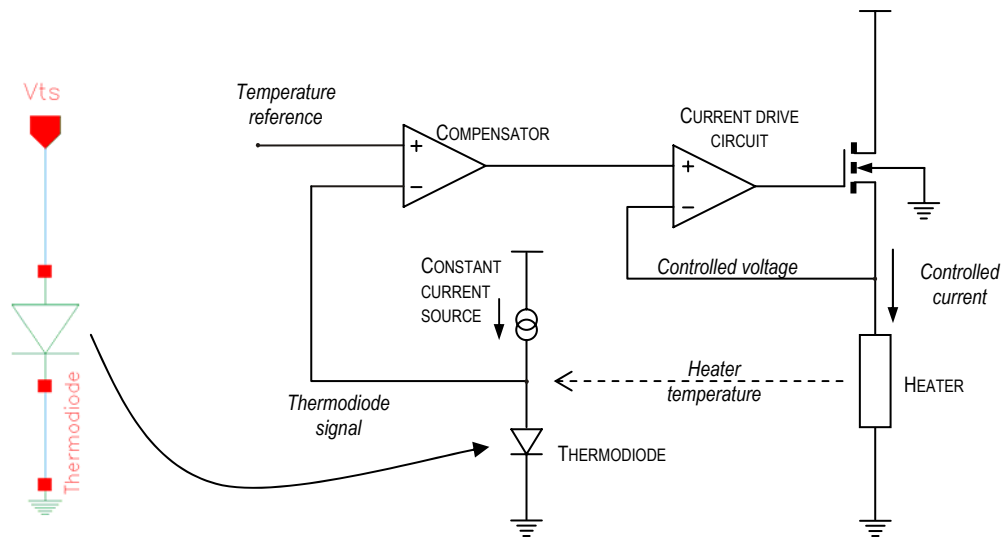


**Figure 3.11** Temperature sensor and temperature control circuit.

### 3.5.2 The temperature set-point circuit

A voltage signal is used as a reference for the temperature set-point. In the circuit, shown in Figure 3.12, the output voltage of the bandgap cell, transmitted by a voltage follower, is applied to a voltage divider in which the second resistor is the external potentiometer *Pot 3* (Figure 3.1) that is connected between the output pin and ground, although it is not shown in this diagram. By digitally adjusting the resistance of this potentiometer, the output of the circuit can be set to the proper size.

The output voltage  $V_{sp}$  is applied as a reference to the input of the two identical circuits that control the operating temperature of the polymer resistors.

The internal resistor, shown in Figure 3.12, is fixed in the design to a value of  $R_{rl} = 10 \text{ K}\Omega$ . The scope limits for the external potentiometer were estimated by assuming that the thermodiodes will operate in the range of 330 to 605 mV for

temperatures between 10°C to 120°C. The approximated values of the resistance required for the potentiometer are obtained from the voltage divider equations, as follows:

$$R_{r2}(10^{\circ}\text{C}) = \frac{0.605R_{r1}}{1.209 - 0.605} = \frac{0.605(10\text{K}\Omega)}{0.604} = 10.02\text{K}\Omega \quad (3.3)$$

$$R_{r2}(120^{\circ}\text{C}) = \frac{0.330R_{r1}}{1.209 - 0.330} = \frac{0.330(10\text{K}\Omega)}{0.879} = 3.75\text{K}\Omega \quad (3.4)$$

Hence, a potentiometer which can vary resistance in this range is enough for the control of the temperature set-point in the range between 10°C to 120°C.

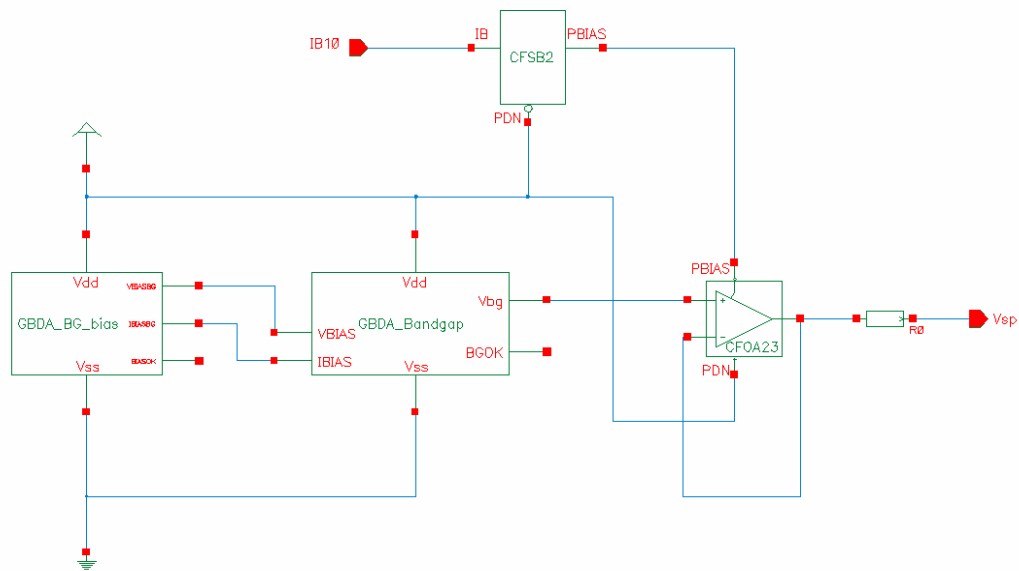


**Figure 3.12** Temperature set-point circuit.

### 3.5.3 The compensator amplifier

A proportional differential amplifier is used to compensate the error between the set-point temperature and the signal of each temperature sensor. Although stability and overshoot problems could arise, the amplifier is designed for a low gain so its response is fast and stable enough, making unnecessary to add derivative or even integral components to the circuit.

The schematic view of the compensator circuit is shown in Figure 3.13. The voltage followers at the inputs take the voltage signals from the set-point and temperature sensor outputs and the difference appears amplified at the output terminal  $V_{comp}$ .

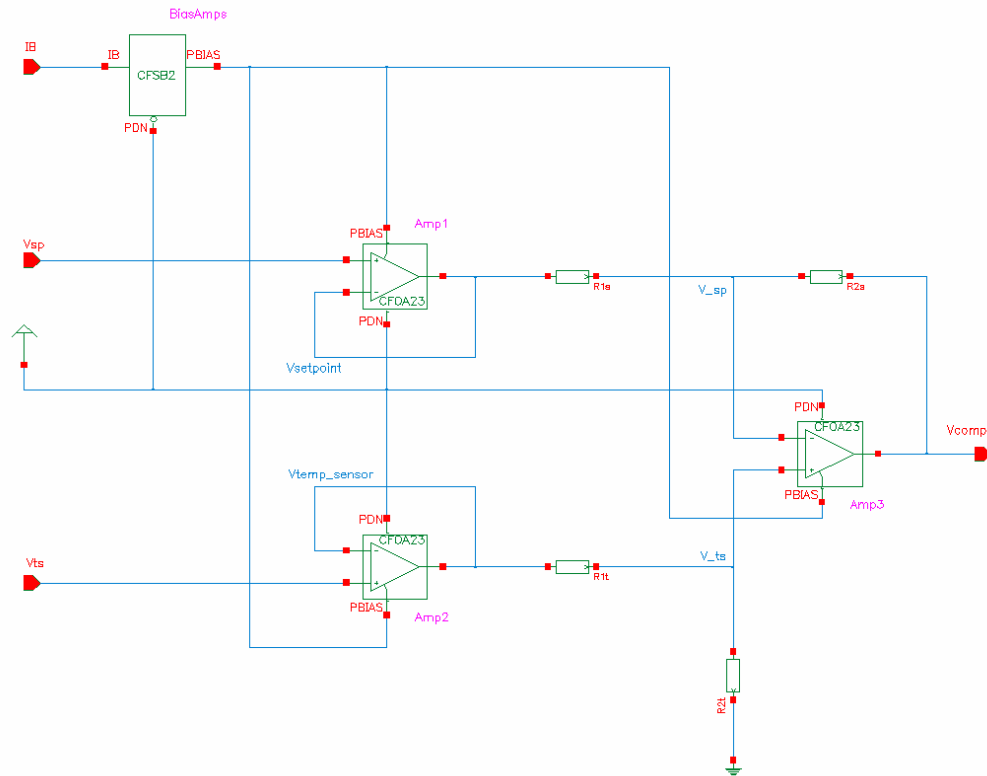


**Figure 3.13** Schematic view of the temperature compensator circuit.

The gain of the amplifier was determined considering that the maximum temperature at which the chip could operate would be 100°C. Given that no previous data were available about the configuration of the heater and electrodes used in this design, it was only estimated, based on reports on similar heaters [14], that a power of 80 mW was required for operation at 100°C.

The heater is designed for a resistance of 50  $\Omega$ . For operation at 80 mW, the required voltage at the heater is 2 V, which corresponds to 40 mA in the intensity of the required current.

The compensator amplifier must have a sufficient gain to raise the temperature from 20°C to 100°C. Considering the expected behaviour of the thermodiode, and according to simulations reported in the next chapter, the voltage of the diode should fall from around 580 mV to 380 mV. Therefore, the expected gain for the amplifier is given by:

$$\text{Differential gain} = \frac{V_{comp}}{V_{20} - V_{100}} = \frac{2.0V}{580mV - 380mV} = 10 \quad (3.5)$$

By choosing  $R_{sp1} = R_{ts1} = R_1 = 1 \text{ k}\Omega$  and  $R_{sp2} = R_{ts2} = R_2 = 10 \text{ k}\Omega$ , i.e.  $R_2 = 10R_1$ , the amplifier gain is set to 10, which will produce the proper compensating signal.

The differential input, which actually compares the temperature of the heater with the reference set-point, produces a compensating amplified signal that is sent to the circuit driving the current for the heater.

### 3.5.4 Current drive circuit

Figure 3.14 shows the current drive circuit. The current is applied to the heater through a low-resistance FET, which actually consists of a parallel array of four standard FET cells. The use of parallel FETs allows the flow of larger currents to the heater and reduces the equivalent forward resistance, which can be too large when compared to the heater resistance.

An operational amplifier drives the gates and the output signal  $V_{comp}$  of the previous circuit is passed directly to the heater that must be connected to the terminal  $I_{heater}$ . The capacitor and resistors included form a compensation network that ensures stability to drive the inputs of the FETs, which may be highly capacitive. The circuit

was adapted from an application bulletin by *Burr-Brown* [15] and it was recalculated in order to keep the same time constants when adjusting the size of the capacitor and resistors to the desired layout dimensions.

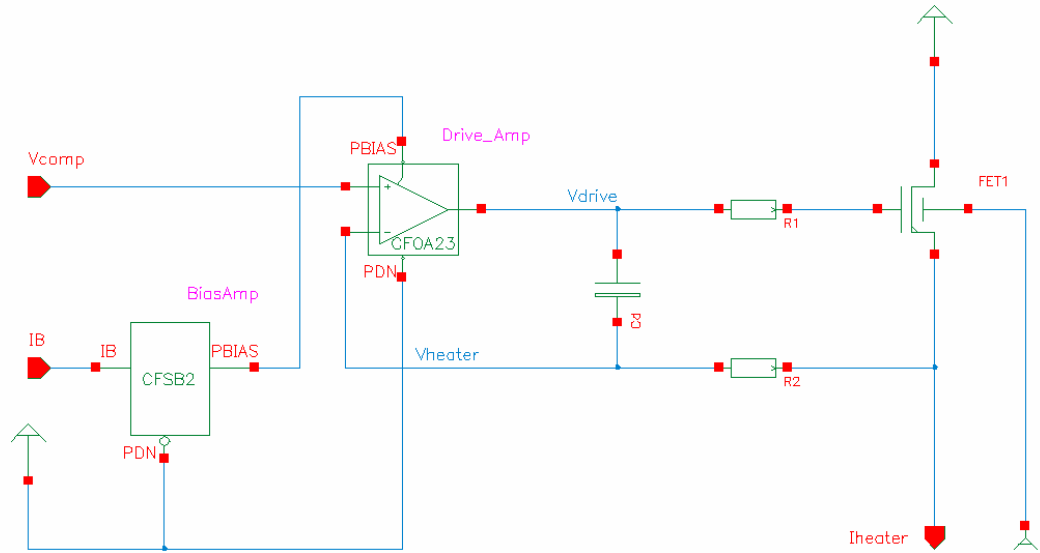


**Figure 3.14** Schematic view of the current drive circuit.

The final specifications of the components are as follows:

$$C_d = 7.5 \text{ pF}, R_1 = 13.3 \text{ k}\Omega, R_2 = 66.67 \text{ k}\Omega.$$

### 3.5.5 The resistive heaters

The resistive heaters, constructed in the *metall* layer of the ASIC, are placed under the electrodes of the polymer resistors in order to produce the required temperature for the operation of the sensors. The resistance of each heater is approximately  $50 \Omega$ .

From the schematic point of view, the heater is represented only as a  $50 \Omega$  resistor, connected to the output of the current drive circuit. From the terminal  $I_{\text{heater}}$ , current flows through the heater and power is dissipated to keep the sensor at the required temperature.

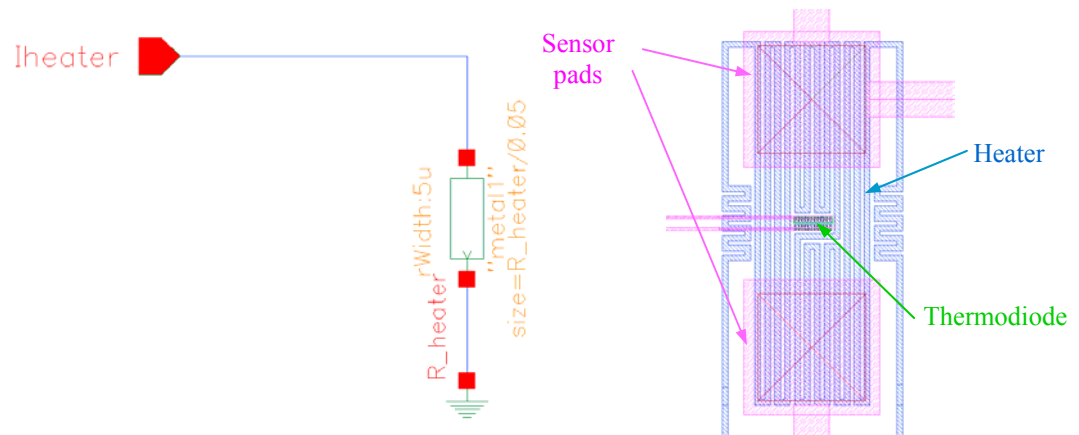


**Figure 3.15** Schematic and layout view of the resistive heater.

Figure 3.15 shows the schematic and layout views of the heater. The resistive track is designed to be placed underneath the sensor electrodes, with the thermodiode in the middle of the gap. Further details of the layout design and characteristics of the fabricated heaters are included in chapters 5 and 6.



### 3.6 ADDITIONAL CIRCUITRY

#### 3.6.1 The ambient temperature sensor

An extra temperature sensor is included in the design to measure the temperature of the ASIC chip. Whereas the other two thermodiodes are placed at the corners of the chips, under the electrode pairs, this third diode is placed near the centre of the chip. This sensor has the same configuration shown in Figure 3.11 and described in section 3.4.1, with the output connected to a non-inverting amplifier. The output of the amplifier, whose schematic is shown in Figure 3.16, is made externally available for additional processing.

Gain of the amplifier is set to 7 by using  $R_1 = 1 \text{ k}\Omega$  and  $R_2 = 6 \text{ k}\Omega$ .

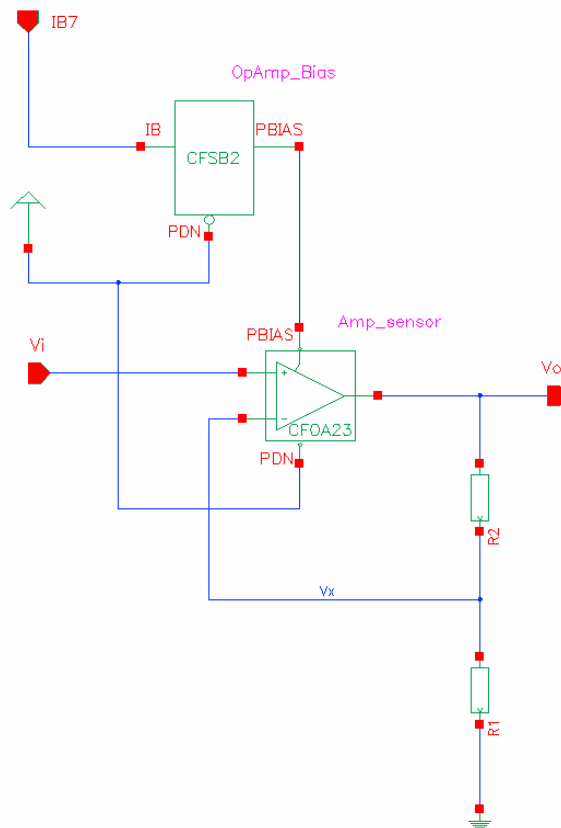


**Figure 3.16** Non-inverting amplifier for the ambient temperature sensor.

### 3.6.2 The bias cells

According to the AMI Semiconductor bias strategy (See section 5.3.1.2), it is required to include bias cells that will provide the negative current required by every operational amplifier. These bias currents are converted to voltages in the slave cells CFSB2 connected to each operational amplifier in the previously described circuits.

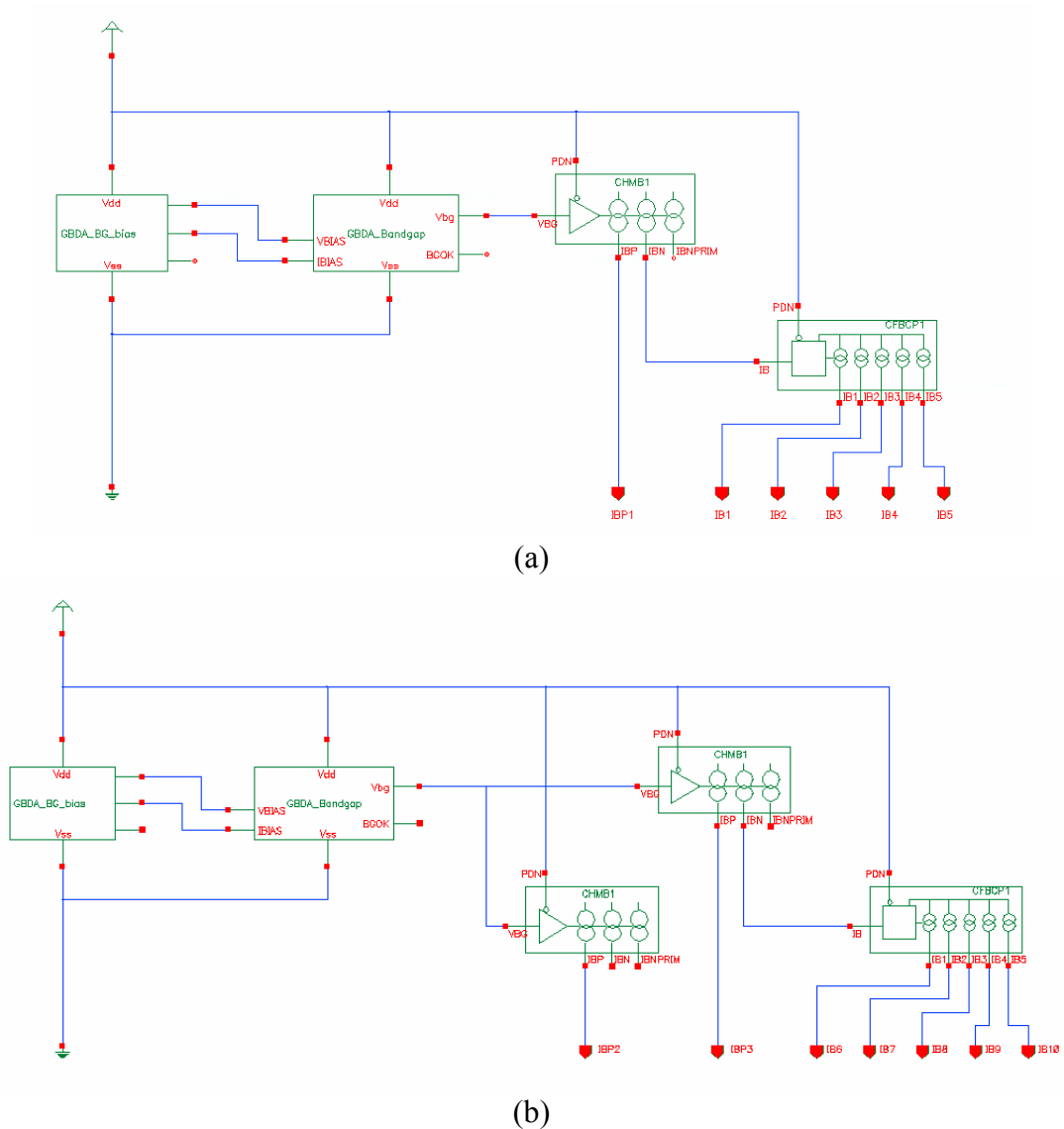


**Figure 3.17** Schematic views of cells: (a) *BIAS1*, (b) *BIAS2*.

Given that the master bias cell CHMB1 has outputs for both negative and positive currents, it is also used to provide the reference current required by the temperature sensors.

The schematic views of the two bias cells that are included in the design are depicted in Figure 3.16 and the assignation of the outputs is shown in Table 3.2.

Table 3.2 Assignation of the pins for the bias cells.

|      | <b>Assignment</b>   |
|------|---|
| IB1  | Instrumentation amplifier   |
| IB2  | Low-pass filter   |
| IB3  | Current drive circuit for the heater of the passive <sup>1</sup> polymer resistor |
| IB4  | Comparator circuit for the heater of the passive polymer resistor                 |
| IB5  | Offset circuit  |
| IB6  | Amplifier of the gas sensor circuit   |
| IB7  | Amplifier for the diode sensing the operating temperature of the ASIC chip        |
| IB8  | Comparator circuit for the heater of the active polymer resistor                  |
| IB9  | Current drive circuit for the heater of the active polymer resistor               |
| IB10 | Temperature set-point circuit.  |
| IBP1 | Diode sensing the operating temperature of the ASIC chip                          |
| IBP2 | Diode sensing the temperature of the heater for the active polymer resistor       |
| IBP3 | Diode sensing the temperature of the heater for the passive polymer resistor      |

<sup>1</sup> The names 'active' and 'passive' are used here only as a reference to distinguish between the two sets of electrodes and the corresponding polymeric resistors. These names are adequate for the case when one active and one passive sensor are used. As explained in Chapter 7, both sensors may be simultaneously active.

### 3.7 CONCLUSIONS

The schematic views of the ratiometric ASIC chip have been described in this chapter. Cadence *Composer* tool was used for the design and the technology adopted was the AMI Semiconductor 0.7  $\mu\text{m}$  analogue CMOS standard process. Whenever available, the components of the circuit were represented using the parameter models of the actual cells included in the layout sent to fabrication. However, custom-designed components such as the heater and thermodiodes, were represented with generic models available in the software at the design stage.

The structure and functioning of the ASIC chip was described step by step from the block level to the components level.

In the gas sensor section a voltage reference is applied to a pair non-inverting amplifiers. One of these circuits contains the gas sensing resistive elements, whilst the other circuit provides a programmable offset signal. The outputs of both the sensor circuit and the offset circuit are connected to the differential input of an instrumentation amplifier, and the output signal is finally obtained after a low-pass filter stage.

The temperature control circuit uses a current-driven resistive heater that is regulated by a proportional feedback signal obtained through a p-n thermodiode. A programmable set-point circuit provides the reference signal which is compared with the temperature feedback through a voltage compensator connected to the current drive circuit.

The performance of each component of the circuit was modelled and simulated as described in the next chapter.

### 3.8 REFERENCES

1. Cole, M., Gardner, J.W., Covington, J.A., Fife, D., Kwok, C.Y., Brignell, J.E. and Bartlett, P.N. (2000). "Active bridge polymeric resistive device for vapour sensing", *Euroensors XIV.*, Copenhagen, Denmark, 895-898.
2. Gardner, J.W., Vidic, M., Ingleby, P., Pike, A.C., Brignell, J.E., Scivier, P. Bartlett, P.N., Duke, A.J., Elliot, J.M. (1998). "Response of a poly(pyrrole) resistive micro-bridge to ethanol vapour", *Sensors and Actuators B*, 48, 289-295.
3. Bruschi, P., Nannini, A. and Neri, B. (1995). "Vapour and gas sensing by noise measurements on polymeric balanced bridge microstructures", *Sensors and actuators B*, **24-25**, 429-432.
4. Hatfield, J. V., Neaves, P., Hicks, P. J., Persaud, K. and Travers, P. (1994). "Towards an integrated electronic nose using conducting polymer sensors", *Sensors and Actuators B*, 18-19, 221-228.
5. Cole, M., Gardner, J.W., Lim, A.W.Y., Scivier, P.K. and Brignell, J.E. (1999). "Polymeric resistive bridge gas sensor array driven by a standard cell CMOS current drive chip", *Sensors and Actuators B*, 58, 518-525.
6. Brokaw, P. (1974). "A simple three-terminal IC bandgap reference", *IEEE Journal of Solid-State Circuits*, **9**, 388-393.
7. Banba, H., Shiga, H., Umezawa, A., Miyaba, T., Tanzawa, T., Atsumi, S., and Sakui, K. (1999). "A CMOS bandgap reference circuit with sub-1-V operation", *IEEE Journal of Solid-State Circuits*, **34**, 670-674.
8. Floyd, T.L. and Buchla, D. (1999). *Fundamentals of analog circuits*, Prentice-Hall, Inc., Upper Saddle River, New Jersey.
9. Horowitz, P. and Hill, W. (1989). *The art of electronics*, 2nd ed., Cambridge University Press. New York, USA.
10. Williams, A.B. (1975). *Active filter design*, Artech House, Inc. Massachusetts, USA.
11. Collins, T.H. (1989). *Analog electronics handbook*, Prentice Hall International (UK) Ltd. London, UK.

12. TEXAS Instruments (2003). "FilterPro™ MFB and Sallen-Key design program", Software available at <http://www.ti.com/>.
13. Gardner, J.W., Cole, M. and Udrea, F. (2002). "CMOS gas sensors and smart devices", *Proceedings of the First IEEE International Conference on Sensors*, Orlando, Florida, USA, **1**, 721-726.
14. Cardinalli, G.C., Dori, L., Fiorini, M., Sayago, I., Faglia, G., Perego, C., Sberveglieri, G., Liberali, V., Maloberti, F. and Tonietto, D. (1997). "A smart sensor system for carbon monoxide detection", *Analog integrated circuits and signal processing*, **14**, No. 3, 275-296.
15. Stitt, R.M. (1990). "Implementation and applications of current sources and current receivers", *Burr-Brown Application Bulletin*, Tucson AZ, USA.

# RATIOMETRIC ASIC CHIP MODELLING AND SIMULATION

## 4.1 INTRODUCTION

This chapter reports on the modelling and simulations that supported the design process of the ratiometric ASIC chip and helped to adapt it to the actual conditions of fabrication. Firstly, a model of the CMOS gas sensor section is presented, showing the response of each cell in the circuit, as it was obtained from simulations made with the final design. Secondly, simulations for the temperature control circuit are also given, showing the expected performance of the thermosensors, heater and other circuit cells.

Lastly, a comprehensive polymer gas sensor *Cadence*<sup>™</sup> model has been developed for this project, and is used to simulate the smart sensor response with respect to gas concentration, at different values of temperature and humidity.

## 4.2 SIMULATION TOOLS AND ENVIRONMENT

Most of the simulations were performed using the *Analog Artist* tool of Cadence™ IC software, version 4.4.3, running on a UNIX workstation Sun Microsystems Ultra 10. The *Spectre* simulator, available under the *Analog Artist* tool, was used for this work. Whenever obtainable, parameter models of the actual cells included in the AMI Semiconductor libraries were used in the simulations, leading to a more realistic design of the features of the circuit. In the case of cells that were custom designed for this project, simulations were performed with the aid of standard cells and using parameters obtained through their expected characteristics.

The model cell used for the study of the chemoresistors response was also developed in Cadence™, using the *Composer* tool for the schematic views and defining the code through *Verilog-A* and *HDL* script.

Variations on the response with varying sensor temperature and humidity were simulated using the same model and the results were plotted with *Matlab* software, version 6.

Additional simulations of the response of the fourth order Bessel filter were obtained through the use of the *Texas Instruments FilterPro™* software.



### 4.3 GAS SENSOR SECTION SIMULATION

In order to verify the performance of the gas sensor section, the circuit was originally tested by applying a constant voltage supply to the voltage reference cell and observing the outputs at every stage of the circuit. After several modifications on the original schematics, the desired voltage levels were obtained.

However, the main interest was focused on the operation of the entire circuit in the pulsed mode, i.e. with a pulsed signal applied to the voltage reference cell, given that this mode increases the benefits of the ratiometric configuration as explained in previous chapters. Simulations presented in this section were therefore obtained with pulses applied to the input of the voltage reference cell (terminal  $V_{pulses}$  in Fig. 3.3) and observing the responses at different stages of the circuit.

#### 4.3.1 Voltage reference signals

The input and output waveforms obtained with the *Spectre* simulator for the voltage reference cell are shown in Figure 4.1. The input was obtained from the cell *vpulse* available for simulation of ideal sources in the standard library *analogLib* of Cadence™. The width of the pulses was set to 10 ms and the period was set to 100 ms.

The output is obtained through the use of the actual model cells provided by AMI Semiconductor for the bandgap and associated cells. The amplitude of the pulses in the signal  $V_{ref}$ , which is sent to the gas sensor and offset circuits, is 1.2 V. The simulation shows the appearance of spike at the raising edge of the output, typical of circuits driven by pulsed signals [1].

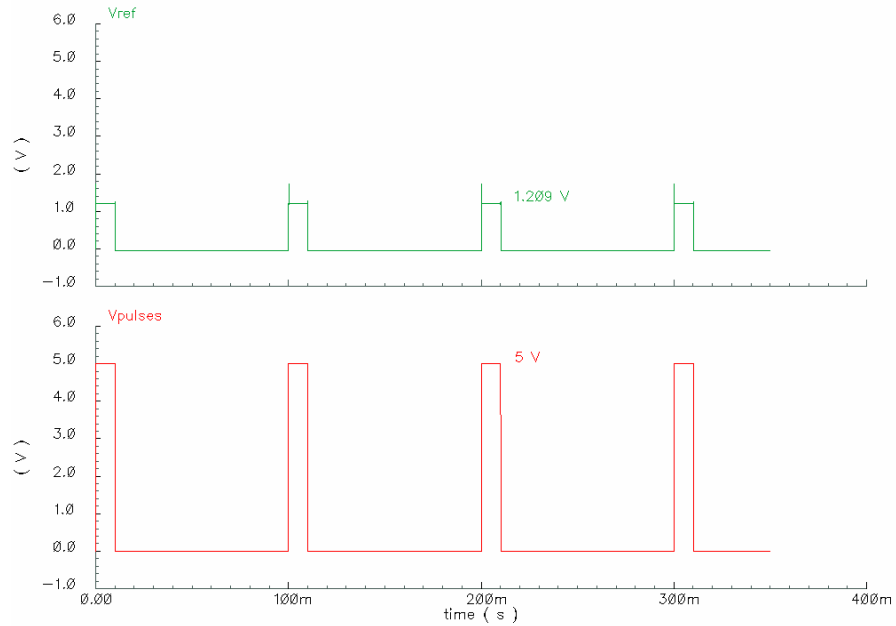


**Figure 4.1** Input and output waveforms in the voltage reference cell.

### 4.3.2 Ratiometric circuit

The performance of the ratiometric circuit is crucial for good behaviour of the sensors in the ASIC. The elimination (or reduction) of the unwanted effects in the sensors response depends on the correct functioning of the ratiometric circuit. Therefore, exhaustive simulations were required and the original circuit was modified several times until the desired response was achieved.

Given that the precise resistances (i.e. range 100  $\Omega$  to 100 k $\Omega$ ) and other characteristics of the polymeric sensors were unknown when the circuit was designed, it was necessary to test the performance of the circuit for a range of different parameters and conditions. In particular, the operation of the FET switches, used to produce the alternating signals on the resistive sensors, required several tests in order to determine the proper size and configuration of the final arrays. This involved considerations about the actual layout that only through simulation permitted to optimise the schematic design.

The resistance of the FETs was originally high when compared to the expected lowest resistance of the sensors, thus impeding the correct adherence to the ratiometric principle for the series switches and polymer resistors. The desired voltage waveforms could not be obtained and, in order to correct this, several FETs in parallel were used, in an attempt to reduce the unwanted effect of switch resistance.

However, a crucial factor in the design of the switches is the selection of the ratio  $W/L = 64$  for the FETs. Simulations showed that this ratio produces the optimal performance of the switching circuit and that this parameter has greater significance than the number of parallel FETs included into each switch. The results of some of these simulations are summarised in Table 4.1.

**Table 4.1** Parameters obtained for the selection of the FET switches.

| N        | W<br>( $\mu\text{m}$ ) | L<br>( $\mu\text{m}$ ) | W/L       | $V_{polymer}$<br>(V) | $V_{sensor}$<br>(V) | $R_{polymer}$<br>( $\text{K}\Omega$ ) |
|----------|------------------------|------------------------|-----------|----------------------|---------------------|---------------------------------------|
| 6        | 128                    | 8                      | 16        | 1.117                | 2.438               | 1                                     |
| 6        | 256                    | 8                      | 32        | 1.157                | 2.420               | 1                                     |
| 6        | 512                    | 8                      | 64        | 1.178                | 2.410               | 1                                     |
| 6        | 256                    | 4                      | 64        | 1.178                | 2.409               | 1                                     |
| 6        | 128                    | 2                      | 64        | 1.178                | 2.408               | 1                                     |
| <b>6</b> | <b>128</b>             | <b>2</b>               | <b>64</b> | <b>1.198</b>         | <b>2.401</b>        | <b>10</b>                             |
| 1        | 128                    | 2                      | 64        | 1.078                | 2.448               | 1                                     |
| 1        | 128                    | 2                      | 64        | 1.187                | 2.405               | 10                                    |
| 8        | 256                    | 8                      | 32        | 1.167                | 2.415               | 1                                     |
| 8        | 128                    | 2                      | 64        | 1.183                | 2.406               | 1                                     |

It can be observed in the last two rows that an increase in the number  $n$  of FETs does not make a significant improvement of the voltage at the output of the sensor circuit  $V_{sensor}$ , which would be 2.400 V under ideal conditions.

On the contrary, an increase on the resistance of the polymer sensors  $R_{polymer}$  produces a considerable improvement of  $V_{sensor}$  as well as in the voltage across the polymer resistors  $V_{polymer}$ , which should be ideally the same as  $V_{ref}$ , i.e. 1.2 V.

Although smaller dimensions with the same ratio would produce slightly better results, it was decided to use for the layout the dimensions  $W = 128 \mu\text{m}$  and  $L = 2 \mu\text{m}$ , with  $W/L = 64$ , as these conformed better to the technology layout rules.

Once the FETs were working properly, simulations showed that the circuit was able to produce the desired response with sensor resistances ranging from 1 k $\Omega$  to 100 k $\Omega$ . However, the design is calculated for optimal performance at 10 k $\Omega$ .

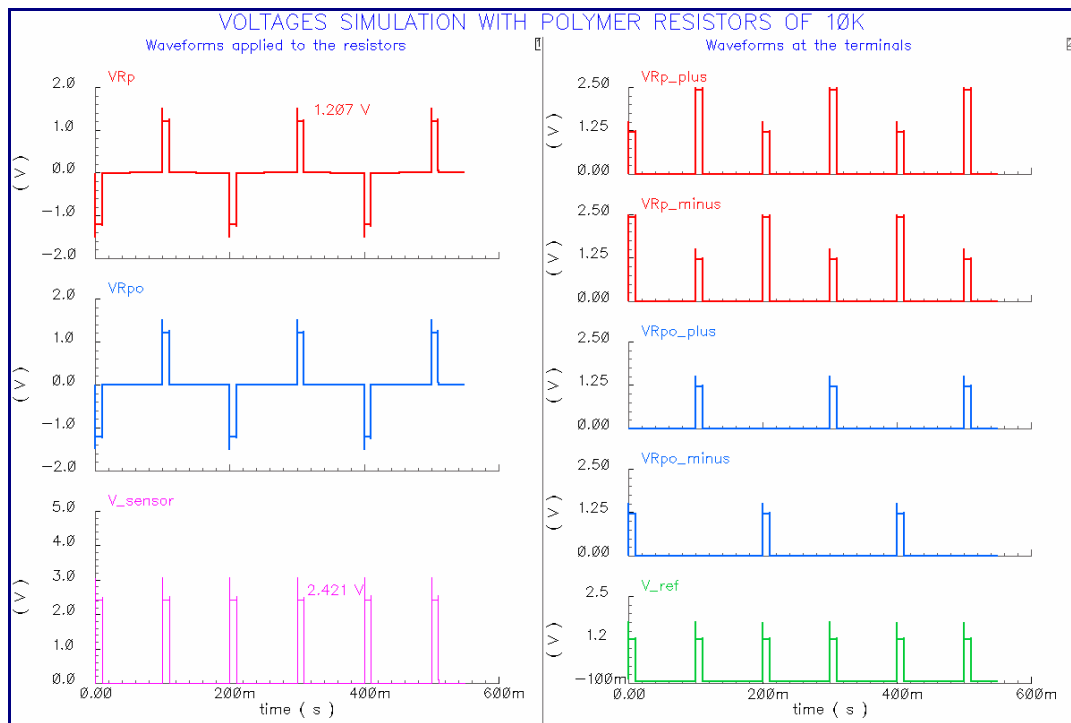


**Figure 4.2** Waveforms simulation for 10 k $\Omega$  polymer resistors.

Figure 4.2 shows the waveforms in the gas sensor circuit (Figure 3.4), obtained with the *Spectre* simulator, assuming resistances of 10 k $\Omega$  for both  $R_p$  and  $R_{po}$  and disregarding any variations due to exposure to gases or vapours.

The left side plots correspond to the actual voltage waveforms at the terminals of the resistors, i.e. the differences in the corresponding positive voltages, plotted on the right side, appearing at the *plus* and *minus* terminals of each resistor. It can be observed how the effect of the switches, pulsed at 5 Hz, results in an alternating signal appearing at the terminals of the chemoresistors. The waveforms for  $V_{ref}$  and  $V_{sensor}$  are also illustrated in the same figure.

Simulations also show that the use of parallel FET switches produces an acceptable response even when the resistance of the sensors is as low as 1 k $\Omega$ . The plots for this case are depicted in Figure 4.3.

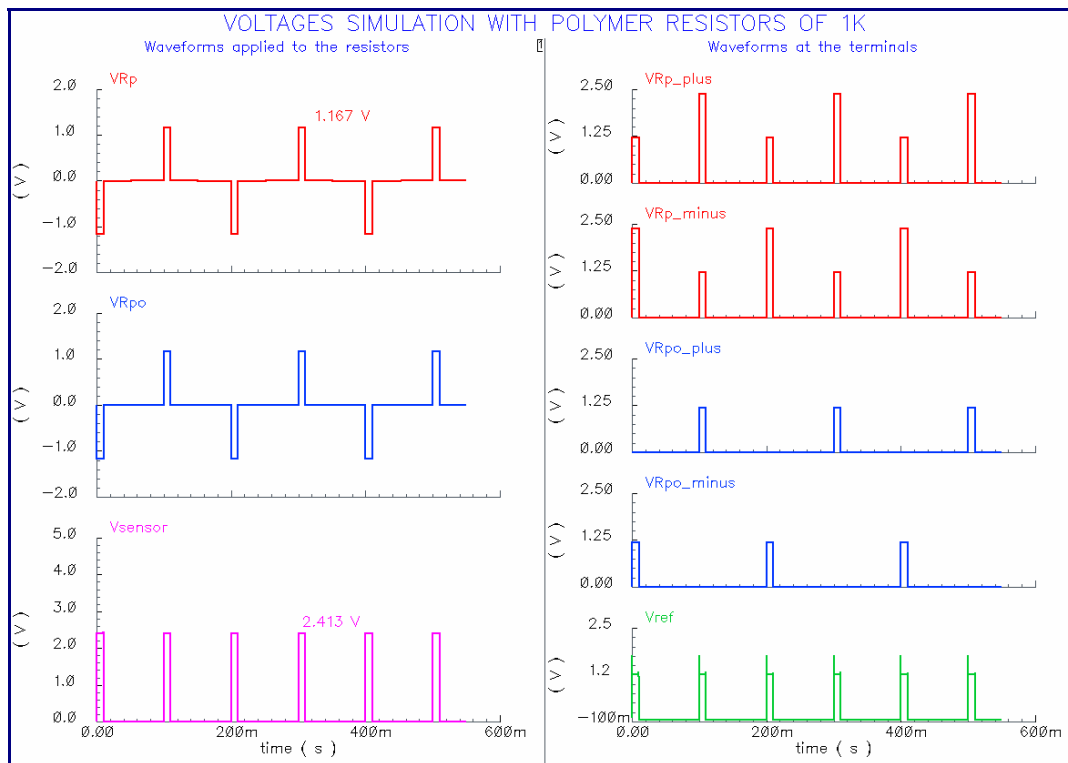


**Figure 4.3** Waveforms simulation for 1 k $\Omega$  polymer resistors.

Table 4.2 summarises the results of further simulations with different resistance values for all the chemosensors, i.e.  $R = R_p = R_{po}$ . It includes the magnitudes of the voltage at the output of the non-inverting sensor circuit,  $V_{sensor}$ ,

and the voltages at the chemoresistors terminals,  $V_{Rp}$  and  $V_{Rpo}$ . The magnitudes of the transient spike produced at the switching edges in each resistor, are also shown in the table.

**Table 4.2** Results of simulations for several values of chemosensors resistance.

| $R$<br>(k $\Omega$ ) | $V_{sensor}$<br>(Volts) | Chemoresistor $R_p$ voltages<br>(Volts) |                          |                          | Chemoresistor $R_{po}$ voltages<br>(Volts) |                          |                          |
|----------------------|-------------------------|---|--------------------------|--------------------------|--|--------------------------|--------------------------|
|                      |                         | $V_{Rp}$                                | Raising<br>edge<br>spike | Falling<br>edge<br>spike | $V_{Rpo}$                                  | Raising<br>edge<br>spike | Falling<br>edge<br>spike |
| 1                    | 2.413                   | 1.167                                   | 0.0                      | 0.00                     | 1.167                                      | 0.0                      | 0.00                     |
| 10                   | 2.421                   | 1.207                                   | 0.3                      | 0.05                     | 1.207                                      | 0.3                      | 0.05                     |
| 100                  | 2.419                   | 1.209                                   | 0.5                      | 0.07                     | 1.209                                      | 0.3                      | 0.07                     |
| 200                  | 2.419                   | 1.209                                   | 0.8                      | 0.12                     | 1.209                                      | 0.3                      | 0.07                     |
| 400                  | 2.419                   | 1.209                                   | 1.2                      | 0.18                     | 1.209                                      | 0.2                      | 0.06                     |
| 600                  | 2.419                   | 1.209                                   | 1.4                      | 0.23                     | 1.209                                      | 0.3                      | 0.07                     |
| 800                  | 2.419                   | 1.209                                   | 1.6                      | 0.30                     | 1.209                                      | 0.3                      | 0.07                     |
| 1000                 | 2.419                   | 1.209                                   | 1.7                      | 0.26                     | 1.209                                      | 0.3                      | 0.06                     |

From the table, it can be noticed that, although the output is free of noise for  $R = 1$  k $\Omega$ , the voltage in the sensors is still below its ideal value (1.2 V), due to the effect of the resistance of the FETs.

For  $R = 10$  k $\Omega$ , conditions are optimal, as the ideal voltage appears across the sensors. The switching spike, although significant when compared with the previous case, is a common effect that is easily removed at the differential input of the amplifier in the next stage of the circuit. The noise components are balanced, i.e. voltage peaks have the same values at both edges of the switching pulses, and they have the same magnitudes as the spike produced in the offset circuit, which is also designed with 10 k $\Omega$  resistors.

For higher resistances, the input impedance of the sensor circuit is greater than that of the offset circuit. This produces an unbalanced spike condition at the resistors, as for  $R_{po}$  it remains at the expected values due to the  $V_{ref}$  voltage being

applied through the operational amplifier, whereas a bigger change is forced to appear through the active resistor  $R_p$ .

The unbalance increases with higher resistance values of the sensors, creating a noise component that is not removed by the differential input of the amplifier, and that will be added to the response of the chemoresistors to gas exposure. This is particularly critical considering that most of the harmonic content of these signals occurs at the same low frequency of  $V_{ref}$  and it also coincides with the response and the flicker noise characteristic of the carbon black/polymer composite sensors, which is modelled and studied in section 4.5.

When resistance of the sensors is 400 k $\Omega$ , the amplitude of the spike noise reaches the same magnitude as the output signal, and it is even greater for higher resistances. Therefore, the simulations suggest that the operation of the circuit is not recommended with resistances greater than 100 k $\Omega$  and it is advisable to try to use sensors with resistance as close to 10 k $\Omega$  as possible, for an optimal performance.

The circuit can be also operated without a pulsed signal, avoiding this way the problem of the spike produced at the switching edges. The use of a constant DC voltage, however, can produce unwanted sensor drift that was mentioned in the two previous chapters.

Regarding the offset circuit, its operation is free from all of these problems. It only produces a replica of the voltage pulses appearing in  $V_{sensor}$ , without any additional spike as there is no switching in this circuit. The 10 k $\Omega$  resistors used in the offset circuit, match the impedance of other cells in the ASIC, including the recommended resistance of the chemosensors.

### 4.3.3 Instrumentation amplifier

When the circuit is being calibrated, both inputs of the instrumentation amplifier receive nominally identical signals, i.e. the differential input is zero. As a result, the voltage at the output terminal of the amplifier is also equal to zero.

The plots in Figure 4.4 correspond to the simulation of the voltages in the instrumentation amplifier under these circumstances. The output of the offset circuit equals the output of the sensor circuit, with pulses sized 2.421 V. Both the differential input and the output of the amplifier are almost zero.

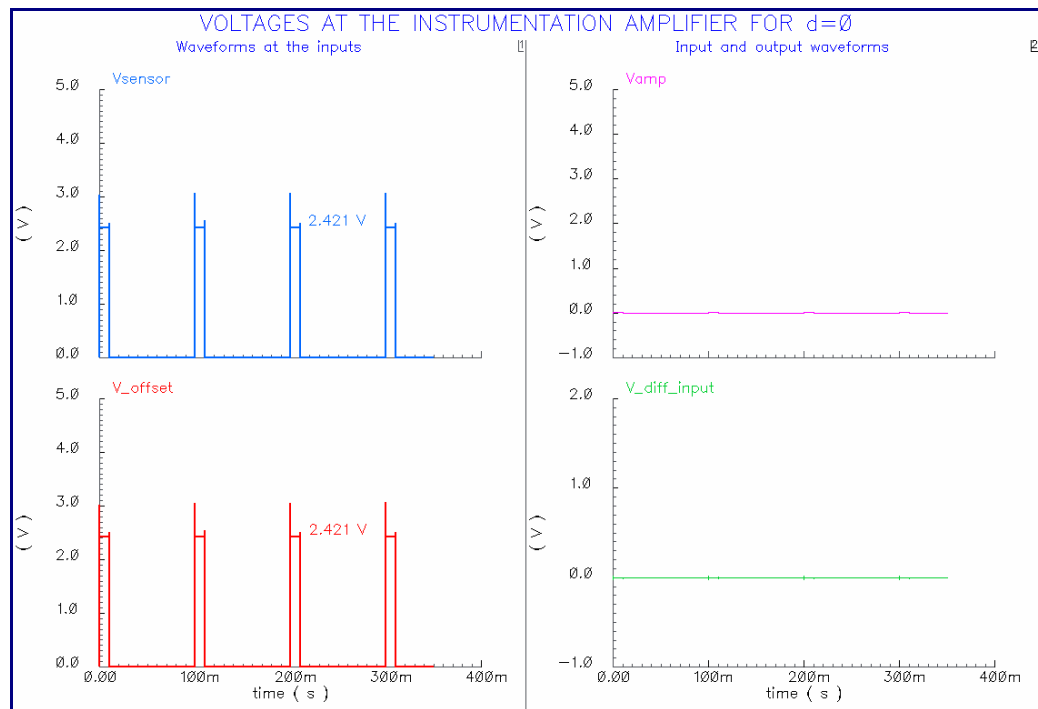


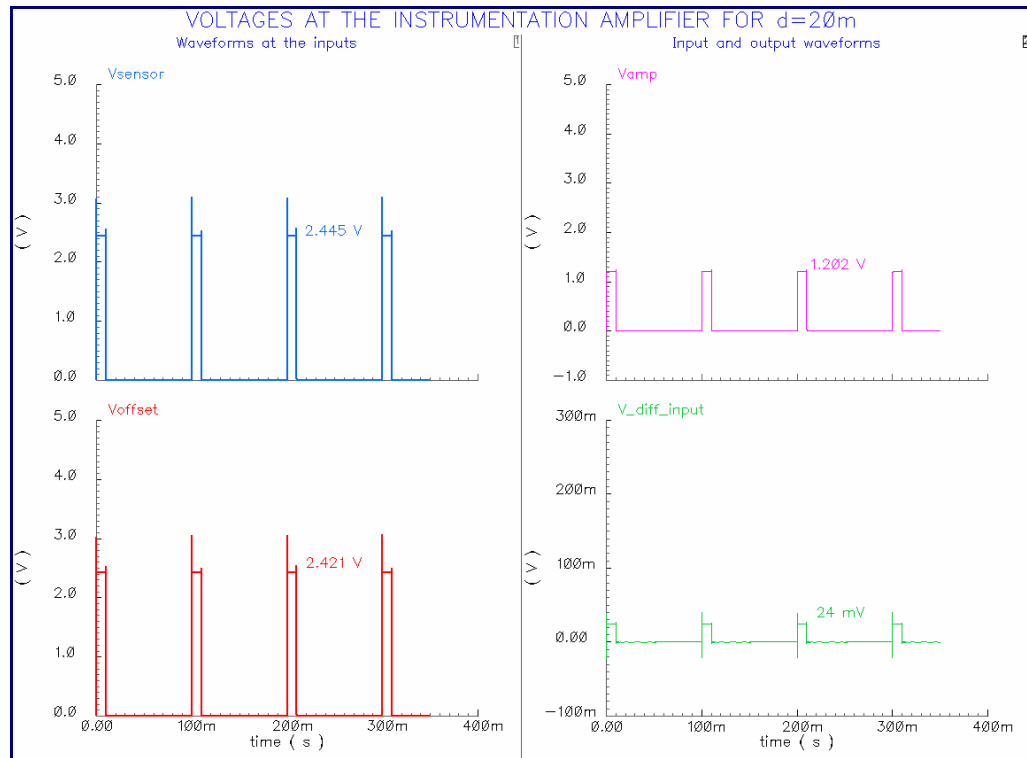
**Figure 4.4** Voltages in the instrumentation amplifier for zero differential input.

The 600 mV common spike produced in the 10 k $\Omega$  resistors of both the sensor and offset circuits is almost entirely cancelled in the differential input of the amplifier, leaving the output at a proper level, ready for the detection of other variations in the resistance and output voltage of the polymeric sensors.



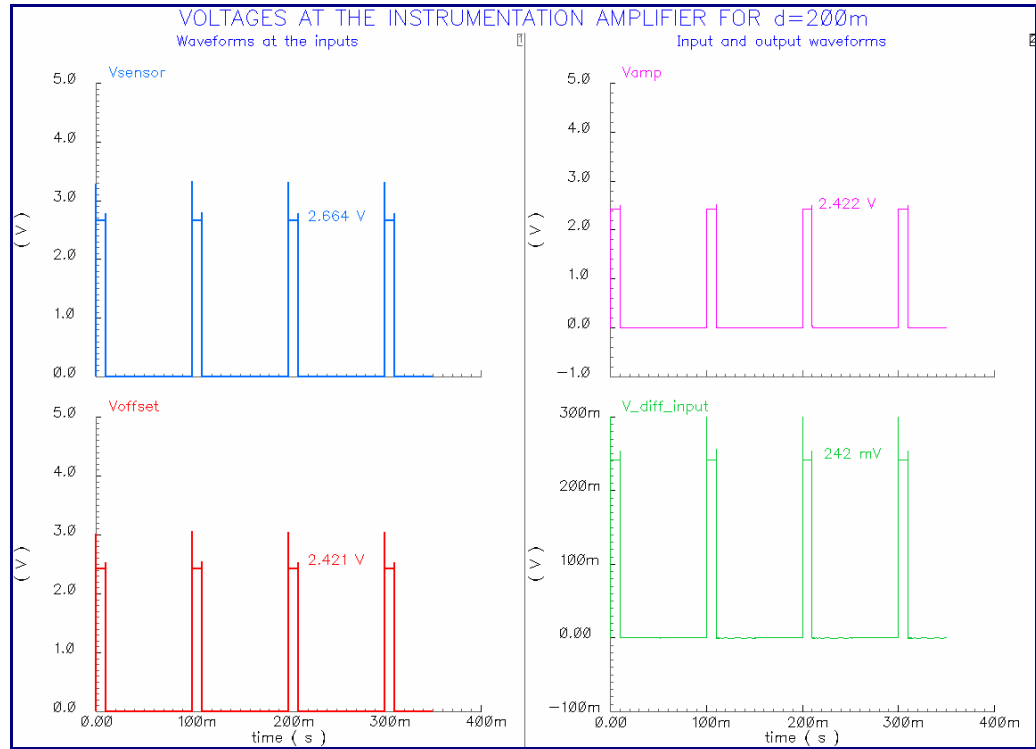
When the sensor system is exposed to a gas, a relative change  $\delta$  will be produced in the polymer resistance, which in turn will cause a voltage difference between the input terminals. Therefore, the voltage at the output will be non-zero, indicating the presence and concentration of the gas.

Figure 4.5 shows the simulation results obtained considering a relative variation of  $\delta = 0.020$ . The gain of the amplifier was adjusted to 50 by setting  $R_{gain}$  in the external potentiometer, raising the output signal to an appropriate level for further processing. As a result, the pulsed voltage difference between  $V_{sensor}$  and  $V_{offset}$ ,  $2.445 - 2.421 = 0.024$  V is applied to the input, where the common spike is cancelled. The output signal has amplitude of 1.20 V, and it is practically free of spiking. Such small variations are expected when the sensor system is exposed to low concentrations of VOC.



**Figure 4.5** Voltage waveforms obtained with  $\delta = 0.020$ .

The response of the circuit to higher variations in the resistance of the chemosensors is illustrated in the plots of Figure 4.6, that was obtained after a simulation with  $\delta = 0.200$  and setting the gain of the amplifier to 10.



**Figure 4.6** Voltage waveforms obtained with  $\delta = 0.200$ .

#### 4.3.4 Fourth order Bessel filter

Apart from its frequency response, it was necessary to verify that the Bessel low-pass filter had the sufficient flat delay characteristic needed to remove the overshoot due to the differences in time delay between the harmonic contents of the raising and falling edges of the voltage pulses used in the circuit.

Also, although it is not critical for this design, attenuation slope near the cut-off frequency was tested and compared with typical values for more conventional filters.

Initial simulations performed with Cadence™ software showed that a fourth-order Bessel filter was appropriate for the required processing of the output signal obtained after the amplification stage. However, it was not easy to transform the *Composer* schematics into the corresponding *Virtuoso* layout views and meet at the same time the sizing specifications suitable for matching the rest of the components in the ASIC chip. The Texas Instruments software *FilterPro*™ was used instead for the simulation of the filter response in the final stages of the design.

Figure 4.7 shows the characteristics obtained with the values mentioned in Table 3.1. The gain (green line) is unity in the pass-band, although not as flat as for a Butterworth filter, with attenuation falling down to  $-70$  dB for  $100$  kHz, which is good for only four poles. Group delay (black line) is flat, free from overshoot and slightly above  $30$  ms for the pass-band, which is much better than the simulated performance for conventional Butterworth and Chebishev responses, which showed group delay spikes from  $40$  to  $60$  ms and from  $50$  to  $100$  ms, respectively.

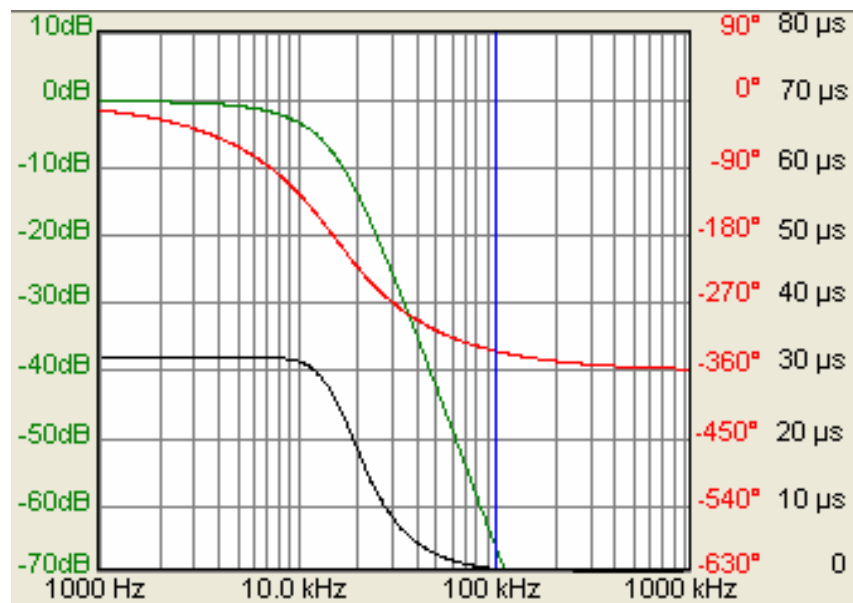


**Figure 4.7** Bessel filter characteristics obtained with *FilterPro*™ software, showing the gain (green line), phase (red line) and group delay (black line).

### 4.3.5 Overall performance

To summarise the description of the gas sensing circuit, a simulation of the voltage waveforms, including from the voltage reference to the filtered output, is shown in Figure 4.8.

The circuit parameters have the values given in the previous sections. The value of the resistance of the chemosensors was set to 10 k $\Omega$ , the relative change in resistance  $\delta$  to 0.200, and the voltage gain of the instrumentation amplifier was 10.

Pulses of amplitude 1.2 V and width 10 ms are applied through the voltage reference cell, at a frequency of 10 Hz. The outputs of both offset circuit and gas sensor circuit have a difference of 242 mV produced by the simulated resistive change  $\delta$  of 0.200. This difference is amplified by a factor of 10 and the output pulses are filtered to produce the final output of the circuit.

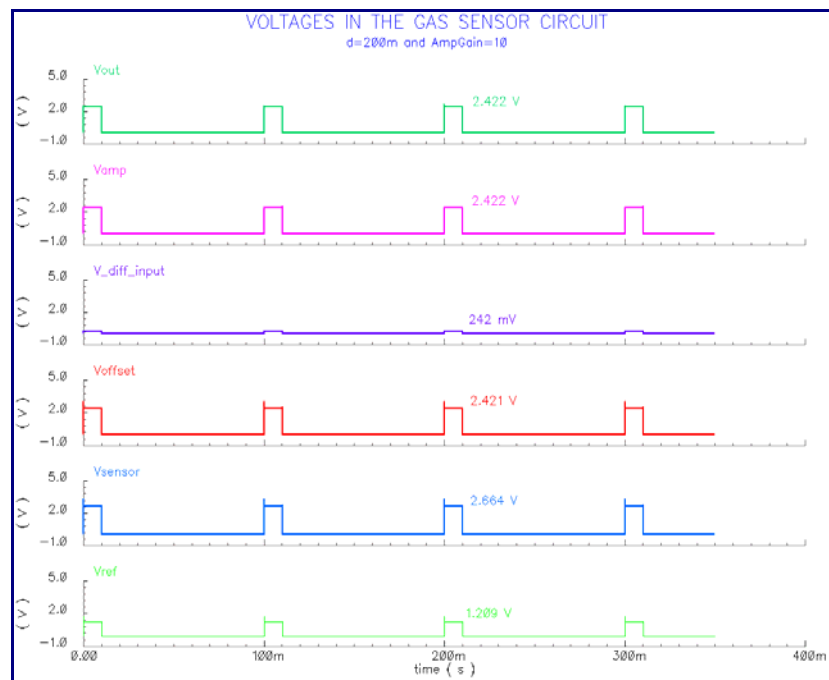


**Figure 4.8** Voltages in the gas sensor section obtained with  $\delta = 0.200$ .

## 4.4 TEMPERATURE CONTROL CIRCUIT SIMULATION

Components of the temperature control circuit were also simulated. In particular, the temperature sensors and heater were simulated using the information available for these custom-designed components. A reasonable estimation of the circuit behaviour was obtained, as verified by results taken from the fabricated ASIC chip.

### 4.4.1 Temperature sensors

As the p-n diode included in the design was not a standard cell, there was no information available about its temperature response. The simulation results given below were obtained with an AMI Semiconductor library model for a diode whose response to a 5  $\mu$ A forward current varies between 580.6 mV and 545.7 mV for the range of temperature between 20°C and 35°C, corresponding to a slope of  $-2.35$  mV/°C, which is above the theoretical value of  $-2.1$  mV/°C for a p-n diode [2]. Approximately linear response for this diode is expected and shown in Figure 4.9. The variation of the forward voltage  $V_{ts}$  decreases with increasing temperature over the working temperature of the sensing element, e.g. +20°C to +100°C.

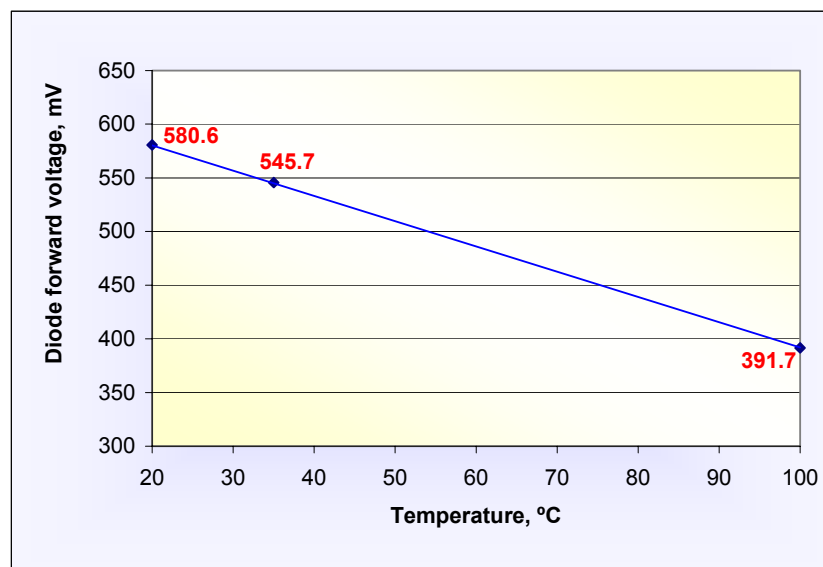


Figure 4.9 Simulated voltage-temperature characteristic of the p-n diode.

The simulated diode characteristic is the same for the three thermosensors in the circuit, one between each pair of electrodes and the third one in the middle of the chip. The only difference in the last one being that output is amplified by a factor of 7, as it was described in section 3.5.1. The results of these simulations differ only slightly from the theoretical values and are close to the values reported in Chapter 6 for the diodes measured in the fabricated ASIC chip.

#### 4.4.2 Heater

The two resistive aluminium heaters were designed to each have a resistance of 50  $\Omega$  and dissipate a maximum of 80 mW of power, enough to operate the sensors at 100°C. Heaters were represented in simulations as linear resistors using only a standard cell available in the *analogLib* library of Cadence™.

According to the simulated response of the thermodiodes, if the heater should reach a temperature of 35°C, the set-point voltage must be 545.7 mV (see Figure 4.9). The equation for the voltage divider gives the required resistance for the external potentiometer in the temperature set-point circuit:

$$R_{tr2} = \frac{0.5457R_{tr1}}{1.209 - 0.5457} = \frac{0.5457(10 \text{ k}\Omega)}{0.6633} = 8.227 \text{ k}\Omega \quad (4.1)$$

Thus, the external potentiometer must be set to 8.227 k $\Omega$  for operation of the heater at 35°C. The value of the internal resistor is fixed in the design to  $R_{tr1} = 10 \text{ k}\Omega$ .

In order to reach a temperature of 100° C, the power of 80 mW must be dissipated by the heater, whose nominal resistance is 50  $\Omega$ . The value of the required current is thus 40 mA, which corresponds to 2 V dropped at the heater terminals. These are the maximum nominal values for the electrical parameters of the heater.

Assuming that the heater starts at  $T = 20^\circ\text{C}$ , then the voltage in the temperature sensor is 580.6 mV. In order to reach a set-point temperature of  $35^\circ\text{C}$  ( $V_{sp} = 545.7$  mV), the voltage that must be initially applied to the heater from the temperature compensator is given by:

$$V_{heater} = \frac{R_2}{R_1}(V_{ts} - V_{sp}) = 10(580.6 - 545.7) = 349 \text{ mV} \quad (4.2)$$

The current driven to the heater at this point is  $I = 349 \text{ mV} / 50\Omega = 6.98 \text{ mA}$ , which corresponds to a power of 2.44 mW.

The simulated performance of the heater, obtained with *Spectre*, is shown in Figure 4.10. In order to raise the temperature of the heater from  $20^\circ\text{C}$  to  $35^\circ\text{C}$ , the applied voltage starts from 349 mV and drops until the required temperature is reached. This allows the transfer of the corresponding power to the heater, by driving through a current which starts at 6.98 mA.

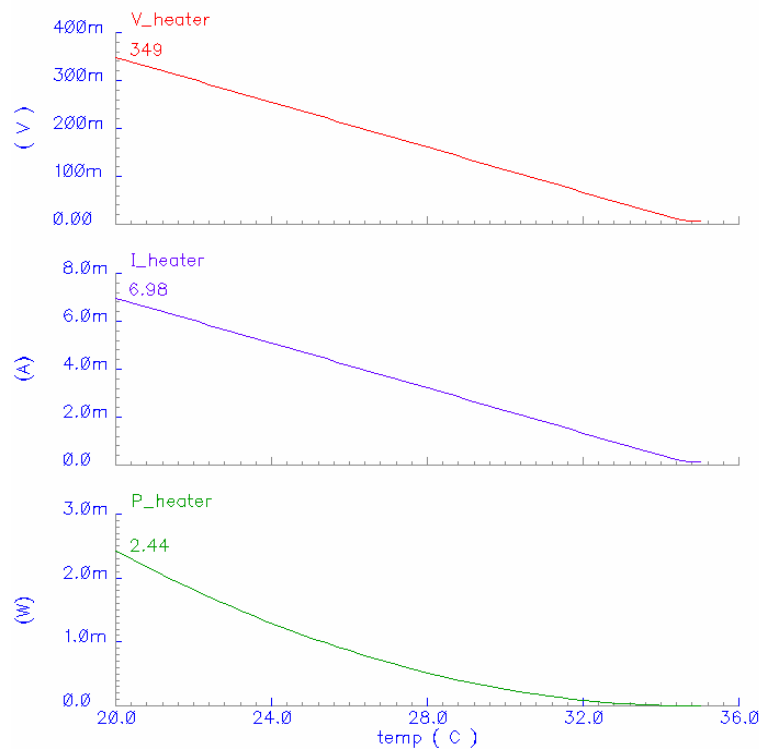


**Figure 4.10** Heater waveforms when temperature increases from  $20^\circ\text{C}$  to  $35^\circ\text{C}$ .

### 4.4.3 Overall performance

The simulation of the overall performance of the temperature control system is presented here, assuming as an example that the circuit is required to drive the heaters up to 35° C, starting from an ambient temperature of 20° C. The thermal behaviour is expected to be approximately linear at these low operating temperatures.

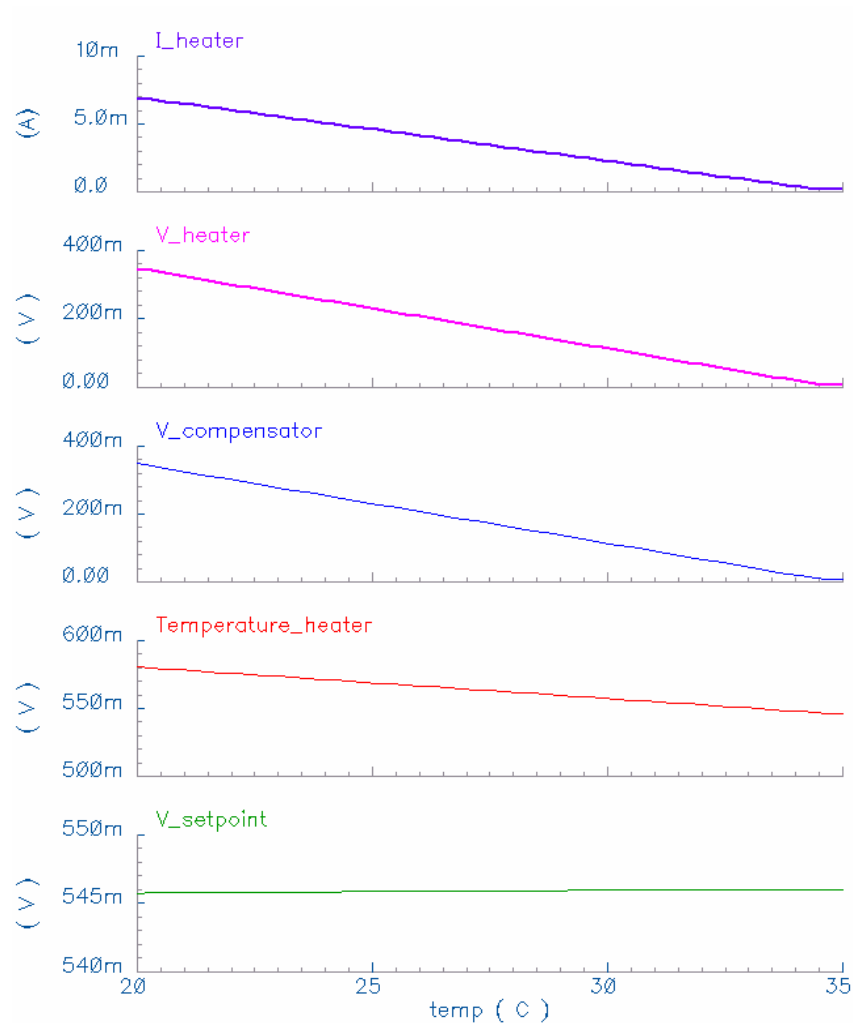


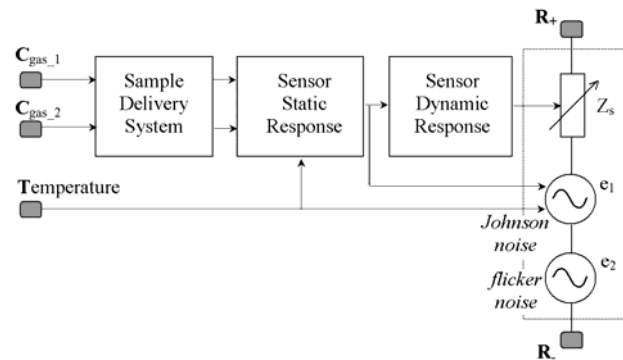
**Figure 4.11** Example of overall performance of the temperature control system.

The plots in Figure 4.11 were obtained with *Spectre* simulator using a Cadence™ library diode model and assuming an *nwell* type external resistor. The variation of voltage in the diode and the compensator output for temperature between 20 and 35°C are also shown. The plot at the top corresponds to the current driven to the heater.



## 4.5 MODELLING AND SIMULATION OF POLYMERIC CHEMORESISTORS<sup>2</sup>

Finally, a parametric model of a polymeric chemoresistor was developed for use in the design and simulation of a smart gas sensor. The model was implemented in Cadence™ software and it allows the simulation of both the static and dynamic response of resistive sensing elements to a mixture of gases. It takes into account temperature and humidity effects and simulates the noise present in polymer resistive sensors, such as Johnson [3] and flicker noise [4-6]. The model also takes into account certain *sample delivery system* (SDS) parameters, such as the volumetric flow rate and mixing volume of the sensor chamber.



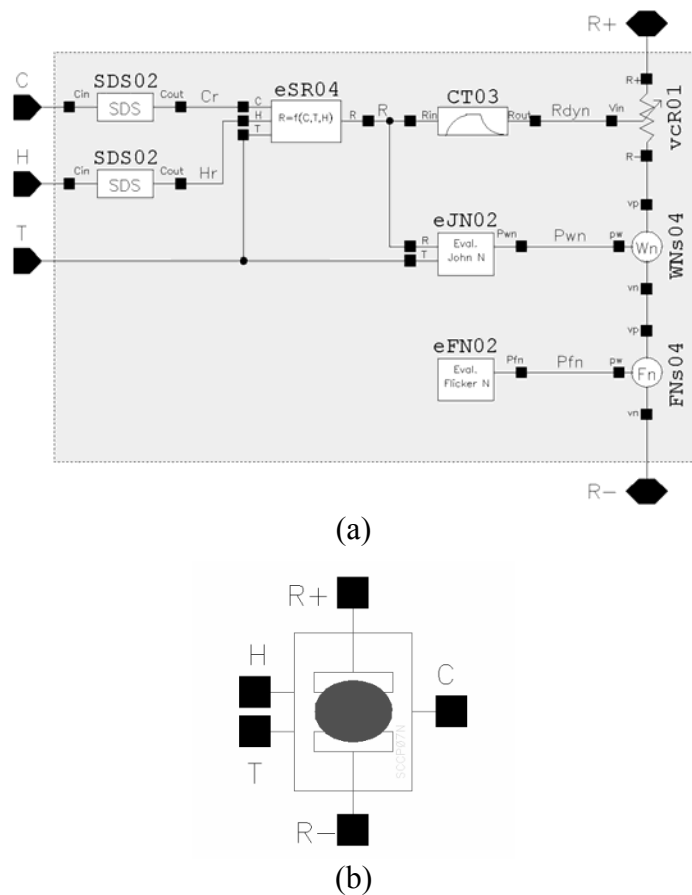
**Figure 4.12** Structure of the polymeric chemoresistor model.

Figure 4.12 shows the basic structure of the proposed model, comprising four blocks that represent the SDS, the static and dynamic responses of the sensor, and the chemoresistor itself. The model has two inputs for different gas concentrations and one input for temperature effect simulation ( $C_{\text{gas}_1}$ ,  $C_{\text{gas}_2}$ , and Temperature) as well as two external ports ( $R_+$ ,  $R_-$ ) for sensors connection within the complete test system. The sensor static response is a function of the input gas concentrations and temperature while the dynamic response depends both on the gas transfer method and the reaction process on, or within, the gas sensitive material. The chemoresistor itself is represented as a complex impedance  $Z_s$  element with two noise generators

<sup>2</sup> The work presented in this section was developed in collaboration with Nicola Ulivieri, from Università di Siena, Italy.

connected in series representing Johnson and flicker noise, which depend on the sensor temperature and sensor resistance [3] and the type of polymer, its volume and its biasing voltage [4-6], respectively.

The schematic view for the model is shown in Figure 4.13(a) with its associated symbol represented in Figure 4.13(b). One of the gas inputs, **H**, is assumed to be the water vapour concentration, i.e. absolute humidity. Each block within the electrical model has been custom designed to perform a desired function or to emulate an electrical device. Two main sections can be distinguished: the block composed from the sub-cells *SDS02*, *eSR04*, *CT03*, *vcR01*, simulating the response of the sensor (i.e. its change in resistance) and the noise generation section which comprises the sub-cells *eJN02*, *eFN02*, *WNs04* and *FNs04*.



**Figure 4.13** Polymeric chemoresistor cell: (a) schematic view, (b) symbol.

The sensor static response is a function of the gas concentration  $C_G$ , the sensor temperature  $T$  and the water vapour concentration  $C_H$ . The dynamic response depends both on the gas transfer method and/or on the gas reaction kinetics. The static resistance of the standard cell,  $R_{SC}$ , is evaluated in the block ‘Sensor Static Response’ (Figure 4.12) which implements the developed model, assuming that carbon-black composite polymer films are used as the gas sensitive material. The cell could be easily modified to model other sensor isotherms, e.g. Langmuir or Freundlich, see reference [7]. The model developed for these materials includes the temperature variations of the baseline resistance and the static resistance is given by:

$$R_{SC} = R_{SCo} \exp\left(\frac{B}{T}\right) \cdot \left[ 1 + k_G C_G^{\gamma_G} \exp\left(\frac{K_{sG}}{T}\right) + k_H C_H^{\gamma_H} \exp\left(\frac{K_{sH}}{T}\right) \right] \quad (4.3)$$

where  $R_{SCo}$  is the baseline sensor resistance (measured in the presence of a reference gas, generally zero grade air or pure nitrogen),  $k_G$ ,  $k_H$  are sensitivity coefficients,  $C_G$ ,  $C_H$  are the gas/vapour concentrations expressed in ppm,  $\gamma_G$ ,  $\gamma_H$  are the power law exponents,  $B$ ,  $K_{sG}$ ,  $K_{sH}$  are the temperature coefficients and  $T$  is the temperature in degrees Kelvin. The subscripts  $G$  and  $H$  refer to the gas and the water vapour, respectively. The sensitivity coefficients can be positive or negative depending on the nature of the gas and the polymer, producing an increase (or decrease) of the sensor resistance after the gas has been introduced.

The transient behaviour of the polymeric gas sensor is simulated by a second order multi-exponential model implemented through a second-order low-pass filter (‘Sensor Dynamic Response’ in Figure 4.12) [8-10]. Since the on-dynamics are generally faster than the off-dynamics, two filters with different poles have been used [3-4]. The sample delivery system is also modelled (‘Sample Delivery System’ in Figure 4.12) in order to include the overall system transfer function. The

performance of the model, and all individual blocks within it, is explained in recent publication [7] and for the sake of completeness has been included in Appendix F.

#### 4.5.1 Discrete chemoresistor model

The resistor model can be used in the voltage divider configuration shown in Figure 4.14 in order to simulate the response of a discrete chemoresistor converting the change in resistance into a change in voltage that can be further processed.

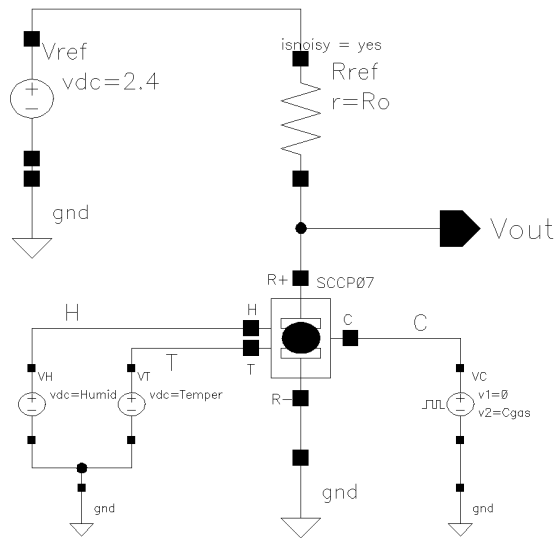


**Figure 4.14** Schematic view of the discrete chemoresistor circuit.

The variation in resistance of the gas-sensitive device, subsequent to exposure to a gas of concentration  $C$ , can then be measured through the change in the output voltage  $V_{out}$  which is function of the sensor resistance  $R_S$ :

$$V_{out} = V_{ref} \frac{R_S(C)}{R_{ref} + R_S(C)} \quad (4.4)$$

The voltage sensitivity  $S$  of the potential divider is defined as

$$S = \frac{dV_{out}}{dR_S} = V_{ref} \frac{R_{ref}}{(R_{ref} + R_S(C))^2} \quad (4.5)$$

which has a maximum for  $R_{ref}=R_S$ . The reference resistance value is chosen to be equal to the sensor baseline value (10 k $\Omega$ ) to maximize sensitivity for small changes of  $R_S$ . Gases injection and sensor temperature are simulated by voltage sources.

### 4.5.2 Ratiometric chemoresistor model

The general parametric model described above can also be used for the modelling of the response of the polymeric chemoresistors in the ratiometric configuration. In the schematic shown in Figure 4.15, the sensor cell  $SCa$  emulates the behaviour of the ‘active’ polymeric sensor, while the cell  $SCp$  emulates the ‘passive’ sensor.

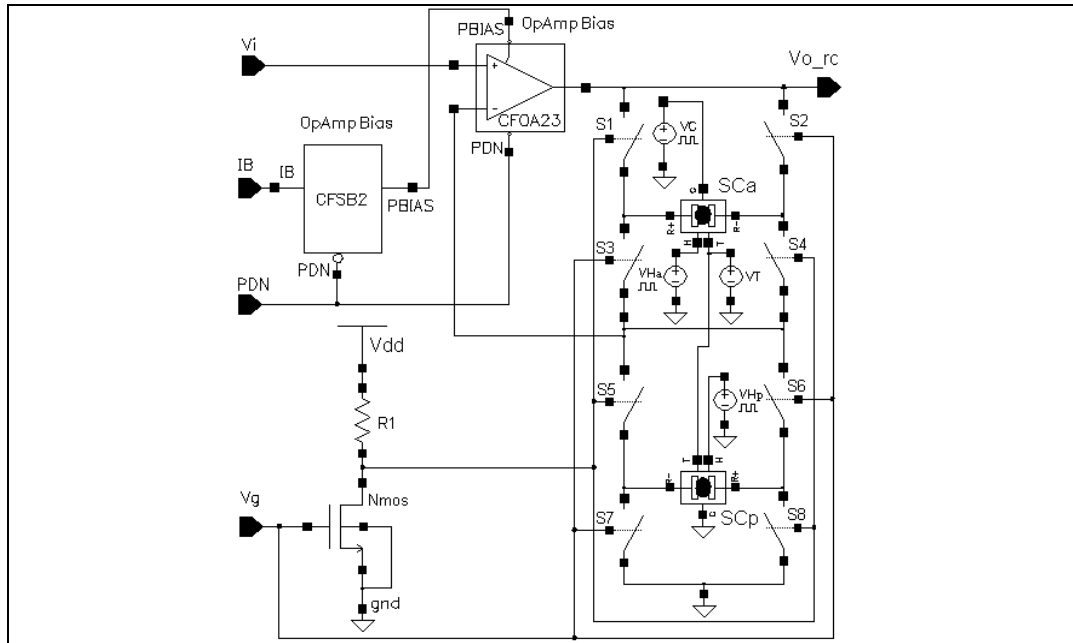


**Figure 4.15** Schematic view of the modelled ratiometric sensor circuit.

The chemoresistor model cell replaces the resistive sensors included in the ratiometric circuit previously described, connected to this via two resistive terminals, while voltage sources simulate the effect of gas concentration, ambient humidity, and sensor temperature. In the circuit shown, the sensor cell  $SCp$  represents the passive condition by having the gas concentration input connected to ground.

The variation in voltage with the changes in resistance of the ratiometric configuration was already studied in section 2.5, where also the equations for every possible measuring case were presented.

Two passivation methods can be analysed in the circuit simulations. In the first case, represented in Figure 4.16(a), one of the polymeric sensors is coated with an inert, passivating material to remove the gas effect. In this way, the passive sensor is sensitive to any temperature variation but will not respond to the gas or ambient humidity. The water vapour concentration is fixed to the concentration present at the moment of the coat deposition (e.g. RH = 40% at 20°C corresponding to 9214 ppm). The gas flow is divided into two paths to expose both sensors simultaneously. The passivation is simulated by connecting the input  $C$  of the  $SCp$  cell to  $gnd$  (gas concentration = 0 ppm) and the input  $H$  to a voltage source (e.g.  $VHp = 9214 \text{ V} \rightarrow 9214 \text{ ppm}$ ).

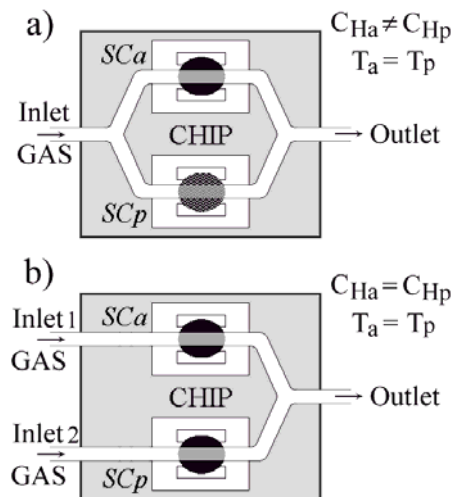


**Figure 4.16** Passivation methods tested in the simulations: (a) one inlet, with one uncoated and one coated sensors (b) two separate inlets, with two uncoated sensors.

The second method requires two separate gas inlets to carry the gas under test and a reference gas to the sensors  $SCa$  and  $SCp$  (Figure 4.16(b)). In this case the sensor  $SCp$  is not coated but it acts as a reference device because the reference gas is injected in the second inlet ('Inlet2 GAS'). This solution theoretically allows a cancelling of the humidity effect when the reference gas has the same water vapour concentration as the gas under test injected in the 'Inlet1 GAS'.

### 4.5.3 Performance simulation

Extensive simulations were carried out, with the aid of the chemoresistor model cell, for the evaluation of the performance of the ratiometric circuit. The response of the polymeric sensors to gases or vapours, their dependence on temperature, and the effect of humidity were all simulated prior to fabrication. A noise analysis was also obtained from the simulations.

Table 4.3 summarises the model parameters values used in the simulations reported in this section.

**Table 4.3** Model parameters used in the simulations <sup>a</sup>.

| Parameter used in the Cadence™ model | Symbols used in the equations | Value(s) <sup>b</sup> | Description   |
|--------------------------------------|-------------------------------|-----------------------|---|
| Cgas                                 | $C_G$                         | 1k                    | Gas concentration (ppm)                                     |
| Humid                                | $C_H$                         | 0-30k                 | Humidity concentration (ppm)                                |
| Temper                               | $T$                           | 40-100                | Sensor temperature (°C)                                     |
| KsH                                  | $K_{sH}$                      | 31.32                 | Temperature coefficient for the humidity (°C)               |
| kH                                   | $k_H$                         | -94n                  | Sensitivity coefficient for the humidity (1/ppm)            |
| gammaH                               | $\gamma_H$                    | 1                     | Power law exponent for the humidity                         |
| Ro                                   | $R_{SCo}$                     | 9512                  | Sensor baseline resistance ( $\Omega$ )                     |
| B                                    | $B$                           | 2                     | Temperature coefficient for sensor baseline resistance (°C) |
| Ks                                   | $K_{sG}$                      | 88.42                 | Temperature coefficient for the gas (°C)                    |
| k1                                   | $k_G$                         | 3.2 $\mu$             | Sensitivity coefficient for the gas (1/ppm)                 |
| Gamma                                | $\gamma_G$                    | 1.07                  | Power law exponent for the gas                              |

<sup>a</sup> A complete list of parameter values can be found in the journal article reproduced in Appendix F.

<sup>b</sup> The values of the parameters used for simulations are obtained from measurements on carbon-black polymer films deposited at the Sensors Research Laboratory of the University of Warwick; the noise measurements were performed in collaboration with the University of Torvegata (Rome).

#### 4.5.3.1 Gas response simulation

Figure 4.17 shows the results of simulations performed using polymer resistors of 10 k $\Omega$  at 40°C under the second passivation method. Gas and humidity concentrations of 1000 ppm and 5000 ppm, respectively, were applied to the sensors terminals.

The changes in resistances of active and passive sensors are shown in figures 4.17 (b) and (c). The output signals from ratiometric and offset sections are also shown. The combination of these variations produces an output which is derived from the modelled response of the chemoresistors (Equation 4.3) and from the ratiometric circuit behaviour, described in section 2.5. The differential input to the amplifier is depicted in Figure 4.17 (f) and the output signal of the gas sensor section is shown in Figure 4.17 (g).

#### 4.5.3.2 Temperature simulation

Figure 4.18 shows the percentage variation of the circuit output voltage with varying sensor temperature. The two sensor configurations depicted in Figure 4.16 are taken into account. The ratiometric configuration shows less sensitivity to temperature variation compared to a single discrete circuit. In particular, the baseline output value is not sensitive to the temperature variation when the configuration with reference gas (two separate inlets) is adopted. These results can be observed in the curves for the ratiometric circuit with  $C_{Ha} = C_{Hp}$ , depicted in figures 4.18 (a) and (b).

This occurs, as expected, because the sensors are assumed to be fabricated under the same conditions and thus should respond to temperature changes with the same coefficient. The plots in figures 4.18 (c) and (d) show that the ratiometric circuit has superior performance when compared to a single chemosensor circuit exposed to gas at different temperatures.



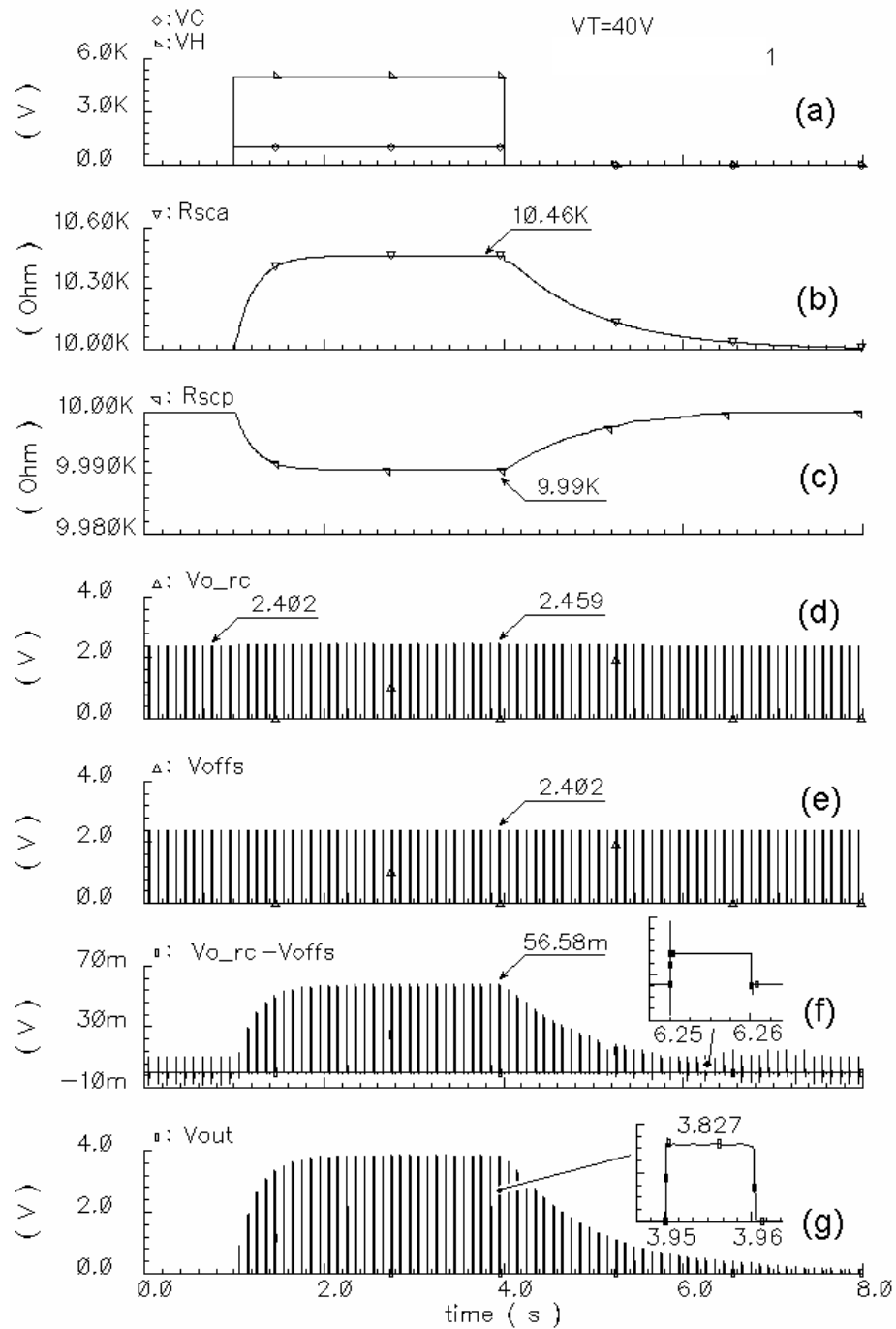


**Figure 4.17** Gas response of the ratiometric circuit for active and passive baseline resistances of  $10\text{ k}\Omega$  at  $40^\circ\text{C}$ , gas concentration = 1000 ppm, water vapour mixed to the gas = 5000 ppm. (a) Voltage pulses applied to the sensor cell SCA simulating the humidity and gas concentration ( $1\text{ V} \leftrightarrow 1\text{ ppm}$ ); (b) resistance of the active sensor; (c) resistance of the passive sensor; (d) output voltage of the ratiometric circuit; (e) output voltage of the offset circuit; (f) differential input of the instrumentation amplifier; (g) output of the gas sensor section.

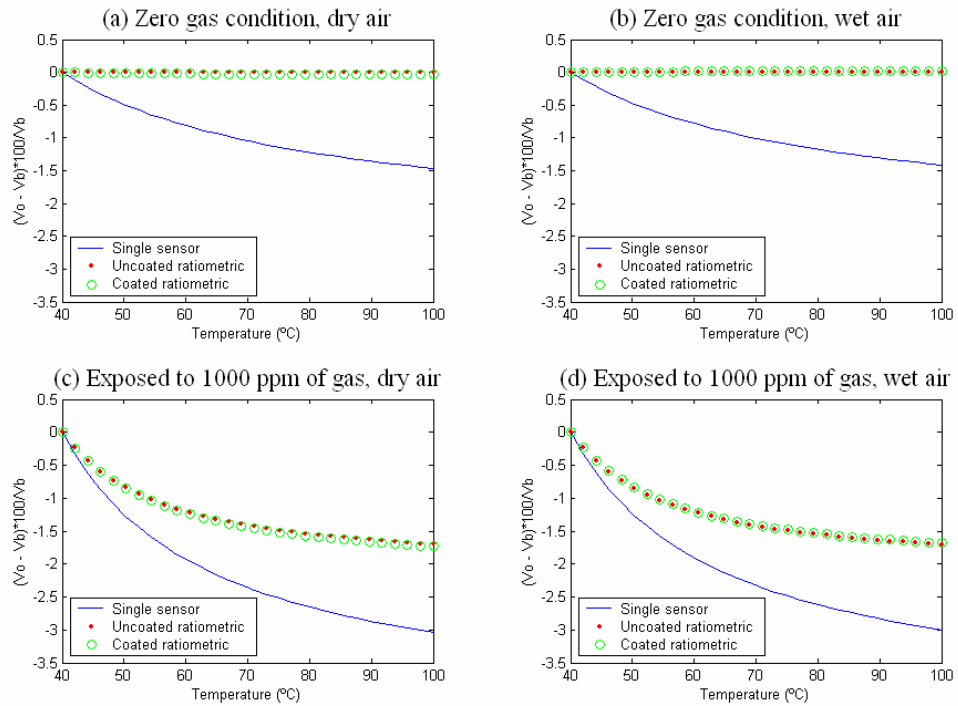


**Figure 4.18** Simulation of the variation of output voltages with changes in sensor temperature.

#### 4.5.3.3 Humidity simulation

The ratiometric circuit shows also better performance in terms of linear humidity dependence<sup>3</sup> (Figure 4.19). The water vapour effect is cancelled in the reference sensor  $SC_p$  when this one is not coated and the two-inlet configuration shown in Figure 4.16 (b) is adopted ( $C_{Ha} = C_{Hp}$ ). If the reference sensor  $SC_p$  is coated with an inert material, as in Figure 4.16 (a), the humidity effect cannot be annulled (ratiometric curves for  $C_{Ha} \neq C_{Hp}$  in Figure 4.19) but the ratiometric circuit is still less sensitive with respect to the voltage divider configuration.

<sup>3</sup> The model adopted here assumes that there is no competition between the gas and water molecules, i.e. the law of linear superposition applies. The model could be changed for a competitive one, e.g. for electroactive conducting polymers.

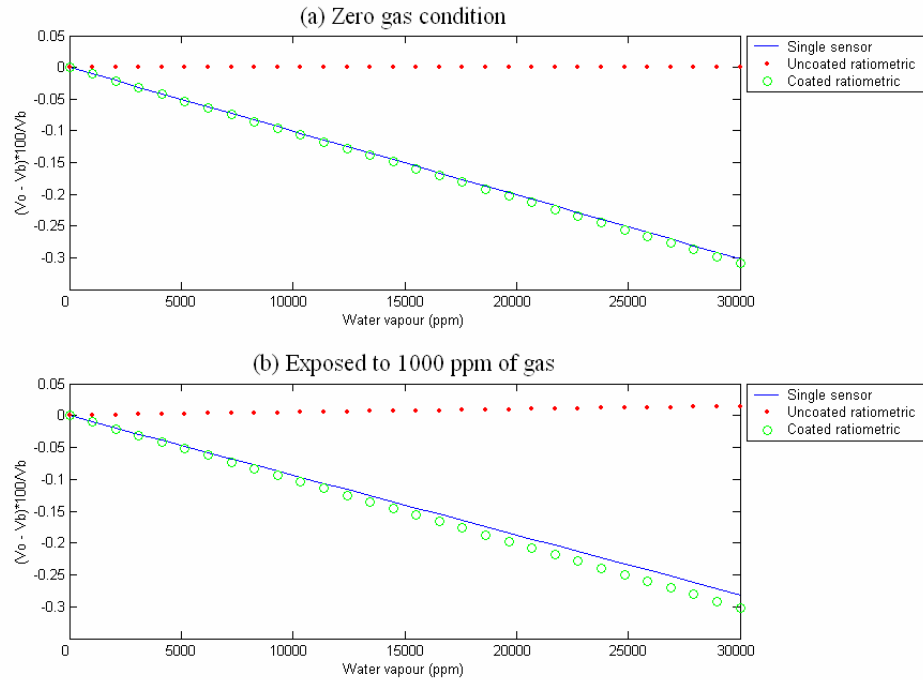


**Figure 4.19** Simulation of the effect of water vapour concentration.

#### 4.5.3.4 Noise simulation

Noise simulation was also performed based on the model developed. Figure 4.20 shows the simulated noise analysis of the ratiometric circuit. It should be noted that in carbon-black polymer resistors flicker noise<sup>4</sup> dominates the thermal noise over the frequency range shown [4].

The operational amplifier CFOA23 (Figure 4.15) gives the main contribution to the total output noise. The RMS value of the noise voltage at the ASIC chip output is evaluated from the simulation results to be  $v_n = 33 \mu\text{V}$ . Considering a RMS signal output of 3.3 V the signal-to-noise ratio is:

$$SNR = 20 \log \left( \frac{3.3}{33 \mu} \right) = 100 \text{ dB} \quad (4.6)$$

<sup>4</sup> Noise was generally 1/f; however possibility of 1/f<sup>2</sup> noise is under investigation.

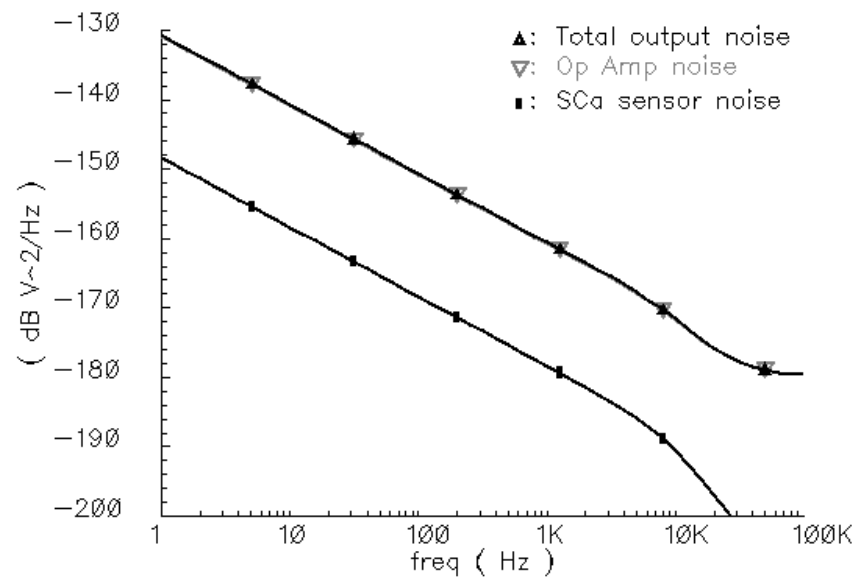


**Figure 4.20** Noise power spectral density at the ratiometric circuit output (From d'Amico, University of Torvegata, Rome).

## **4.6 CONCLUSIONS**

The performance of each part of the circuit was tested prior to fabrication, with the use of available library parameter models provided by AMI Semiconductor and by predicting the required additional parameters for the custom designed components. In particular, a generalised parametric model was developed for the chemoresistive sensors, and it was used for the simulation of the response of the whole smart sensor system.

Simulations show that every component of the ratiometric ASIC chip performs according to the expectations and predicts superior performance to a conventional single resistive polymer sensor. On-chip compensation of temperature and humidity variations, and pulsed-mode cancellation of polarisation effects and voltage-induced drifting, were built-in to the simulations.

## 4.7 REFERENCES

1. Horowitz, P. and Hill, W. (1989). *The art of electronics*, 2nd ed., Cambridge University Press. New York, USA.
2. Gardner, J.W., Varadan, V.K. and Awadelkarim, O.O. (2001). *Microsensors, MEMS, and smart devices*, John Wiley & Sons, Ltd., Chichester, England.
3. Bell, D.A. (1985). *Noise and the solid state*, Pentech Press, London.
4. Briglin, S.M., Freund, M.S., Tokumaru, P., Lewis, N.S. (2002). "Exploitation of spatio-temporal information and geometric optimisation of signal/noise performance using arrays of carbon black-polymer composite vapor detectors", *Sensors and Actuators B*, **82**, 54-74.
5. Kolek, A. and Dzedzic, A. (2000). "Low-frequency noise of polymer thick-film resistors: analysis of volume and contact effects", *Proceedings 22nd International Conference on Microelectronics*, Nis, **2**, 531-534.
6. Dzedzic, A. and Kolek, A. (1998). "1/f noise in polymer thick-film resistors", *J. Phys. D: Appl. Phys.*, **31**, 2091-2097.
7. Cole, M., Olivieri, N., Garcia-Guzman, J., and Gardner, J.W. (2003). "Parametric model of a polymeric chemoresistor for use in smart sensor design and simulation", *Microelectronics Journal*, **34**, 865-875.
8. Samitier, J., López-Villegas, J.M., Marco, S., Cámara, L., Pardo, A., Ruiz, O. and Morante, J.R. (1994). "A new method to analyse signal transients in chemical sensors", *Sensors and Actuators B*, **18/19**, 308-312.
9. Gardner, J.W., Llobet, E. and Hines, E.L. (1999). "PSPICE model for resistive gas and odour sensors", *IEE Proc.-Circuits Devices Syst.*, **146**, No. 3, 101-104.
10. Llobet, E., Vilanova, X., Brezmes, J., López, D. and Correig, X. (2001). "Electrical equivalent models of semiconductor gas sensors using PSpice", *Sensors and Actuators B*, **77**, 275-280.

# RATIOMETRIC ASIC CHIP LAYOUT AND CHECKING

## 5.1 INTRODUCTION

A description of the layout views of the whole ASIC chip and of each cell included in the design is presented in this chapter. AMI Semiconductor cells are described in terms of functionality and a brief explanation of the bias strategy required by the 0.7  $\mu\text{m}$  CMOS technology is included for a better understanding of the overall design.

Whenever appropriate, details of the custom-designed cells are given and some calculations are also included. Design parameters that were used for the simulations presented in the previous chapter are annotated together with the layout views of the cells.

Verification and rule checking steps are also reported in this chapter, and a summary of the post layout testing is also included.

## 5.2 CAD AND TECHNOLOGY CONSIDERATIONS

The layout view for the ASIC chip was obtained with the *Virtuoso* layout editor included in Cadence™ IC version 4.4.3 software package. It was designed according to the layout rules of the AMI Semiconductor 0.7  $\mu\text{m}$  CMOS technology and it was fabricated through the *Europractice IC Service* at the *Interuniversity MicroElectronics Center* (IMEC), Belgium.

Although Cadence™ IC software offers extended capabilities for the design of layout views derived from the schematic views, and for the complete verification of the correspondence between equivalent views of a given design, it is always limited by the availability of the required sets of parameters in the technology selected for the design.

In the case of the AMI Semiconductor 0.7  $\mu\text{m}$  silicon CMOS process, parameter models for the components were obtainable but a direct link between schematic and layout views was not available for the automated synthesis of the design. This led to the need of a complete step-by-step design process for the layout views, and it also impeded the direct use of the electrical verification tools included in the Cadence™ software.

However, the support provided by the *Europractice IC Service* team at IMEC, complemented the verification process and aided the design by running several tests with the software available in Belgium while the required modifications to the design were performed at the Warwick SRL laboratories.

As a result, the ASIC chip design was optimised by the use of the most up to date CAD software and technology libraries available. Verification and rule checking



was also exhaustively performed through state-of-the-art software in order to ensure the proper functioning of the design.

The AMI Semiconductor 0.7  $\mu\text{m}$  CMOS C07M-A technology is a mixed Analogue/Digital process, derived from an originally pure digital process but extended by precision resistors and capacitors, plus an additional special PMOS transistor. It is a single polysilicon and double metal layer process.

Standard cell libraries in the process include the digital libraries MTC-22000, MTC-22200, MTC-22400, MTC 23000, and the analogue library MTC-22500, whose characteristics are further described in Appendix B. Access to the libraries and layout rules, as well as support for the use of this technology, was obtained via the *Europractice IC Manufacturing Service*.

As mentioned in Chapter 3, the choice of the AMI Semiconductor 0.7  $\mu\text{m}$  CMOS technology forced the use of some special cells. In particular, the bias cells, demanded mainly by amplifiers, increased the complexity of the overall design.

## 5.3 LAYOUT VIEWS

The layout views of every component on the design are described in this section. Standard cells are described first and then every cell that was custom designed for this project. Then, a description of the interconnections and distribution of the cells is presented, showing also the characteristics of the elements provided for the external connectivity of the chip. Finally, an overall view of the circuit layout is shown.

### 5.3.1 Standard cells

Several standard cells were selected directly from the AMI Semiconductor libraries for the design of the components of the circuit, whenever those were appropriate for the purposes of the project. These standard cells are described here in terms of its functionality within the design of this ASIC chip in particular.

#### 5.3.1.1 *GBDA\_Bandgap*

This cell produces an output voltage that is equal to the bandgap voltage of silicon. Its functionality and schematic view have already been described in section 3.3.1, because it is the same cell that was used to obtain the voltage reference for the circuits. As explained previously, it requires the use of the bias cell *GBDA\_BG\_bias*, and together with this one they constitute one of the largest building blocks used in the chip.

The bandgap cell is used to obtain the reference voltage needed for the temperature set-point described in section 3.4.2, and again to produce the voltage signals that feed the bias cells (section 3.5.2).

Figure 5.1 shows the general aspect and metal frames of the bandgap cell and its associated bias cell as they were assembled within the ASIC chip structure.

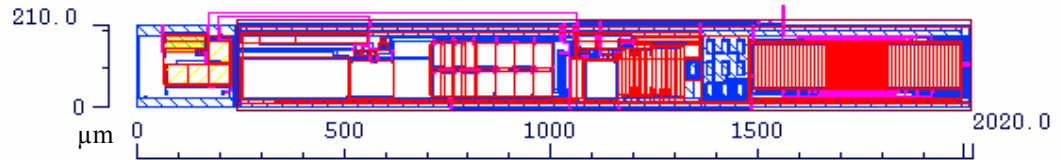


**Figure 5.1** General aspect of cells *GBDA\_Bandgap* and *GBDA\_BG\_bias*.

### 5.3.1.2 Bias strategy and required cells

In analogue cells, components are often biased with a controlled amount of current in order to set them to their required characteristics. The particular bias strategy required by the 0.7  $\mu\text{m}$  CMOS technology avoids the use of individual bias-current generators in each cell, using instead a reference current which is generated only once and is distributed to the whole circuit. This strategy is illustrated in the block diagram in Figure 5.2.

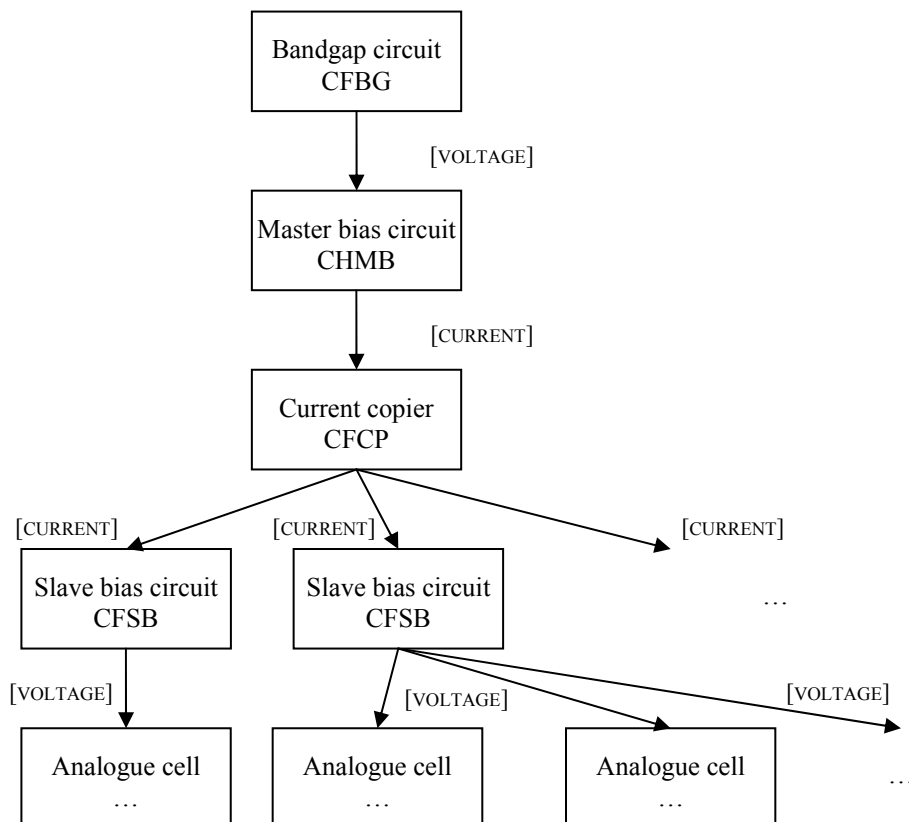


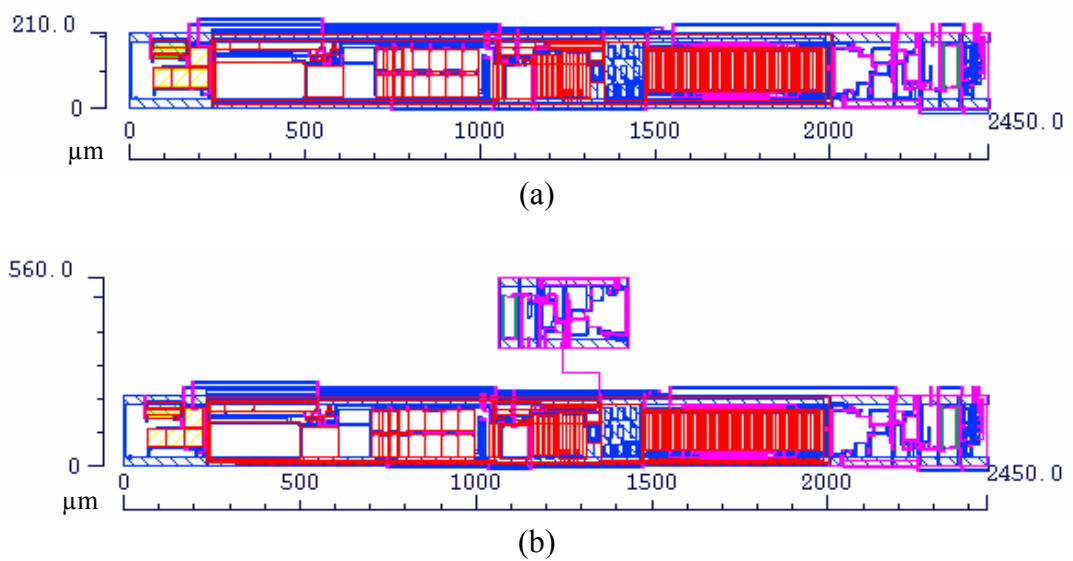
**Figure 5.2** Bias strategy for the AMI Semiconductor 0.7  $\mu\text{m}$  CMOS technology.

A constant voltage is generated by the bandgap cell, as explained before. Then, the voltage is converted to a reference current in the *master bias circuit* CHMB1, which in turn feeds the *current copier* CFCP1. From this cell, copies of the master reference current can be provided to the *slave bias circuit* cells CFSB2 which convert the reference currents into bias voltages because they are needed by operational amplifiers and other analogue cells.

The symbols and main characteristics of the cells involved in the bias process are summarized in Table 5.1.

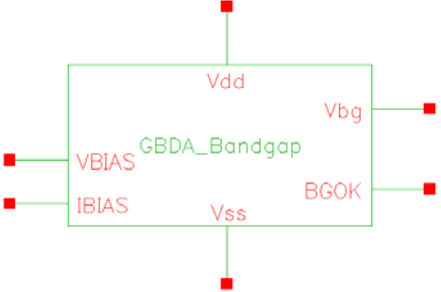
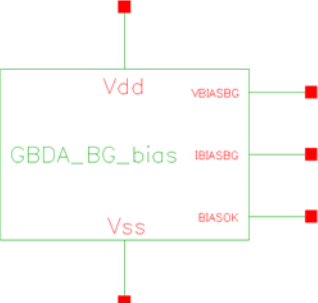
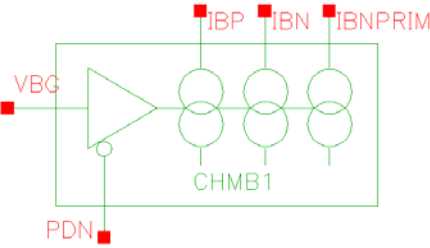
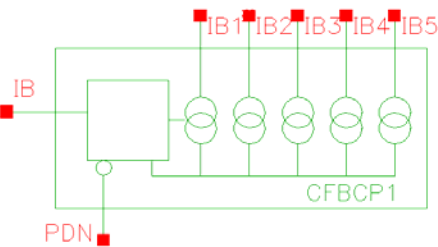
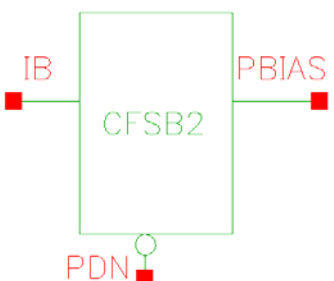
A power-down (PDN) terminal is available in each analogue cell for cutting the current when required. The pin must be high (5 V) during normal operation and low (0 V) when in power-down mode.

All the required bias cells were integrated in the cells *BIAS1* and *BIAS2* previously described in Chapter 3. The general aspect of the resulting layout views of *BIAS1* and *BIAS2* are shown in Figure 5.3.



**Figure 5.3** General aspect of cells (a) *BIAS1* and (b) *BIAS2*.

**Table 5.1** Symbols and functions of standard cells in the bias process.

| Cell                                | Symbol   | Function  |
|-------------------------------------|--|---|
| <i>Bandgap</i><br>GBDA_Bandgap      |    | Generates a reference voltage equal to the bandgap voltage of silicon.          |
| <i>Bandgap bias</i><br>GBDA_BG_bias |    | Produces the voltage and current required to bias the bandgap cell.             |
| <i>Master bias circuit</i><br>CHMB1 |  | Generates the reference current from the output voltage of the bandgap circuit. |
| <i>Current copier</i><br>CFBCP1     |  | Takes a reference current and generates several copies of that.                 |
| <i>Slave bias circuit</i><br>CFSB2  |  | Converts the reference current to bias voltage.                                 |

### 5.3.1.3 Operational amplifier

The standard operational amplifier selected for the ASIC chip was the two-stage cell CFOA23, whose main characteristics are given in Table 5.2. The cell needs to be biased with a reference voltage, which is obtained through the slave bias cell CFSB2, that is biased at 5  $\mu\text{A}$ . This cell needs to be placed as close as possible to the operational amplifier cell, in order to minimize voltage drops in the supply lines.

**Table 5.2** Main characteristics of operational amplifier CFOA23.

|                        |                    |
|------------------------|--------------------|
| Minimum supply voltage | 2.7 V              |
| Maximum supply voltage | 5.5 V              |
| Minimum DC Gain        | 100 dB             |
| Gain bandwidth         | 350 kHz            |
| Cell width             | 468 $\mu\text{m}$  |
| Minimum output current | -340 $\mu\text{A}$ |
| Maximum output current | +340 $\mu\text{A}$ |

### 5.3.2 Custom and semi-custom designed cells

Several cells were designed specifically for this research project, and some others were constructed from generic standard cells that were adapted to the particular requirements of the design. This section summarizes the characteristics of these cells, giving particular details of their layout views.

#### 5.3.2.1 Sensor electrodes and heaters

The sensor area of the layout is shown in Figure 5.4. The electrodes, in layer *Metal2*, are 96  $\mu\text{m}$   $\times$  96  $\mu\text{m}$  in size, with 80  $\mu\text{m}$  inter-electrode gap, in order to achieve

resistance of approximately 10 k $\Omega$  when using the carbon-black polymer composite films made in the SRL [1]. Overlay openings of 76  $\mu\text{m} \times 76 \mu\text{m}$  down to layer *Metal2* were specified for the post-CMOS deposition of the sensing materials, altering intentionally the layout rules but still following the standard CMOS process. However, although special care was given to the geometry of the electrodes, the actual resistance of the sensors was difficult to control due to variation in the film thickness and precise carbon loading in the semi-automated deposition process.

The heaters are constructed underneath the electrodes in the layer *Metal1*, which has a nominal sheet resistance of 50 m $\Omega$ /sq. Each heater has a nominal design resistance of 50  $\Omega$ , obtained from a metal serpentine with a width of 4  $\mu\text{m}$  and an approximate length of 4000  $\mu\text{m}$ . Metal spacing is 3  $\mu\text{m}$ . An opening has been provided in the centre of the heater in order to allocate a thermodiode, also shown in Figure 5.4.

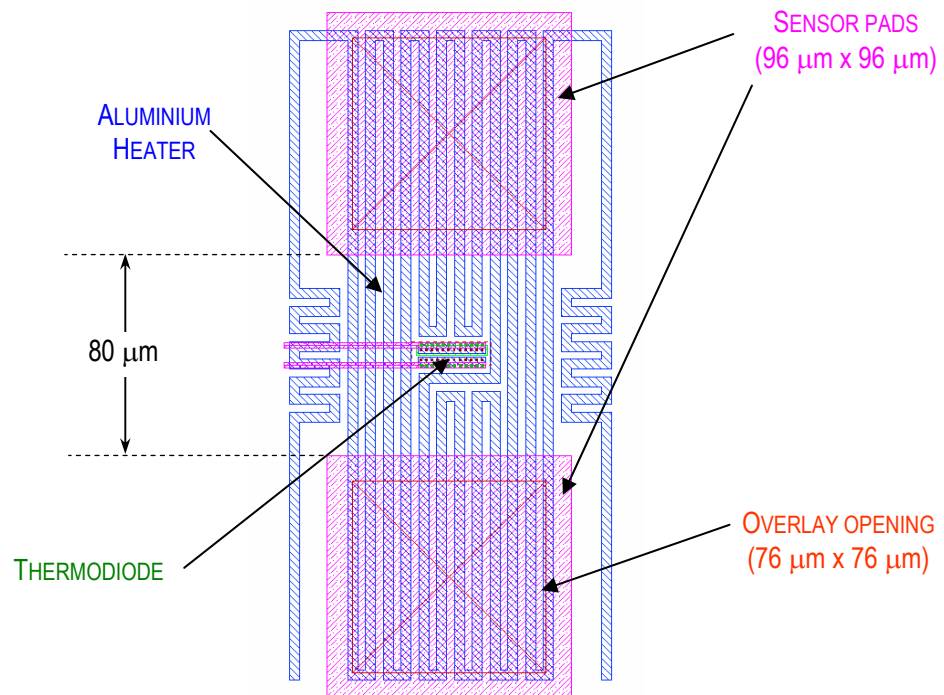


**Figure 5.4** Layout view of the sensor area.

### 5.3.2.2 Diode

The thermodiodes are placed in the centre of the heater regions, just between the electrodes. Figure 5.5 shows the layout view of the diode, custom designed for this project using the junction from  $P+$  diffusion to  $Nwell$  region, forward biased for measuring the anode voltage with respect to ground.

These thermodiodes are used for each sensor region, as shown in Figure 5.4, and for the temperature monitoring of the centre of the ASIC chip.

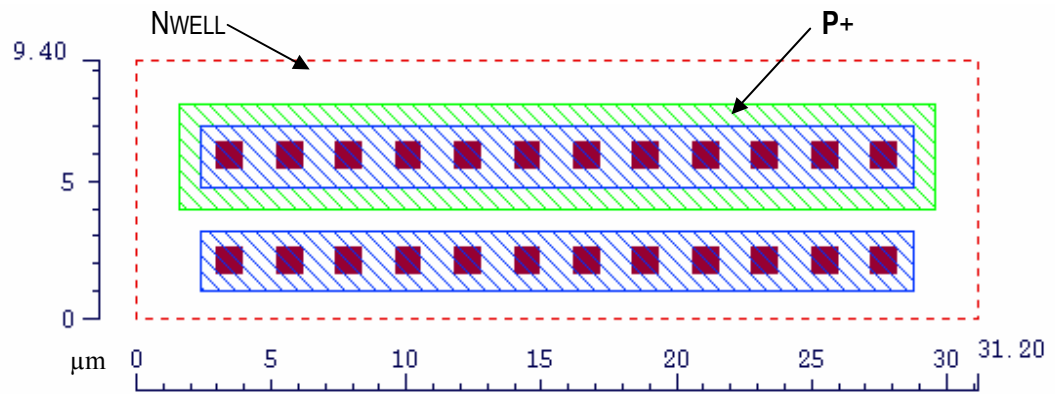


**Figure 5.5** Layout view of the custom designed thermodiode.

### 5.3.2.3 Capacitors

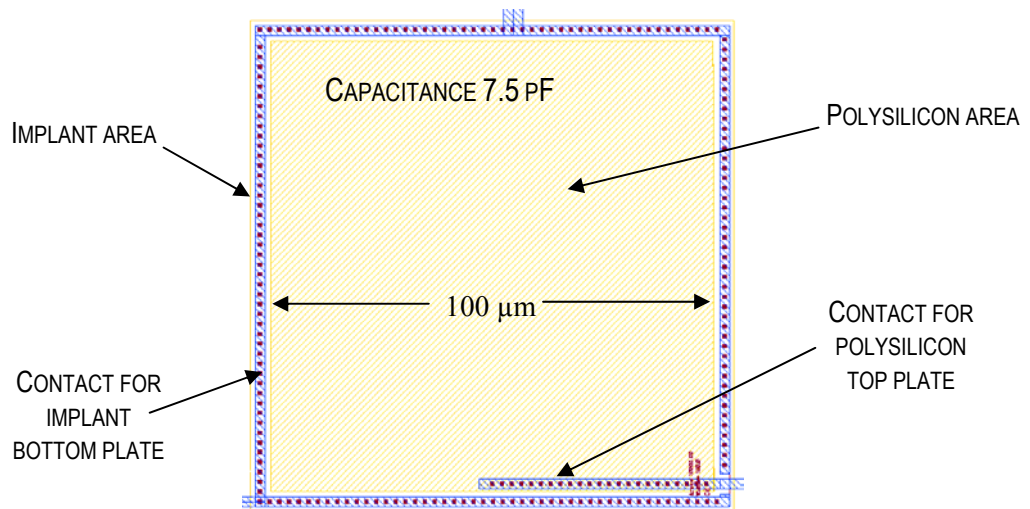
Capacitors were obtained from the cell *npc\_poly\_cap* available in the libraries for the analogue version of the AMI Semiconductors process, C07M-A. This cell allows the semi-custom design of precision analogue capacitors, formed between a bottom plate made with implanted N-type dopants and a top plate defined by a polysilicon mask over active area. The nominal capacitance per unit area is calculated to be  $0.75 \text{ fF}/(\mu\text{m})^2$ .



**Table 5.3** Specifications for the layout of capacitors.

| Instance  | Used in cell           | Capacitance (pF) | Area ( $\mu\text{m}^2$ ) | Width ( $\mu\text{m}$ ) |
|-----------|------------------------|------------------|--------------------------|-------------------------|
| Ca1 = Ca2 | Bessel low-pass filter | 20.0             | 26667                    | 163.3                   |
| Cb1       | Bessel low-pass filter | 14.7             | 19600                    | 140.0                   |
| Cb2       | Bessel low-pass filter | 7.5              | 10000                    | 100.0                   |
| Cd        | Current drive circuit  | 7.5              | 10000                    | 100.0                   |

Four capacitors were used in the Bessel low-pass filter and two more in the current drive circuits. The data for all of them are summarised in Table 5.3 and the layout of one of them is shown in Figure 5.6.

**Figure 5.6** Layout view of a 7.5 pF capacitor.

#### 5.3.2.4 Resistors

Two types of resistors were used in the layout of the ASIC chip: Nwell resistors in most of the cases, obtained from the cell *npc\_Nwell\_res*, and high ohmic polysilicon (HIPO) resistors when higher resistances were required, obtained from the cell *npc\_hipo\_res*. Both cells are available in the libraries of the C07M-A process.

HIPO resistors are a special type of component created by defining low doped polysilicon regions in order to achieve high sheet resistance. Nominal sheet resistance for HIPO resistors that are more than  $2\ \mu\text{m}$  wide is  $2000\ \Omega/\text{sq}$ , whereas the sheet resistance for Nwell resistors is between 1200 and  $1400\ \Omega/\text{sq}$ .

Whenever possible, resistances values chosen were  $10\ \text{k}\Omega$ , trying to match the expected resistance of the polymer sensors. Resistors in the Bessel low-pass filter, which had the highest values in the ASIC in order to allow reasonable sizes for the capacitors, were designed with HIPO type, being  $3\ \mu\text{m}$  in width and calculated with the nominal sheet resistance of  $2000\ \Omega/\text{sq}$ . The rest of resistors in the design are Nwell type, with  $5\ \mu\text{m}$  in width, and calculated at  $1200\ \Omega/\text{sq}$ .

The specifications for the layout of every semi-custom resistor designed in the ASIC chip are given in Table 5.4.

**Table 5.4** Specifications for the layout of resistors.

| Instance | Used in cell        | Type  | Resistance (k $\Omega$ ) | Width ( $\mu\text{m}$ ) | Sheets $\times$ resistors |
|----------|---------------------|-------|--------------------------|-------------------------|---------------------------|
| Ra1      | Bessel filter       | HIPO  | 402                      | 3                       | $67 \times 3$             |
| Rb1      | Bessel filter       | HIPO  | 1050                     | 3                       | $35 \times 15$            |
| Ra2      | Bessel filter       | HIPO  | 687                      | 3                       | $68.7 \times 5$           |
| Rb2      | Bessel filter       | HIPO  | 956                      | 3                       | $23.9 \times 20$          |
| Several  | Several             | Nwell | 100                      | 5                       | $83.33 \times 1$          |
| Several  | Several             | Nwell | 10                       | 5                       | $8.333 \times 1$          |
| Several  | Several             | Nwell | 1                        | 5                       | $0.8333 \times 1$         |
| R1       | Current drive       | Nwell | 13.3                     | 5                       | $11.11 \times 1$          |
| R2       | Current drive       | Nwell | 66.67                    | 5                       | $55.56 \times 1$          |
| R2       | Amplifier for diode | Nwell | 6                        | 5                       | $5 \times 1$              |

Figure 5.7 shows the layout views of two of the designed resistors. The first one is the most used  $10\text{ k}\Omega$  Nwell resistor and the second one is the  $1.05\text{ M}\Omega$  HIPO resistor. Views are not at the same scale.

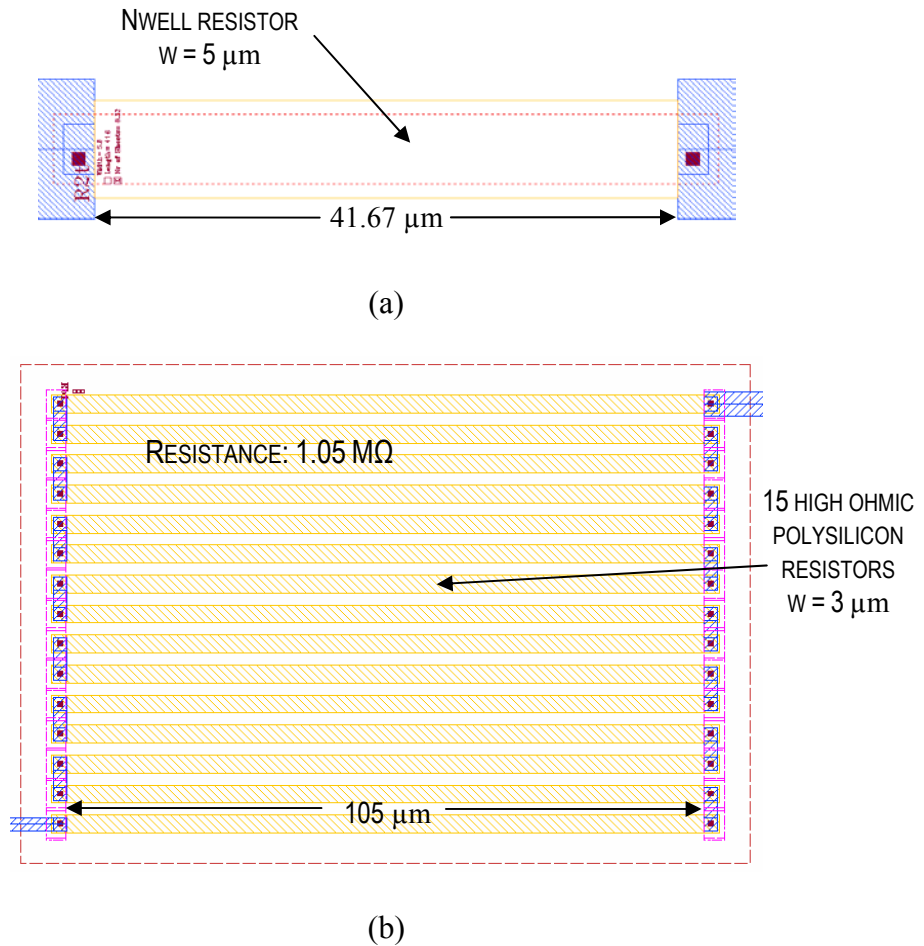


**Figure 5.7** Layout view of: (a)  $10\text{ k}\Omega$  Nwell resistor; (b)  $1.05\text{ M}\Omega$  HIPO resistor.

### 5.3.2.5 NMOSFETs

Semi-custom designed NMOSFETs were obtained starting with the cell *npc\_Mos* available in the libraries of the analogue process C07M-A. Figure 5.8 shows the layout view of the NMOSFET used in the current drive circuit, which consists of the parallel combination of four individual cells although it was actually designed as a cell with four gates.

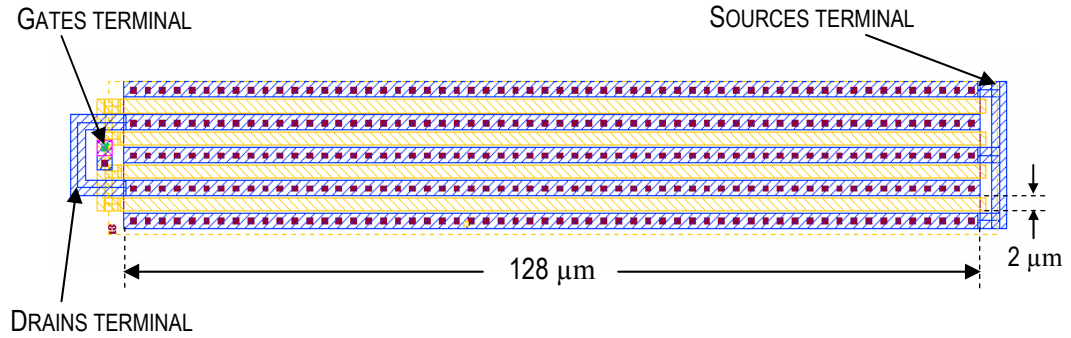


**Figure 5.8** Layout view of the NMOSFET used in the current drive circuit.

All the NMOSFETs designed for the ASIC chip have the dimensions shown in Figure 5.8, varying only in the number of gates. There are six gates or parallel cells in each of the FET-switches used to alternate the signal in the gas sensor circuit, and only one gate in the FET receiving the pulsed signal  $V_{gates}$  (see Figure 3.4).

Additional connections were required for the substrate by the sides of the NMOSFETs. These can be seen in Figure 5.9, which shows the array used to switch alternatively the terminals of the polymer gas sensors. Four switches, each one consisting of six parallel NMOSFETs, are interconnected and placed near each electrodes area.

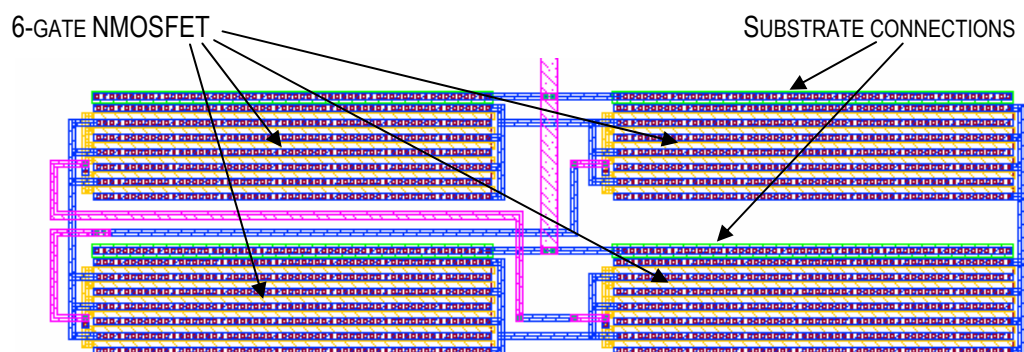


**Figure 5.9** Layout view of the switches array.

### 5.3.3 Cells distribution and overall layout view

All the analogue cells in the libraries of the C07M-A process have a height of 210  $\mu\text{m}$ , with different widths. Each cell is surrounded by P+ diffusion at substrate voltage, sharing this P+ ring with the neighbouring cells. Analogue pins are placed at the top side and digital pins are at the bottom side. Power and ground lines, built in *Metal1* layer, are 25 micron width each and they are placed at the top and the bottom of the cell respectively. [2].

Whenever it was possible, the cells were distributed symmetrically along eight rows, sharing the power lines and trying to minimise the distances for the connections between components. Slave bias cells were always placed in the same row as the cells they bias. Semi-custom designed components were placed at the top side of the standard cells to which they are primarily connected.

Figure 5.10 shows the actual location of every main functional block in the final layout view of the ASIC chip.

The electrodes for the gas sensors are placed in the top left and bottom right corners, just in front of the corresponding set of FET switches and the row containing the temperature compensator and the current drive circuit.

The bias cells are placed near the circuits that they are biasing, minimising in this way the lengths of connections. The instrumentation amplifier and the Bessel low-pass filter are located in the second row from top, with several operational amplifiers sharing voltage bias cells.

The two middle rows contain the voltage reference cells, one of them providing the signal for the ratiometric gas sensor and offset circuits, and the other,

located below, for the temperature set-point. The operational amplifier at the left of the first voltage reference corresponds to the offset circuit and the one at the right of the temperature set-point cell is the voltage follower passing the reference signal for the temperature control.

Just above the last row there are two amplifiers. The one at the left side is for the output of the temperature sensor located at the centre of the chip, which measures the operating temperature of the ASIC chip. The other amplifier corresponds to the ratiometric gas sensor circuit. The identification of the chip, which has the number SRL-194, is just at the right of these amplifiers.

The overall dimensions of the chip are 3300  $\mu\text{m}$  x 3750  $\mu\text{m}$ .

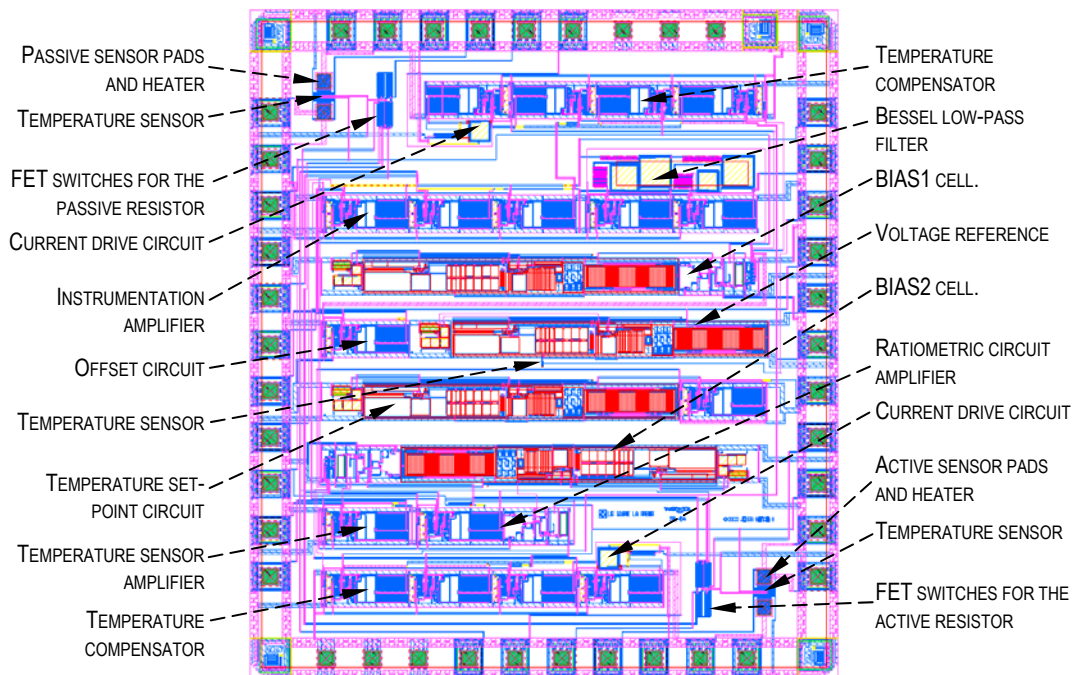


**Figure 5.10** Overall layout view of the 0.7  $\mu\text{m}$  CMOS ASIC chip.

### 5.3.4 Power rails, bondpads and ESD protection

The power rails form two rings around the cells and they contain 33 bondpads for external connections of the chip components, as well as five pads structured for *electrostatic discharge* (ESD) protection.

Figure 5.11 shows in detail one of the corners of the ASIC chip. Power lines are built into layer *Metal2*, with the ground rail in the external side. Different types of pads were used for every particular purpose.

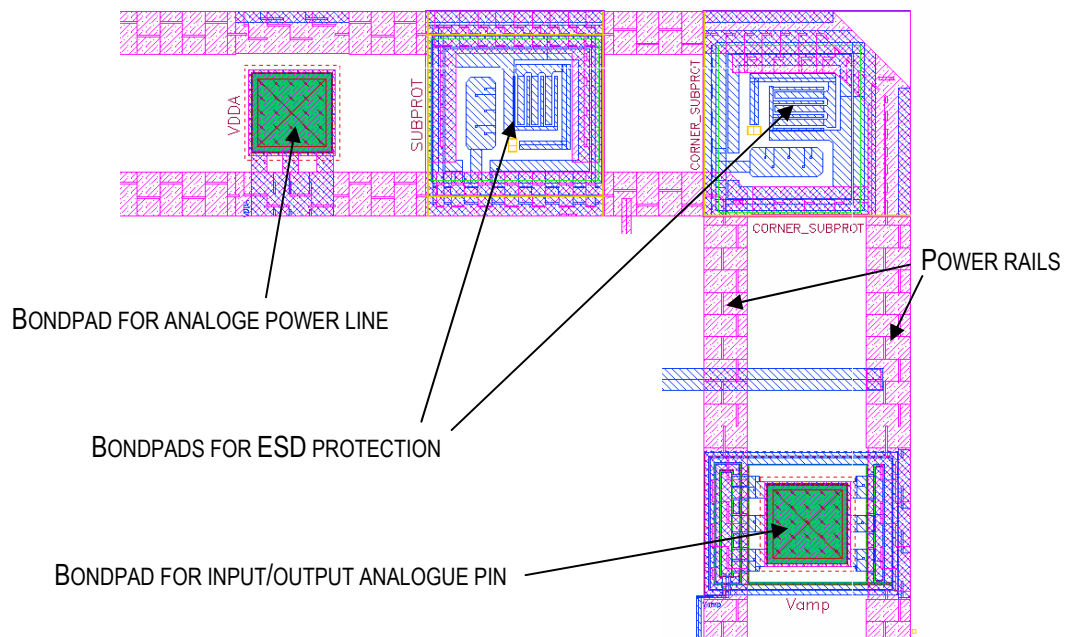


**Figure 5.11** Detail of power rails and bondpads.

Analogue pins are available for testing every component of the ASIC separately. Every point required for the monitoring of the signals reported in the simulations has been made also available. Likewise, there are pins that allow the use of some external components instead the internal ones, for testing purposes. A detailed description of the pins configuration is given in Chapter 6.

## 5.4 VERIFICATION AND RULE CHECKING

As mentioned at the beginning of this chapter, it was not possible to link directly the schematic and layout views of the design, because of the limitations in the libraries provided. However, although a direct *layout versus schematic* (LVS) test was not performed, the functionality of the layout was extensively tested and verified.

First, *Diva* check tools available within the Cadence software were used for basic *design rule check* (DRC) in the layout views. Accessed from the *Virtuoso* layout editor, *Diva* DRC was performed to verify the correspondence of the layout views with the design rules file *mtcn0u7iV.drc* provided by AMI Semiconductors. Cells and rows of cells were tested individually using the layout views of every component designed. Once the required corrections were made, verification of the whole layout view was also performed, until the design was free of edge and shape errors.

In order to attempt the LVS test, *extracted* views were obtained with the aid of the rules file *mtcn0u7iV.ext*. The extracted views were compared to the schematic views with the *Diva* LVS checker according to the rules file *mtcn0u7iV.lvs2*. A complete verification was not possible because parameters were not available for all the cells used in the design. In particular, the bandgap cell, which was new when the design was submitted for fabrication, included several error messages and warnings that affected the flow of the test.

The design was, however, extensively inspected step-by-step before sending it to IMEC for final post-layout testing.



## 5.5 POST-LAYOUT TESTING AND VERIFICATION

After running basic design rule checks with *Diva* on the layout and making all required corrections, the design was sent to the *Europractice* IMEC in Belgium for further testing and verification. Once there, the design was checked using the *Dracula* software, running more detailed tests that allowed the further detection and amendment of errors. Extracted views and verification reports were sent back to the SRL, where the *Dracula* output was fed back into the *Virtuoso* editor to locate and correct layout problems. Although design rule problems had been practically eliminated before using *Dracula*, importing its error cells over the ASIC chip layout allowed the recognition and correction of minor errors that were not detected previously by *Diva* tools.

However, the reports generated by the *Dracula* electrical rule check tool allowed the detection and correction of errors that were not considered before, and they also permitted the verification of the electrical functions of custom and semi-custom cells, namely thermodiodes, FETs, resistors and capacitors.

Finally, *substrate checks* were also performed with *Dracula* tools, allowing the correction of details about physical connections to the substrate.

After making minor modifications to the circuit layout, every design error was corrected and check passed. Only a few messages about errors that were no relevant for the aims of the project remained unattended, such as those produced by the intentionally requested openings on top of the electrode pads.

## 5.6 CONCLUSIONS

In spite of some limitations in the AMI Semiconductor technology, and after checking and verifying carefully every layout cell, a complete and reliable design was finally obtained. Special considerations were requested about the overlay openings on top of the sensor electrodes over the *Metal2* layer, as these were required for the post-CMOS deposition of the polymeric sensing materials.

The final layout design was submitted under the *Europractice IC Manufacturing Service* and approved for fabrication by IMEC in the run 730 scheduled for May of 2002. A total of 20 samples were ordered at an educational charge of €2476.

The characteristics of the actual ratiometric ASIC chips obtained after fabrication are described in the next chapter.

## 5.7 REFERENCES

1. Covington J.A. (2001). "CMOS and SOI CMOS FET-based gas sensors", PhD Thesis, University of Warwick, Coventry, UK.
2. AMI Semiconductor (2002). *Library MTC 22500*, Revision 1.0, Information accessed under permission of the proprietor.

# ELECTRICAL CHARACTERISATION OF FABRICATED RATIOMETRIC ASIC CHIP

## 6.1 INTRODUCTION

The ASIC chip was fabricated through the AMI Semiconductor 0.7  $\mu\text{m}$  standard CMOS process via the *Europractice IC Manufacturing Service* at IMEC, Belgium. The design was submitted in May 2002, and after a delay in the fabrication run, the chips were received at Warwick SRL by October 2002. Thanks to the support of the staff at IMEC, a total count of 105 ASIC chips were produced instead of the 20 samples originally requested. A photograph of the resulting chip, measuring 3.30 mm  $\times$  3.75 mm, is shown in Figure 6.1.

This chapter describes the electrical characterisation of the ASIC chip and its preparation, including bonding, packaging and the design of a single-chip electronic interface, for the testing of each component of the circuit.

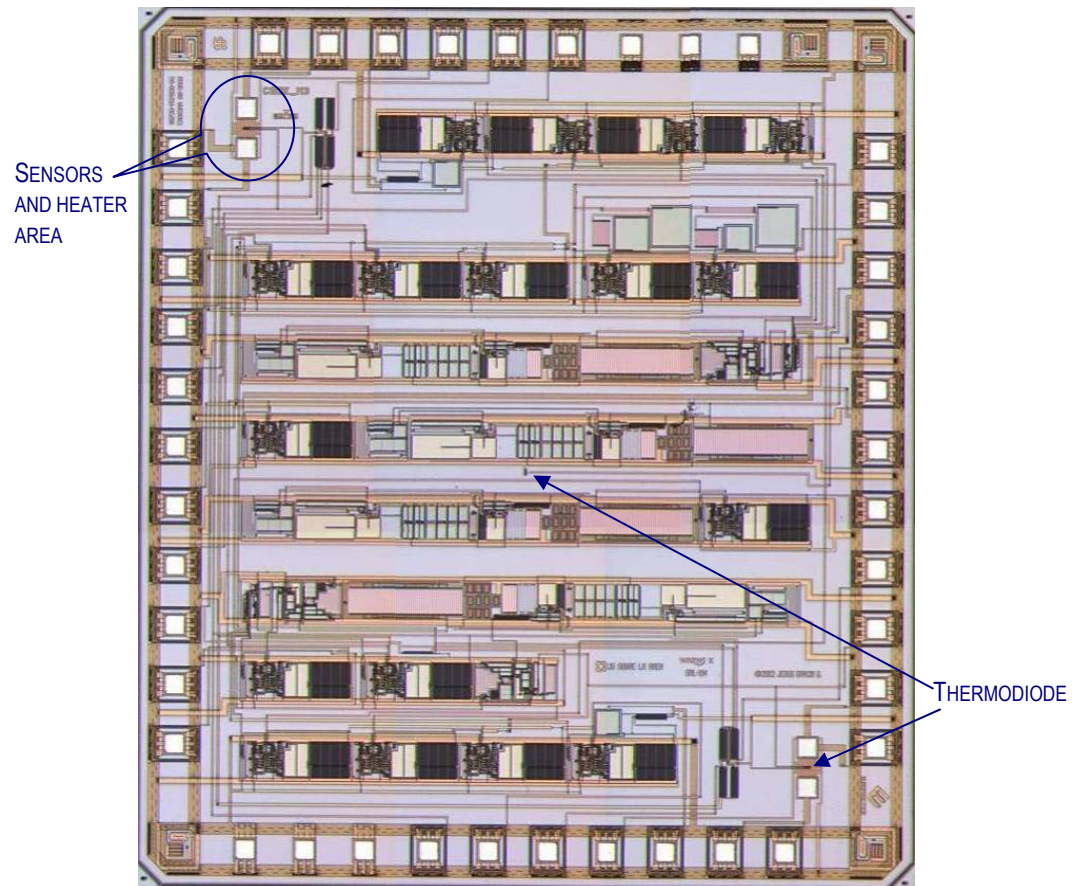


**Figure 6.1** Photograph of the fabricated ASIC chip, sized 3.30 mm × 3.75 mm.

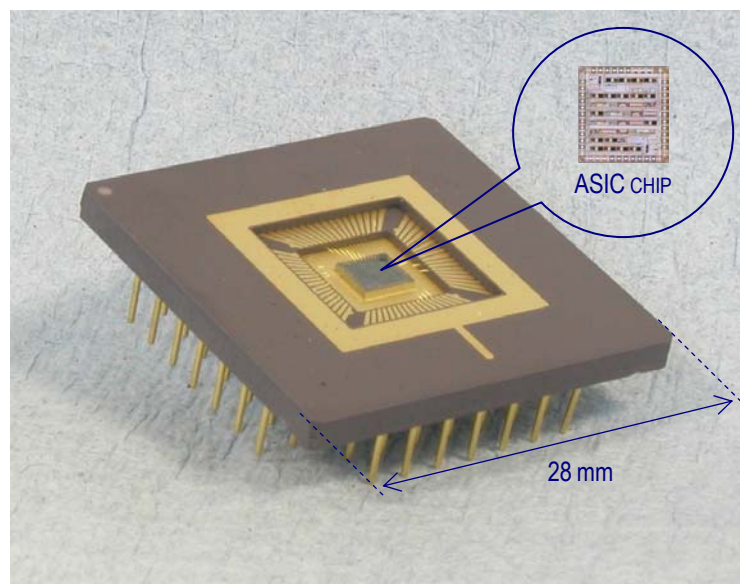


**Figure 6.2** The ratiometric ASIC chip, bonded in the PGA 68-pin package.

## 6.2 PACKAGING AND BONDING

The fabricated ASIC chips were packaged using a standard ceramic *Pin Grid Array* (PGA) 68-pin package shown in Figure 6.2. The complete list of the pins, with the names of the points of the circuit they connect, is given in Table 6.1, where the numbers in the first column correspond to the pin numbers in the package.

**Table 6.2.** Complete list of pins of the ASIC chip.

| No. | Name              | Description   |
|-----|-------------------|---|
| 5   | VSSA (GROUND)     | To be connected to 0 VDC, analogue ground                           |
| 7   | VSENSOR           | Voltage at the output of the ratiometric sensor                     |
| 8   | VCOMP_A           | Output of the temperature compensator (active resistor)             |
| 10  | RACT_PLUS_RETURN  | Return point for the “positive” terminal of the active resistor     |
| 12  | HEATER_A          | Input terminal of the heater under the active resistor              |
| 13  | VDRIVE_A          | Output of the current drive circuit (active resistor)               |
| 14  | RACT_MINUS        | “Negative” terminal of the active resistor                          |
| 22  | RACT_PLUS         | “Positive” terminal of the active resistor                          |
| 23  | TEMP_HEATER_A     | Output from the temperature sensor near the active resistor         |
| 24  | RACT_MINUS_RETURN | Return point for the “negative” terminal of the active resistor     |
| 25  | RTR2              | Terminal for the external resistor of the temperature reference     |
| 26  | VSP               | Input/return terminal for the temperature set-point                 |
| 27  | VPULSES           | Input of pulses for the voltage reference                           |
| 28  | VREF              | Output of the voltage reference                                     |
| 29  | TEMP_DIODE_IN     | Terminal of the anode of the thermodiode                            |
| 30  | VOUT              | Output voltage of the sensor section after amplifying and filtering |
| 31  | VAMP              | Output of the instrumentation amplifier                             |
| 39  | VDDA              | Analogue power supply, to be connected to +5 VDC                    |
| 41  | VCOMP_P           | Output of the temperature compensator (passive resistor)            |
| 43  | RPAS_PLUS_RETURN  | Return point for the “positive” terminal of the passive resistor    |
| 45  | HEATER_P          | Input terminal of the heater under the passive resistor             |
| 47  | VDRIVE_P          | Output of the current drive circuit (passive resistor)              |
| 48  | RPAS_MINUS        | “Negative” terminal of the passive resistor                         |
| 56  | RPAS_PLUS         | “Positive” terminal of the passive resistor                         |
| 57  | TEMP_HEATER_P     | Output from the temperature sensor near the passive resistor        |
| 58  | RPAS_MINUS_RETURN | Return point for the “negative” terminal of the passive resistor    |
| 59  | RGAIN2            | Output to the terminal 2 of the potentiometer for gain setting      |
| 60  | ROFF_EXT          | Terminal for the external potentiometer of the offset circuit       |
| 61  | VOFFSET           | Output voltage of the offset circuit                                |
| 62  | RGAIN1            | Output to the terminal 1 of the potentiometer for gain setting      |
| 63  | VGATES            | Input of pulses for the gates of the switches                       |
| 64  | TEMP_DIODE_OUT    | Terminal of the current source and input to the amplifier           |
| 65  | TEMP_ASIC         | Output of the amplifier of the thermodiode                          |

The guidelines for bonding each pin of the ratiometric ASIC chip to the external pins of the package are given in the diagram shown in Figure 6.3.

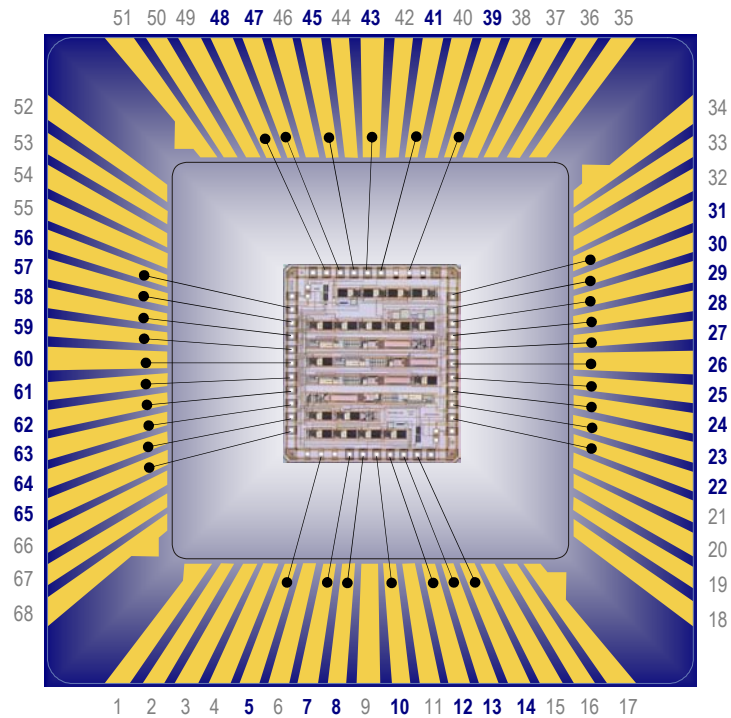


**Figure 6.3** Diagram showing the bonding guidelines for the ratiometric ASIC chip. Pins labelled with bold typeface are employed (33 out of 68).

### 6.3 PRELIMINARY SINGLE-CHIP TESTING BOARD DESIGN

In order to test and characterize the components of the fabricated ASIC chip, an interface printed circuit board (PCB) was designed. The board also served to test the implementation of both the complementary circuitry and the additional software for the use of the ASIC chip in an automated testing system. A photograph of the board fabricated in-house, designed to test a single ASIC chip, is shown in Figure 6.3.

Three digital potentiometers available in the *Xicor's* X9241A [1] chip are externally programmed in order to achieve the calibration of three signals: the offset level, the gain of the instrumentation amplifier, and the set-point of the temperature circuit. The board is also provided with a set of analogue potentiometers, selectable through jumpers, which alternatively allow manual calibration of the same signals.

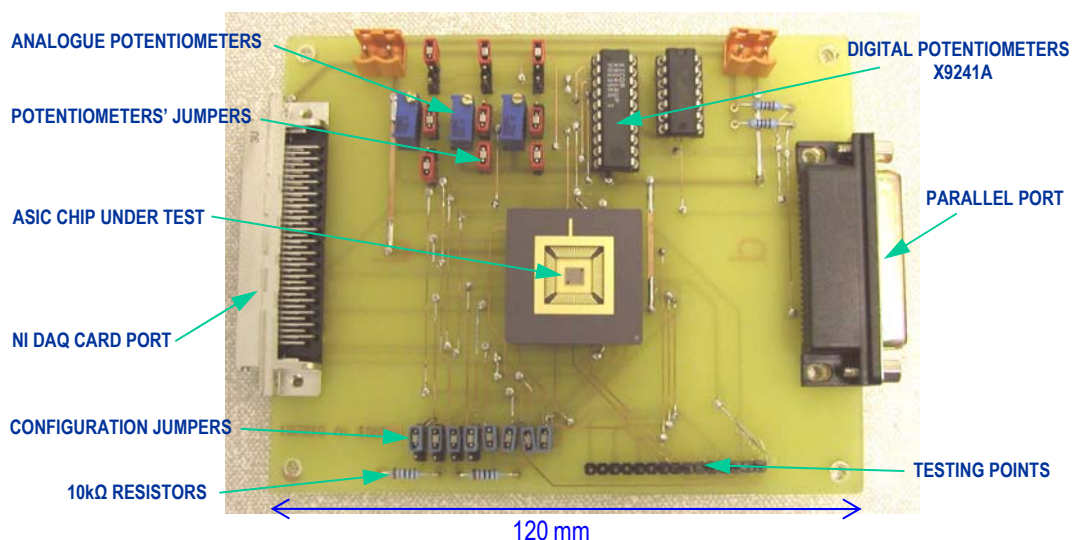


**Figure 6.4** The testing PCB for the characterisation of a single ASIC chip.

The test board is connected to a personal computer through the parallel port, for the control of the digital potentiometers, and through a *National Instruments* data acquisition card (NI-DAQ), for processing the required input and output signals. A



number of jumpers and test points were included in the design of the board to facilitate the testing of individual components of the chip at different stages.

Both the test board and the ASIC chip design allow the testing of the whole system prior to the deposition of the polymeric sensing resistors, by connecting instead a pair of precision resistors included in the board or any other set of external resistors.

*LabView*® virtual instruments (VI) have been written for both controlling and monitoring the operation of the ASIC chip. Analogue inputs and outputs can respectively be sent and obtained by means of the NI-DAQ; the processed output signals are monitored and analysed in a personal computer.

Details and specifications of the circuitry designed are given in Appendix C. Likewise, Appendix D includes a description of the virtual instrumentation written for the programming of digital potentiometers and for the automated control of the testing process.

## 6.4 ELECTRICAL CHARACTERISATION AND TESTING

Using the interface PCB described in the previous section, the ASIC chip was tested and the semi-custom designed components were characterised. First, an overall verification of signals, for both the gas sensor section and the temperature control section, was performed. Several samples of the ASIC chip were tested, using 10 k $\Omega$  precision resistors connected between the sensor electrodes. In this way, every voltage signal that was previously simulated was verified on the actual ASIC chip, showing the results expected from the simulations.

The setup for these tests consisted of basic laboratory equipment: a power supply, providing the +5 VDC required by the test board; an oscilloscope, to register the signals; a multi-meter and the ASIC chip test board. A personal computer, running *LabView* software with the virtual instruments written for the tests, was used for the control of the input and output signals, interfaced to the test board through the NI-DAQ and through the parallel port.

### 6.4.1 The voltage reference

The main signal inside the system is the output of the voltage reference cell, as it is used to drive the rest of the components of the circuit, both in the gas sensor section and in the temperature control section.

Measurements of the voltage  $V_{ref}$ , at the output of the voltage reference cell in a sample of 20 ASIC chips, averaged 1.23 V, with a standard deviation of 8.37 mV. This value was obtained when the supply voltage was  $VDD = +5$  VDC. The same magnitude was produced when pulses with a period of 100 ms and width of 10 ms were applied to the input  $V_{pulses}$ . No difference in phase was observed. The actual

output of the voltage reference cell corresponds, therefore, to the expected values of 1.2 V and 1.209 V predicted by the process specifications and the results of the simulations, respectively.

#### 6.4.2 The ratiometric gas sensor circuit

The non-inverting ratiometric array was tested with the aid of a pair of 10 k $\Omega$  precision resistors available in the PCB, connected to the corresponding operational amplifier bypassing the sensor electrodes with the aid of the jumpers provided. As these precision resistors have identical resistances, the gain of the circuit was set to 2 and the expected output was the double of the input, which corresponded to the previously tested signal  $V_{ref}$ . The average amplitude of the output  $V_{sensor}$  was 2.42 V, with a standard deviation of 8.83 mV, which is very close to the expected values.

The signals obtained in the simulations described in section 4.3.2, for the response of the ratiometric gas sensor circuit, were actually obtained in the experimental set up when the pulsed signals  $V_{pulses}$  and  $V_{gates}$  were applied to the inputs of the ASIC chip. The pulsed inputs were generated through a VI developed in *LabView* software and interfaced to the test board via the NI-DAQ (see appendices C and D).

It was observed that the semi-custom FET-switches were also working as expected, alternating the input pulses to reduce the constant voltage drifting effect, as the waveforms obtained for the voltage signals in the resistors corresponded to the simulations reported in Chapter 4.

### 6.4.3 Offset circuit

As explained in Chapter 3, the offset circuit uses the same configuration as the ratiometric gas sensor circuit. In the offset circuit, the two resistors forming the voltage divider at the output of the operational amplifier are theoretically identical, and designed to have 10 k $\Omega$  resistances.

In the actual ASIC chip, however, the resistances obtained differ from the values in the design by a significant amount as a result of variations in the fabrication process. Also, different types of resistors were used in the design of the offset circuit, as one of them is built inside the chip in the *Nwell* type, whereas the other one is obtained from the digital potentiometers in the Xicor's X9241A integrated circuit.

The offset circuit was tested by applying the voltage reference  $V_{ref}$  to the input and calibrating its output through the programmable potentiometer in such a way that the voltage  $V_{offset}$  matched the voltage  $V_{sensor}$ , obtained from the gas sensor circuit.

Variations in resistance produced no significant effects on the operation of the offset circuit, given that differences are cancelled according to the ratiometric principle. Tests showed that when the 10 k $\Omega$  precision resistors were used in the ratiometric circuit, the variable digital resistor needed to be adjusted to an average value of 16.5 k $\Omega$  with a standard deviation of 0.43 k $\Omega$  in order to obtain identical output in the offset circuit. This value corresponds to the indirect measurement of the resistance of the internal offset resistor, including the interfacing wiring and contacts.

The offset circuit worked as predicted in the design specifications. The functionality of the digital potentiometers and the controlling software was also tested.

#### 6.4.4 Amplified and filtered output

Although the voltage levels at every point of the circuit matched the values predicted by the simulations, it was found that the gain of the instrumentation amplifier was higher than expected. As it happened also within the offset circuit, the reason for this was found to be in the variations of the fabricated *Nwell* type resistors, which differ significantly from the nominal values in the design.

According to Equation 3.2, the gain of the amplifier depends on the values of the resistors  $R_1$ , built in *Nwell* type inside the ASIC chip, and  $R_{gain}$ , obtained with one of the Xicor's digital potentiometers. Measurements of gain with samples of the ASIC chip showed that the actual value of  $R_1$  was as large as 150 k $\Omega$ , which is far from the 100 k $\Omega$  specified in the design. Programmability of  $R_{gain}$ , however, allowed enough control over the gain of the circuit, being the only change with respect to the design that the minimum possible gain obtained is 7 instead of the designed value of 5. There is no maximum limit for the gain of the amplifier, but it is actually restricted by the saturation condition of the operational amplifiers. Details of the actual amplifier cell CFOA23 are given in Appendix B.

The output of the instrumentation amplifier was observed to be zero when identical signals were applied to its inputs. Positive differences  $V_{sensor} - V_{offset}$  applied to the input produced correctly amplified outputs. When negative differences were applied during the tests, the output was also reduced to zero, as it was expected from the amplifier design and the power supply limitations (0 to +5 VDC).

Figure 6.5 shows the approximately linear response of the amplifier, obtained by averaging the outputs of five samples of the ASIC chip for three different values

of gain when  $R_{gain}$  was set to 47 k $\Omega$ , 36 k $\Omega$  and 23 k $\Omega$ . The average resistance of  $R_1$  was 149.7 k $\Omega$ , with standard variation of 3.87 k $\Omega$ .

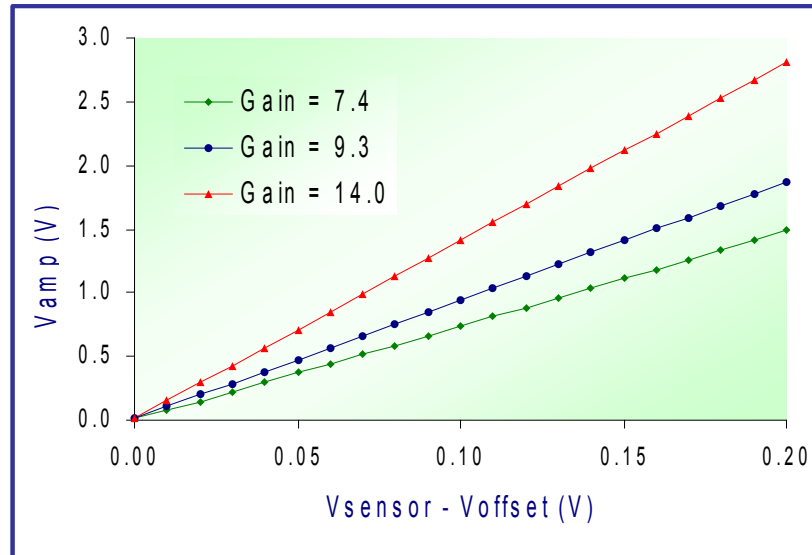


**Figure 6.5** Response of the instrumentation amplifier for different values of gain.

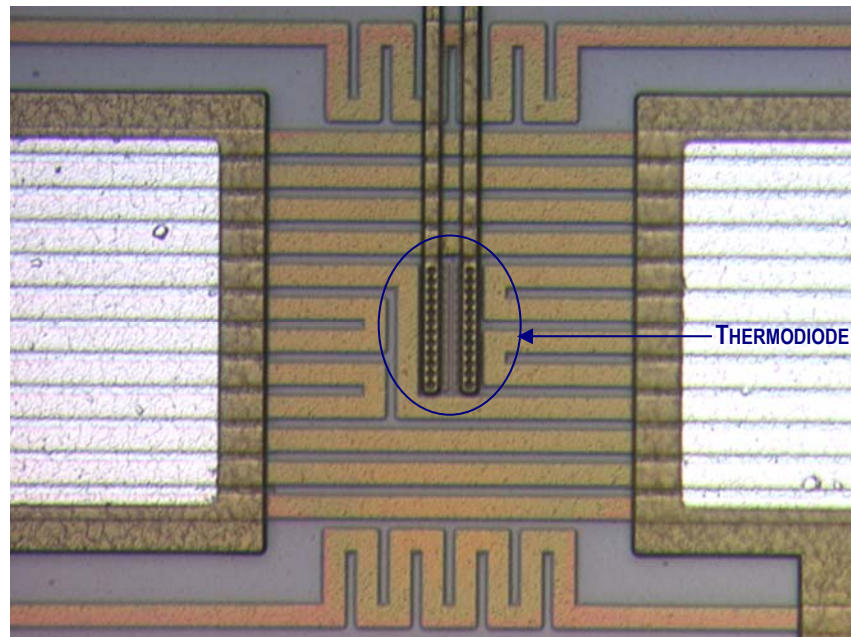
Resistors in the Bessel low-pass filter, which were fabricated in the HIPO type, matched correctly the specifications of the design. The filter response showed unity gain and no change in phase for all the measurements and this was later confirmed when the ASIC chip was used for polymeric sensors characterisation.

#### 6.4.5 Thermodiode characterisation

Characterisation of the n-p thermodiode designed for this project showed that data proposed for the simulations corresponded with a good approximation to the actual fabricated device.

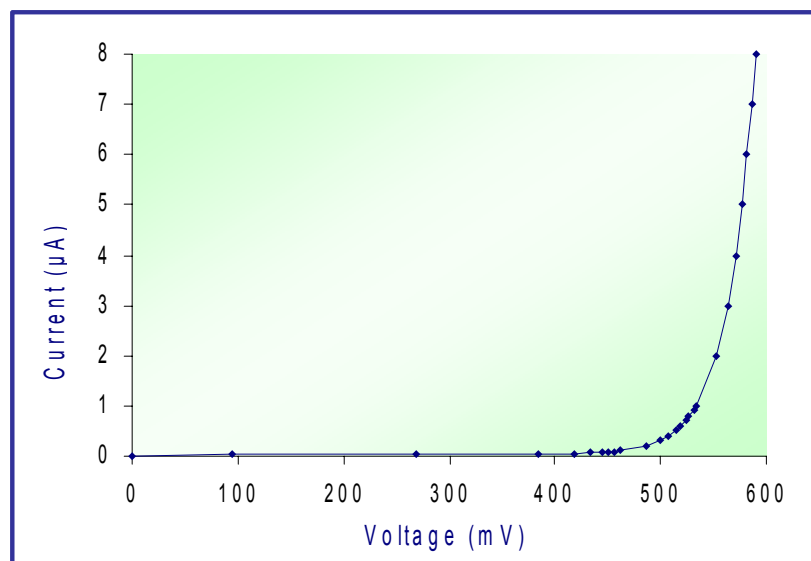
Thermodiodes are located in the middle of the space between each pair of electrodes, in the centre of the heater area, in order to measure the temperature of the polymer resistors. An identical diode is also used in the centre of the ASIC chip for

the measurement of its operating temperature. Figure 6.6 shows a photograph of one of the thermodiodes.



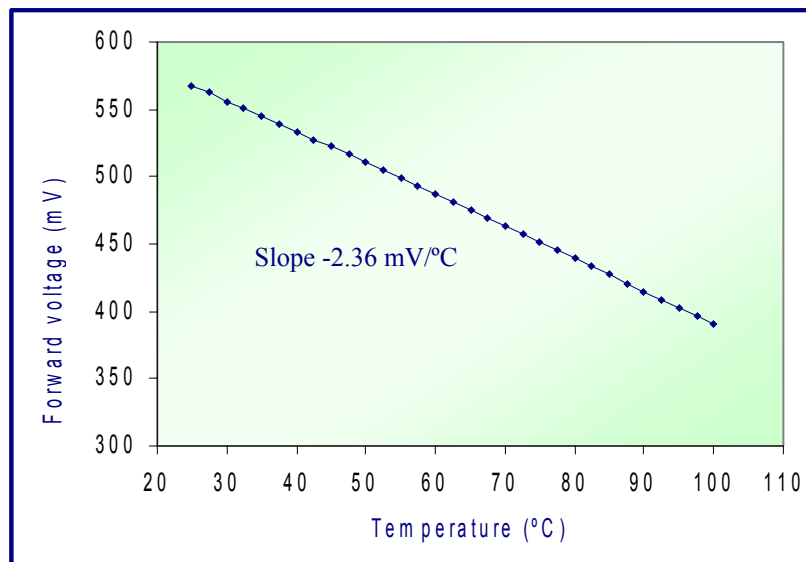
**Figure 6.6** Photograph of a p-n thermodiode, between the heater and electrodes.

Figure 6.7 shows the average I-V characteristic of the p-n diode in the forward region. The forward voltage drop is in the typical range just above 500 mV and the I-V curve follows the expected diode behaviour.



**Figure 6.7** I-V characteristic of the thermodiode.

The diodes showed a linear response to temperature, with an average sensitivity of  $-2.36 \text{ mV}/^\circ\text{C}$ , as it is depicted in Figure 6.8. The actual response is similar to that obtained in the simulations, but differs slightly from the theoretical value of  $-2.1 \text{ mV}/^\circ\text{C}$  [2].



**Figure 6.8** Temperature characteristic of the thermodiode.

#### 6.4.6 Heater characterisation

The characteristics of the designed heater and the results of the simulations were described in previous chapters. The photograph in Figure 6.9 corresponds to the sensor pads and heater area

An external variable current source was applied to the heaters in a set of five ASIC chips and the characteristic I-V was obtained by measuring voltage, producing the averaged response shown in Figure 6.10, where the reciprocal of the slope corresponds to the actual resistance of the heater, averaged to  $62.8 \Omega$  with standard deviation of  $5.65 \Omega$ . The reasons for the difference with respect to the nominal design value of  $50 \Omega$  are not easy to understand but it might be the combined result of the variations in the fabrication process and the errors introduced by the wiring and equipment used during the tests.



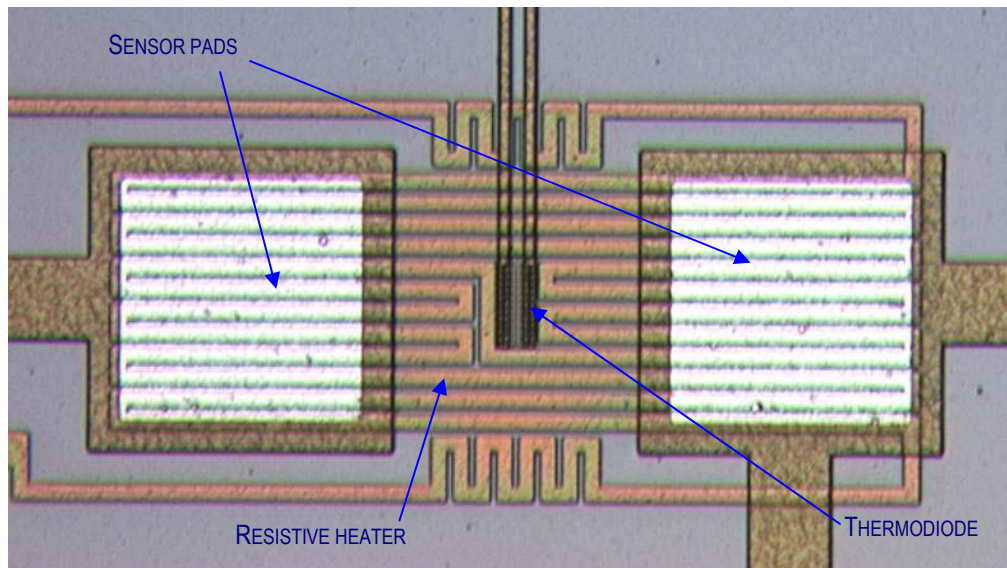


**Figure 6.9** Photograph of the sensor pads and heater area.

The values of current and voltage used during the tests correspond to the operating conditions expected during the actual application of the ratiometric ASIC chip. The response of the heater showed linearity within this range.

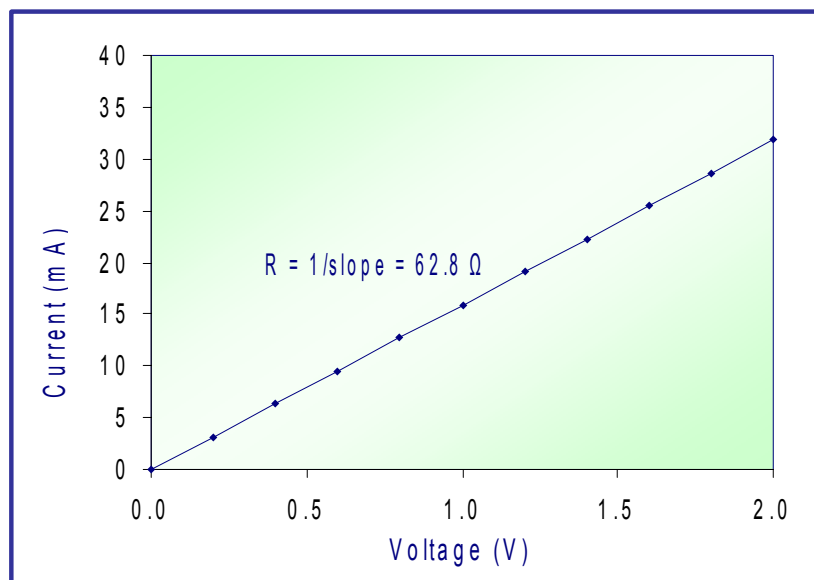


**Figure 6.10** Averaged I-V characteristic of the heaters in the ASIC chip.

### 6.4.7 Temperature control circuit

As mentioned before for other components of the fabricated ASIC chip, *Nwell* type resistors have different resistance values with respect to the design. However, due to the fact that not all the terminals were externally available for testing, it was not possible to measure directly the actual values of resistance of all these elements in the temperature compensator circuit and in the current drive circuit.

Indirect measurements in the temperature compensator circuit showed that the possible variations in its internal *Nwell* resistors did not affect the gain, which was calculated by testing voltages at the inputs and output of the circuit. This also suggests that variations in the resistance occurred at a constant percentage and they are therefore cancelled through the ratio of the resistors involved.

In the current drive circuit, the variations in the resistance of the two *Nwell* resistors could have modified the transient response and it is possible that a slight capacitive effect could appear in the input of the FET. However, there were not signs of instability observed and the circuit drives current to the heater as expected.

The temperature set-point circuit is also affected by the changes in the *Nwell* resistance, but the changes can still be compensated via the external digital potentiometer  $R_{tr2}$ . The internal resistor  $R_{tr1}$ , which was designed for 10 k $\Omega$ , resulted to be around 16 k $\Omega$  in the fabricated ASIC chips. The use of a 0-50 k $\Omega$  potentiometer for  $R_{tr2}$  allows the compensation of that difference and the reference for temperature can still be set to any desired value within the operating range of the ASIC chip.

## **6.5 CONCLUSIONS**

After testing a number of samples as explained in this chapter, it was found that the fabricated ASIC chip performed mainly according to the design specifications, and that they were ready for the deposition of polymeric materials and for further experimentation in the automated testing system.

The variations in the resistances and temperature coefficients of the resistors in the circuit do not affect significantly the overall performance of the ASIC chip, which also showed its ability for the compensation of such differences through the use of either ratiometric relationships of resistors or externally programmable potentiometers.

The main section of the ASIC chip, which corresponds to the ratiometric gas sensor circuit, responded as expected in the original design. Its ability to compensate for variations in parameters such as resistance of the sensors, temperature, humidity, and for the cancellation of voltage-induced drifting, showed that the chip is highly suitable for application in combination with gas sensing materials.

The components in the temperature control section were also characterized and the results showed that its behaviour follows the design specifications. In particular, the responses of the custom-designed heater and diode are very close to the theoretical predictions. A more detailed analysis of the overall functioning of this section can still be performed, as it is proposed in Chapter 8.

The next chapter describes the incorporation of chemoresistive sensors into the ASIC chip and the results obtained when exposing the ratiometric ASIC chip to the presence of VOC.

## 6.6 REFERENCES

1. XICOR (2002). “X9241A Quad digital controlled potentiometers (XD<sup>TM</sup>CP)”, Datasheet available at [www.xicor.com](http://www.xicor.com), Rev 1.1.13 12/09/02.
2. Gardner, J.W., Varadan, V.K. and Awadelkarim, O.O. (2001). *Microsensors, MEMS, and smart devices*, John Wiley & Sons, Ltd., Chichester, England.

## **CHAPTER 7**

# **SMART SENSORS CHARACTERISATION**

### **7.1 INTRODUCTION**

Chemoresistors are devices whose resistance changes with the concentration of gas that is present. Even when they may not exhibit specificity to a particular gas, it is still possible to use them in the form of sensing arrays and extract from them information that can be used for the identification of specific gases, vapours or odours.

This chapter describes two types of chemoresistive devices fabricated at Warwick SRL and evaluates the performance of the smart ratiometric ASIC chip when the system was exposed to toluene and ethanol vapours in air under different testing conditions.

## 7.2 POST-CMOS FABRICATION OF CHEMORESISTIVE SENSORS

As explained in chapters 5 and 6, the metal electrodes on the ratiometric ASIC chip can be accessed through the overlay openings made during the fabrication process thus allowing the deposition of resistive materials to create two embedded chemoresistors. Alternatively, the layout of the ASIC bond-pads also permits the connection of the interface circuitry to external resistive sensors.

Polymer-carbon black composite films are used here as a gas sensitive material both to demonstrate the practical application of the ratiometric ASIC chip and to study the response of two different types of smart devices. These films, firstly reported by Lewis at the California Institute of Technology, USA, consist of conducting carbon black nanospheres dispersed into a non-conducting base polymer film [1-4]. When exposed to VOC, the polymer within the composite film absorbs the vapour and generally swells reversibly. This swelling causes the distances between the conductive carbon black nanoparticles to increase and thus, induces a resistance increase in the composite film [1, 3].

Carbon black polymer composite film-based sensors are not selective toward a specific gas but they show different sensitivities to different gases. However, the pattern response of an array of several sensors made up by different polymer composite films can be used as a 'fingerprint' to classify different gas or chemical mixtures [5, 6] using multivariate pattern recognition methods.

The chemoresistors were created through a post-fabrication stage via in-house spray coating of carbon black/polymer composite materials across the electrodes. The aluminium electrodes required a gold layer, attached using ultrasonic wedge bonding, before the deposition of the sensing materials. Effort has been made to

obtain resistance values as close to 10 k $\Omega$  as possible for each chemoresistor, but most importantly, special care was given to matching the resistances of the sensor pair and therefore take maximum advantage from the benefits of the ratiometric configuration.

Mixtures of 20% carbon black with poly(ethylene-co-vinyl acetate) (PEVA) and poly(caprolactone) (PCL) polymers have been deposited onto the openings for the electrodes of the ASIC chips. The resistive layer obtained acts as a sensing element which reacts both quantitatively and qualitatively to the presence of VOC. A cross-section of the general structure of the chemoresistors is shown in Figure 7.1. For simplicity, the gold layer on top of the metal electrodes, and the heater in the first metal layer underneath the electrodes, are not shown. Figure 7.2 shows photographs of two of the resulting sensors embedded inside the ratiometric ASIC chip.

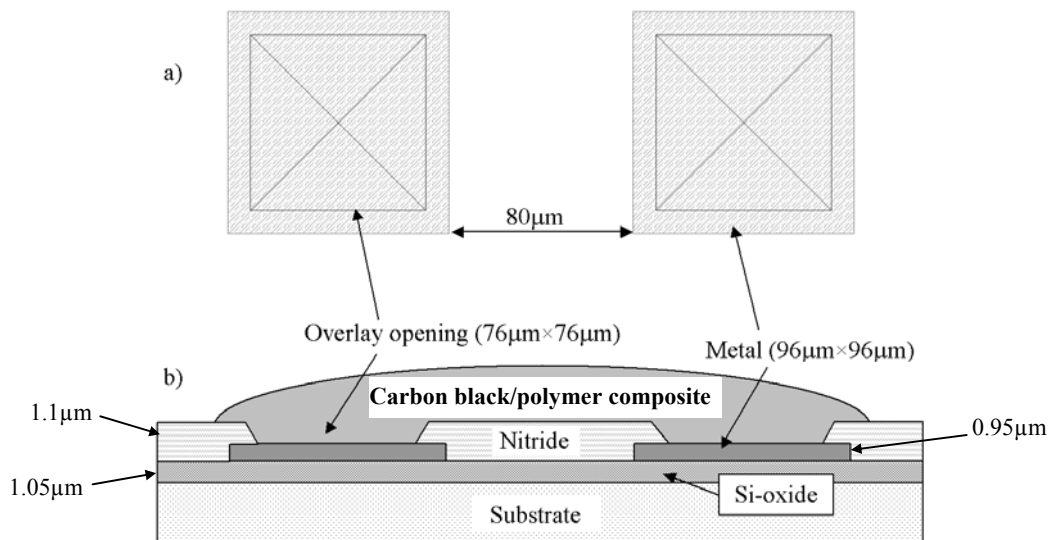


**Figure 7.1** Cross-section of the general structure of the chemoresistors fabricated onto the ASIC chips.

A description of the fabrication and characterisation of two types of devices is given below. In the first type, both chemoresistors in the ASIC chip are based in

the same material, with one of them exposed to the presence of a VOC while the other is covered to make it immune to the exposure. The second type uses a different material for each chemoresistor and both sensors are exposed to the presence of VOC. Current research at Warwick includes the application of the ratiometric ASIC chip with other materials and under different novel configurations, which are briefly commented in the final chapter of this thesis.

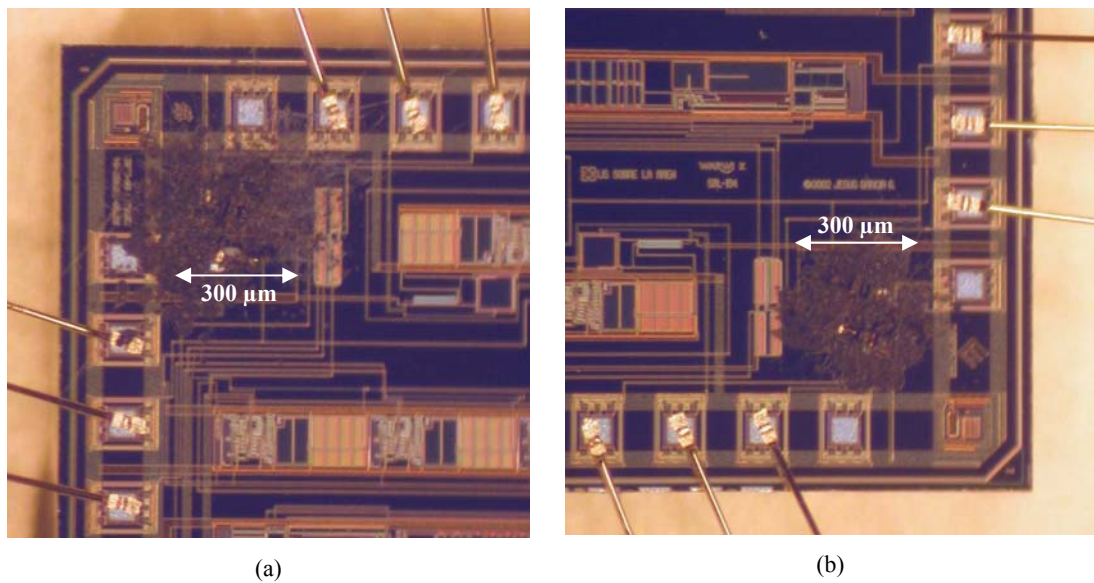


**Figure 7.2** Aspect of two of the chemoresistors obtained by spray coating carbon black/polymer composite onto the electrode areas. Resistances averaged over a 17 weeks period at 24°C are: (a) 9.7 k $\Omega$  and (b) 8.9 k $\Omega$ .

### 7.2.1 *Monotype* ratiometric devices

In the first type of device tested, both chemoresistors were made out of the same material. One of them was covered with a non-corrosive adhesive/sealant<sup>5</sup> in order to make it passive to the VOC effects, whilst the other sensor remained completely exposed. In this way, the active sensor responds to the variations in gas concentration and humidity, whereas the passive resistor remains at constant humidity and does not

<sup>5</sup> Dow Corning® 3145 RTV MIL-A-46146.



respond to the presence of a VOC. However, both of the sensors in the array are sensitive to temperature changes, drift and other variations, which are mostly eliminated through the circuit response previously described, as a consequence of the ratiometric relationship.

Although it was difficult in practice to obtain sensors with actual resistances of 10 k $\Omega$ , the circuit also showed excellent response with values out of this range. More important than the actual resistance value, the *resistance ratio* ( $rr$ )  $R_1/R_2$  was kept within the range  $\frac{1}{2} < rr < 2$  and as close to 1.0 as possible (0.96 in average, with standard deviation of 0.070). Devices with sensors based on PEVA material were labelled 122 $n$ , being  $n$  the number of the sample, whereas devices based on PCL composite are identified as 133 $n$ . The resistances of some of the samples tested are shown in Table 7.1.

**Table 7.1** Resistances of several samples of devices based on a single material – *monotype* ratiometric devices.

| Sensing materials      | Device ID | $R_1$ (k $\Omega$ ) | $R_2$ (k $\Omega$ ) | $rr = R_1 / R_2$ |
|------------------------|-----------|---------------------|---------------------|------------------|
| PEVA + carbon<br>black | 1221      | 8.70                | 8.90                | 0.98             |
|                        | 1222      | 36.2                | 34.55               | 1.05             |
|                        | 1223      | 9.39                | 11.28               | 0.83             |
|                        | 1224      | 12.10               | 12.20               | 0.99             |
| PCL + carbon<br>black  | 1331      | 9.70                | 10.00               | 0.97             |
|                        | 1332      | 5.29                | 5.23                | 1.01             |
|                        | 1333      | 8.85                | 9.65                | 0.92             |

In these samples,  $R_1$  is the resistance of the uncoated or active chemoresistor, whilst  $R_2$  is the resistance of the coated or passive element. Characterisation of these devices is reported in section 7.4.

### 7.2.2 Duo-type ratiometric devices

In the second type of devices reported, each sensor possesses a different material and both of them are exposed to VOC and humidity variations. The idea behind this configuration is to take advantage of the contrasting responses of different materials when exposed to the same VOC. This means that two materials showing different responses to a given VOC will produce an enhanced output derived from the ratiometric configuration, provided that the partial outputs of the sensors have opposite signs in sensitivity, in order to obtain the adding effect in the expression for

the output of the sensor circuit given in equation 2.23:  $\frac{V_{ref}}{R_2^2} (R_2 dR_1 - R_1 dR_2)$ .

In order to test this idea, several sample devices were prepared using the carbon black/PEVA and carbon black/PCL materials, the first of them for  $R_1$  and the latter for  $R_2$ . In this configuration, none of the sensors was coated, so both of them can be exposed to gas and humidity effects. Table 7.2 shows data for some of these devices, labelled 323 $n$ , being  $n$  the number of the sample.

The responses showed by these samples are reported in section 7.5.

**Table 7.2** Resistances of several samples of devices based on contrasting materials – *duo-type* ratiometric devices.

| Sensing materials               | Device ID | $R_1$ (k $\Omega$ ) | $R_2$ (k $\Omega$ ) | $rr = R_1/R_2$ |
|---------------------------------|-----------|---------------------|---------------------|----------------|
| PEVA + carbon black<br>in $R_1$ | 3231      | 1.53                | 1.53                | 1.00           |
|                                 | 3232      | 5.94                | 7.04                | 0.84           |
| PCL + carbon black<br>in $R_2$  | 3233      | 18.27               | 15.19               | 1.20           |
|                                 | 3234      | 22.30               | 12.66               | 1.76           |

### 7.3 AUTOMATED TESTING SYSTEM FOR DEVICE CHARACTERISATION

Devices were tested and characterised using an automated system. A dual-chip test board was used for interfacing a pair of ASIC chips to the rest of the system, consisting on the following components:

- A *Flow Injection Analysis* (FIA) test station [7] for the automated exposure of the ASIC chips to vapours.
- A data acquisition system and interface electronics for the control of the FIA test station.
- A data acquisition system for the control of the ASIC chips and the collection of output data.
- An I<sup>2</sup>C-bus data control system for the programming of the external set of digital potentiometers used with the ASIC chips.
- Virtual instrumentation written in *LabView*<sup>TM</sup> for the automated control of the whole testing process.

The FIA test station and the corresponding data acquisition software and electronics were available at the SRL as they were designed and fabricated for previous research work [7]. The rest of the components were designed specifically for this project. A diagram of the components of the whole testing system is shown in Figure 7.3.

#### 7.3.1 Dual-chip testing board design

A PCB was designed and constructed for the simultaneous and automated testing of two ASIC chips within the gas testing chamber. The dual-chip testing board consists basically on the duplication of the components included in the single-chip board described in section 6.3. However, the dual-chip version is provided with a

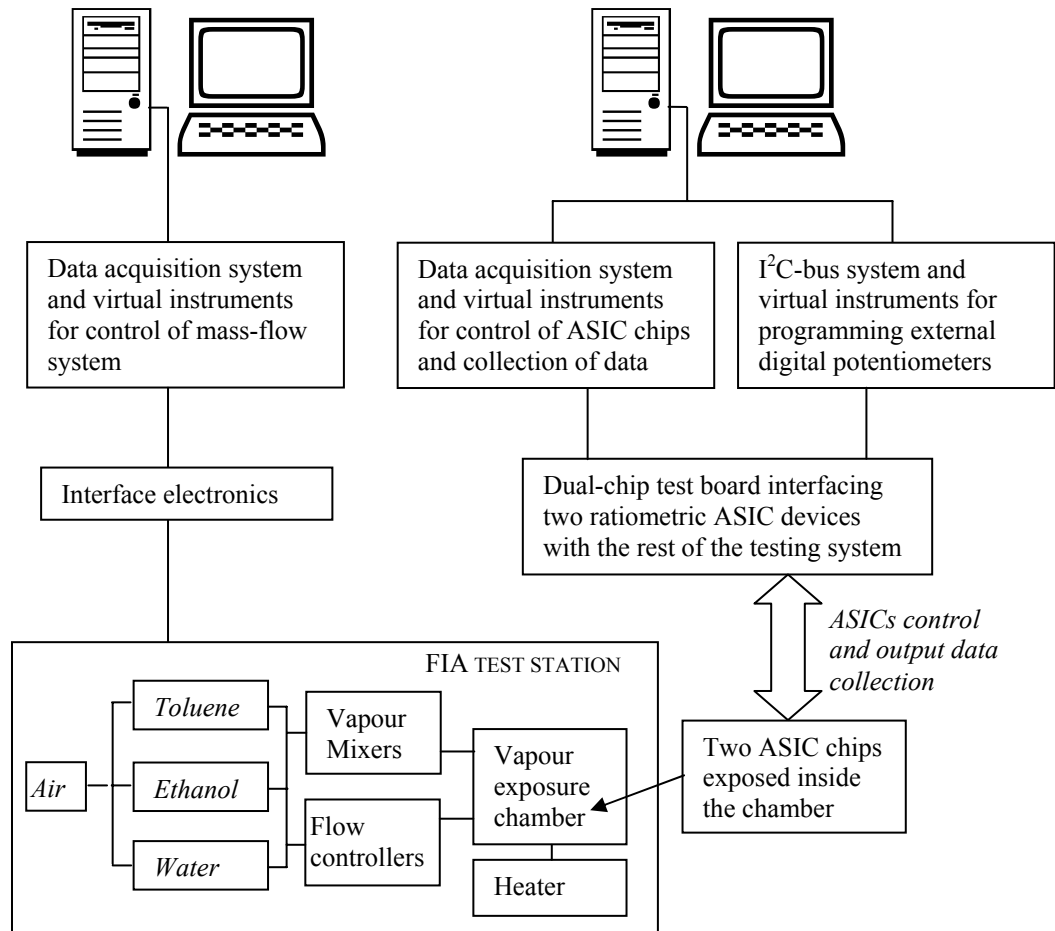
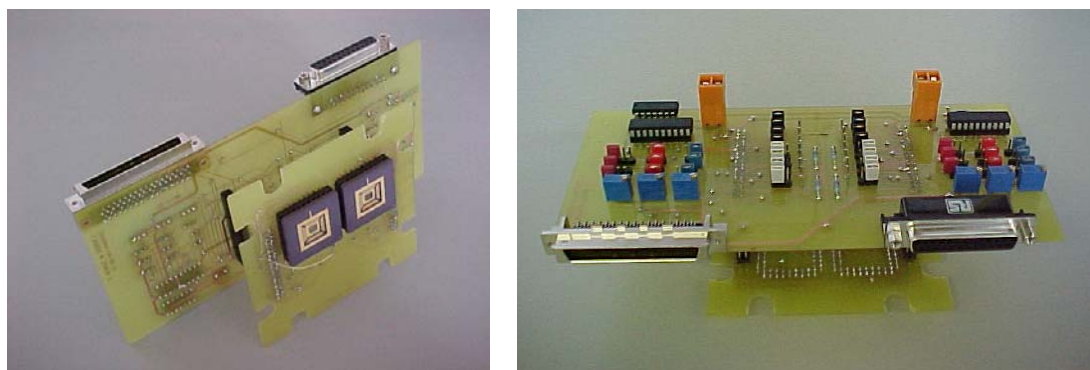


**Figure 7.3** Diagram of the testing system for smart sensor characterisation.



(a)

(b)

**Figure 7.4** Dual-chip test board for the characterisation of smart ratiometric ASIC devices, showing: (a) two packaged chips connected for preliminary testing, and (b) 68-pin and 25-pin PC connectors, and additional electronics for testing.

complementary board that can be directly fitted to the metallic chamber where the ASIC chips are exposed to VOC. Photographs of the dual-chip test board are shown in Figure 7.4, and further details about it are included in Appendix C.

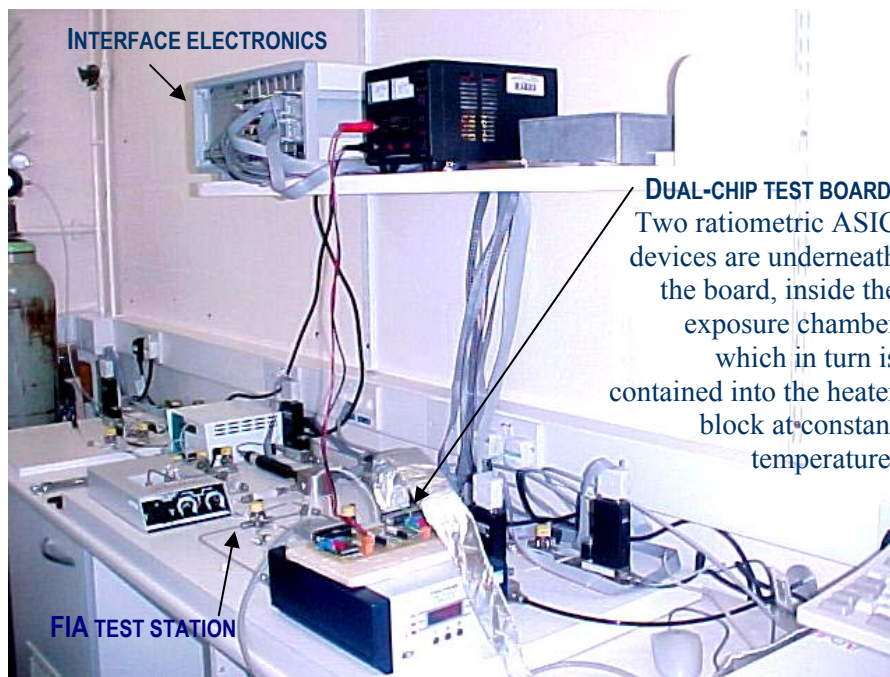
### 7.3.2 FIA test station

Testing and characterisation of the ASIC chips were performed with the aid of a previously developed automated FIA test station [7]. The FIA test station was constructed for previous research work with the aim of controlling accurately atmosphere conditions, and its design allows the exposure and characterisation of ASIC chips to mixtures of water and analyte vapours in air, at controlled concentrations.

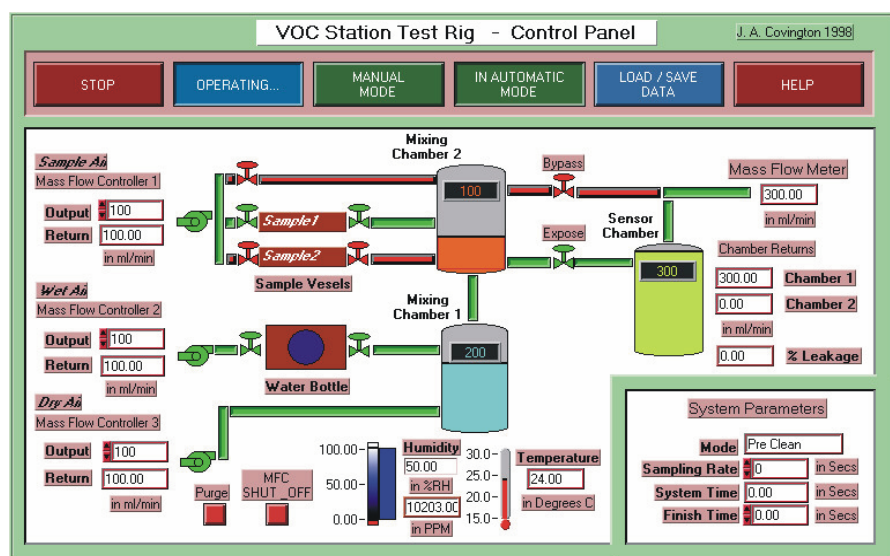
#### 7.3.2.1 Hardware

Basically, the FIA test station (Figure 7.5(a)) controls the mix of air with analyte vapours under test and under particular conditions of humidity and temperature. For the purposes of the research project described in this thesis, analytes tested were toluene and ethanol vapours. Air is injected through the system and the concentrations of analyte and water vapours are regulated through mass flow controllers, producing a mix that is taken to the gas exposure chamber, where the ASIC chips are placed. For each test, the chamber was maintained at constant temperature inside a controlled heating unit. The action of valves and mass flow controllers is commanded through an electronic interface connected to a standard personal computer via a National Instruments Lab-PC-1200 card. A complete description of the FIA test station is given in [7].

The configuration adopted for the exposure of the ratiometric ASIC chips, is that where both sensors are exposed to the same flow, although one of them can be covered by an inert material, as described in chapter 4 (Figure 4.16 (a)).



(a)



(b)

**Figure 7.5** (a) Photograph of the FIA test station, its interface electronics and the dual-chip test board as they were arranged for the tests. The ratiometric ASIC devices are in the exposure chamber, placed inside the heater block just underneath the dual-chip test board. (b) The front panel of the FIA control software, showing a schematic view of the FIA test station [7].

### 7.3.2.2 Virtual instrumentation

Operation of the FIA test station is completely automated and controlled from software running on a standard PC. Virtual instrumentation was written in *LabView*<sup>™</sup> for Windows version 5.0 and its structure, organisation and presentation has been thoroughly described elsewhere [7].

The FIA test station software allows the programming of automated test sequences, in which analyte samples are mixed with air and water vapour at regulated concentrations. These analyte concentrations and humidity values are usually given in a series of parameters that determine the exposure times of the ASIC devices to the programmed sequence of analyte sample, vapour concentration, and humidity. Once started, the whole test runs without need of user intervention. Figure 7.5(b) shows the front panel of the FIA control software [7].

### 7.3.3 Data acquisition system for the control of ASIC devices

A data acquisition system was implemented for the control of input and output signals of the ratiometric ASIC devices under test. The voltage signals required for the operation of the ASIC devices, as described in chapter 3, were provided through National Instruments software and hardware, installed and running on a standard PC. The same system was also used for the data acquisition of the output signals produced by the ASIC devices.

#### 7.3.3.1 Hardware

A National Instruments data acquisition card NI 6036E was installed in a desktop personal computer and connected to the corresponding 68-pin port available in the dual-chip test board previously described. The NI 6036E card has sixteen channels of

16-bit analogue input, eight lines of digital input-output, two channels of 16-bit analogue output, and a 68-pin connector. The NI 6036E card was found suitable for the data acquisition system required by this particular application, where analogue signals were obtained from the ratiometric ASIC devices. However, data acquisition cards produce distortion in the frequency spectrum as their analogue output glitches due to updating with new values [8], and this effect was reflected in the data collected from the ASIC devices responses, making necessary additional data processing.

The two 16-bit analogue output channels were used for the delivery of the input voltage signals required by the ASIC devices, namely  $V_{\text{pulses}}$ , which activates the voltage reference cell, and  $V_{\text{gates}}$ , which allows the operation of the FET switches in the ratiometric sensor circuit.

The outputs of the ASIC devices are acquired through the analogue input channels of the NI 6036E card. Four channels were assigned to each ASIC chip, to register the amplified and filtered output voltage of the sensor response and to monitor the outputs of the three temperature sensors. With two chips under test, only eight of the sixteen available channels were used, but the system can be easily expanded in order to test four ASIC devices simultaneously.

A R6868 ribbon cable was used for the connection between the NI 6036E and the dual-chip test board.

Further details on the connections, pin assignment and configuration of the NI 6036E card and related hardware are given in Appendix C.



### 7.3.3.2 Virtual instrumentation

*LabView*<sup>TM</sup> software was written by the author for the automated control of the vapour exposure process that allowed the characterisation of the response obtained from the sensors in the ratiometric ASIC devices. The software runs in the desktop computer where the NI 6036E card is installed and, through this data acquisition device, it controls input and output signals of the ASIC chips connected via the dual-chip test board.

There are two main functions in the data acquisition system for the control of the ASIC devices:

a) *Generation of the input voltage pulses which drive the ASIC chips:*

A square waveform of 10 Hz and a duty cycle of 10% is used for energizing the voltage reference cell which produces the basic signal for the gas sensor circuit. A second square waveform of 5 Hz and duty cycle of 50% is required in order to alternately invert the polarity of the voltage applied to the sensing chemoresistors through the set of FET-based switches. Both square waveforms are generated with *LabView*<sup>TM</sup> and they are sent to the ASICs through the analogue outputs of the NI 6036E card.

b) *Data acquisition of the output voltages from the ASIC chips*

The output of the ratiometric ASIC chips is monitored through the analogue input channels of the NI 6036E card and the sampled response is saved to files in the desktop computer by using *LabView*<sup>TM</sup> software.

A virtual instrument was written in *LabView*<sup>TM</sup> version 6.1 for each of these functions and the whole process is controlled from a main module that integrates the corresponding sub-programs.

The front panel of the main module for ratiometric ASIC devices test is shown in Figure 7.6. When the program is run, it starts immediately the virtual instrument that produces the input pulses for the two ASIC chips under test. The input pulses produce in turn pulses in the voltage reference cell and from here all the corresponding parts of the circuit respond to the pulsed stimuli. The waveforms of the input pulses are shown in the left-side sub-panel.

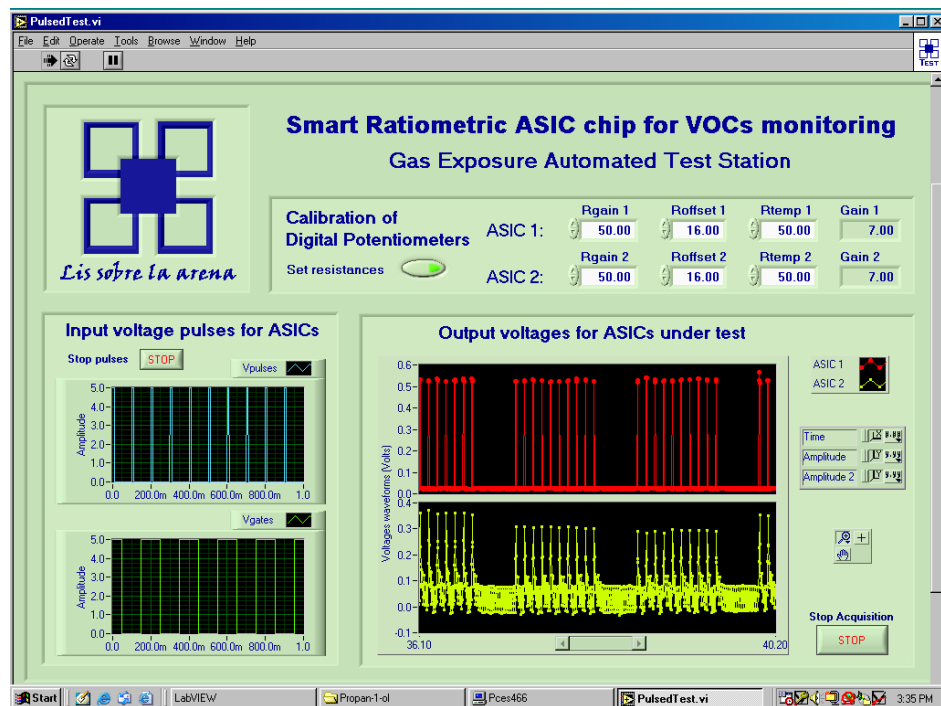


**Figure 7.6** Front panel of the data acquisition system for characterisation of the smart ratiometric ASIC devices.

The right-side sub-panel corresponds to the acquisition of data from the output of the ASIC chips. From the main panel the actual acquisition of data can be started and finished, obtaining a file with the sampled values of voltages in a tabular form. The waveforms of the output voltages are shown as they are obtained through the input analogue channels of the NI 6036E card.

The block diagrams and additional information of the virtual instrumentation written for this project are included in Appendix D.

### 7.3.4 I<sup>2</sup>C-bus data control system for digital potentiometers

Three programmable digital potentiometers are used with each ASIC chip for the adjustment of the following variables: the gain of the instrumentation amplifier, the offset voltage signal which calibrates the output of the sensor circuit, and the voltage corresponding to the set-point of the temperature control. The resistance values of these potentiometers are set through a piece of *LabView*<sup>TM</sup> software which communicates with them using an I<sup>2</sup>C-bus [9] data stream via the parallel port of the computer.

#### 7.3.4.1 Hardware

The programmable digital potentiometers are obtained from the Xicor's X9241A integrated circuit [10], which contains four 50 k $\Omega$  potentiometers. There are two X9241A in the dual-chip test board, one to be used with each ASIC device.

Communication between the desktop computer and the X9241A is achieved through an I<sup>2</sup>C-bus standard protocol [9], which uses the parallel port of the computer to send two lines of data, namely a serial clock signal and a serial data stream. Serial data are buffered with the aid of a 74SL07 integrated circuit, while routing of data to the proper X9241A chip for each ASIC device is achieved by identifying the chips with different digital device addresses.

A standard 25-pin shielded cable was used for the connection between the parallel port in the desktop computer and the corresponding connector in the dual-chip test board.

Additional details and diagrams of the I<sup>2</sup>C-bus data control circuitry used in the dual-chip test board are included in Appendix C.

#### 7.3.4.2 Virtual instrumentation

The front panel of the main module described in the previous section, also contains a sub-panel for the calibration of the digital potentiometers connected to the two ratiometric ASIC devices under test. This sub-panel is shown on top of the input and output waveforms panels in Figure 7.6.

The virtual instrumentation written for the calibration of the digital potentiometers generates the serial clock signal and the serial data stream required by the I<sup>2</sup>C-bus protocol. The serial data bytes needed to automatically transfer and set the resistance values for each potentiometer are generated in a sub-module which the user does not need to access.

The resistance values can be directly varied from 0 to 50 k $\Omega$  through the controls in the main panel, adjusting in this way the proper levels of gain, offset voltage and temperature set-point.

Complete diagrams and details of the virtual instruments for calibration of X9241A digital potentiometers are also included in Appendix D.

## 7.4 RESPONSE OF MONOTYPE RATIOMETRIC DEVICES

Following the spray coating of carbon black/polymer composite materials, the responses of the resulting ASIC devices to toluene and ethanol vapours in air have been characterised in the automated testing system. Each test consisted in the exposure of the ASIC to a series of concentrations of vapours in air at two given fixed humidity levels, while holding the chip at constant temperature (30, 35, 40, 45 and 50°C). The variations of the output voltage were automatically registered through the VI software and using the PCB previously described. A summary of the results of the experiments is presented here. A more complete set of plots and results is included in Appendix G.

The ASICs were tested at 442, 619, 884, 1946, 2918 and 4156 ppm of toluene vapour in air. Likewise, concentrations of 805, 1127, 1610, 3542, 5312 and 7566 ppm of ethanol vapour were also applied to the devices. Each series of analyte concentrations was tested under two different humidity conditions: 9853 ppm and 3000 ppm of water vapour.

### 7.4.1 Response of monotype devices to ethanol and toluene vapours

Samples of monotype devices (as referred in Table 7.1) were exposed to the presence of ethanol and toluene vapours in air. It was observed that carbon black/PEVA devices have a better response to polar ethanol vapours in air, whereas the carbon black/PCL ASICs responded much better when exposed to non-polar toluene vapours.

#### 7.4.1.1 Response of monotype devices to ethanol concentration

Figure 7.7 shows the typical response to ethanol vapours in air obtained with the poly(ethylene-co-vinyl acetate) ASIC samples maintained at 35°C. The plot in Figure

7.7(a) corresponds to the amplified voltage at the output of the ASIC. The change in output voltage of the sensor itself before any amplification is plotted in Figure 7.7(b). As expected, the magnitude of the change in the output voltage increases with the concentration of vapours, with a typical sensitivity coefficient to ethanol of  $3.2 \mu\text{V}/\text{ppm}$ , prior to amplification, or with a minimum of  $22.4 \mu\text{V}/\text{ppm}$  in the amplified output, at  $35^\circ\text{C}$ .

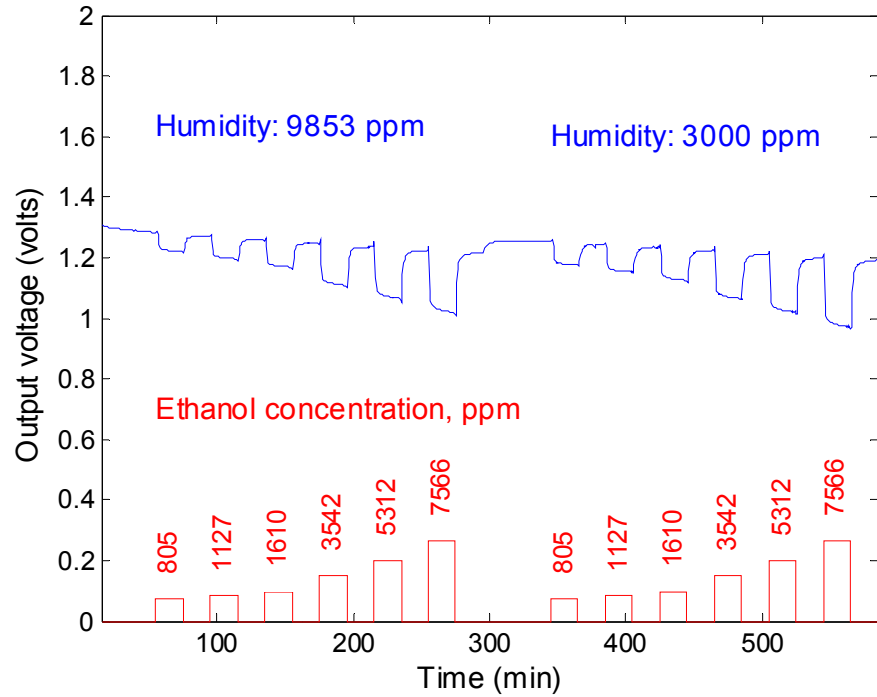
The response of the carbon black/PCL ASIC devices to ethanol vapours in air was lower, with a sensitivity coefficient to ethanol of around  $1.9 \mu\text{V}/\text{ppm}$  without amplification, at  $35^\circ\text{C}$ .

As a consequence of the ratiometric configuration, there is no considerable drift on the baseline voltage of the output.

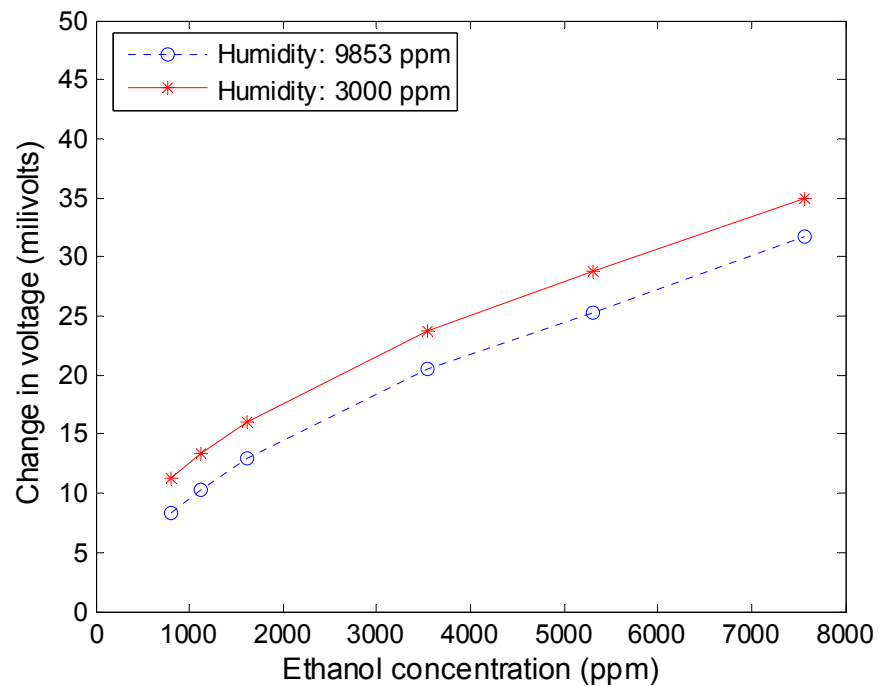
#### *7.4.1.2 Response of monotype devices to toluene concentration*

Figure 7.8(a) shows the response to toluene vapours in air obtained with the poly(caprolactone) ASIC samples at  $35^\circ\text{C}$  at the amplified output of the circuit. This device responds with a voltage sensitivity coefficient to toluene of  $8.6 \mu\text{V}/\text{ppm}$  before amplification. Figure 7.8(b) shows the near elimination of humidity dependence on the response of the ASIC chip to VOC. The change in voltage is plotted as obtained prior to any amplification. Again, there is no significant drifting on the baseline voltage of the output.

Samples of the carbon black/PEVA devices responded with less sensitivity ( $2.6 \mu\text{V}/\text{ppm}$  prior to amplification) to toluene vapours, although the ASICs were too sensitive ( $14.7 \mu\text{V}/\text{ppm}$  without amplification) to the raising edge of the pulses, as is shown by the spikes in the time response plot (Figure 7.9).

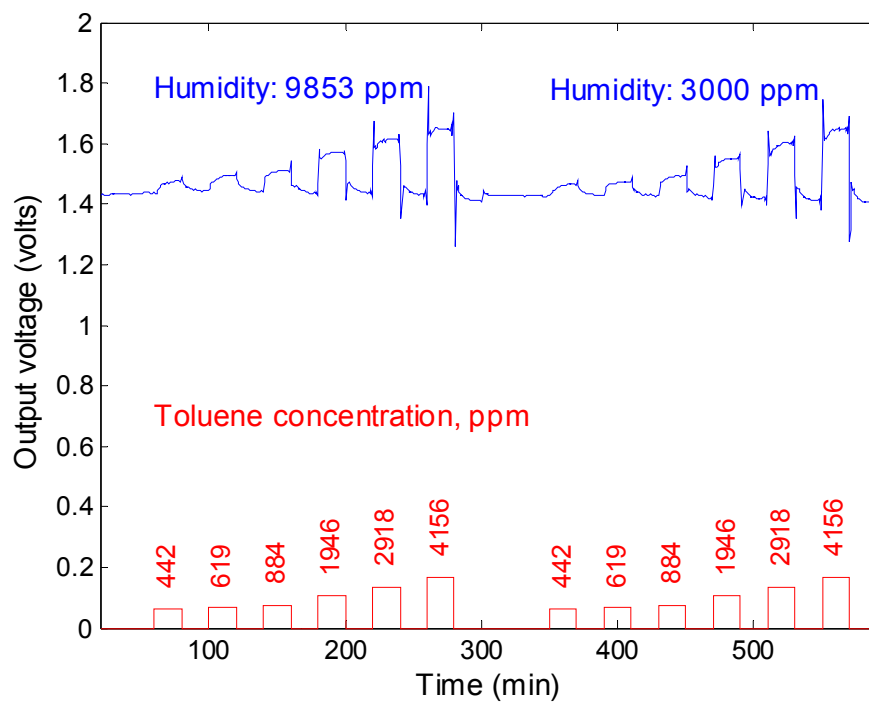


(a)

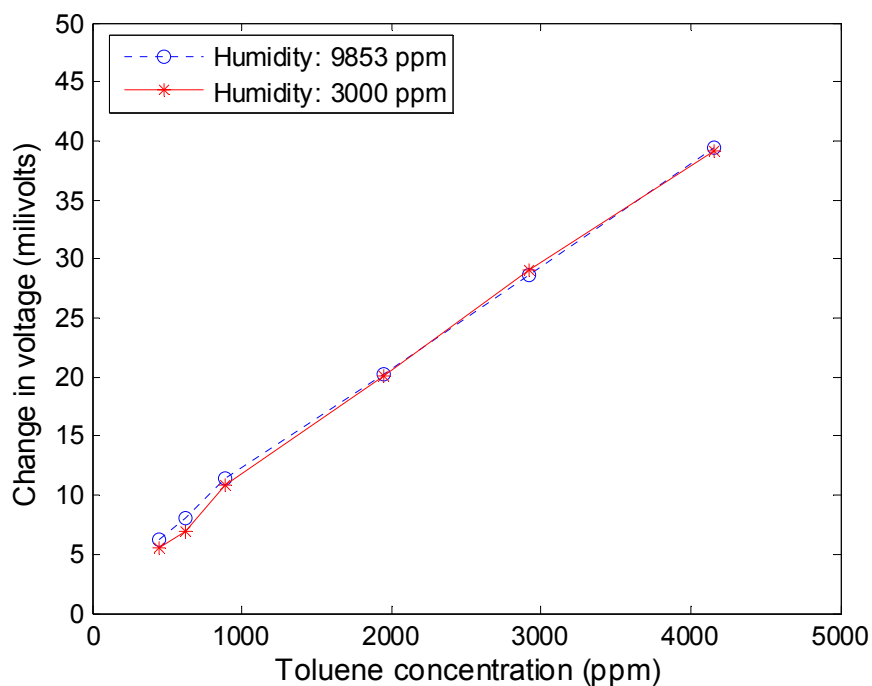


(b)

**Figure 7.7** Typical response of the poly(ethylene-co-vinyl acetate) ASIC devices to different concentrations of ethanol vapours in air at 35°C. (a) Amplified output voltage. (b) Change in voltage prior to amplification.



(a)



(b)

**Figure 7.8** Typical response of the poly(caprolactone) ASIC devices to different concentrations of toluene vapours in air at 35°C. The output shows very small drifting and low humidity dependence. (a) Amplified output voltage. (b) Change in voltage prior to amplification.



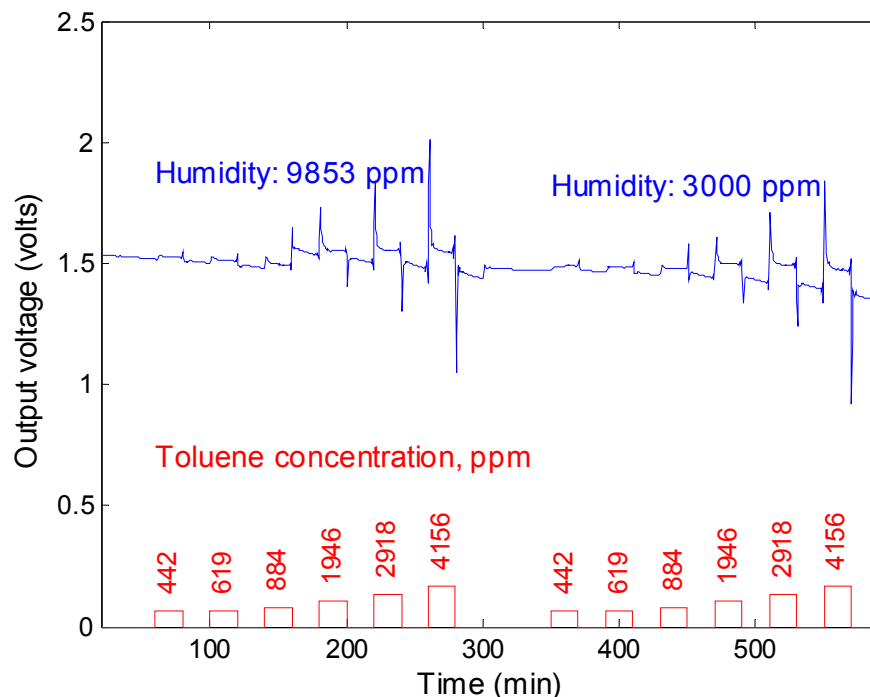


**Figure 7.9** Typical time response of carbon black/PEVA devices to different concentrations of toluene vapours in air at 35°C.

#### 7.4.2 Response of monotype devices to humidity

Monotype devices were tested using the configuration in which one of the chemoresistors is coated and therefore the reference humidity remained constant during the tests and different to ambient humidity. The active chemoresistor, on the contrary, was exposed to changes in humidity and the output shows a slight difference for the concentrations of water vapour that were tested.

Previous research at SRL had revealed that these carbon-based polymeric resistive sensors show a smaller variation in response with water concentration than conducting polymers, on both the baseline resistance and on the effect of ethanol and toluene vapours [7]. This was confirmed by the tests performed at water concentrations of 3000 and 9853 ppm, and at constant temperature. The responses are almost the same for both humidity tests, although there is a slight difference that may

be produced either by the immunity to these changes obtained with the coating on the passive sensor or by the linear additive water term modelled elsewhere [7].

Although variations due to humidity are small, it could be noticed that PEVA based devices had a larger average response ( $0.503 \mu\text{V}/\text{ppm}$  with toluene and  $-0.477 \mu\text{V}/\text{ppm}$  with ethanol) to water vapour than PCL based devices ( $0.021 \mu\text{V}/\text{ppm}$  with toluene and  $-0.246 \mu\text{V}/\text{ppm}$  with ethanol).

#### *7.4.2.1 Response of monotype devices to humidity and ethanol vapours*

Ethanol vapour tends to mix with water vapour and the result is a slight decrease in the response of the sensors with an increase in water vapour concentration. Coefficients measured were  $-0.477 \mu\text{V}/\text{ppm}$  for PEVA based devices and  $-0.226 \mu\text{V}/\text{ppm}$  for PCL based devices, averaged at the four ethanol concentrations tested.

#### *7.4.2.2 Response of monotype devices to humidity and toluene vapours*

Contrasting with the effect of humidity on the response to ethanol, toluene vapours produce an increase on the output with an increase in the water vapour concentration. Averaged humidity sensitivities for toluene were  $0.503 \mu\text{V}/\text{ppm}$  for PEVA based devices and  $0.021 \mu\text{V}/\text{ppm}$  for PCL based devices.

Figure 7.10 shows the response with humidity of one the poly(caprolactone) devices at four fixed toluene vapour concentrations in air. Humidity coefficients are  $0.083$ ,  $0.020$ ,  $-0.063$  and  $0.045 \mu\text{V}/\text{ppm}$  for 884, 1946, 2918 and 4156 ppm of toluene, respectively.

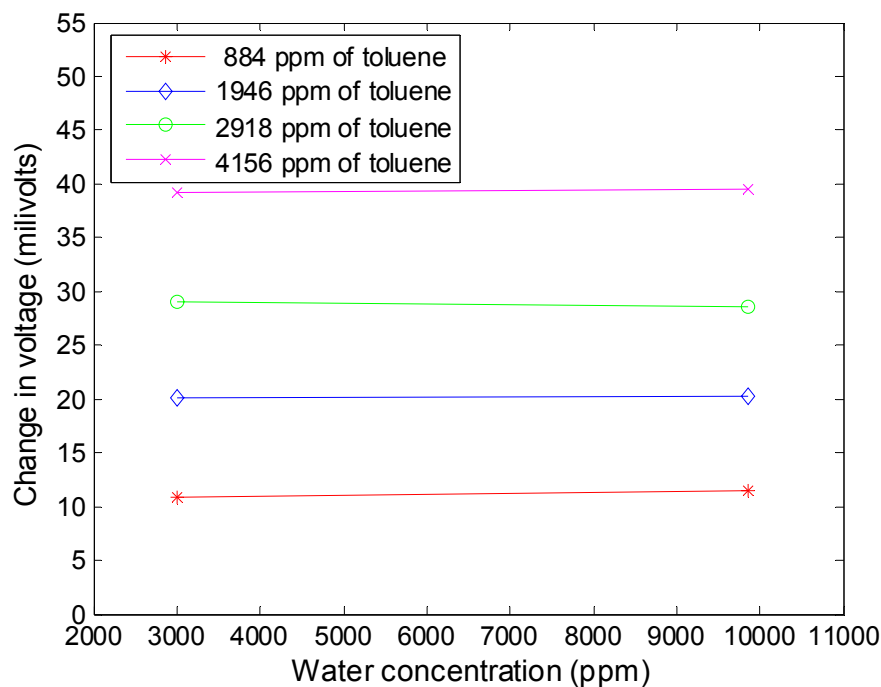


**Figure 7.10** Humidity dependence of the response of poly(caprolactone) devices at several concentrations of toluene vapour.

### 7.4.3 Response of monotype devices to temperature

As expected from results in previous work with resistive composite polymers [7], the response of monotype devices decreased with increasing temperature.

The fact that only one active chemoresistor sensor is used in the monotype configuration, produces the same behaviour for the response to temperature as in the case of single resistive sensors. Common variations in sensor resistance that are originated by variations in temperature are cancelled because of the ratiometric configuration adopted. Therefore, the effect of temperature on the baseline resistance is minimum, as it is mostly cancelled in the ratio of the two sensor resistances.

However, the effect of increasing temperature on the boiling point of the analyte is reflected as a reduction in the response of the ASIC sensing devices.

### 7.4.3.1 Response of monotype devices to temperature and ethanol vapour

The ratiometric ASIC devices based on poly(ethylene-co-vinyl acetate) showed a response almost linear to temperature when they were exposed to ethanol vapour in air. The reduction in the response with increasing temperature produced coefficients as low as  $-0.157 \text{ mV}/^\circ\text{C}$  in average, with standard deviation of only  $0.01 \text{ mV}/^\circ\text{C}$ .

Figure 7.11 shows the almost linear response to temperature of monotype PEVA-based ASIC devices, when exposed at several concentrations of ethanol vapour in air.

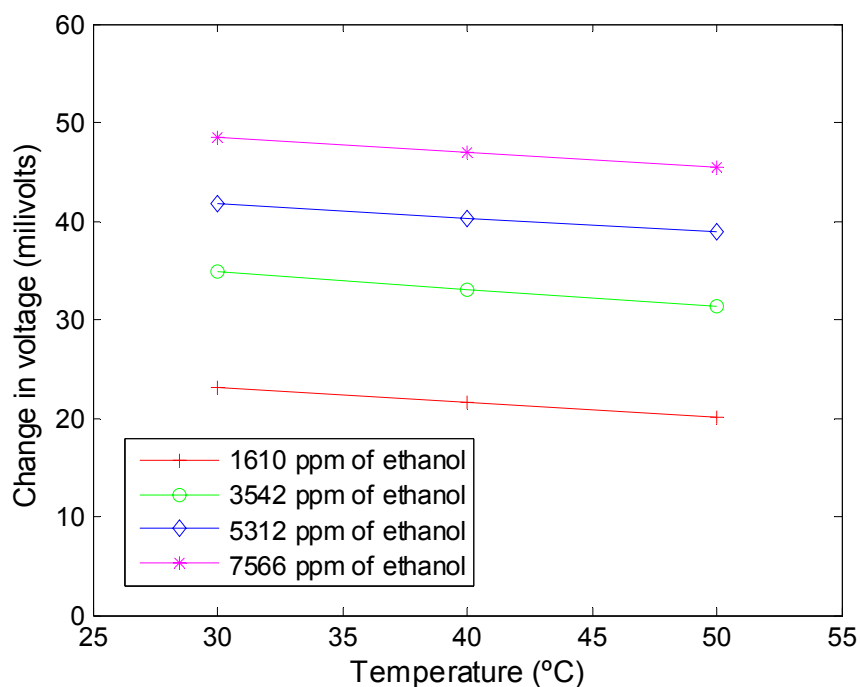


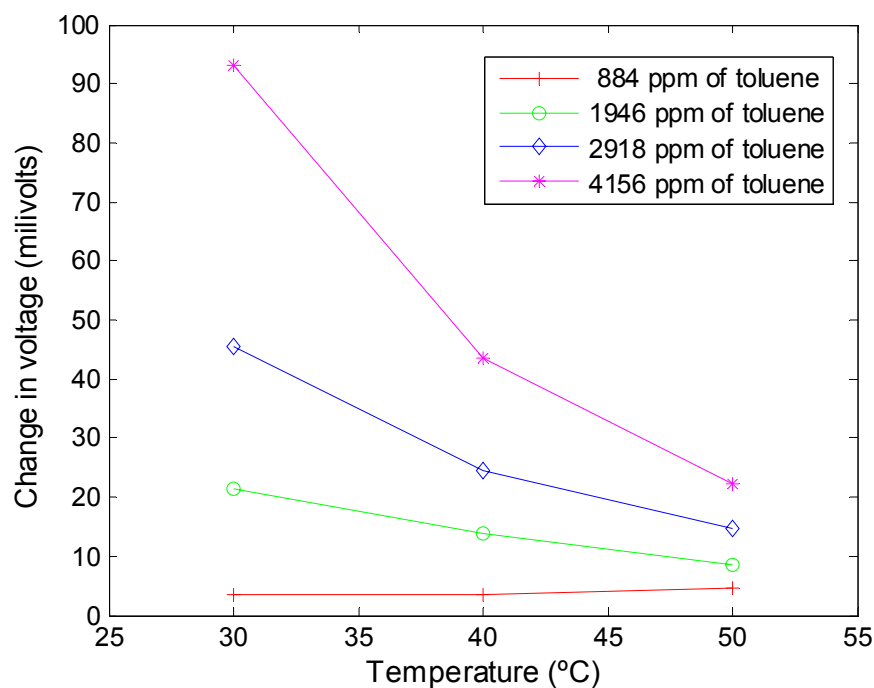
**Figure 7.11** Temperature dependence of monotype PEVA-based ASIC devices at several concentrations of ethanol vapour in air.

Poly(caprolactone) ASIC devices produced a similar response to temperature when exposed to ethanol vapour. Average temperature coefficient was  $-0.027 \text{ mV}/^\circ\text{C}$ , with standard deviation of  $0.04 \text{ mV}/^\circ\text{C}$ .

#### 7.4.3.2 Response of monotype devices to temperature and toluene vapours

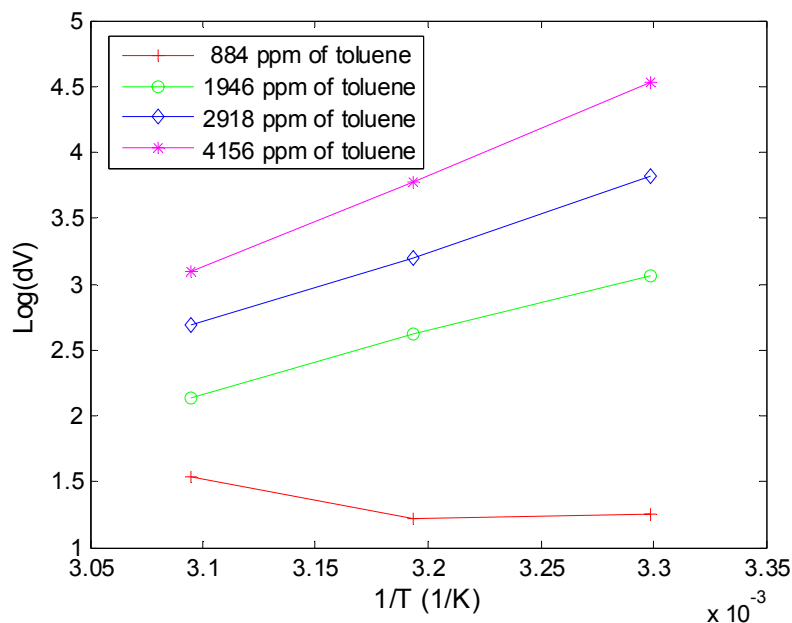
Temperature dependence of monotype ASIC devices showed higher first and second order gradients for tests with toluene vapours. Both PEVA and PCL devices averaged temperature sensitivities of  $-1.420$  mV/°C, but standard deviation was larger for PCL-based ASIC devices ( $1.56$  mV/°C) than for PEVA-based ASIC devices ( $0.92$  mV/°C).

The response to temperature at four concentrations of toluene for PCL-based ratiometric ASIC devices is shown in Figure 7.12.



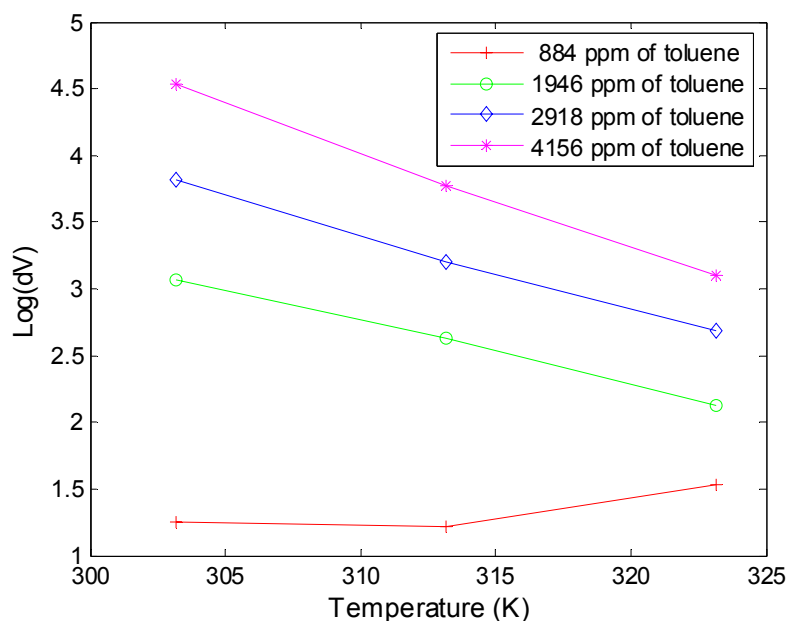
**Figure 7.12** Temperature dependence of monotype PCL-based ratiometric ASIC devices at several concentrations of toluene vapour in air.

Figure 7.13 shows the plot of  $\log(\Delta V)$  vs.  $1/T$  for the same set of data. It is observed that, for high concentrations of toluene, the increasing temperature produces a reduction in the response of the PCL devices, following a log model close to linearity, which can be approximately scaled to the concentration of the analyte.



**Figure 7.13** Log plot of temperature dependence of monotype PCL-based ratiometric ASIC devices for several concentrations of toluene vapour in air.

A more precise fit can be obtained by representing  $\log(\Delta V)$  vs.  $T$ , as shown in Figure 7.14 where for the same higher concentrations the logarithmic plots are closer to linearity, in correspondence with the analyte boiling point model studied in [7].



**Figure 7.14** Logarithmic plots showing how increasing temperature produces a decrease on the response of monotype PCL-based ratiometric ASIC devices.

## 7.5 RESPONSE OF DUO-TYPE DEVICES

The innovative idea of using two materials with contrasting responses for the sensing elements connected to the ratiometric circuit has been tested with a combination of Warwick sensors. The combined use of two different carbon black/polymer composite materials was tested with the samples listed in Table 7.2.

### 7.5.1 Response of duo-type devices to ethanol and toluene vapours

It was observed that the combined responses of PEVA and PCL composites to ethanol vapours in air virtually cancelled the output of the circuit, whereas the differences in their dynamical responses to toluene vapours produced a considerable change in output voltage. Initial results show a promising significant increase in sensitivity, even though the phenomenon is still under investigation. The response, however, is only significant from medium to high concentrations of the vapours. Although with a difference in magnitude, all the samples tested showed similar responses.

#### 7.5.1.1 Response of duo-type devices to ethanol concentration

The plots in Figure 7.15 correspond to the typical response to ethanol vapours in air of the duo-type devices with a carbon black/PEVA sensor in  $R_1$  and a carbon black/PCL sensor in  $R_2$ , tested at 35°C. It is clear that the output has been mostly cancelled for ethanol vapour, with an average response of 0.24  $\mu\text{V/ppm}$  before amplification, contrasting with the response of the same devices to toluene, which is described below.

The explanation for this behaviour comes from the contrasting partial responses of the combination of sensors when the products  $R_2 dR_1$  and  $R_1 dR_2$  are equal, cancelling the total variation in the output voltage given by Equation 2.23 in Chapter 2.

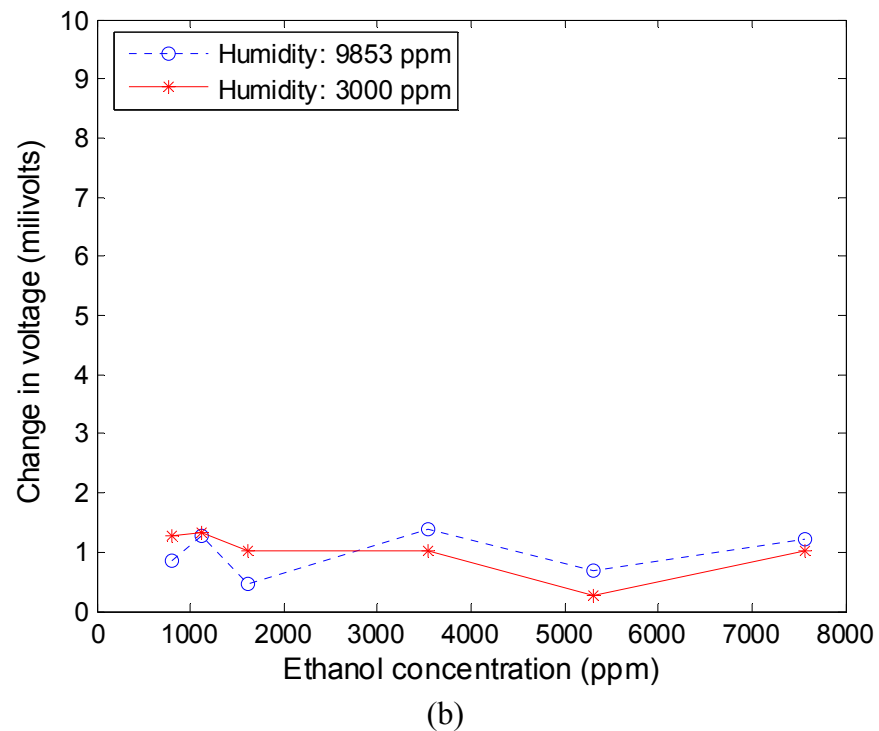
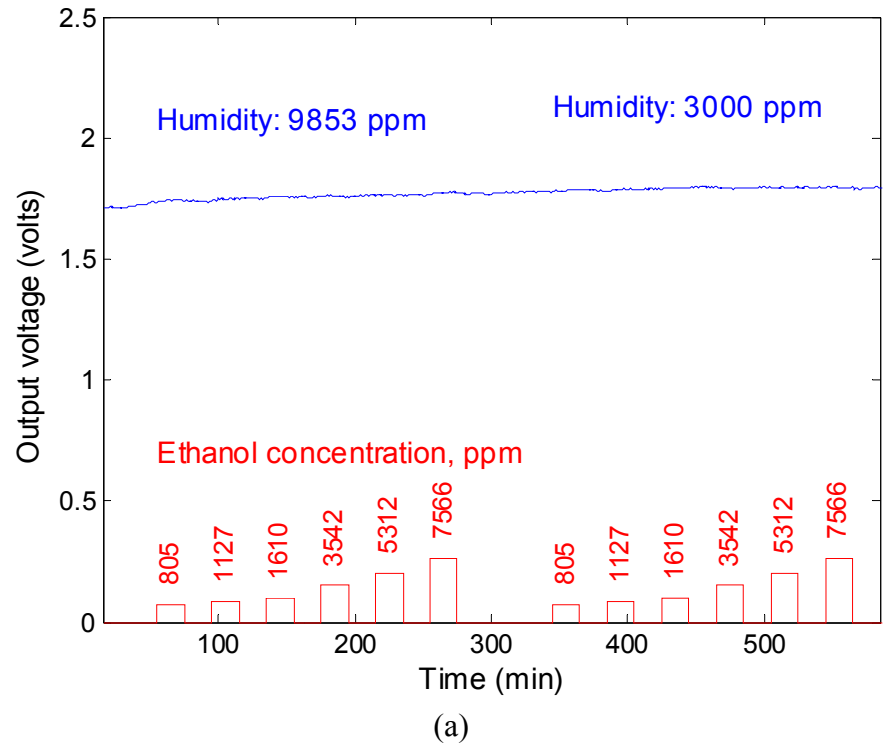


**Figure 7.15** Typical almost null response of the duo-type devices to different concentrations of ethanol vapours in air at 35°C. (a) Output voltage. (b) Change in voltage prior to amplification.



### *7.5.1.2 Response of duo-type devices to toluene concentration*

The response of the duo-type devices to toluene has been significantly increased, with respect to the responses of the two composites used in the monotype devices, reaching a notable voltage sensitivity coefficient of  $30.5 \mu\text{V}/\text{ppm}$  prior to any amplification. The plots in Figure 7.16 show the typical response of a duo-type device to toluene vapours.

### **7.5.2 Response of duo-type devices to humidity**

Derived from the particular ratiometric configuration adopted and given that both chemoresistors in the sensor array are exposed to any variations in the environment conditions, changes due to different humidity levels are reduced to a minimum in the duo-type devices.

There is, however, a difference produced by the larger response to humidity of the PEVA based sensors when compared to the PCL based ones, in particular when the ratiometric ASIC devices are exposed to toluene vapours.

#### *7.5.2.1 Response of duo-type devices to humidity and ethanol vapours*

Besides the observation that the duo-type devices produce virtually no response to ethanol vapours, the comparable sensitivities of PEVA and PCL based sensors to water vapour contribute to generate an overall output which is barely sensitive to humidity changes.

The average sensitivity coefficient to water vapour concentration for the duo-type devices exposed to ethanol vapours in air at  $35^\circ\text{C}$  was  $0.056 \mu\text{V}/\text{ppm}$ . The plots in Figure 7.17 show the typical response of duo-type devices to humidity, for different concentrations of ethanol vapour.

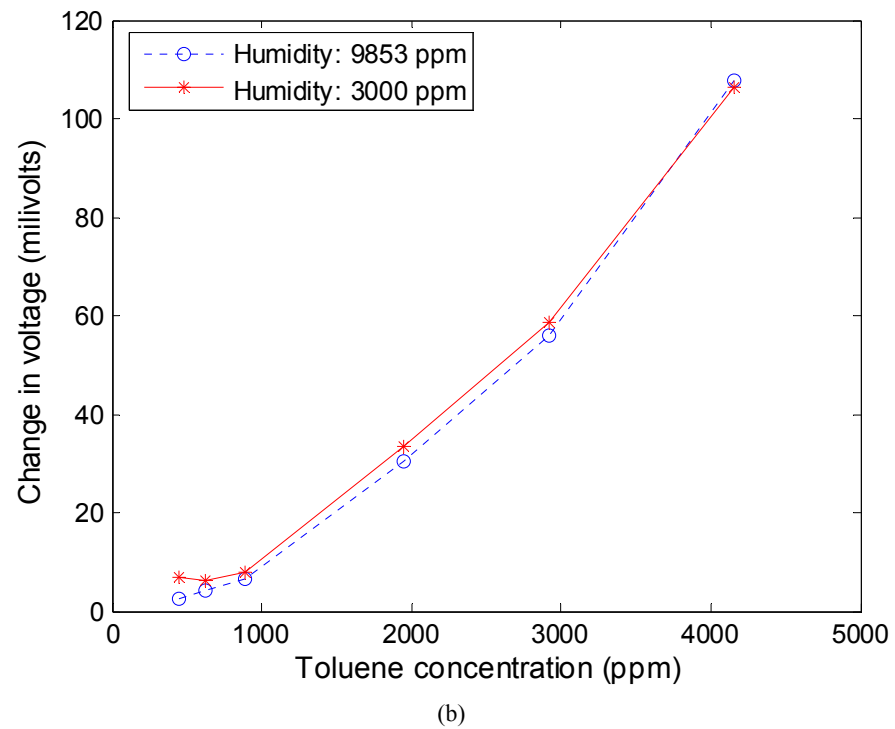
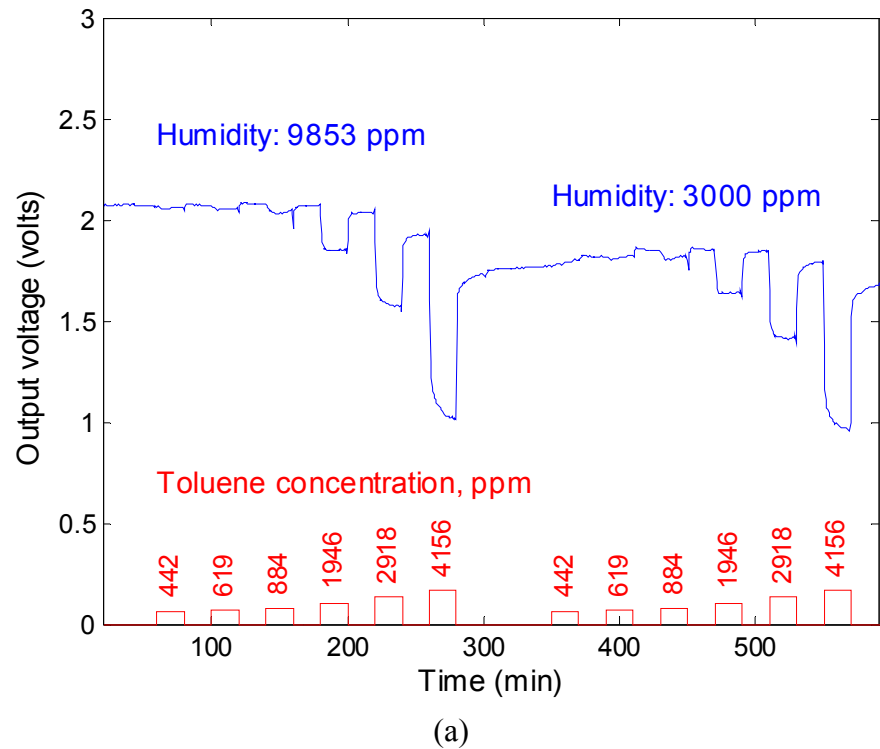


**Figure 7.16** Typical response of the PEVA/PCL duo-type devices to different concentrations of toluene vapours in air at 35°C. (a) Output voltage. (b) Change in voltage prior to amplification.

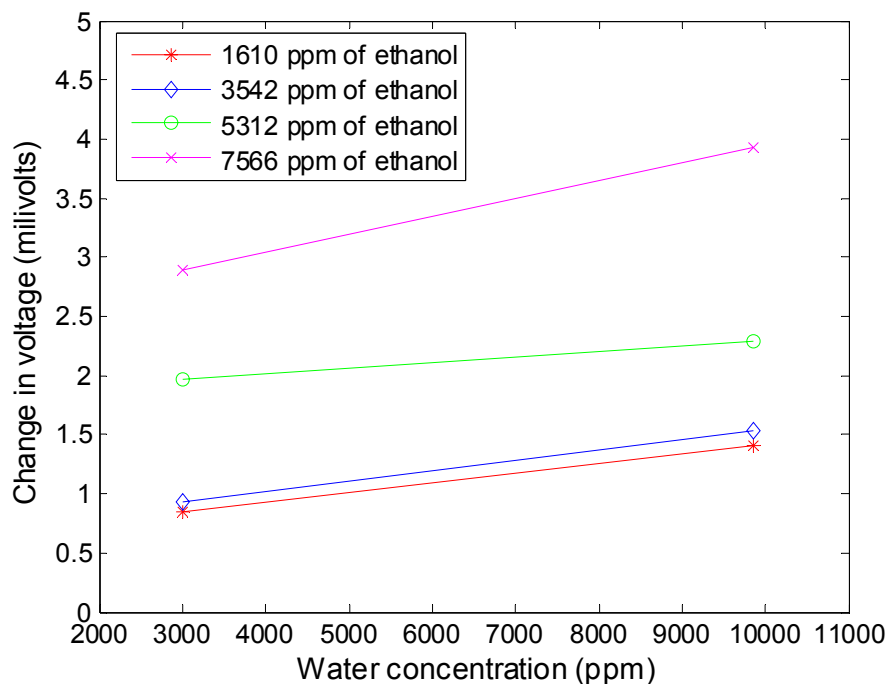


**Figure 7.17** Typical response of the duo-type ASIC chips to different concentrations of water vapour when exposed to ethanol vapours in air at 35°C.

#### 7.5.2.2 Response of duo-type devices to humidity and toluene vapours

The sensitivity of PEVA composites to toluene vapours is significantly larger than the sensitivity of the PCL based sensors, and the interaction with water vapour produces also a difference in the response of the two types of sensors at different humidity values.

The sensitivity to water vapour concentration for the duo-type devices exposed to different concentrations of toluene vapour in air at 35°C averaged 0.390  $\mu\text{V/ppm}$ . Figure 7.18 shows the typical response of duo-type devices to humidity, obtained with different concentrations of toluene vapour.

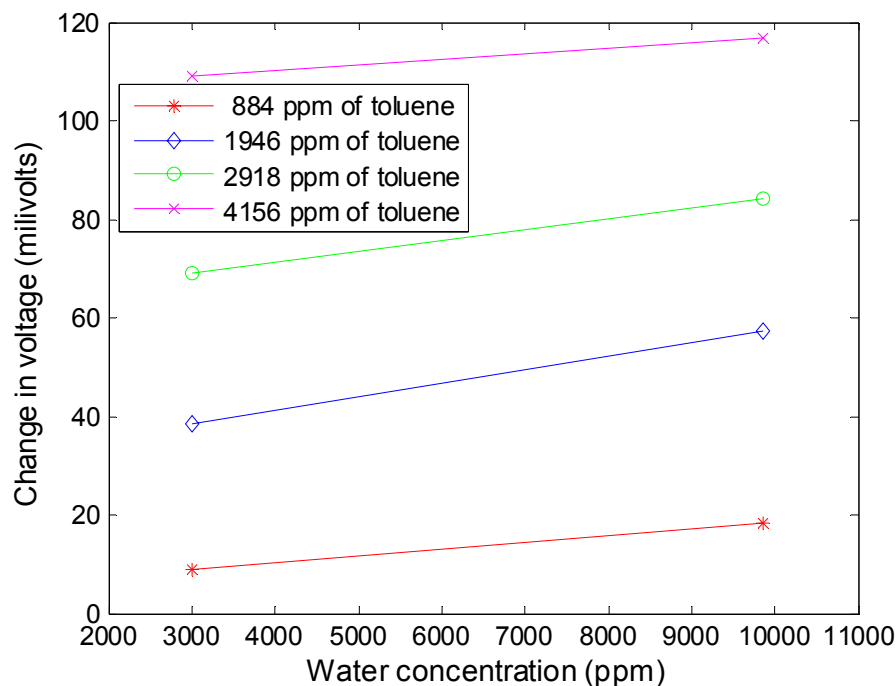


**Figure 7.18** Typical response of the duo-type ASIC chips to different concentrations of water vapour when exposed to toluene vapours in air at 35°C.

### 7.5.3 Response of duo-type devices to temperature

The main characteristic of the duo-type ASIC devices is the selective response to the analytes tested. Whereas for ethanol the response is practically cancelled, the contrasting responses of PEVA and PCL sensors act additively for toluene vapours. This phenomenon was also observed with respect to temperature dependence, given that very low temperature coefficients were obtained with ethanol vapour whilst the temperature response was significantly increased with toluene exposure.

#### 7.5.3.1 Response of duo-type devices to temperature and ethanol vapours

Given the low response to ethanol that the duo-type ASIC devices produced, there is not much that can be observed regarding the effect of temperature. The low averaged coefficient ( $-0.010$  mV/°C) obtained for temperature dependence with ethanol has no significance when the overall output of the duo-type devices is practically nil.

### 7.5.3.2 Response of duo-type devices to temperature and toluene vapours

Temperature dependence is highly significant in the response of the duo-type ASIC devices to toluene vapours. The differences in the responses to temperature showed by the PEVA and PCL materials have in this case an additive effect.

A comparison of responses obtained with the same duo-type device at 35°C and 45°C is shown in Figure 7.19. The increase in temperature produces a lessening in the magnitude of the response, modifying the voltage sensitivity coefficient to toluene vapour from 30.5  $\mu\text{V}/\text{ppm}$  at 35°C to 10.5  $\mu\text{V}/\text{ppm}$  at 45°C for the duo-type ASIC device at the humidity values tested. It can also be noticed that the differences between the two humidity tests are minimised.

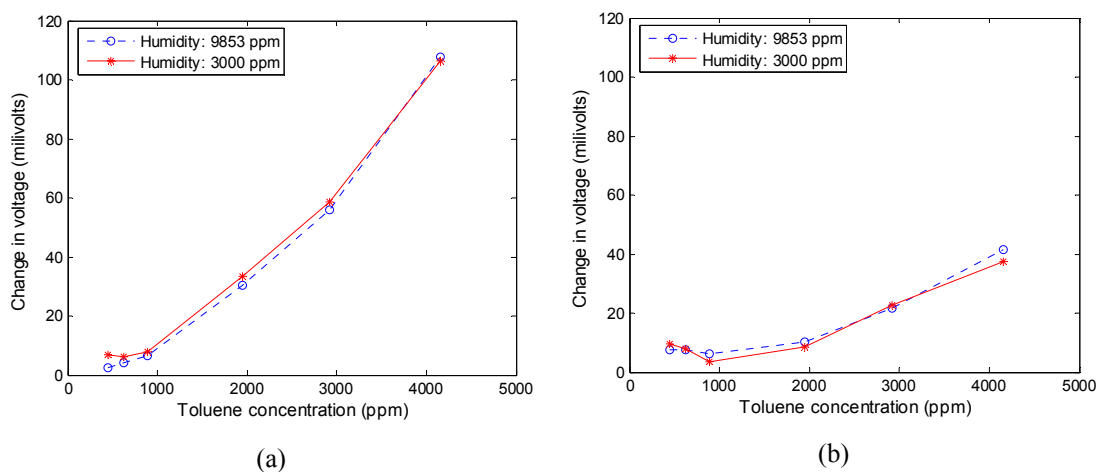


**Figure 7.19** Response of one of the duo-type ASIC chips with the contrasting PEVA-PCL array of sensors to different concentrations of toluene vapours in air at (a) 35°C and (b) 45°C.

Temperature dependence of the duo-type ratiometric ASIC device is shown in Figure 7.20 for different concentrations of toluene vapour in air. Average sensitivity is  $-3.123 \text{ mV}/^\circ\text{C}$ , with standard deviation of  $1.99 \text{ mV}/^\circ\text{C}$ . The combined response of the two sensing materials did not follow the same log model shown by the monotype devices.

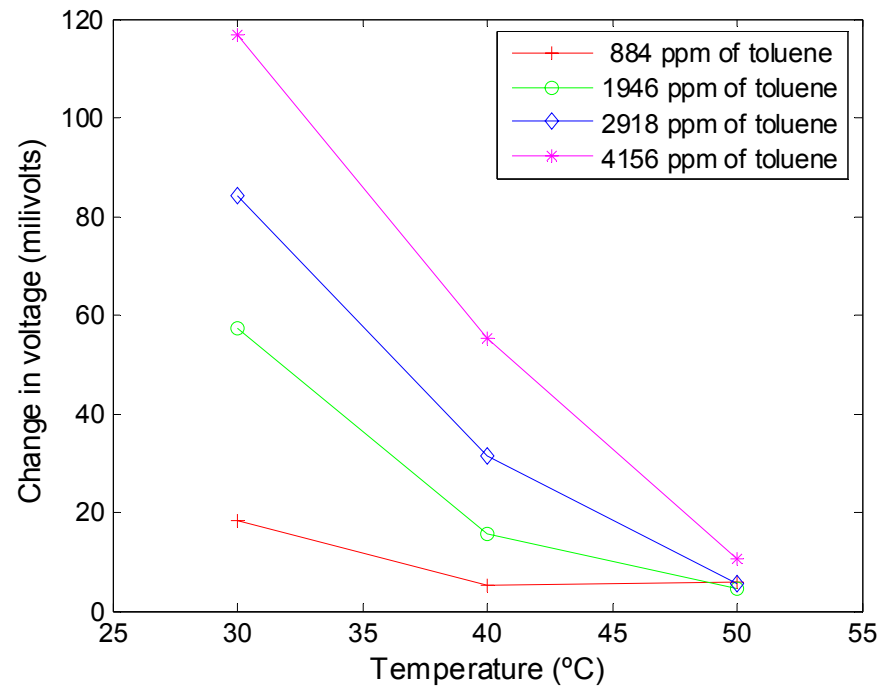


**Figure 7.20** Temperature dependence of duo-type ratiometric ASIC devices at several concentrations of toluene vapour in air.

## 7.6 OVERALL PERFORMANCE

The two types of ratiometric ASIC devices that were tested produced results within the expectations and predictions based on simulations reported in chapter 4 of this work.

Characterisation shows two consistent types of devices performing with clearly defined patterns and confirming the behaviour envisaged from the analysis of the characteristics of both the sensing materials employed and the configurations in which they were applied within the ratiometric ASIC devices.

For the first type of them, i.e. the monotype devices, it was observed a limited selectivity of the composite material to the analytes. The use of PEVA based resistive sensors produced a type of device with a response slightly better to ethanol ( $3.2 \mu\text{V/ppm}$ ) than the one for toluene ( $2.6 \mu\text{V/ppm}$ ), whereas the devices based on PCL resistive sensors showed a much better response to toluene ( $8.6 \mu\text{V/ppm}$ ) than the one for ethanol ( $1.9 \mu\text{V/ppm}$ ).

Duo-type devices based on combined active PEVA and PCL resistive sensors showed a highly improved selectivity to the same analytes, clearly discriminating between toluene, with typical sensitivity as high as  $30.5 \mu\text{V/ppm}$ , and ethanol, whose response was as low as  $0.24 \mu\text{V/ppm}$ , which gives a rejection ratio of 127.

Mono and duo-types of devices are compared in terms of sensitivity as shown in Figure 7.21. The voltage sensitivity coefficient to toluene for the PEVA/PCL duo-type ratiometric device, estimated as  $30.5 \mu\text{V/ppm}$  at the tested concentrations, outperforms that of the monotype ASIC devices, whose sensitivity coefficients to toluene are only  $8.6 \mu\text{V/ppm}$  (PCL devices), and  $2.6 \mu\text{V/ppm}$  (PEVA devices).

For ethanol, the response of the duo-type PEVA/PCL devices is almost zero (0.24  $\mu\text{V/ppm}$ ) at concentrations tested, whereas the monotype devices responded with sensitivity coefficients of 3.2  $\mu\text{V/ppm}$  (PEVA devices) and 1.9  $\mu\text{V/ppm}$  (PCL devices).

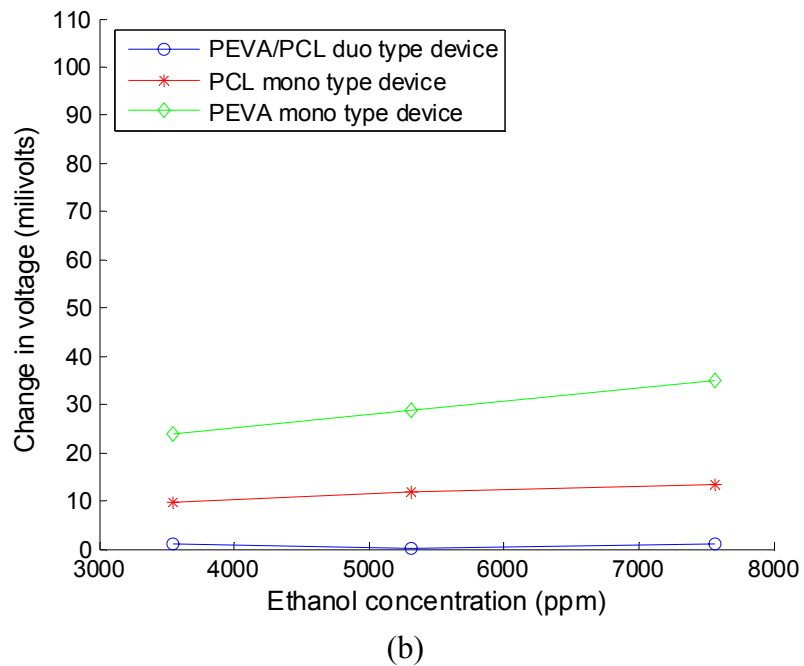
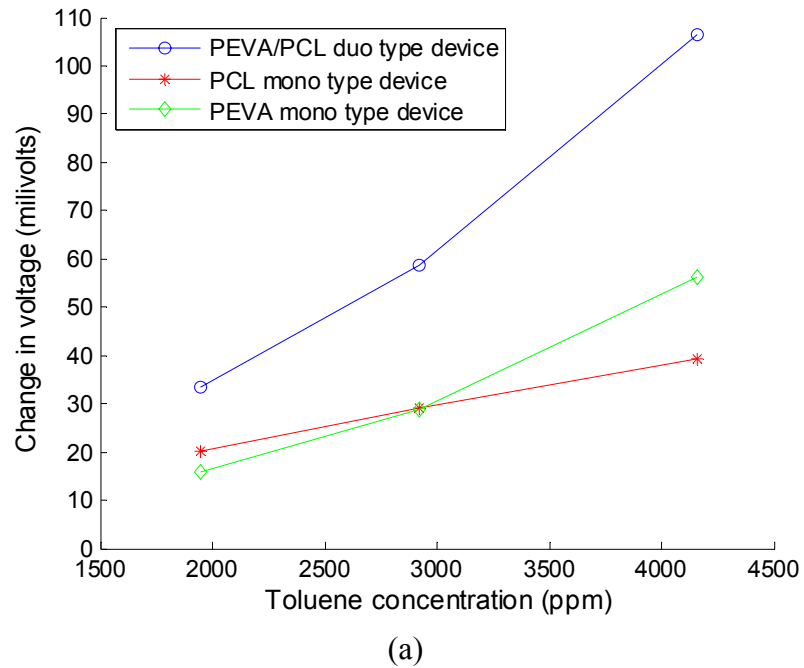


**Figure 7.21** Comparison of voltage sensitivities of duo-type and monotype ratiometric ASIC devices to (a) toluene, and (b) ethanol.



A summary of the typical response coefficients for all the types of ratiometric ASIC devices tested is presented in Table 7.3.

**Table 7.3** Response coefficients to vapours in air for ratiometric ASIC devices.

| Ratiometric ASIC devices        | Toluene ( $\mu\text{V}/\text{ppm}$ ) | Ethanol ( $\mu\text{V}/\text{ppm}$ ) | Rejection ratio Toluene/Ethanol | Water vapour ( $\mu\text{V}/\text{ppm}$ ) |         |
|---------------------------------|--------------------------------------|--------------------------------------|---------------------------------|---|---------|
|                                 |                                      |                                      |                                 | Toluene                                   | Ethanol |
| Mono type devices based on PEVA | 2.6                                  | 3.2                                  | 0.81                            | 0.503                                     | -0.477  |
| Mono type devices based on PCL  | 8.6                                  | 1.9                                  | 4.53                            | 0.021                                     | -0.246  |
| Duo-type devices PEVA/PCL       | 30.5                                 | 0.24                                 | 127                             | 0.390                                     | 0.056   |

In terms of humidity, it was noticed that, for the monotype devices tested, the sensitivity to water vapour was positive for toluene and negative for ethanol, reflecting the differences in the affinity of these analytes to water. The ratiometric configuration used with monotype devices had also some effect on the response to humidity, as only one of the chemoresistors in a given ASIC device was exposed to variations in water vapour concentration, whereas the passive chemoresistor remained at a fixed humidity during the tests, resulting in a higher sensitivity when compared to that of the duo-type devices. Typical values of the response coefficients to humidity are also included in Table 7.3.

Duo-type devices, on the contrary, showed no difference in the sign of sensitivity coefficients to water vapour for the analytes tested. However, the fact that the PEVA and PCL sensors were both active and they acted on complementary

resistive and conductive effects, respectively, gave as a result that the response to humidity of the duo-type devices was also different with respect to that of the monotype ones. The response of the PEVA/PCL devices to the mix of toluene and water vapours ( $0.390 \mu\text{V}/\text{ppm}$ ) was not as high as it was for the PEVA monotype devices ( $0.503 \mu\text{V}/\text{ppm}$ ). Also, duo-type devices showed a very low sensitivity to the mix of ethanol and water vapours ( $0.056 \mu\text{V}/\text{ppm}$ ), derived from the ability of the PEVA/PCL combination for the near elimination of the response to ethanol.

Increasing temperature caused a reduction in the response for all the ASIC devices tested. Near linearity was observed for ethanol vapours, where the decreasing of the response was almost null, as it is confirmed by the summary of coefficients presented in Table 7.4.

The figures shown for the duo-type devices are not relevant at all, given the fact of the very low response of these devices to ethanol vapours.

**Table 7.4** Temperature coefficients for ratiometric ASIC devices obtained at different concentrations of ethanol vapour in air.

| Ratiometric ASIC devices        | Temperature coefficients<br>( $\mu\text{V} / ^\circ\text{C}$ ) |          |          |          |                     |                    |
|---------------------------------|--|----------|----------|----------|---------------------|--------------------|
|                                 | 1610 ppm   | 3542 ppm | 5312 ppm | 7566 ppm | Average sensitivity | Standard deviation |
| Mono type devices based on PCL  | -78.8  | -14.8    | -14.6    | 1.4      | -26.7               | 35.6               |
| Mono type devices based on PEVA | -151.0   | -175.7   | -149.8   | -149.7   | -156.6              | 12.8               |
| Duo-type devices PEVA/PCL       | -50.9  | 9.0      | -11.7    | 12.3     | -10.3               | 29.1               |

The effect of increasing temperature on the reduction of the response was larger when the ratiometric ASIC devices were exposed to toluene vapours in air. The difference in results with respect to ethanol suggest that the temperature effect is mainly related to the analyte boiling point, as it has been extensively analysed and modelled in previous research work [7]. These differences are made more noticeable by the use of the uncoated duo-type devices, whose temperature coefficients for toluene are larger ( $-3123 \mu\text{V}/^\circ\text{C}$  in average) than those obtained for the monotype devices (averaged  $-1420 \mu\text{V}/^\circ\text{C}$ ). A summary of temperature coefficients for different concentrations of toluene vapour in air is presented in Table 7.5.

**Table 7.5** Temperature coefficients for ratiometric ASIC devices obtained at different concentrations of toluene vapour in air.

| Ratiometric ASIC devices        | Temperature coefficients ( $\mu\text{V} / ^\circ\text{C}$ ) |          |          |          |                     |                    |
|---------------------------------|---|----------|----------|----------|---------------------|--------------------|
|                                 | 884 ppm   | 1946 ppm | 2918 ppm | 4156 ppm | Average sensitivity | Standard deviation |
| Mono type devices based on PCL  | 56.1  | -647.6   | -1542.7  | -3545.5  | -1420               | 1561               |
| Mono type devices based on PEVA | -281.9  | -1131.9  | -1868.1  | -2398.8  | -1420               | 919.6              |
| Duo-type devices PEVA/PCL       | -625.2  | -2629.9  | -3932.6  | -5304.1  | -3123               | 1991.2             |

The tests also revealed that the ratiometric configuration practically eliminated the temperature dependence of the baseline output voltage for the monotype devices, as a consequence of the cancellation of the common temperature effect through the ratio of the resistances of the sensors.

## 7.7 CONCLUSIONS

Two types of smart sensors have been characterised using the ratiometric ASIC chip designed in this project. Chemoresistors made out of carbon black/polymer composite were arranged in two different ratiometric configurations, called monotype and duo-type. In the first of these, both the active and the passive resistive sensors were fabricated with the same polymer material. The passive chemoresistor acted as a reference while the active one responded to the ethanol and toluene vapours applied in the tests. In the second type of array both chemoresistors responded actively to the vapours applied, but each one was fabricated with a different sensing material.

Samples of both types of smart ratiometric devices were tested in an automated station in order to test their response to different concentrations of ethanol and toluene vapours in air. The tests were performed at different values of humidity and temperature, in order to study the effect of these variables on the response of the sensors, but most of all, to observe and validate the performance of the ratiometric ASIC chip.

Additional electronics designed for the control of the tests with the ASIC devices worked as expected. The virtual instrumentation written for the same purpose allowed the automated calibration of the devices prior to the tests and the automatic recording of the output voltage data while the ASIC devices were exposed to the programmed concentrations of analyte vapours.

The results obtained with the monotype ASIC devices confirmed the response that was predicted by the simulations. It was remarkable, however, the near

elimination of the temperature dependence on the baseline output voltage, produced by the ratiometric configuration of the circuit.

Also noticeable were the results obtained with the duo-type ASIC devices, given that the use of the combined effect of different active materials had not been reported before. The resulting devices showed high selectivity for the analytes tested, achieved also through the ratiometric arrangement of the sensors.

The reported results also illustrate additional benefits of the ratiometric principle applied for the design of the ASIC chip. Low drift in the baseline output voltage was observed and a considerable reduction of the dependence on humidity was also found. Some of the devices were available for several months and it was also confirmed that the circuit minimises long-term drift and ageing effects of the sensing materials, by producing consistent responses.

The complete set of results obtained with all the tests performed is included in Appendix G.

Overall conclusions about the project and some proposals for additional work with the ratiometric ASIC chip are presented in the last chapter of this work.

## 7.8 REFERENCES

1. Lonergan, M.C., Severin, E.J., Doleman, B.J., Beaber, S.A., Grubbs, R.H., Lewis, N.S. (1996). "Array-based vapor sensing using chemically sensitive carbon-black-polymer resistors", *Chem. Mater.*, **8**, 2298-2312.
2. Tsubokawa, N., Tsuchida, M., Chen, J., Nakazawa, Y. (2001). "A novel contamination sensor in solution: the response of the electric resistance of a composite based on crystalline polymer-grafted carbon black", *Sensors and Actuators B*, **79**, 92-97.
3. Dickson, J.A. and Goodman, R.M. (2000). "Integrated chemical sensors based on carbon black and polymer films using a standard CMOS process and post-processing", *Proceedings of the IEEE International Symposium on Circuits and Systems (ISCAS)*, Geneva, Switzerland, 341-344.
4. Zee, F. and Judy, J.W. (2001). "Micromachined polymer-based chemical gas sensor array", *Sensors and Actuators B*, **72**, 120-128.
5. Gardner, J.W. and Bartlett, P.N. (1999). *Electronic noses: principles and applications*, Oxford University Press, New York.
6. Gardner, J.W., Pearce, T.C., Friel, S., Bartlett, P.N., Blair, N. (1994). "A multisensor system for beer flavour monitoring using an array of conducting polymers and predictive classifiers", *Sensors and Actuators B*, **18**, 240-243.
7. Covington J.A. (2001). "CMOS and SOI CMOS FET-based Gas Sensors", PhD Thesis, University of Warwick, Coventry, UK.
8. National Instruments™ (2002). *DAQ NI 6034E/6035E/6036E User manual, Multifunction I/O devices*, Part number 322339D-01, Austin, Texas, USA.
9. Phillips Semiconductors (2002). "The I<sup>2</sup>C-bus specification", Document available at [www.semiconductors.phillips.com](http://www.semiconductors.phillips.com).
10. XICOR (2002). "X9241A Quad digital controlled potentiometers (XDCP™)", Datasheet available at [www.xicor.com](http://www.xicor.com), Rev 1.1.13 12/09/02.

# CONCLUSIONS AND FURTHER WORK

### 8.1 AIMS REVIEWED

A novel ratiometric ASIC chip has been designed, fabricated and characterised with resistive vapour sensors made out of carbon black/polymer composite materials in two ratiometric configurations. Its smart capabilities of drift reduction and self-calibration demonstrate its potential application in a micro-power hand-held unit for the monitoring of VOC.

A review of the aims of the project, enunciated at the end of chapter 1, shows a positive balance on the achievements of this work. Not only the all goals were more than satisfactorily reached, but also additional findings and possibilities were envisaged and explored after the successful fabrication of the ratiometric ASIC chip.

In effect, the proposed CMOS ASIC chip was fabricated and characterised after being designed, modelled and simulated in order to accomplish the required features for its application in the smart monitoring of VOC or gases. All the stages of the process were described along previous chapters and the characterisation of the fabricated ASIC chip and resulting smart sensing devices were also presented.

As put forward from the aims of the project, chemoresistors and processing circuitry were integrated into a single chip. Post-fabrication tests demonstrated that the designed ratiometric ASIC devices fulfilled all the expectances when the gas sensitive material was added to the CMOS chips.

The post-CMOS fabrication of the chemoresistors complemented the ASIC chip design. Whenever possible, resistances of the sensors were tried to match when the carbon black/polymer composites were deposited within every ASIC device. However, the unavoidable variations due to the fabrication process were effectively compensated through the ratiometric array used in the ASIC design. Additionally, the ASIC chip allows the use of a large range of values of resistances in the sensors around the nominal design value of  $10\text{k}\Omega$ . Resistances of at least one order of magnitude, both above and below this nominal value, were satisfactorily tested in the simulations presented in Chapter 4.

Effects of environmental variations such as temperature and humidity were also reduced and a substantial improvement has being obtained with respect to previous attempts [1-6]. Changes in ambient temperature are automatically compensated on sensors made out of identical material, given that variations are absorbed in the ratio of their resistances. As a consequence of this ratiometric relationship, temperature dependence of the baseline voltage was practically



eliminated in the monotype devices. The effect of humidity, although negligible for the type of resistive sensors used, was also found to be lessened for the ratiometric monotype devices, reaching values below than  $0.50 \mu\text{V/ppm}$  and as low as  $0.021 \mu\text{V/ppm}$  for mixtures with toluene, and within the same range of magnitude for mixtures with ethanol (See Table 7.3).

Expecting to gain better control and independence of ambient variations, a temperature control circuit was also included in the design. The circuit relies on the use of resistive heaters which are controlled by thermodiodes and powered via a proportional feedback system, which compensates for differences in temperature between the heaters regions and a previously established set-point. The temperature control circuit, however, was not required in the experimental part of this work, given that the tests were performed with the ASIC devices within a heater block included in the automated test station. The availability of the temperature control circuitry, however, expands the versatility of the ASIC chip for the use of other resistive materials which may require operation at different temperatures, as it was explained in section 3.4.

Carbon black/polymer composites were used as resistive sensing materials in order to produce the smart devices that were tested using some of the different ratiometric configurations allowed by the ASIC chip design. Availability and performance of the ASIC chip allowed both the testing of the benefits of the ratiometric configuration in the monotype devices and the exploration of a novel sensing design in the duo type devices.

In summary, the application of the ratiometric principle to the design, fabrication and testing of the smart ASIC devices reported in this work, demonstrated the following benefits:

- The circuit compensates for unwanted variations in the fabrication of the resistive sensors, allowing the use of *resistance ratios* between  $\frac{1}{2}$  and 2 in the chemoresistors of the ratiometric array.
- Apart from the wide range allowed in the resistance ratios, the ASIC chip operates accurately with chemoresistors varying widely (from 1 k $\Omega$  to 100 k $\Omega$ ) around the nominal design value of 10 k $\Omega$ , avoiding the need for the use of multiplexed current sources or other methods to accommodate range of polymer resistances.
- Temperature dependence of the baseline output voltage was practically eliminated in the monotype devices, and its effect was negligible in the case of the duo-type devices (Figures were given in tables 7.4 and 7.5).
- The drift problem originated by the use of constant voltage sources has been eliminated by driving the chemoresistors with a pulsed voltage that is alternated by a FET-switched circuit.
- Important progress has been made in the reduction of long-term drift, given that ageing occurs simultaneously and in the same proportion in the chemoresistors, thus cancelling differences in the ratio of their resistances.
- Humidity dependence of the output, although negligible for the carbon black/polymer composite materials employed in the tests, was also

substantially reduced through the partial cancellation in the ratio of resistances of the sensor configuration.

- The design of the ASIC chip allowed the testing and characterisation of different ratiometric configurations, namely monotype and duo-type devices. Its flexibility is not limited only to these types, but other innovative configurations can also be implemented, as it is proposed below.
- The ASIC chip can work with practically any resistive sensing material, internal or external to the chip; the only practical limitation being the size of the electrodes area. Carbon black/polymer composite materials were characterised in this project, but modelling and simulation performed (Chapter 4) show the adaptability of the circuit to any other type of chemoresistors.

A comparison of the aims set at the beginning of the project with the conclusions and findings summarised in this chapter, shows how the global achievements of this work exceed the goals originally proposed. Moreover, the successful design, modelling, simulation, fabrication and testing of the ratiometric ASIC chip has opened the possibilities for more advanced and innovative research based on the application of the fully functional product of this project.

## 8.2 THE ASIC TOP-DOWN DESIGN

Although the original proposal of the project considered the fabrication of the smart ASIC chip in two separated steps, all the original targets were achieved within a single design stage. This was possible by following a complete top-down process for the design and fabrication of the ASIC chip, ensuring that every feature required by the expected final product was successively:

- a) included in the design since the first schematic version (presented in chapter 3), defining particular and global functions of every component,
- b) modelled either by available parameter sets obtained from the technology vendors or by parameter models explicitly written for this project (reported in chapter 4),
- c) simulated under operating conditions and redesigned until each part performed as it was proposed (also reported in chapter 4),
- d) included in the layout of the ASIC chip (as described in chapter 5) according to the characteristics and requirements of the CMOS process adopted, and verified against its design rules prior to the fabrication step,
- e) tested and characterised after fabrication (as summarised in chapter 6), in order to compare the actual performance of the ASIC chips with the predictions of the simulations,

Once all these steps were accomplished in that order and with the proper feedback reconsiderations, the resulting ratiometric ASIC chip proved to work efficiently when the carbon black/polymer composite were integrated to the chip (as reported in chapter 7).

### 8.3 SMART SENSORS CHARACTERISATION

Two different configurations of carbon black/polymer composite chemoresistors were used for the complete characterisation of smart sensors based on the ratiometric ASIC chip, namely: monotype devices and duo-type devices. In the first one of them, monotype devices, the sensing resistors were made out of the same material, with one being active while the other was prevented from gas exposure. Characterisation of these ASIC devices led to the following conclusions:

- a) The response of the devices increased with increasing concentration of toluene and ethanol vapours in air.
- b) Humidity effect on the response was negligible with the sensing materials and analytes tested, even after considering the difference produced with respect of the coated chemoresistor, which was maintained at constant humidity.
- c) Temperature dependence of the baseline voltage was eliminated by the use of the ratiometric configuration.

The characterisation of the novel duo-type devices allowed the exploration of the combined properties of two different materials and also permitted the use of two active sensing elements in the ratiometric array, i.e. no passive sensors were used in this configuration. From these experiments, it was concluded that:

- a) Duo-type ASIC devices were proposed, fabricated and tested for the first time in this project. The novel devices are also based on the ratiometric principle and its operation was successfully characterised.

- b) Duo-type devices responded with superior sensitivity to VOC concentration with respect to the monotype devices (figures reported in Table 7.3). Compared to the monotype devices, sensitivity to toluene was clearly superior for the duo-type devices, resulting 3.55 times greater than for the PCL-based monotype devices and 11.73 times greater than for the PEVA-based monotype devices.
- c) The duo-type ASIC devices tested showed clear selectivity for the two analytes used in the tests. The average voltage response to toluene was 127 times greater than the response to ethanol, which is much higher than the 4.53 ratio obtained with the most selective samples of monotype devices. Data were given in Table 7.3.

## 8.4 ADDITIONAL BENEFITS OF THE RATIOMETRIC DESIGN

The benefits of the ratiometric design have already been described in the sections 8.1 and 8.3 and in the conclusions of Chapter 7. In general, the ratiometric ASIC chip proved to be effective in the reduction of drift problems and for the compensation of unwanted variations that affect in the same proportion to both resistive sensors of the array.

Additionally, the use of the ratiometric configuration showed several beneficial consequences. First of all, the ratiometric ASIC chip possesses extensive flexibility and adaptability, being able to work with a number of nano-materials and combinations thereof and producing coherent results, as it was revealed after its experimental application with two types of carbon black/polymer composite sensors. Moreover, the implementation of innovative configurations, such as duo type devices, also showed that the sensitivity and selectivity of the device as a whole can be enhanced.

Also, the versatile pad design applied in the structure of the chip allowed the use of both internal and external resistive sensors and the straight access to the supporting electronics for interconnectivity and testing of every component. Interfacing electronics also worked as expected both for electrical characterisation of the ASIC chip and for the characterisation of the smart ratiometric devices under vapour exposure.

Even variations in the CMOS fabrication process that were not considered at the moment of the design, were cancelled through the resistance ratios adopted thoroughly in the circuit. That was the case of the *Nwell* resistors used, whose actual resistance differed from nominal values given in the technology specifications, but differences were compensated through the ratiometric relationship, as it was deduced from indirect measurements in those points that were not available for direct testing.

## **8.5 PROPOSED FURTHER WORK**

Although the design and fabrication project was successfully completed, capabilities of the ASIC chip are still too extensive and there are a number of projects which can be derived from its applications and possible improvements. Some proposals for the possible further work derived from this project are given below, with basic guidelines for its practical implementation.

### **8.5.1 Application of the ASIC chip with novel nano-materials**

The designed ratiometric ASIC chip is capable to drive not only the carbon black/polymer composite sensors reported in the previous chapter, but it also works with any set of external resistive sensors, provided these matched the general requirements regarding the absolute resistance and, most of all, the proper resistance ratio. In fact, the precision 10 k $\Omega$  resistors used for the initial electrical tests of the chips are a good example of the adaptability of the ASIC to any external resistive element connected through the available sensor pads.

The ratiometric circuit concept applied in the design allows the use of practically any resistive sensing material, as it was also shown through the modelling described in Chapter 4, section 4.5. The designed structure of the sensor electrodes allowed the deposition or spray coating of polymer-based materials, but other chemoresistive elements can be used, especially if electroless plating is applied onto the aluminium electrodes.

There is, however, a more concrete possibility already under development. Discrete gas sensor chips with different gas sensing materials have been used together with the ratiometric ASIC to obtain novel hybrid devices that are currently under characterisation.



The first of these microsensors is a special chemoresistor type based on gold-nanoparticle/organic linker films developed and provided by the Materials Science Laboratories of Sony International (Europe) [7-8]. In these discrete chemoresistors, the organic linker allows the absorption of the analytes, while the gold nanoparticles provide electric conductivity to the film, [7, 9-10], resembling the behaviour of the carbon black/polymer composites. The films show linear current-voltage characteristics, with resistance increasing when exposed to solvent vapours. The electrical response to the concentration of the absorbed analyte is also linear [8].

Research with these materials is currently undertaken at the SRL using the ratiometric ASIC chip and all the testing equipment described in this work, with expectancies for the development of better sensing devices. Likewise, other chemoresistive nano-materials can be studied by exploiting the possibilities of the ratiometric ASIC chip.

### **8.5.2 Application of the ASIC chip with novel configurations**

The design of the ratiometric ASIC chip is also adaptable to the use of different configurations that can be obtained through the addition of post-CMOS components for the experimentation with other innovative structures.

In chapter 4, section 4.5.2, two methods are described for the exposure of the sensors to the sample vapour under test. Although both of these methods were tested in the simulations, only the one with the coated passive sensor was used in the characterisation of the smart devices. The second method, consisting on the use of two separate flows in the gas exposure chamber, still requires practical investigation.

A review of the configuration proposed in figure 4.16(b) reveals the need of an appropriate package which will allow the *dual-input line ratiometric method* to be implemented. This will require of a precise design in order to expose one of the sensors to the analyte under test, while the second sensor is exposed to a reference gas within the chamber. As studied in simulations, a more detailed analysis could be obtained of the individual contribution of each sensor to the overall response of the device, in terms of applied concentrations of analytes and water vapours.

Other possibilities for the experimentation with novel configurations can be derived after the success of the duo-type devices tested and after developing micro-channel structures like the one required for the dual-input line method just mentioned. This would eventually lead to more selective devices for more gas sensing applications.

### **8.5.3 Characterisation and use of the temperature control circuit**

Although most of the experimental work reported here is related to the gas sensor section of the ASIC chip, the availability of the temperature control circuit within the design offers the opportunity for further research in the use of this feature.

The components of the temperature control circuit have been individually tested as described in chapter 6. However, a more detailed characterisation is still required, covering both electrical and thermal behaviour of heaters, thermodiodes, and the corresponding circuitry providing the control function.

In particular, developing a proper thermal model would be useful in order to show the distribution of heat in the electrodes area. Although such a model would not be easily applied in the case of the spray coated polymeric materials used in this

project, it will be accurate enough in the case of materials more evenly deposited, or even for sensing materials arranged onto new electrodes and heater structures designed for other resistive sensors, like the gold nanoparticle/organic linker films mentioned above.

Operation of the temperature control circuit needs also be studied in detail. Stability of the system can be analysed, the speed of the response can be determined and the heater power can be characterised in terms of proportionality and performance. Looking for optimisation of the control system in future versions of the ASIC, it would be useful to find the proper value of gain that could keep the system stable in order to obtain a faster response. Also, analysis in the frequency domain could help to evaluate whether the noise in the thermosensors is low enough and does not produce significant fluctuations on the heater power. If so, the possible benefits of adding a derivative effect to the circuit could be considered.

Another possibility for further study could be that related to the difference in the type of resistors used in the voltage divider of the set-point circuit. Whereas the first resistor is fabricated in the *Nwell* type available in the CMOS process adopted, the resistor of the divider is taken from one of the external potentiometers in the Xicor chip, which are fabricated as series arrays of small resistive elements [11]. The differences in fabrication make the resistors have different temperature coefficients and this leads to an unwanted displacement of the set point.

There are two possible ways, which can be the subject of new research, to overcome this problem. The first proposed approach consists in the study of the differences on the temperature response of the two resistors in the voltage divider. Once the difference is well identified, corrective action can be taken either by

programming a self-adjusted setting of the external potentiometer or by externally correcting the action of the compensator circuit. A second approach would be suitable in the case of the design of new generations of the chip, as proposed below. In this case, an alternative way to match the temperature response of the resistors could be implemented, such as the use of two external potentiometers for the voltage divider used in the temperature set-point circuit.

#### **8.5.4 Improving the design: new generations of the ASIC chip**

Since the first ratiometric ASIC chip has proved to work accordingly with expectances, the design of a new generation of the same devices would aim more for additional innovations than for simple modifications to the previous design.

A second generation of the ratiometric ASIC chip would improve its predecessor by considering modifications and innovations such as the following:

- a) Using a complete external set-point voltage divider, to avoid differences in temperature coefficients of resistors, as it was commented in the previous sub-section.
- b) Increasing the resistance ratios that the circuit can handle, by using a larger potentiometer range in the offset circuit. It might also be included a circuit which allows the scaling of the offset to different resistance levels, making the ASIC adaptable to the use of a much wider range of resistances in the sensors.
- c) Providing external access to the voltage in each individual sensor, allowing the monitoring and better study of the variations produced.

- d) Including an internal section in the ASIC chip for the conversion of the analogue signals to digital format. In this way, on-chip basic signal processing could be achieved and the output would be more easily adaptable for the use of standard micro-controllers. Also, current spike phenomena produced by the analogue output of the ASIC chip through the data acquisition cards would be substantially reduced.
- e) Additionally, the implementation of a standard interface protocol such as the IEEE 1451 will enable the ASIC chip with the capability of network communication, following the recent trends in smart sensors technology [12].

### **8.5.5 The hand-held instrument**

As stated in the aims and objectives of the project (section 1.4), the ratiometric ASIC chip is intended to be the main component of a micro-power hand-held instrument for the monitoring of VOC.

The diagram in Figure 3.1 showed an initial proposal for the integration of a complete instrument, by adding the required external potentiometers and a micro-controller unit. The ratiometric ASIC chip was designed following that structure for the sensor system. The functions of the micro-controller unit were performed in the experimental stage by a desktop computer interfaced to the ASIC chip with a data acquisition card and running LabView™ virtual instrumentation.

Given that the smart sensor system have shown adequate performance based on this configuration, a further project would consider the consolidation of the instrument into a smaller unit. This would mainly require the translation of the

functions currently assigned to the desktop computer into a properly programmed micro-controller. Possibilities for the forthcoming application of the ASIC chip in a VOC-monitoring hand-held instrument are as close to reality as outlined in other theoretical proposals [13].

Additionally, an appropriate analogue-to-digital interface would be required, although this could also be included in a newer version of the ASIC chip, as it is proposed above.

A display unit would also be necessary, showing values and settings in the instrument. An input numeric pad will complement the user interface.

The exposure of the chemoresistors to gas or VOC would require of a proper interface which must accomplish the basic functions of the current vapour exposure chamber used in the FIA test station described in chapter 7.

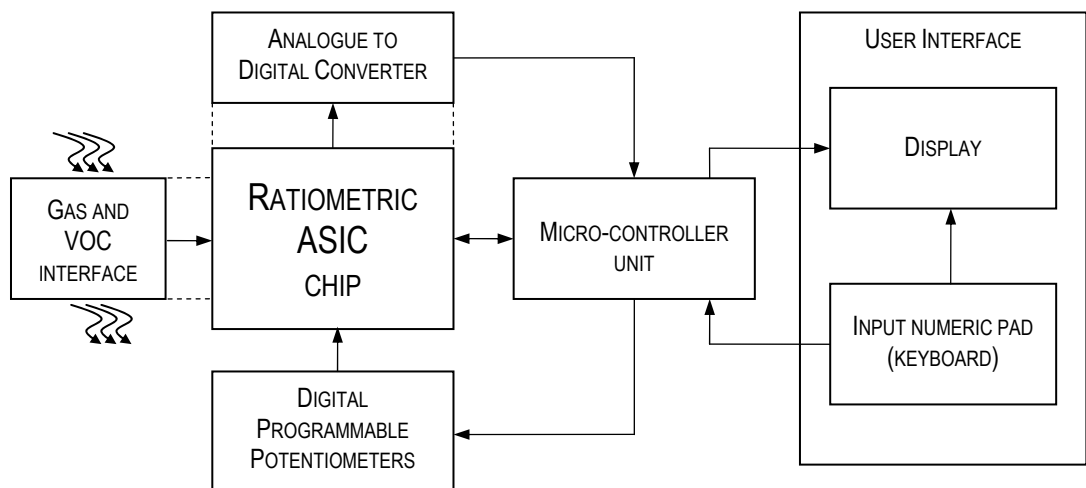


**Figure 8.1.** Block diagram of the proposed hand-held VOC monitoring instrument.

The block diagram of the proposed hand-held instrument is shown in Figure 8.1. A list of specifications for the signals in the main micro-controller unit is given

in Appendix E. Programming of the micro-controller unit should follow the functions developed for the *LabView*<sup>TM</sup> virtual instruments described in Appendix D.

The possibilities for this hand-held instrument, when considered together with the options for new nano-materials and new configurations described above, clearly envisage a promising future for the practical application of the ratiometric ASIC chip developed in this project.

## 8.6 A FINAL SUMMARY

A CMOS ratiometric ASIC chip for the monitoring of VOC has been successfully designed, modelled, simulated, fabricated and characterised in this project.

The following important smart features were included in the ASIC chip:

- a) The ratiometric measurement principle was employed in the design of the circuit with the chemoresistive sensors. This allowed the nearly elimination of the temperature dependence of the baseline output voltage, provided compensation for variations in the resistance of the sensors, and made the circuit capable of operating correctly with a wide range of resistances (from 1 k $\Omega$  to 100 k $\Omega$ ).
- b) A programmable offset circuit complements the ratiometric configuration, permitting the use of a wide range of *resistance ratios* in the chemoresistors of the ratiometric array, i.e. compensating for differences between the two resistive elements of the array.
- c) The instrumentation amplifier is provided with programmable gain, which allows a proper setting of the output signal and improves the sensitivity of the device as a whole.
- d) The sensor circuit can be operated either in constant mode or in a pulsed-mode, the latter allowing low-power consumption, which is highly desirable for application in commercial instruments.
- e) The chemoresistors are driven by applying a pulsed voltage that is alternated by a FET-switched circuit. This would eliminate the drift



problems associated with the use of constant voltage sources, especially with conducting polymers as gas sensitive materials.

- f) A dual temperature control circuit is provided for the operation of the chemoresistors under regulated thermal conditions.

Smart ratiometric ASIC devices were tested by depositing carbon black/polymer composite materials across the electrodes of the chip. The results of the experiments confirmed that through the ratiometric principle applied in the design, common problems found in discrete resistive gas sensors, such as humidity and temperature dependence of the response, induced voltage drift, and variations in the resistance of fabricated chemoresistors were reduced.

Furthermore, the design of the ratiometric ASIC chip allows the use of other gas sensitive materials, with no more internal limitations than the size of the electrodes area. In particular, the use of electroless plating on the aluminium electrodes would extend the possibilities for the employment of new nano-materials. In addition, its adaptability for being used in hybrid configuration with external chemoresistors makes the ASIC chip suitable for practically any resistive gas sensing material.

The novel *duo-type* ratiometric devices, proposed for the first time in this project, were successfully tested with the aid of the developed ASIC chip. The combined application of two active sensing materials produced results that have revealed an increase in the selectivity (average rejection ratio of 127 for toluene/ethanol) of the devices when compared to the mono-type devices (rejection ratio averaged only 4.53 for the same analytes). Sensitivity to VOC was also improved for the duo-type devices, resulting 3.55 times greater than for the PCL-

based monotype devices and 11.73 times greater than for the PEVA-based monotype devices.

Several research projects have already been proposed, and some of them are already underway, in order to continue the work related to the ratiometric ASIC chip described in this thesis. The success of its design has brought the opportunity to investigate new gas sensing materials and novel ratiometric configurations. Improvements for a new generation of the chip have been recommended, and the structure of a hand-held instrument for VOC monitoring based on the ASIC chip has also been outlined.

It is believed that the functionality, benefits and possibilities of the designed ratiometric ASIC chip have exceeded the original expectations and aims of the project.

## 8.7 REFERENCES

1. Cole, M., Gardner, J.W. and Bartlett, P.N. (2001). "Low-drift odour and vapour ratiometric resistive elements for analogue CMOS smart sensors", *Electrochemical Society Proceedings*, **15**, 117-120.
2. West, C. (2001). "Design of an ASIC chip for a hand held gas detector", BEng Final Report, University of Warwick, Coventry, UK.
3. Cole, M., Gardner, J.W., Covington, J.A., Fife, D., Kwok, C.Y., Brignell, J.E. and Bartlett, P.N. (2000). "Active bridge polymeric resistive device for vapour sensing", *Euroensors XIV.*, Copenhagen, Denmark, 895-898.
4. Cole, M., Gardner, J.W., Lim, A.W.Y., Scivier, P.K. and Brignell, J.E. (1999). "Polymeric resistive bridge gas sensor array driven by a standard cell CMOS current drive chip", *Sensors and Actuators B*, **58**, 518-525.
5. Gardner, J.W., Vidic, M., Ingleby, P., Pike, A.C., Brignell, J.E., Scivier, P. Bartlett, P.N., Duke, A.J., Elliot, J.M. (1998). "Response of a poly(pyrrole) resistive micro-bridge to ethanol vapour", *Sensors and Actuators B*, **48**, 289-295.
6. Pike, A.C. (1996). "Design of chemoresistive silicon sensors for application in gas monitoring", PhD Thesis, University of Warwick, Coventry, UK.
7. Krasteva, N., Besnard, I., Guse, B., Bauer, R.E., Müllen, K., Yasuda, A. and Vossmeier, T. (2002). "Self-Assembled Gold Nanoparticle/Dendrimer Composite Films for Vapor Sensing Applications", *Nano Letters*, **2**, No. 5, 551-555.
8. Joseph, Y., Krasteva, N., Besnard, I., Guse, B., Rosenberger, M., Wild, U., Knop-Gericke, A., Schlögl, R., Krustev, R., Yasuda, A. and Vossmeier, T. (2004). "Gold nanoparticle/organic linker films: self-assembly, electronic and structural characterisation, composition and vapour sensitivity." *Faraday Discussions*, **125**, 77-97.
9. Krasteva, N., Guse, B., Besnard, I., Yasuda, A. and Vossmeier, T. (2003). "Gold nanoparticle/PPI-dendrimer based chemoresistors vapor-sensing properties as a function of the dendrimer size", *Sensors and Actuators B*, **92**, 137-143.

10. Vossmeier, T., Guse, B., Besnard, I., Bauer, R.E., Müllen, K. and Yasuda, A. (2002). "Gold nanoparticle/polyphenylene dendrimer composite films: preparation and vapor-sensing properties", *Advanced Materials*, **14**, No. 3, 238-242.
11. XICOR (2002). "X9241A Quad Digital Controlled Potentiometers (XDCP™)", Datasheet available at [www.xicor.com](http://www.xicor.com), Rev 1.1.13 12/09/02.
12. Ferrari, P., Flammini, A., Marioli, D. and Taroni, A. (2002). "A low-cost Internet-enabled smart sensor", *Proceedings of the First IEEE International Conference on Sensors*, Orlando, Florida, USA, **2**, 1549-1554.
13. Seguine, D. (2002). "Just add sensor -- Integrating analog and digital signal conditioning in a programmable system on chip", *Proceedings of the First IEEE International Conference on Sensors*, Orlando, Florida, USA, **1**, 665-668.

## BIBLIOGRAPHY

- Ahlskog, M. and Reghu, M. (1999). "The localization-interaction model for the DC-conductivity of metallic conducting polymers", *Synthetic Metals*, **101**(1-3), 367-368.
- Albert, K.J. and Walt, D.R. (2003). "Information coding in artificial olfaction multisensor arrays", *Anal. Chem.*, **75**, 4161-4167.
- Albert, K.J., Walt, D.R., Gill, D.S. and Pearce, T.C. (2001). "Optical multibead arrays for simple and complex odor discrimination", *Analytical Chemistry*, **73**, No. 11, 2501-2508.
- AMI Semiconductor (2002). *Library MTC 22500*, Revision 1.0, Information accessed under permission of the proprietor.
- Amrani, M.E.H. and Payne, P.A. (1999). "Multi-frequency interrogation technique applied to conducting polymer gas and odour sensors", *IEE Proceedings - Science, Measurement and Technology*, **146**, No. 2, 95-101.
- Amrani, M.E.H., Payne, P.A. and Persaud, K.C. (1996). "Multi-frequency measurements of organic conducting polymers for sensing of gases and vapours", *Sensors and Actuators B*, **33**, 137-141.
- Analog Devices (2002). "Passive and active analog filtering", Application note 281 available at [www.analog.com](http://www.analog.com).
- Baca, A.G., Heller, E.J., Hietala, V.M., Casalnuovo, S.A., Frye-Mason, G.C., Klern, J.F. and Drummond, T.J. (1999). "Development of a GaAs monolithic surface acoustic wave integrated circuit", *IEEE Journal of Solid-State Circuits*, **43**, 1254-1258.
- Baker, B. (1993). "Single-supply, low power measurements of bridge networks", *Burr-Brown Application Bulletin*, Tucson, AZ, USA.

- Baker, R.J., Li, H.W. and Boyce, D.E. (1998). *CMOS Circuit design, layout, and simulation*, IEEE Press, New York.
- Bakker, A. (2000). "High-accuracy CMOS smart temperature sensors", Thesis, Delft University of Technology, Delft, The Netherlands.
- Bakker, A. (2002). "CMOS smart temperature sensors – An overview", *Proceedings of the First IEEE International Conference on Sensors*, Orlando, Florida, USA, **2**, 1423-1427.
- Baltes, H. (1993). "CMOS as sensor technology", *Sensors and Actuators A*, **37-38**, 51-56.
- Baltes, H. and Brand, O. (2000). "CMOS-based microsensors", *Euroensors XIV.*, Copenhagen, Denmark, 1-8.
- Banba, H., Shiga, H., Umezawa, A., Miyaba, T., Tanzawa, T., Atsumi, S., and Sakui, K. (1999). "A CMOS bandgap reference circuit with sub-1-V operation", *IEEE Journal of Solid-State Circuits*, **34**, 670-674.
- Barrentino, D., Graf, M., Song, W.H., Kirstein, K.U., Hierlemann, A. and Baltes, H. (2004). "Hotplate-based monolithic CMOS microsystems for gas detection and material characterization for operating temperatures up to 500 °C", *IEEE Journal of Solid-State Circuits*, **39**, No. 7, 1202-1207.
- Bateman, C. (2003). "Testing and characterisation of a smart ratiometric ASIC chip for a palm-top VOC monitor", BEng Final Year Report, University of Warwick, Coventry, UK.
- Becker, T., Mühlberger, S., Bosch-v.Braunmühl, C., Müller, G., Meckes, A. and Benecke, W. (2000). "Gas mixture analysis using silicon micro-reactor systems", *Journal of Microelectromechanical Systems*, **9**, No. 4, 478-484.
- Becker, T., Mühlberger, S., Bosch-v.Braunmühl, C., Müller, G., Meckes, A. and Benecke, W. (2001). "Microreactors and microfluidic systems: an innovative approach to gas sensing using tin oxide-based gas sensors", *Sensors and Actuators B*, **77**, 48-54.
- Bednarczyk, D. and DeWeerth, S.P. (1995). "Smart chemical sensing arrays using tin oxide sensors and analog winner-take-all signal processing", *Sensors and Actuators B*, **26-27**, 271-274.
- Bell, D.A. (1985). *Noise and the solid state*, Pentech Press, London.
- Benecke, W., Meckes, A. (1998). "A smart gas sensing microsystem", *Proceedings of the IEEE International Symposium on Industrial Electronics*, **1**, 263-266.
- Bentley, J.P. (1995). *Principles of measurement systems*, 3<sup>rd</sup> ed., Longman Group Limited, Essex, England.

- Berouille, V., Bertrand, Y., Latorre, L. and Nouet, P. (2003). "Monolithic piezoresistive CMOS magnetic field sensors", *Sensors and Actuators A*, **103**, 23-32.
- Besnard, I. (2003). "Development of an array of smart chemical sensors based on gold nanoparticle films", Technical annex, Confidential.
- Bishop, J., Trump, B. and Stitt, R.M. (2001). "FilterPro™ MFB and Sallen-Key low-pass filter design program", Application report SBFA001A available at TEXAS Instruments web page, <http://www.ti.com/>.
- Boeker, P., Horner, G. and Rösler, S. (2000). "Monolithic sensor array based on a quartz microbalance transducer with enhanced sensitivity for monitoring agricultural emissions", *Sensors and Actuators B*, **70**, 37-42.
- Bolton, W. (1996). *Measurement and instrumentation systems*, Newnes, Oxford.
- Briand, D., van der Schoot, B., de Rooij, N.F., Sundgren, H. and Lundström, I. (2000). "A low-power micromachined MOSFET gas sensor", *Journal of Microelectromechanical Systems*, **9**, No. 3, 303-308.
- Briglin, S.M., Freund, M.S., Tokumaru, P., Lewis, N.S. (2002). "Exploitation of spatio-temporal information and geometric optimisation of signal/noise performance using arrays of carbon black-polymer composite vapor detectors", *Sensors and Actuators B*, **82**, 54-74.
- Brignell, J. and White, N. (1996). *Intelligent sensor systems*, Institute of Physics Publishing, Bristol.
- Brignell, J.E. (1991). "Software techniques for sensor compensation", *Sensors and Actuators A*, **25-27**, 29-35.
- Brignell, J.E. (1993). "Quo vadis smart sensors?", *Sensors and Actuators A*, **37-38**, 6-8.
- Brignell, J.E. (1996). "The future of intelligent sensors: a problem of technology or ethics?", *Sensors and Actuators A*, **56**, 11-15.
- Brokaw, P. (1974). "A simple three-terminal IC bandgap reference", *IEEE Journal of Solid-State Circuits*, **9**, 388-393.
- Bruschi, P., Nannini, A. and Neri, B. (1995). "Vapour and gas sensing by noise measurements on polymeric balanced bridge microstructures", *Sensors and actuators B*, **24-25**, 429-432.
- Burl, M.C., Sisk, B.C., Vaid, T.P. and Lewis, N.S. (2002). "Classification performance of carbon black-polymer composite vapor detector arrays as a function of array size and detector composition", *Sensors and Actuators B*, **87**, 130-149.

- Burr-Brown. (1993). "Dual current source/current sink", REF200, Tucson, AZ, USA.
- Cai, Q.Y., Park, J., Heldsinger, D., Hsieh, M.D. and Zellers, E.T. (2000). "Vapor recognition with an integrated array of polymer-coated flexural plate wave sensors", *Sensors and Actuators B*, **62**, 121-130.
- Cané, C., Gràcia, I., Götz, A., Fonseca, L., Lora-Tamayo, E., Horrillo, M.C., Sayago, I., Robla, J.I., Rodrigo, J. and Gutiérrez, J. (2000). "Detection of gases with arrays of micromachined tin oxide gas sensors", *Sensors and Actuators B*, **65**, 244-246.
- Cardinalli, G.C., Dori, L., Fiorini, M., Sayago, I., Faglia, G., Perego, C., Sberveglieri, G., Liberali, V., Maloberti, F. and Tonietto, D. (1997). "A smart sensor system for carbon monoxide detection", *Analog integrated circuits and signal processing*, **14**, No. 3, 275-296.
- Carmona, F. and Ravier, J. (2002). "Electrical properties and mesostructure of carbon black-filled polymers", *Carbon*, **40**, 151-156.
- Casans, S., Navarro, A.E., Ramírez, D., Pelegrí, J., Balde, A. and Abramova, N. (2001). "Novel constant current driver for ISFET/MEMFETs characterisation", *Sensors and Actuators B*, **76**, 629-633.
- Chaudry, A.N., Hawkins, T.M. and Travers, P.J. (2000). "A method for selecting an optimum sensor array", *Sensors and Actuators B*, **69**, 236-242.
- Clark, D.T. (1994). "Surface, transforms and interfaces; the SMART direction for polymer science", *Synthetic Metals*, **67**, 63-70.
- Cole, M., Gardner, J.W. and Bartlett, P.N. (2001). "Low-drift odour and vapour ratiometric resistive elements for analogue CMOS smart sensors", *Electrochemical Society Proceedings*, **15**, 117-120.
- Cole, M., Gardner, J.W., Covington, J.A., Fife, D., Kwok, C.Y., Brignell, J.E. and Bartlett, P.N. (2000). "Active bridge polymeric resistive device for vapour sensing", *Euroensors XIV.*, Copenhagen, Denmark, 895-898.
- Cole, M., Gardner, J.W., Lim, A.W.Y., Scivier, P.K. and Brignell, J.E. (1999). "Polymeric resistive bridge gas sensor array driven by a standard cell CMOS current drive chip", *Sensors and Actuators B*, **58**, 518-525.
- Cole, M., Ulivieri, N., Garcia-Guzman, J., and Gardner, J.W. (2003). "Parametric model of a polymeric chemoresistor for use in smart sensor design and simulation", *Microelectronics Journal*, **34**, 865-875.
- Collins, T. H. (1989). *Analog electronics handbook*, Prentice Hall International (UK) Ltd., London, UK.



- Cornila, C., Hierlemann, A., Lenggenhager, R., Malcovati, P., Baltes, H., Noetzel, G., Weimar, U. and Göpel, W. (1995). "Capacitive sensors in CMOS technology with polymer coating", *Sensors and Actuators B*, **24-25**, 357-361.
- Costa Freitas, A.M., Parreira, C., and Vilas-Boas, L. (2001). "The use of an electronic aroma-sensing device to assess coffee differentiation—Comparison with SPME gas chromatography-mass spectrometry aroma patterns", *Journal of Food Composition and Analysis*, **14**, 513-522.
- Covington J.A. (2001). "CMOS and SOI CMOS FET-based gas sensors", PhD Thesis, University of Warwick, Coventry, UK.
- Covington, J.A., Gardner, J.W., Briand, D. and de Rooij, N.F. (2001). "A polymer gate FET sensor array for detecting organic vapours", *Sensors and Actuators B*, **77**, 155-162.
- Covington, J.A., Tan, S.L., Gardner, J.W., Hamilton, A., Koickal, T.J. and Pearce, T.C. (2003). "Combined smart chemFET/resistive sensor array", *Proceedings of the IEEE International Conference on Sensors*, Toronto, Canada, **2**, 1120-1123.
- Cunningham, B., Weinberg, M., Pepper, J., Clapp, C., Bousquet, R., Hugh, B., Kant, R., Daly, C. and Hauser, E. (2001). "Design, fabrication and vapor characterization of a microfabricated flexural plate resonator sensor and application to integrated sensor arrays", *Sensors and Actuators B*, **73**, 112-123.
- Dahan, M., Deniz, A.A., Ha, T., Chemla, D.S., Schultz, P.G. and Weiss, S. (1999). "Ratiometric measurement and identification of single diffusing molecules", *Chemical Physics*, **247**, 85-106.
- Das, R.R., Shukla, K.K., Dwivedi, R. and Srivastava, A.R. (1999). "Discrimination of individual gas/odor using responses of integrated thick film tin oxide sensor array and fuzzy-neuro concept", *Microelectronics Journal*, **30**, 793-800.
- Datskos, P.G., Sepaniak, M.J., Tipple, C.A. and Lavrik, N. (2001). "Photomechanical chemical microsensors", *Sensors and Actuators B*, **76**, 393-402.
- De Jong, P.C., Riedijk, F.R. and van der Meer, J. (2002). "Smart silicon sensors - Examples of Hall-effect sensors", *Proceedings of the First IEEE International Conference on Sensors*, Orlando, Florida, USA, **2**, 1440-1444.
- Dickson, J.A. and Goodman, R.M. (2000). "Integrated chemical sensors based on carbon black and polymer films using a standard CMOS process and post-processing", *Proceedings of the IEEE International Symposium on Circuits and Systems (ISCAS)*, Geneva, Switzerland, 341-344.
- Doebelin, E.O. (1990). *Measurement systems: application and design*, 4th ed., McGraw-Hill, Inc., New York.

- Dyer, D.C. and Gardner, J.W. (1997). "High precision intelligent interface for a hybrid electronic nose", *Sensors and Actuators A*, **62**, 724-728.
- Dziedzic, A. and Kolek, A. (1998). "1/f noise in polymer thick-film resistors", *J. Phys. D: Appl. Phys.*, **31**, 2091-2097.
- Ehrmann, S., Jüngst, J., Goschnick, J. and Everhard, D. (2000). "Application of a gas sensor microarray to human breath analysis", *Sensors and Actuators B*, **65**, 247-249.
- Ercan, A.O., Xiao, F., Liu, X., Lim, S.H., El Gamal, A. and Wandell, B. (2002). "Experimental high speed CMOS image sensor system and applications", *Proceedings of the First IEEE International Conference on Sensors*, Orlando, Florida, USA, **1**, 15-20.
- Ferrari, P., Flammini, A., Marioli, D. and Taroni, A. (2002). "A low-cost Internet-enabled smart sensor", *Proceedings of the First IEEE International Conference on Sensors*, Orlando, Florida, USA, **2**, 1549-1554.
- Fewster, A. (1995). "Design, modelling and application of analogue switches and multiplexers", *Electronic Engineering*, 83-92.
- Fife, D. (2000). "The design, analysis and implementation of two analogue CMOS chips for incorporation in hand-held gas sensing equipment", BEng final report, University of Warwick, Coventry, UK.
- Figliola, R.S. and Beasley, D.E. (2000). *Theory and design for mechanical measurements*, 3rd ed., John Wiley & Sons, Inc., New York.
- Flammini, A., Ferrari, P., Sisinni, E., Marioli, D. and Taroni, A. (2002). "Sensor interfaces: from field-bus to Ethernet and Internet", *Sensors and Actuators A*, **101**, 194-202.
- Flammini, A., Ferrari, P., Sisinni, E., Marioli, D. and Taroni, A. (2003). "Sensor integration in industrial environment: from field-bus to web sensors", *Computer Standards & Interfaces*, **25**, 183-194.
- Floyd, T.L. and Buchla, D. (1999). *Fundamentals of analog circuits*, Prentice-Hall, Inc., Upper Saddle River, New Jersey.
- Frank, R. (1996). *Understanding smart sensors*, Artech House, Inc., Massachusetts, USA.
- Gardner, J. W. (1995). "Intelligent gas sensing using an integrated sensor pair", *Sensors and actuators B*, **26-27**, 261-266.
- Gardner, J.W. (1994). *Microsensors: principles and applications*, John Wiley & Sons Ltd., Chichester, U. K.

- Gardner, J.W. and Bartlett, P.N. (1994). "A brief history of electronic noses", *Sensors and Actuators B*, **18-19**, 211-220.
- Gardner, J.W. and Bartlett, P.N. (1995). "Application of conducting polymer technology in microsystems", *Sensors and Actuators A*, **51**, 57-66.
- Gardner, J.W. and Bartlett, P.N. (1996). "Performance definition and standardization of electronic noses", *Sensors and Actuators B*, **33**, 60-67.
- Gardner, J.W. and Bartlett, P.N. (1999). *Electronic noses: principles and applications*, Oxford University Press, New York.
- Gardner, J.W. and Cole, M. (2003). "Integrated electronic noses and microsystems for chemical analysis", Chapter 10 in *Handbook of machine olfaction.*, Pearce, T.C., Schiffman, S.S., Nagle, H.T. and Gardner, J.W., Ed. Weinheim, Germany: Wiley-VCH.
- Gardner, J.W., Cole, M. and Udrea, F. (2002). "CMOS gas sensors and smart devices", *Proceedings of the First IEEE International Conference on Sensors*, Orlando, Florida, USA, **1**, 721-726.
- Gardner, J.W., Iskandarani, M.Z. and Bott, B. (1992). "Effect of electrode geometry on gas sensitivity of lead phthalocyanine thin films", *Sensors and Actuators B*, **9**, 133-142.
- Gardner, J.W., Llobet, E. and Hines, E.L. (1999). "PSPICE model for resistive gas and odour sensors", *IEE Proc.-Circuits Devices Syst.*, **146**, No. 3, 101-104.
- Gardner, J.W., Pearce, T.C., Friel, S., Bartlett, P.N., Blair, N. (1994). "A multisensor system for beer flavour monitoring using an array of conducting polymers and predictive classifiers", *Sensors and Actuators B*, **18**, 240-243.
- Gardner, J.W., Pike, A., de Rooij, N.F., Koudelka-Hep, M., Clerc, P.A., Hierlemann, A. and Göpel, W. (1995). "Integrated array sensor for detecting organic solvents", *Sensors and Actuators B*, **26-27**, 135-139.
- Gardner, J.W., Shin, H.W., Hines, E.L. and Dow, C.S. (2000). "An electronic nose system for monitoring the quality of potable water", *Sensors and actuators B*, **69**, 336-341.
- Gardner, J.W., Varadan, V.K. and Awadelkarim, O.O. (2001). *Microsensors, MEMS, and smart devices*, John Wiley & Sons, Ltd., Chichester, England.
- Gardner, J.W., Vidic, M., Ingleby, P., Pike, A.C., Brignell, J.E., Scivier, P. Bartlett, P.N., Duke, A.J., Elliot, J.M. (1998). "Response of a poly(pyrrole) resistive micro-bridge to ethanol vapour", *Sensors and Actuators B*, **48**, 289-295.
- Gerard, M., Chaubey, A. and Malhotra, B.D. (2002). "Application of conducting polymers to biosensors", *Biosensors & Bioelectronics*, **17**, 345-359.

- Giachino, J.M. (1986). "Smart sensors", *Sensors and Actuators*, **10**, 239-248.
- Goodey, A., Lavigne, J.J., Savoy, S.M., Rodriguez, M.D., Curey, T., Tsao, A., Simmons, G., Wright, J., Yoo, S.J., Sohn, Y., Anslyn, E.V., Shear, J.B., Neikirk, D.P. and McDevitt, J.T. (2001). "Development of multianalyte sensor arrays composed of chemically derivatized polymeric microspheres localized in micromachined cavities", *Journal of the American Chemical Society*, **123**, 2559-2570.
- Göpel, W. (1995). "Sensors and 'smart' molecular structures: components for future information technologies" in *Sensors: a comprehensive survey*, **8**, *Micro- and nanosensor technology/ Trends in sensor markets*, Meixner, H. and Jones, R., Ed. Cambridge: VCH, 295-336.
- Graf, M., Barrentino, D., Zimmermann, M., Hierlemann, A., Baltes, H. and Hahn, S. (2004). "CMOS monolithic metal-oxide sensor system comprising a microhotplate and associated circuitry", *IEEE Sensors Journal*, **4**, No. 1, 9-16.
- Graf, R.F. (1985). *The encyclopedia of electronic circuits*, TAB Books, Blue Ridge Summit, PA.
- Gregory, B.A. (1981). *An introduction to electrical instrumentation and measurement systems*, 2nd ed., The Macmillan Press Ltd., London.
- Hagleitner, C., Hierlemann, A., Lange, D., Kummer, A., Kerness, N., Brand, O. and Baltes, H. (2001). "Smart single-chip gas sensor microsystem", *Nature*, **414**, 293-296.
- Hallewell, G., Crawford, G., McShurley, D., Oxoby, G. and Reif, R. (1988). "A sonar-based technique for the ratiometric determination of binary gas mixtures", *Nuclear Instruments and Methods in Physics Research*, **A264**, 219-234.
- Hammond, P.A., Cumming, D.R.S. and Ali, D. (2002). "A single-ship pH sensor fabricated by a conventional CMOS process", *Proceedings of the First IEEE International Conference on Sensors*, Orlando, Florida, USA, **1**, 350-355.
- Hastings, A. (2001). *The art of analog layout*, Prentice-Hall, Inc., New Jersey.
- Hatfield, J. V., Neaves, P., Hicks, P. J., Persaud, K. and Travers, P. (1994). "Towards an integrated electronic nose using conducting polymer sensors", *Sensors and Actuators B*, 18-19, 221-228.
- Heaney, M.B. (1995). "Measurement and interpretation of nonuniversal critical exponents in disordered conductor-insulator composites", *Physical Review B*, **52**, No. 17, 12 477-12 480.
- Heaney, M.B. (1996). "Resistance-expansion-temperature behaviour of a disordered conductor-insulator composite", *Appl. Phys. Lett.*, **69**(17), 2602-2604.

- Heer, F., Franks, W., Blau, A., Tachini, S., Ziegler, C., Hierlemann, A. and Baltes, H. (2004). "CMOS microelectrode array for the monitoring of electrogenic cells", *Biosensors and Bioelectronics*, **20**, 358-366.
- Hierlemann, A. and Baltes, H. (2003). "CMOS-based chemical microsensors", *Analyst*, **128**(1), 15-28.
- Hierlemann, A., Brand, O., Hagleitner, C. and Baltes, H. (2003). "Microfabrication techniques for chemical/biosensors", *Proceedings of the IEEE*, **91**, No. 6, 839-863.
- Hierlemann, A., Lange, D., Hagleitner, C., Kerness, N., Koll, A., Brand, O. and Baltes, H. (2000). "Application-specific sensor systems based on CMOS chemical microsensors", *Sensors and actuators B*, **70**, 2-11.
- Hilburn, J.L. (1973). *Manual of active filter design*, McGraw-Hill, Inc. New York, USA.
- Hirano, S. and Kishimoto, A. (1998). "Effect of heating rate on positive-temperature-coefficient-of-resistivity behaviour of conductive composite thin films", *Appl. Phys. Lett.*, **73**(25), 3742-3744.
- Horowitz, P. and Hill, W. (1989). *The art of electronics*, 2nd ed., Cambridge University Press. New York, USA.
- Hosticka, B.J. (1998). "CMOS sensor systems", *Sensors and Actuators A*, **66**, 335-341.
- Hosticka, B.J., Brockherde, W. and Hammerschmidt, D. (1997). "Silicon sensor systems", *Analog Integrated Circuits and Signal Processing*, **14**, 261-273.
- Howe, R.T. and Sodini, C.G. (1997). *Microelectronics: an integrated approach*, Prentice-Hall International, Inc., New Jersey, USA.
- Huijsing, J.H. and Meijer, G.C.M. Ed., (1997). *Smart Sensor Interfaces*, Delft University of Technology, The Netherlands, Kluwer Academic Publishers, Boston.
- Huijsing, J.H., Riedijk, F.R. and van der Horn, G. (1994). "Developments in integrated smart sensors", *Sensors and Actuators A*, **43**, 276-288.
- Hurley, R.E. and Gamble, H.S. (1995). "Some recent advances in silicon microtechnology and their dependence on processing technique", *Vacuum*, **46**(3), 287-293.
- Ingleby, P., Gardner, J.W. and Bartlett, P.N. (1999). "Effect of micro-electrode geometry on response of thin-film poly(pyrrole) and poly(aniline) chemoresistive sensors", *Sensors and Actuators B*, **57**, 17-27.

- Ishida, H., Tokuhiko, T., Nakamoto, T. and Moriizumi, T. (2002). "Improvement of olfactory video camera: gas/odour visualization system", *Sensors and Actuators B*, **83**, 256-261.
- Ishida, H., Yamanaka, T., Cusida, N., Nakamoto, T. and Moriizumi, T. (2000). "Study of real-time visualization of gas / odor flow image using gas sensor array", *Sensors and Actuators B*, **65**, 14-16.
- Ismail, M. and Fiez, T. (1994). *Analog VLSI: signal and information processing*, McGraw-Hill, Inc. New York.
- Johns, D. and Martin, K. (1997). *Analog Integrated Circuit Design*, John Wiley & Sons, Inc., New York.
- Johnson, C.L., Schwank, J.W. and Wise, K.D. (1994). "Integrated ultra-thin-film gas sensors", *Sensors and Actuators B*, **20**, 55-62.
- Jones, M.H. (1995). *A practical introduction to electronic circuits*, 3rd ed., Cambridge University Press, Cambridge, UK.
- Joseph, Y., Besnard, I., Rosenberger, M., Guse, B., Nothofer, H.G., Wessels, J.M., Wild, U., Knop-Gericke, A., Su, D., Schlögl, R., Yasuda, A. and Vossmeier, T. (2003). "Self-assembled gold nanoparticle/alkanedithiol films: preparation, electron microscopy, XPS-analysis, charge transport, and vapor-sensing properties", *J. Phys. Chem. B*, **107**, 7406-7413.
- Joseph, Y., Guse, B., Yasuda, A. and Vossmeier, T. (2004). "Chemoresistor coatings from PT- and Au-nanoparticle/nonanedithiol films: sensitivity to gases and solvent vapors", *Sensors and Actuators B*, **98**, 188-195.
- Joseph, Y., Krasteva, N., Besnard, I., Guse, B., Rosenberger, M., Wild, U., Knop-Gericke, A., Schlögl, R., Krustev, R., Yasuda, A. and Vossmeier, T. (2004). "Gold nanoparticle/organic linker films: self-assembly, electronic and structural characterisation, composition and vapour sensitivity." *Faraday Discussions*, **125**, 77-97.
- Klaassen, K.B. (1996). *Electronic measurement and instrumentation*, Cambridge University Press, Cambridge.
- Kleinfelder, S., Lim, S.H., Liu, X. and El Gamal, A. (2001). "A 10,000 frames/s CMOS digital pixel sensor", *IEEE Journal of Solid-State Circuits*, **36**, 2049-2059.
- Ko, W.H. (1996). "The future of sensor and actuator systems", *Sensors and Actuators A*, **56**, 193-197.
- Kolek, A. and Dziedzic, A. (2000). "Low-frequency noise of polymer thick-film resistors: analysis of volume and contact effects", *Proceedings 22nd International Conference on Microelectronics*, Nis, **2**, 531-534.

- Krasteva, N., Besnard, I., Guse, B., Bauer, R.E., Müllen, K., Yasuda, A. and Vossmeier, T. (2002). "Self-assembled gold nanoparticle/dendrimer composite films for vapor sensing applications", *Nano Letters*, **2**, No. 5, 551-555.
- Krasteva, N., Guse, B., Besnard, I., Yasuda, A. and Vossmeier, T. (2003). "Gold nanoparticle/PPI-dendrimer based chemoresistors vapor-sensing properties as a function of the dendrimer size", *Sensors and Actuators B*, **92**, 137-143.
- Krasteva, N., Krustev, R., Yasuda, A. and Vossmeier, T. (2003). "Vapour sorption in self-assembled gold nanoparticle/dendrimer films studied by specular neutron reflectometry", *Langmuir*, **19**, 7754-7760.
- Krummenacher, P. and Oguey, H. (1990). "Smart temperature sensor in CMOS technology", *Sensors and Actuators A*, **21-23**, 636-638.
- Kutz, M. (1968). *Temperature control*, John Wiley & Sons, Inc., New York.
- Lahav, M., Shipway, A.N., Willner, I., Nielsen, M.B., and Stoddart, J.F. (2000). "An enlarged bis-bipyridinium cyclophane-Au nanoparticle superstructure for selective electrochemical sensing applications", *Journal of Electroanalytical Chemistry*, **482**, 217-221.
- Lankinen, E., Sundholm, G., Talonen, P., Laitinen, T. and Saario, T. (1998). "Characterization of a poly(3-methyl thiophene) film by an in-situ dc resistance measurement technique and in-situ FTIR spectroelectrochemistry", *Journal of Electroanalytical Chemistry*, **447**, 135-145.
- Lauwers, E., Suls, J., Gumbrecht, W., Maes, D., Gielen, G. and Sansen, W. (2001). "A CMOS multiparameter biochemical microsensor with temperature control and signal interfacing", *IEEE Journal of Solid-State Circuits*, **36**, No. 12, 2030-2038.
- Lee, S.M. (2002). "Low-power silicon planar micro-calorimeter employing nanostructured catalyst", PhD Thesis, University of Warwick, Coventry, UK.
- Lim, A.W.Y. (1998). "The characterisation on a hex constant-current ASIC chip to drive an array of microbridge devices for an electronic nose", BEng final report, University of Warwick, Coventry, UK.
- Lim, J.W., Kang, D.W., Lee, D.S., Huh, J.S. and Lee, D.D. (2001). "Heating power-controlled micro-gas sensor array", *Sensors and Actuators B*, **77**, 139-144.
- Llobet, E., Brezmes, J., Ionescu, R., Vilanova, X., Al-Khalifa, S., Gardner, J.W., Bârsan, N. and Correig, X. (2002). "Wavelet transform and fuzzy ARTMAP-based pattern recognition for fast gas identification using a micro-hotplate gas sensor", *Sensors and Actuators B*, **83**, 238-244.
- Llobet, E., Ionescu, R., Al-Khalifa, S., Brezmes, J., Vilanova, X., Correig, X., Bârsan, N. and Gardner, J.W. (2001). "Multicomponent gas mixture analysis

- using a single tin oxide sensor and dynamic pattern recognition", *IEEE Sensors journal*, **1**, No. 3, 207-213.
- Llobet, E., Rubio, J., Vilanova, X., Brezmes, J., Correig, X., Gardner, J.W. and Hines, E.L. (2001). "Electronic nose simulation tool centred on Pspice", *Sensors and Actuators B*, **76**, 419-429.
- Llobet, E., Vilanova, X., Brezmes, J., López, D. and Correig, X. (2001). "Electrical equivalent models of semiconductor gas sensors using PSpice", *Sensors and Actuators B*, **77**, 275-280.
- Lonergan, M.C., Severin, E.J., Doleman, B.J., Beaver, S.A., Grubbs, R.H., Lewis, N.S. (1996). "Array-based vapor sensing using chemically sensitive carbon-black-polymer resistors", *Chem. Mater.*, **8**, 2298-2312.
- Lundström, I. (2000). "Artificial noses: picture the smell", *Nature*, **406**, 682-683.
- Lundström, I., Erlandsson, R., Frykman, U., Hedborg, E., Spetz, A., Sundgren, H., Welin, S. and Winquist, F. (1991). "Artificial 'olfactory' images from a chemical sensor using a light-pulse technique", *Nature*, **352**, 47-50.
- Maloberti, F. and Malcovati, P. (1997). "Microsystems and smart sensor interfaces: a review", *Analog integrated circuits and signal processing*, **15**, 9-26.
- McLachlan, D.S. and Heaney, M.B. (1999). "Complex ac conductivity of a carbon black composite as a function of frequency, composition, and temperature", *Physical Review B*, **60**, No. 18, 12 746-12 751.
- Meijer, G.C.M. (1994). "Concepts and focus point for intelligent sensor systems", *Sensors and Actuators A*, **41-42**, 183-191.
- Middelhoek, S. and Hoogerwerf, A.C. (1985). "Smart sensors: when and where?", Paper presented at the *Third International Conference on Solid-State Sensors and Actuators (Transducers '85)*, Philadelphia, PA, U.S.A.
- Misselbrook, T.H., Hobbs, P.J. and Persaud, K.C. (1997). "Use of an electronic nose to measure odour concentration following application of cattle slurry to grassland", *Journal of Agricultural Engineering Research*, **66**, 213-220.
- Müller, T., Brandl, M., Brand, O. and Baltes, H. (2000). "An industrial CMOS process family adapted for the fabrication of smart silicon sensors", *Sensors and Actuators A*, **84**, 126-133.
- Musio, F., Amrani, M.E.H. and Persaud, K.C. (1995). "High-frequency a.c. investigation of conducting polymer gas sensors", *Sensors and Actuators B*, **23**, 223-226.
- National Instruments™ (2002). *DAQ NI 6034E/6035E/6036E User manual, Multifunction I/O devices*, Part number 322339D-01, Austin, Texas, USA.



- Neaves, P. I. and Hatfield, J. V. (1994). "An analogue current-mode signal processing ASIC for interrogating resistive sensor arrays", *Proceedings of the 1994 IEEE International Symposium on Circuits and Systems*, London, **5**, 405-408.
- Neaves, P. I. and Hatfield, J. V. (1994). "Current-mode multiplexer for interrogating resistive sensor arrays", *Electronic letters*, **30**, No. 12, 942-943.
- Neaves, P. I. and Hatfield, J. V. (1995). "A new generation of integrated electronic noses". *Sensors and Actuators B*, **26-27**, 223-231.
- NOSE, "Standards Commission of NOSE II", Information available at <http://www.nose-network.org/members/wg/default.asp>.
- Ong, C.K., Huang, J.L. and Cheng, K.T. (2002). "Testing second-order delta-sigma modulators using pseudo-random patterns", *Microelectronics Journal*, **33**, 807-814.
- Pallàs-Areny, R. and Webster, J.G. (2001). *Sensors and signal conditioning*, 2nd ed., John Wiley & Sons, Inc., New York.
- Palmqvist, E., Kriz, C.B., Svanberg, K., Khayyami, M. and Kriz, D. (1995). "DC-resistometric urea sensitive device utilizing a conducting polymer film for the gas-phase detection of ammonia", *Biosensors and Bioelectronics*, **10**, 283-287.
- Passeraub, P.A., Besse, P.A., de Raad, C. and Popovic, R.S. (1997). "A differential relaxation oscillator as a versatile electronic interface for sensors", *Sensors and actuators A*, **58**, 141-148.
- Pearce, T.C., Koickal, T.J., Mari, C.F., Covington, J.A., Tan, S.L., Gardner, J.W. and Hamilton, A. (2004). "Silicon-based neuromorphic olfactory pathway implementation", Brain Inspired Cognitive Systems Conference, Scotland, UK, BIS6.3 1-6.
- Phillips Semiconductors (2002). "The I<sup>2</sup>C-bus specification", Document available at [www.semiconductors.phillips.com](http://www.semiconductors.phillips.com).
- Pike, A.C. (1996). "Design of chemoresistive silicon sensors for application in gas monitoring", PhD Thesis, University of Warwick, Coventry, UK.
- Pons, P., Blasquez, G. and Behocaray, R. (1993). "Feasibility of capacitive pressure sensors without compensation circuits", *Sensors and Actuators A*, **37-38**, 112-115.
- Puers, R. (1999). "Sensor, sensor interfacing and front-end data management for stand-alone microsystems", *J. Micromech. Microeng*, **9**, R1-R7.
- Pui, B.H., Hayes-Gill, B., Clark, M., Somekh, M., See, C., Morgan, S. and Ng, A. (2002). "The design of a real time VLSI optical centroid processor",

*Proceedings of the First IEEE International Conference on Sensors*, Orlando, Florida, USA, **1**, 5-10.

Ramsay, D.C. (1996). *Principles of engineering instrumentation*, Arnold, London.

Randy, F. (1996). *Understanding smart sensors*, Artech House, Inc., Massachusetts, USA.

Razavi, B. (2001). *Design of analog CMOS integrated circuits*, McGraw-Hill, New York, USA.

Rickerby, D.G., Wächter, N., Horrillo, M.C., Gutiérrez, J., Gràcia, I. And Cané, C. (2000). "Structural and dimensional control in micromachined integrated solid state gas sensors", *Sensors and Actuators B*, **69**, 314-319.

Rösch, O.J., Schilling, K. and Roth, H. (2002). "Haptic interfaces for the remote control of mobile robots", *Control Engineering Practice*, **10**, 1309-1313.

Rostov, Y., Harás, M. and Rao, G. (2001). "Ratiometric sensing using dual-frequency lifetime discrimination", *Analytical Biochemistry*, **297**, 105-108.

Russell, R.A. (2004). "Robotic location of underground chemical sources", *Robotica*, **22**(1), 109-115.

Russell, R.A. and Purnamadajaja, A.H. (2002). "Odour and airflow complementary senses for a humanoid robot", *Proceedings of the IEEE International Conference on Robotics and Automation*, Washington DC, 1842-1847.

Samitier, J., López-Villegas, J.M., Marco, S., Cámara, L., Pardo, A., Ruiz, O. and Morante, J.R. (1994). "A new method to analyse signal transients in chemical sensors", *Sensors and Actuators B*, **18/19**, 308-312.

Schöning, M.J., Buß, G., Faßbender, F., Glück, O., Emons, H., Schmitt, G., Schultze, J.W. and Lüth, H. (2000). "A silicon-based microelectrode array for chemical analysis", *Sensors and Actuators B*, **65**, 284-287.

Sedra, A.S. and Smith, K.C. (1998). *Microelectronic circuits*, 4th. ed., Oxford University Press, New York, USA.

Seguine, D. (2002). "Just add sensor -- Integrating analog and digital signal conditioning in a programmable system on chip", *Proceedings of the First IEEE International Conference on Sensors*, Orlando, Florida, USA, **1**, 665-668.

Sessions, K.W. (1978). *IC schematic sourcemaster*, John Wiley & Sons, Inc., USA.

Shevade, A.V., Ryan, M.A., Homer, M.L., Manfreda, A.M., Zhou, H. and Manatt, K.S. (2003). "Molecular modeling of polymer composite-analyte interactions in electronic nose sensors", *Sensors and Actuators B*, **93**, 84-91.

- Sisk, B.C. and Lewis, N.S. (2003). "Estimation of chemical and physical characteristics of analyte vapors through analysis of the response data of arrays of polymer-carbon black composite vapor detectors", *Sensors and Actuators B*, **96**, 268-282.
- Sisk, B.C. and Lewis, N.S. (2005). "Comparison of analytical methods and calibration methods for correction of detector response drift in arrays of carbon black-polymer composite vapor detectors", *Sensors and Actuators B*, **104**, 249-268.
- Sohn, J.H., Smith, R., Yoong, E., Leis, J. and Galvin, G. (2003). "Quantification of odours from piggery effluent ponds using an electronic nose and an artificial neural network", *Biosystems Engineering*, **86**, 399-410.
- Stitt, R.M. (1990). "Implementation and applications of current sources and current receivers", *Burr-Brown Application Bulletin*, Tucson, AZ, USA.
- Stitt, R.M. (1994). "Make a precision current source or current sink", *Burr-Brown Application Bulletin*, Tucson, AZ, USA.
- Stitt, R.M. and Kunst, D. (1991). "Diode-based temperature measurement", *Burr-Brown Application Bulletin*, Tucson, AZ, USA.
- Stitzel, S.E., Stein, D. R. and Walt, D.R. (2003). "Enhancing vapor sensor discrimination by mimicking a canine nasal cavity flow environment", *Journal of the American Chemical Society*, **125**, 3684-3685.
- Stratigakis, N. (2001). "Electronics interface circuit for a cMOS 5-element microbridge sensor", BEng Final Year Report, University of Warwick, Coventry, UK.
- Stuetz, R.M., Engin, G. and Fenner, R.A. (1998). "Sewage odour measurements using a sensory panel and an electronic nose", *Water Science and Technology*, **38**, 331-335.
- Tan, S.L., Covington, J.A. and Gardner, J.W. (2004). "Ultra-fast chemical sensing microsystem employing resistive nanomaterials", *SPIE 11<sup>th</sup> International Symposium on Smart Structures and Materials*, San Diego, **5389**, 366-376.
- Tan, S.L., Covington, J.A. and Gardner, J.W. (2004). "Velocity-optimised diffusion for ultra-fast polymer-based resistive gas sensors", Submitted for publication on *IEE-Science, Measurement and Technology*.
- Taner, A.H. and Brignell, J.E. (1995). "Aspects of intelligent sensor reconfiguration", *Sensors and Actuators A*, **46-47**, 525-529.
- Taner, A.H. and Brignell, J.E. (1997). "Virtual instrumentation and intelligent sensors", *Sensors and Actuators A*, **61**, 427-430.

- Texas Instruments (1999). "Noise analysis in operational amplifier circuits", Application report SLVA043A, Document available at The Web pages of Texas Instruments.
- Texas Instruments (2001). "Op Amp noise theory and applications", Literature number SLOA082, Document available at The Web pages of Texas Instruments.
- Texas Instruments (2003). "FilterPro™ MFB and Sallen-Key design program", Software available at <http://www.ti.com/>.
- The Royal Swedish Academy of Sciences (2000). "The 2000 Nobel Prize in Chemistry", Information for the public available at <http://www.nobel.se>.
- The Royal Swedish Academy of Sciences. (2000). "The 2000 Nobel Prize in Chemistry, 2000: Conductive polymers", Information available at <http://www.nobel.se>.
- Tresoldi, S. (1999). "Sniffing robot: robotic odor perception", *Circuit Cellar Magazine*, **108**, 12-16.
- Trieu, H.K., Kordas, N. and Mokwa, W. (2002). "Fully CMOS compatible capacitive differential pressure sensors with on-chip programmabilities and temperature compensation", *Proceedings of the First IEEE International Conference on Sensors*, Orlando, Florida, USA, **2**, 1451-1455.
- Tsubokawa, N., Tsuchida, M., Chen, J., Nakazawa, Y. (2001). "A novel contamination sensor in solution: the response of the electric resistance of a composite based on crystalline polymer-grafted carbon black", *Sensors and Actuators B*, **79**, 92-97.
- Uchida, H., Filippini, D. and Lundström, I. (2004). "Unsupervised scanning light pulse technique for chemical sensing", *Sensors and Actuators B*, **103**, 225-232.
- Udrea, F., Gardner, J.W., Setiadi, D., Covington, J.A., Dogaru, T., Lu, C.C. and Milne, W.I. (2001). "Design and simulations of SOI CMOS micro-hotplate gas sensors", *Sensors and Actuators B*, **78**, 180-190.
- Ulmer, H., Mitrovics, J., Weimar, U. and Göpel, W. (2000). "Sensor arrays with only one or several transducer principles? The advantage of hybrid modular systems", *Sensors and Actuators B*, **65**, 79-81.
- Valente, A., Morais, R., Couto, C. and Correia, J.H. (2004). "Modeling, simulation and testing of a silicon soil moisture sensor based on the dual-probe heat-pulse method", *Sensors and Actuators A*, **115**, 434-439.
- Van der Horn, G. and Huijsing, J.H. (1997). "Integrated smart sensor calibration", *Analog Integrated Circuits and Signal Processing*, **14**, No. 3, 207-222.

- Van der Horn, G. and Huijsing, J.L. (1998). *Integrated smart sensors: design and calibration*, Kluwer Academic Publishers, The Netherlands.
- Viarani, L., Stoppa, D., Gonzo, L., Gottardi, M. and Simoni, A. (2002). "A CMOS smart pixel for active 3D vision applications", *Proceedings of the First IEEE International Conference on Sensors*, Orlando, Florida, USA, 11-14.
- Vidic, M. and Gardner, J.W. (1997). "ASIC Project: progress report", University of Warwick, Coventry, UK.
- Vossmeyer, T., Guse, B., Besnard, I., Bauer, R.E., Müllen, K. and Yasuda, A. (2002). "Gold nanoparticle/polyphenylene dendrimer composite films: preparation and vapor-sensing properties", *Advanced Materials*, **14**, No. 3, 238-242.
- Wang, A.Z., Feng, H.G., Gong, K., Zhan, R.Y. and Stine, J. (2001). "On-chip ESD protection design for integrated circuits: an overview for IC designers", *Microelectronics Journal*, **32**, No. 9, 733-747.
- West, C. (2001). "Design of an ASIC chip for a hand held gas detector", BEng Final Report, University of Warwick, Coventry, UK.
- Williams, A.B. (1975). *Active filter design*, Artech House, Inc. Massachusetts, USA.
- Williams, C.D.H. (2001). "Feedback and temperature control", Information available at <http://newton.ex.ac.uk/teaching/CDHW/Feedback/>.
- Wilson, D.M. (1996). "Compact CMOS circuit for outlier removal", *Electronic letters*, **32**, No. 11, 991-992.
- Wojslaw, C. (2000). "A compendium of application circuits for Xicor's digitally-controlled (XDCP) potentiometers", Application note 115 available at [www.xicor.com](http://www.xicor.com).
- Wojslaw, C. (2000). "Putting analog on the bus", Application note 133 available at [www.xicor.com](http://www.xicor.com).
- Woodward, S. and Wojslaw, C. (2000). "Sensor circuits and digitally controlled potentiometers (XDCPs)", Application note 135 available at [www.xicor.com](http://www.xicor.com).
- Wycisk, R., Poźniak, R. and Pasternak, A. (2002). "Conductive polymer materials with low filler content", *Journal of Electrostatics*, **56**, 55-66.
- XICOR (2000). "X9258 Quad digital controlled potentiometers (XDCP™)", Datasheet available at [www.xicor.com](http://www.xicor.com), Rev 1.1.1 10/15/00.
- XICOR (2002). "X9241A Quad digital controlled potentiometers (XDCP™)", Datasheet available at [www.xicor.com](http://www.xicor.com), Rev 1.1.13 12/09/02.

- XICOR Applications Staff (2000). "A Primer on Digitally-Controlled Potentiometers", Application note 124 available at [www.xicor.com](http://www.xicor.com).
- XICOR Applications Staff (2000). "Evaluation circuits for XDCP™", Application note 88 available at [www.xicor.com](http://www.xicor.com).
- XICOR Applications Staff (2000). "Interfacing the X9421 XDCPs to 8051 Microcontrollers", Application note 20 available at [www.xicor.com](http://www.xicor.com).
- XICOR Applications Staff (2000). "Op Amp gain and offset trim using XICOR digitally controlled potentiometers (XDCPs)", Application note 50 available at [www.xicor.com](http://www.xicor.com).
- XICOR Applications Staff (2000). "Understanding the Xicor 3-Wire XDCPTM Interface", Application note 92 available at [www.xicor.com](http://www.xicor.com).
- Xu, X. and Lucas, M.S.P. (1995). "Variable-sampling-rate sigma-delta modulator for instrumentation and measurement", *IEEE Transactions on Instrumentation and Measurement*, **44**, No. 5, 929-932.
- Yazdi, N., Mason, A., Najafi, K. and Wise, K.D. (2000). "A generic interface chip for capacitive sensors in low-power multi-parameter microsystems", *Sensors and Actuators A*, **84**, 351-361.
- Zee, F. and Judy, J.W. (2001). "Micromachined polymer-based chemical gas sensor array", *Sensors and Actuators B*, **72**, 120-128.

## **APPENDIX A**

# **DESIGN AND SIMULATION ENVIRONMENT AND TOOLS**

## SOFTWARE

| <b>Purpose</b>                                   | <b>Software package used</b>                              |
|--|---|
| General ASIC design, simulation and verification | <i>Cadence<sup>TM</sup> IC, version 4.4.3</i>             |
| Schematic design                                 | <i>Composer-Schematic</i>                                 |
| Simulation                                       | <i>Analog artist, with Spectre simulator, included in</i> |
| Layout design                                    | <i>Virtuoso tool included in Cadence</i>                  |
| Verification and design rule checks(DRC)         | <i>Diva DRC</i>   |
| Additional verification at IMEC Belgium          | <i>Dracula tools</i>                                      |
| Additional filter calculations                   | <i>FilterPro<sup>TM</sup>, by Texas Instruments</i>       |
| Data processing and plots                        | <i>Matlab, version 6<br/>Excel, Office 2000</i>           |

## HARDWARE

| <b>Purpose</b>                                   | <b>Hardware used</b>                                  |
|--|---|
| General ASIC design, simulation and verification | <i>UNIX workstation Sun Microsystems<br/>Ultra 10</i> |
| Windows based software                           | <i>Standard desktop PC</i>                            |



## **APPENDIX B**

# **AMI SEMICONDUCTORS 0.7 $\mu\text{M}$ CMOS TECHNOLOGY DESCRIPTION**

## CMOS TECHNOLOGY

|  |  |
|--|--|
| Process                                  | AMI Semiconductor 0.7 $\mu\text{m}$ CMOS C07M-A  |
| Characteristics                          | Mixed analogue/digital process, single polysilicon and double metal layer.             |
| Digital Libraries                        | MTC-22000, MTC-22200, MTC-22400, MTC-23000   |
| Analogue Library                         | MTC-22500  |
| Fabrication facilities:                  | Europractice IC Service at the Interuniversity MicroElectronics Center (IMEC), Belgium |
| Design rules file                        | <i>mtcn0u7iV.dcr</i>   |
| Extracted rules file                     | <i>mtcn0u7iV.ext</i>   |
| Layout versus schematic (LVS) rules file | <i>mtcn0u7iV.lvs2</i>  |
| Date of design submission                | May 2002   |
| Registration of design                   | MPW run 730, reference number of the registration is 68730/A37630/01                   |
| Date of ASIC chips delivery              | October 2002   |
| Cost of production                       | €2476  |
| Number of samples produced               | 20 samples ordered + 85 free additional samples  |
| Overall dimensions                       | 3.30 mm $\times$ 3.75 mm   |

### AMI SEMICONDUCTORS CELLS USED IN THE DESIGN

| COMPONENT           | SCHEMATIC                  | LAYOUT                           |
|---------------------|----------------------------|----------------------------------|
| Bandgap             | c07_bandgap / GBDA_Bandgap | c07_bandgap / GBDA_Bandgap       |
| Bandgap Bias        | c07_bandgap / GBDA_BG_bias | c07_bandgap / GBDA_BG_bias       |
| Resistors           | transistorLib / M_R        | cmos07NewPCells / npc_Nwell_res  |
| Resistors (LPF)     | transistorLib / M_R        | cmos07NewPCells / npc_hipo_res   |
| Capacitors          | transistorLib / M_C        | cmos07NewPCells / npc_poly_cap   |
| NMOSFET             | transistorLib / M_NMOS     | cmos07NewPCells / npc_Mos        |
| Diode               | transistorLib / M_D        | Designed at SRL for this project |
| Op Amps             | MTC-22500 / CFOA23         | MTC-22500 / P_CFOA23             |
| Master Bias circuit | MTC-22500 / CHMB1          | MTC-22500 / P_CHMB1              |
| Current copier      | MTC-22500 / CFBCP1         | MTC-22500 / P_CFBCP1             |
| Slave Bias circuit  | MTC-22500 / CFSB2          | MTC-22500 / P_CFSB2              |

## SELECTED AMIS DOCUMENTATION

Important information about the AMI Semiconductor 0.7  $\mu\text{m}$  CMOS technology<sup>§</sup> is included here, under permission of the proprietor, as a reference for the reported design. These pages contain details about the following topics:

Characteristics of the 0.7  $\mu\text{m}$  CMOS technology family C07M

Bias and power-down strategy

Datasheet of the operational amplifier CFOA23

Selection guide for operational amplifiers

---

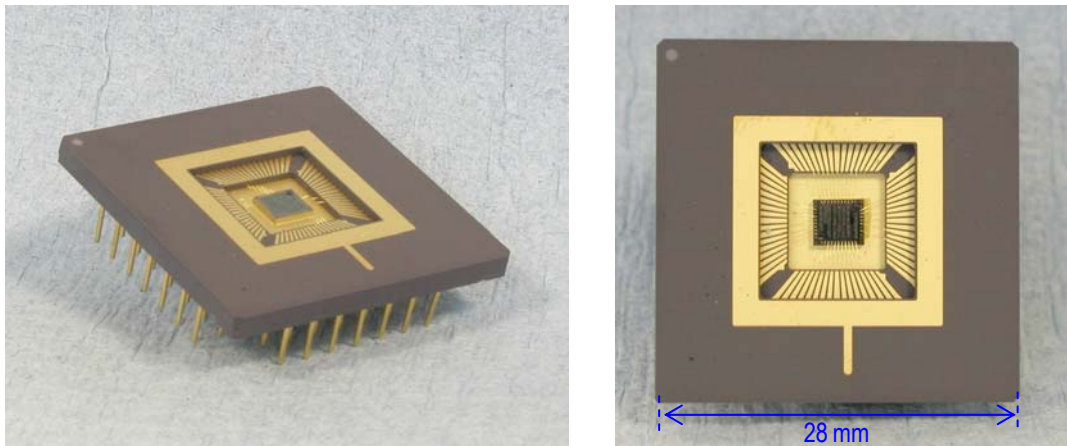
<sup>§</sup> AMI Semiconductor (2002). *Library MTC 22500*, Revision 1.0, Information accessed under permission of the proprietor.

## **APPENDIX C**

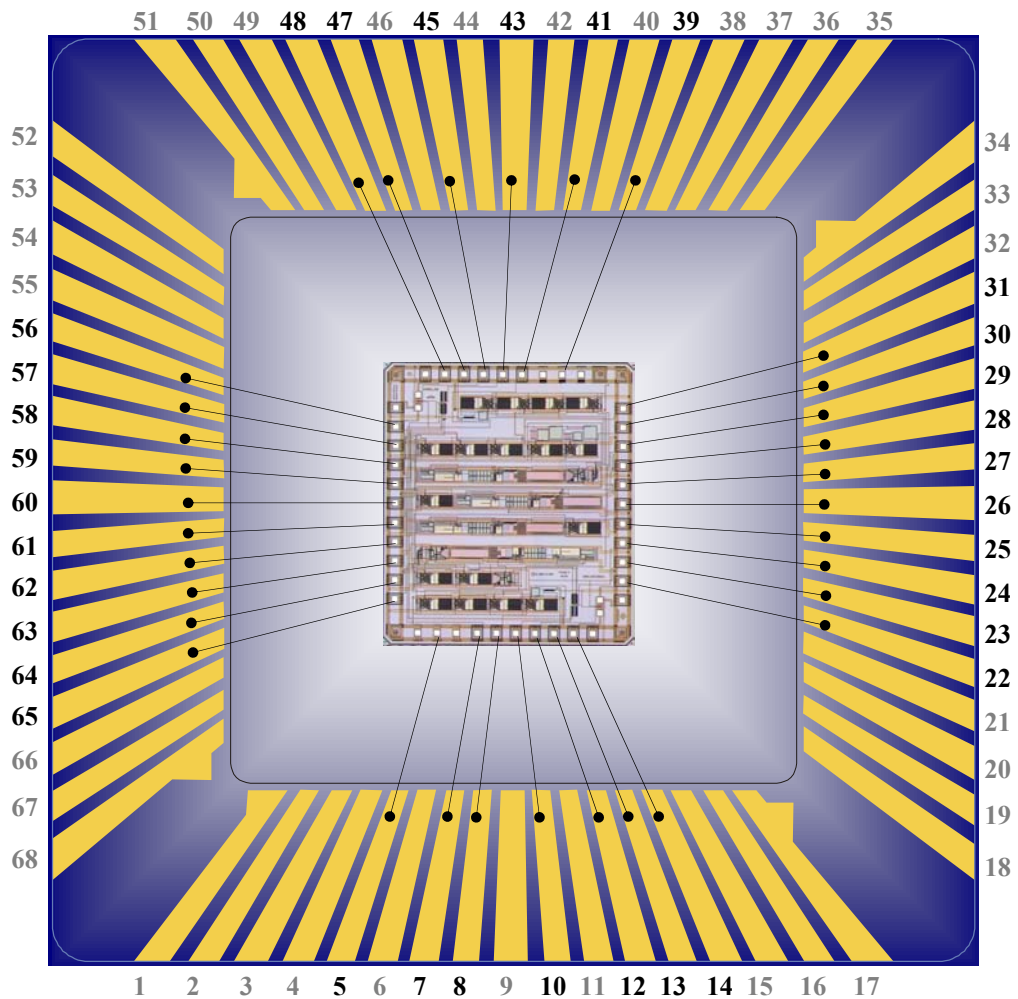
# **DETAILS AND ESPECIFICATIONS OF ADDITIONAL CIRCUITRY DESIGNED**

## ASIC PACKAGING

A ceramic PGA 68 pin package was used according to the bonding guidelines given below.



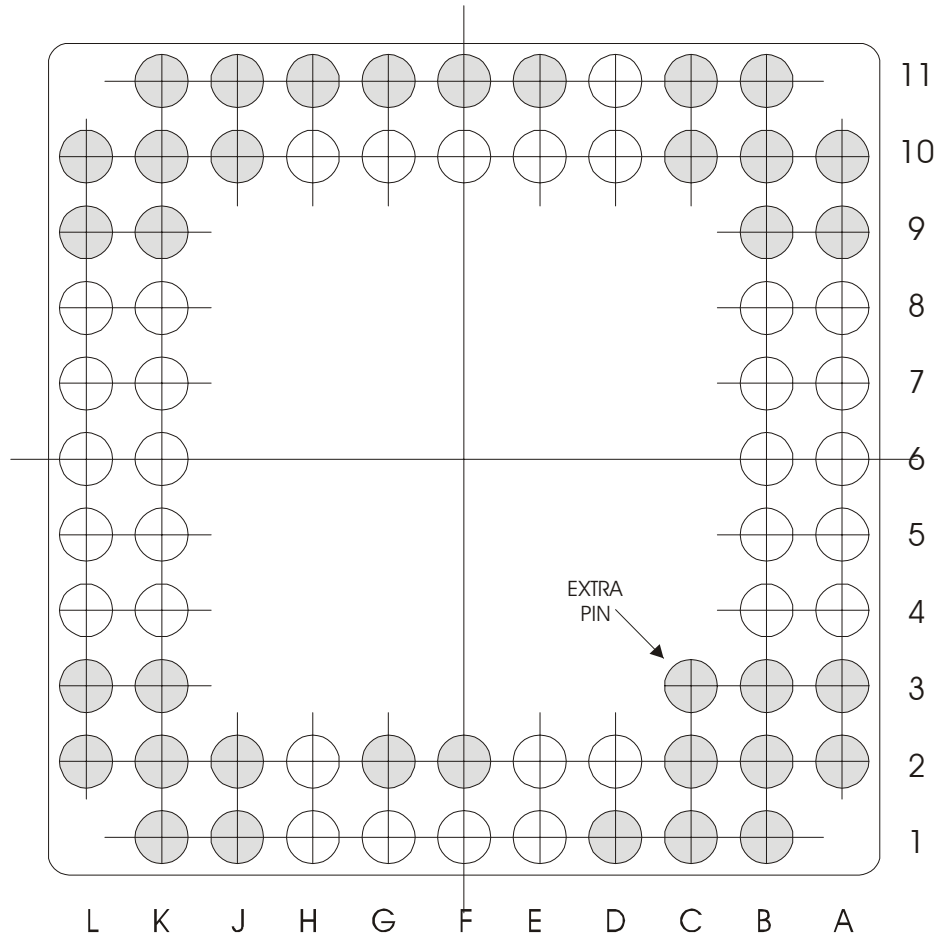
(a)



(b)

**Figure C.1** (a) The ceramic PGA 68-pin package and (b) the bonding guidelines.

### DIAGRAM OF PIN DISTRIBUTION



### CONNECTION TABLE

| PAD | PIN | PAD | PIN | PAD | PIN | PAD | PIN |
|-----|-----|-----|-----|-----|-----|-----|-----|
| 1   | B2  | 18  | K2  | 35  | K10 | 52  | B10 |
| 2   | B1  | 19  | L2  | 36  | K11 | 53  | A10 |
| 3   | C2  | 20  | K3  | 37  | J10 | 54  | B9  |
| 4   | C1  | 21  | L3  | 38  | J11 | 55  | A9  |
| 5   | D2  | 22  | K4  | 39  | H10 | 56  | B8  |
| 6   | D1  | 23  | L4  | 40  | H11 | 57  | A8  |
| 7   | E2  | 24  | K5  | 41  | G10 | 58  | B7  |
| 8   | E1  | 25  | L5  | 42  | G11 | 59  | A7  |
| 9   | F2  | 26  | K6  | 43  | F10 | 60  | B6  |
| 10  | F1  | 27  | L6  | 44  | F11 | 61  | A6  |
| 11  | G2  | 28  | K7  | 45  | E10 | 62  | B5  |
| 12  | G1  | 29  | L7  | 46  | E11 | 63  | A5  |
| 13  | H2  | 30  | K8  | 47  | D10 | 64  | B4  |
| 14  | H1  | 31  | L8  | 48  | D11 | 65  | A4  |
| 15  | J2  | 32  | K9  | 49  | C10 | 66  | B3  |
| 16  | J1  | 33  | L9  | 50  | C11 | 67  | A3  |
| 17  | K1  | 34  | L10 | 51  | B11 | 68  | A2  |

NOTES:

Numbers in grey indicate that pins are not connected.

Cavity size: .291 in x .291 in.

Index mark corresponds to pin number 1.

Connection table is referred to the attached pin diagram.

SSM Part No. CPG 06844

|  |                                |                     |
|--|--------------------------------|---------------------|
|  | SRL-194: RATIOMETRIC ASIC CHIP |                     |
|  | <b>ASIC TESTING BOARD</b>      |                     |
|  | PGA PIN DISTRIBUTION           | August 2002         |
|  | PhD project                    | JESÚS GARCÍA GUZMÁN |

## COMPLETE LIST OF PINS OF THE ASIC CHIP AND PACKAGE

| No. | Name              | Description   |
|-----|-------------------|---|
| 5   | VSSA (GROUND)     | To be connected to 0 VDC, analog ground                             |
| 7   | VSENSOR           | Voltage at the output of the ratiometric sensor                     |
| 8   | VCOMP_A           | Output of the temperature compensator (active resistor)             |
| 10  | RACT_PLUS_RETURN  | Return point for the "positive" terminal of the active resistor     |
| 12  | HEATER_A          | Input terminal of the heater under the active resistor              |
| 13  | VDRIVE_A          | Output of the current drive circuit (active resistor)               |
| 14  | RACT_MINUS        | "Negative" terminal of the active resistor                          |
| 22  | RACT_PLUS         | "Positive" terminal of the active resistor                          |
| 23  | TEMP_HEATER_A     | Output from the temperature sensor near the active resistor         |
| 24  | RACT_MINUS_RETURN | Return point for the "negative" terminal of the active resistor     |
| 25  | RTR2              | Terminal for the external resistor of the temperature reference     |
| 26  | VSP               | Input/return terminal for the temperature set-point                 |
| 27  | VPULSES           | Input of pulses for the voltage reference                           |
| 28  | VREF              | Output of the voltage reference                                     |
| 29  | TEMP_DIODE_IN     | Terminal of the anode of the thermodiode                            |
| 30  | VOUT              | Output voltage of the sensor section after amplifying and filtering |
| 31  | VAMP              | Output of the instrumentation amplifier                             |
| 39  | VDDA              | Analog power supply, to be connected to +5 VDC                      |
| 41  | VCOMP_P           | Output of the temperature compensator (passive resistor)            |
| 43  | RPAS_PLUS_RETURN  | Return point for the "positive" terminal of the passive resistor    |
| 45  | HEATER_P          | Input terminal of the heater under the passive resistor             |
| 47  | VDRIVE_P          | Output of the current drive circuit (passive resistor)              |
| 48  | RPAS_MINUS        | "Negative" terminal of the passive resistor                         |
| 56  | RPAS_PLUS         | "Positive" terminal of the passive resistor                         |
| 57  | TEMP_HEATER_P     | Output from the temperature sensor near the passive resistor        |
| 58  | RPAS_MINUS_RETURN | Return point for the "negative" terminal of the passive resistor    |
| 59  | RGAIN2            | Output to the terminal 2 of the potentiometer for gain setting      |
| 60  | ROFF_EXT          | Terminal for the external potentiometer of the offset circuit       |
| 61  | VOFFSET           | Output voltage of the offset circuit                                |
| 62  | RGAIN1            | Output to the terminal 1 of the potentiometer for gain setting      |
| 63  | VGATES            | Input of pulses for the gates of the switches                       |
| 64  | TEMP_DIODE_OUT    | Terminal of the current source and input to the amplifier           |
| 65  | TEMP_ASIC         | Output of the amplifier of the thermodiode                          |



SRL-194: RATIOMETRIC ASIC CHIP

ASIC TESTING BOARD

PGA-ASIC PINS

August 2002

PhD project


JESÚS GARCÍA GUZMÁN



## PRELIMINARY SINGLE-CHIP TESTING BOARD DESIGN

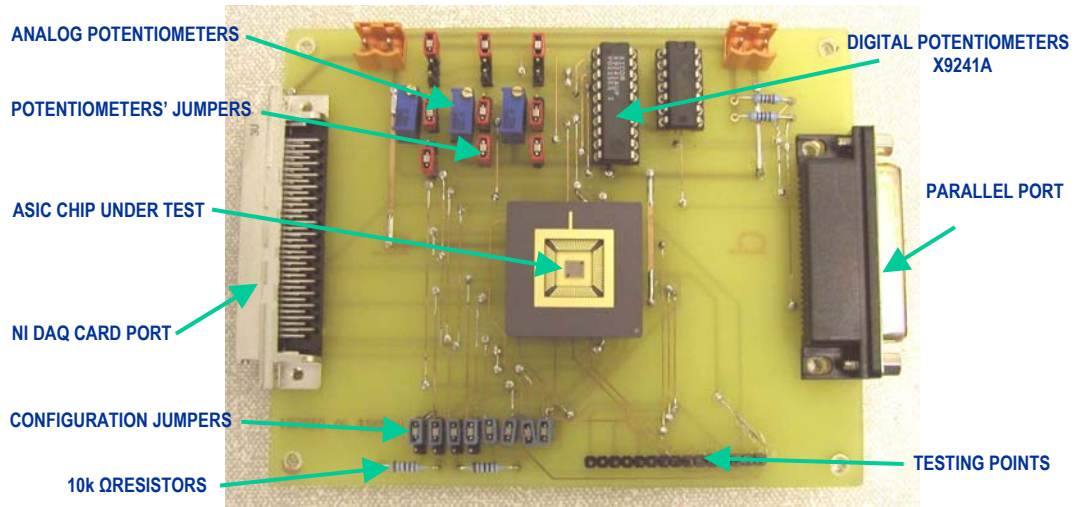


**Figure C.2** The testing board for the characterisation of a single ASIC chip.

|  |                                  |                     |
|--|----------------------------------|---------------------|
|  | SRL-194: RATIOMETRIC ASIC CHIP   |                     |
|  | <b>SINGLE-ASIC TESTING BOARD</b> |                     |
|  | PHOTOGRAPH                       | <i>August 2002</i>  |
|  | <i>PhD project</i>               | JESÚS GARCÍA GUZMÁN |

## DUAL-CHIP TEST BOARD

This is a modification of the previous single testing board used to test the components. This new dual-chip board will be used for the test rig experiments and it must fit into the existing chamber, having the dimensions of previous designs. Two ASIC chips will be tested simultaneously and this will require the use of a circuit in the board capable of controlling the data for both of them.

Two identical circuits will be used, sharing the same PC connectors to the DAQ card and the parallel port. All connections are identical in both of the circuits, namely A and B or either 1 and 2.

The connections for the parallel port remain the same, giving its signals to both the first and second sets of [X9241A + 74LS07 + 4.7k Resistors], from pins 2, 3 and 11.

The connections for the DAQ card are different for each set, as is shown in the following table:

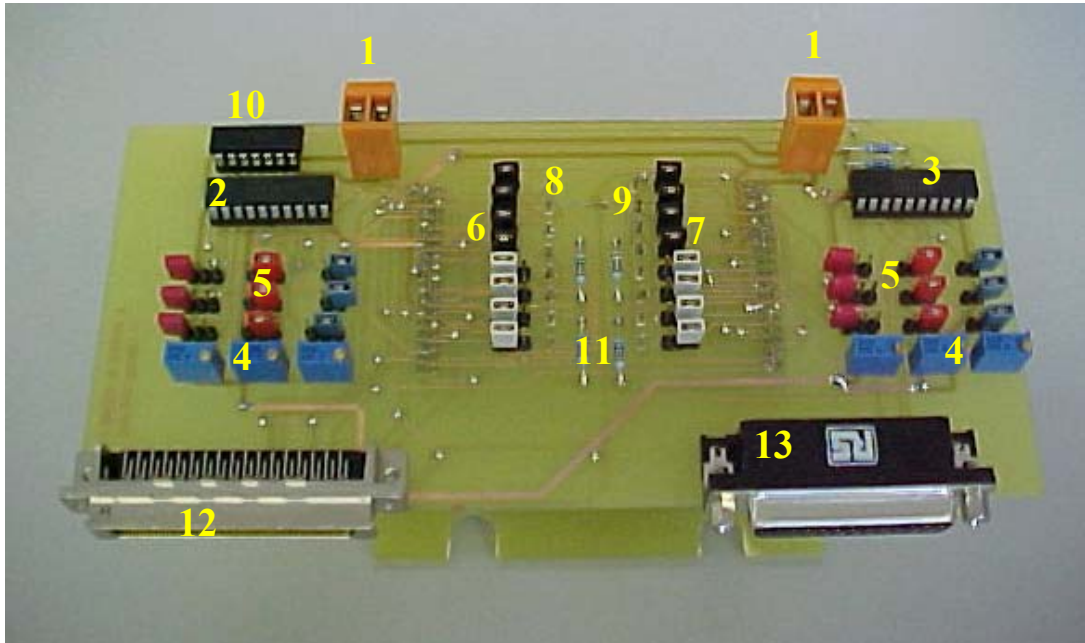
| PIN | NAME          | ASIC 1 connected to | ASIC 2 connected to |
|-----|---------------|---------------------|---------------------|
| 5   | VSSA (GROUND) | AIGND [64]          | AIGND [64]          |
| 23  | TEMP_HEATER_A | ACH8 [34]           | ACH10 [31]          |
| 27  | VPULSES       | DAC1OUT[21]         | DAC1OUT[21]         |
| 30  | VOUT          | ACH0 [68]           | ACH2 [65]           |
| 57  | TEMP_HEATER_P | ACH4 [28]           | ACH15 [23]          |
| 63  | VGATES        | DAC0OUT[22]         | DAC0OUT[22]         |
| 65  | TEMP_ASIC     | ACH12 [61]          | ACH7 [57]           |

The connections for the X9241 vary in the pins determining the device address.

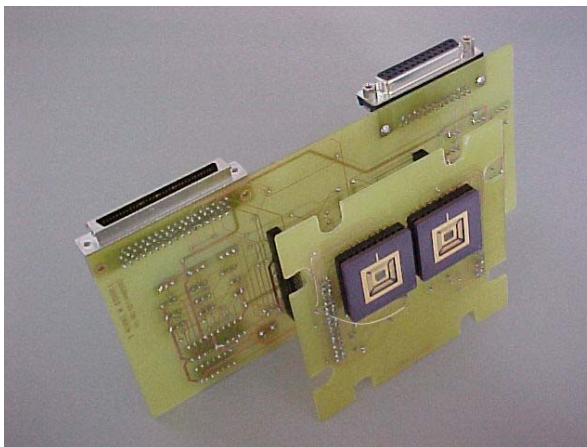
| PIN | NAME | XDCP 1 CONNECTED TO | XDCP 2 CONNECTED TO |
|-----|------|---------------------|---------------------|
| 4   | A0   | GND                 | +5V (VCC)           |
| 16  | A1   | GND                 | GND                 |
| 5   | A2   | GND                 | GND                 |
| 15  | A3   | GND                 | GND                 |

Power supply connectors do not need to be repeated.

## DUAL-CHIP TEST BOARD PHOTOGRAPHS



1. Power supply connector +5 VDC (only one is required)
2. Digital potentiometers XDCP1
3. Digital Potentiometers XDCP2
4. Analog potentiometers
5. Jumpers for potentiometers
6. Jumpers for ASIC1
7. Jumpers for ASIC2
8. Test points for ASIC1
9. Test points for ASIC2
10. 74LS07
11. Resistors 10k
12. NI-DAQ card connector
13. Parallel port



ASIC chips must be connected as shown, with gold reference line pointing in the same direction as the PC connectors.

Connection between the two PCBs is allowed only in one way, with the two sockets aligned towards the PC connectors.

The left side chip is the ASIC1, on the side of the NI-DAQ connector, whereas ASIC2 is at the right side, near the parallel port.



Lis sobre la arena

SRL-194: RATIOMETRIC ASIC CHIP

ASIC TESTING BOARD

PHOTOGRAPHS

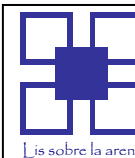
August 2002

PhD project

JESÚS GARCÍA GUZMÁN

## ASIC CHIP CONNECTIONS

| PIN NO |     | NAME              | ASIC 1 connected to | ASIC 2 connected to |
|--------|-----|-------------------|---------------------|---------------------|
| 5      | D2  | VSSA (GROUND)     | AIGND [64]          | AIGND [64]          |
| 7      | E2  | VSENSOR           | TP1                 | TP1                 |
| 8      | E1  | VCOMP_A           | TP2                 | TP2                 |
| 10     | F1  | RACT_PLUS_RETURN  | JP1-B               | JP1-B               |
| 12     | G1  | HEATER_A          | JP5-A               | JP5-A               |
| 13     | H2  | VDRIVE_A          | JP5-B & TP3         | JP5-B & TP3         |
| 14     | H1  | RACT_MINUS        | JP2-A               | JP2-A               |
| 22     | K4  | RACT_PLUS         | JP1-A               | JP1-A               |
| 23     | L4  | TEMP_HEATER_A     | ACH8 [34]           | ACH10 [31]          |
| 24     | K5  | RACT_MINUS_RETURN | JP2-B               | JP2-B               |
| 25     | L5  | RTR2              | JPT-A & JP6-A       | JPT-A & JP6-A       |
| 26     | K6  | VSP               | JP6-B               | JP6-B               |
| 27     | L6  | VPULSES           | DAC1OUT[21]         | DAC1OUT[21]         |
| 28     | K7  | VREF              | TP4                 | TP4                 |
| 29     | L7  | TEMP_DIODE_IN     | JP7-B               | JP7-B               |
| 30     | K8  | VOUT              | ACH0 [68]           | ACH2 [65]           |
| 31     | L8  | VAMP              | TP5                 | TP5                 |
| 39     | H10 | VDDA              | +5VDC               | +5VDC               |
| 41     | G10 | VCOMP_P           | TP6                 | TP6                 |
| 43     | F10 | RPAS_PLUS_RETURN  | JP3-B               | JP3-B               |
| 45     | E10 | HEATER_P          | JP8-A & TP7         | JP8-A & TP7         |
| 47     | D10 | VDRIVE_P          | JP8-B               | JP8-B               |
| 48     | D11 | RPAS_MINUS        | JP4-A               | JP4-A               |
| 56     | B8  | RPAS_PLUS         | JP3-A               | JP3-A               |
| 57     | A8  | TEMP_HEATER_P     | ACH4 [28]           | ACH15 [23]          |
| 58     | B7  | RPAS_MINUS_RETURN | JP4-B               | JP4-B               |
| 59     | A7  | RGAIN2            | JPG-A2              | JPG-A2              |
| 60     | B6  | ROFF_EXT          | JPO-A               | JPO-A               |
| 61     | A6  | VOFFSET           | TP8                 | TP8                 |
| 62     | B5  | RGAIN1            | JPG-A1              | JPG-A1              |
| 63     | A5  | VGATES            | DAC0OUT[22]         | DAC0OUT[22]         |
| 64     | B4  | TEMP_DIODE_OUT    | JP7-A               | JP7-A               |
| 65     | A4  | TEMP_ASIC         | ACH12 [61]          | ACH7 [57]           |



Las sobre la arena

SRL-194: RATIOMETRIC ASIC CHIP

**ASIC TESTING BOARD**

ASIC CONNECTIONS August 2002

PhD project

JESÚS GARCÍA GUZMÁN

### XDCPs CONNECTIONS

| PIN No | NAME | FUNCTION              | XDCP1 CONNECTED TO:                     | XDCP2 CONNECTED TO:                     |
|--------|------|-----------------------|---|---|
| 14     | SCL  | SERIAL CLOCK          | D0 [2] & R2                             | D0 [2] & R4                             |
| 9      | SDA  | SERIAL DATA           | $\overline{S7}$ [11] & R1 & 74LS07-A[2] | $\overline{S7}$ [11] & R3 & 74LS07-B[2] |
| 4      | A0   | DEVICE ADDRESS        | GND                                     | +5V (VCC)                               |
| 16     | A1   | DEVICE ADDRESS        | GND                                     | GND                                     |
| 5      | A2   | DEVICE ADDRESS        | GND                                     | GND                                     |
| 15     | A3   | DEVICE ADDRESS        | GND                                     | GND                                     |
| 2      | RL0  | POTENTIOMETER 0 LOW   | JPT-L                                   | JPT-L                                   |
| 3      | RH0  | POTENTIOMETER 0 HIGH  | JPT-H                                   | JPT-H                                   |
| 1      | RW0  | POTENTIOMETER 0 WIPER | JPT-W                                   | JPT-W                                   |
| 7      | RL1  | POTENTIOMETER 1 LOW   | JPO-L                                   | JPO-L                                   |
| 8      | RH1  | POTENTIOMETER 1 HIGH  | JPO-H                                   | JPO-H                                   |
| 6      | RW1  | POTENTIOMETER 1 WIPER | JPO-W                                   | JPO-W                                   |
| 18     | RL3  | POTENTIOMETER 3 LOW   | JPG-L                                   | JPG-L                                   |
| 17     | RH3  | POTENTIOMETER 3 HIGH  | JPG-H                                   | JPG-H                                   |
| 19     | RW3  | POTENTIOMETER 3 WIPER | JPG-W                                   | JPG-W                                   |
| 20     | VCC  | DIGITAL POWER SUPPLY  | +5V (VCC)                               | +5V (VCC)                               |
| 10     | VSS  | DIGITAL GROUND        | GND                                     | GND                                     |



Lis sobre la arena

SRL-194: RATIOMETRIC ASIC CHIP

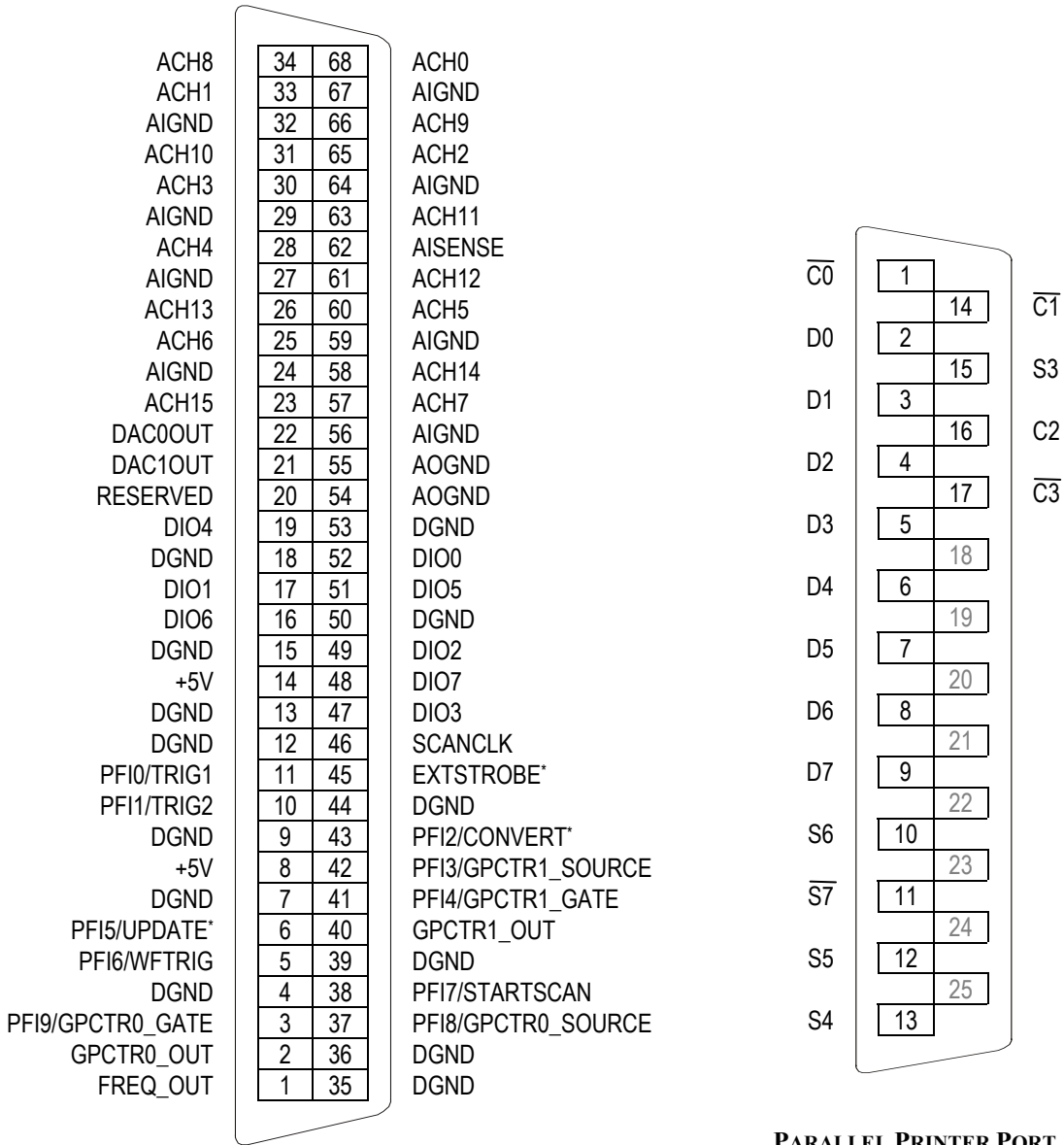
ASIC TESTING BOARD

XDCPs CONNECTIONS August 2002

PhD project

JESÚS GARCÍA GUZMÁN


### PC D-CONNECTORS FOR THE TEST BOARD



**PARALLEL PRINTER PORT**  
25-way Female D-Type Connector

### NI 6036 DAQ CARD

I/O Connector Pin Assignment for the NI 6036E

|  |                                |                     |
|--|--------------------------------|---------------------|
|  | SRL-194: RATIOMETRIC ASIC CHIP |                     |
|  | <b>ASIC TESTING BOARD</b>      |                     |
|  | PC D-CONNECTORS                | August 2002         |
|  | PhD project                    | JESÚS GARCÍA GUZMÁN |

## TEST POINTS SIGNALS

| TP | SIGNAL   | DESCRIPTION   |
|----|----------|---|
| 1  | VSENSOR  | Output voltage from the ratiometric sensor circuit                  |
| 2  | VCOMP_A  | Output voltage from the compensator circuit, for the active sensor  |
| 3  | VDRIVE_A | Voltage applied to the heater for the active sensor                 |
| 4  | VREF     | Voltage reference applied to the input of the ratiometric circuit   |
| 5  | VAMP     | Voltage at the output of the instrumentation amplifier              |
| 6  | VCOMP_P  | Output voltage from the compensator circuit, for the passive sensor |
| 7  | VDRIVE_P | Voltage applied to the heater for the passive sensor                |
| 8  | VOFFSET  | Output voltage from the offset circuit                              |



Lis sobre la arena

SRL-194: RATIOMETRIC ASIC CHIP

**ASIC TESTING BOARD**

TEST POINTS

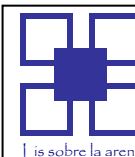
*August 2002*

*PhD project*

JESÚS GARCÍA GUZMÁN

## JUMPERS CONNECTIONS

| JP | PINS | IS CONNECTING:  |
|----|------|---|
| 1  | A-B  | ACTIVE RESISTOR (PLUS PIN) TO THE INTERNAL CIRCUIT                    |
| 1  | B-C  | INTERNAL CIRCUIT TO THE DUMMY ACTIVE RESISTOR (PLUS PIN)              |
| 2  | A-B  | ACTIVE RESISTOR (MINUS PIN) TO THE INTERNAL CIRCUIT                   |
| 2  | B-C  | INTERNAL CIRCUIT TO THE DUMMY ACTIVE RESISTOR (MINUS PIN)             |
| 3  | A-B  | PASSIVE RESISTOR (PLUS PIN) TO THE INTERNAL CIRCUIT                   |
| 3  | B-C  | INTERNAL CIRCUIT TO THE DUMMY PASSIVE RESISTOR (PLUS PIN)             |
| 4  | A-B  | PASSIVE RESISTOR (MINUS PIN) TO THE INTERNAL CIRCUIT                  |
| 4  | B-C  | INTERNAL CIRCUIT TO THE DUMMY PASSIVE RESISTOR (MINUS PIN)            |
| 5  | A-B  | HEATER_A TO VDRIVE_A; APPLIES VOLTAGE TO THE HEATER (ACTIVE)          |
| 6  | A-B  | RTR2 TO VSP; SET-POINT VOLTAGE APPLIED TO THE CIRCUIT                 |
| 7  | A-B  | TEMP_DIODE_OUT TO TEMP_DIODE_IN; THERMODIODE CONNECTED TO THE CIRCUIT |
| 8  | A-B  | HEATER_P TO VDRIVE_P; APPLIES VOLTAGE TO THE HEATER (PASSIVE)         |



*Lo es sobre la arena*

SRL-194: RATIOMETRIC ASIC CHIP

**ASIC TESTING BOARD**

JUMPERS 1-8

*August 2002*

*PhD project*

JESÚS GARCÍA GUZMÁN



## JUMPERS FOR POTENTIOMETERS

| JP | PINS  | IS CONNECTING:   |
|----|-------|--|
| G  | A1-W  | RGAIN1 TO DIGITAL POTENTIOMETER                                  |
| G  | A1-G1 | RGAIN1 TO ANALOG POTENTIOMETER                                   |
| G  | A2-L  | RGAIN2 TO DIGITAL POTENTIOMETER                                  |
| G  | A2-G2 | RGAIN2 TO ANALOG POTENTIOMETER                                   |
| G  | H-V   | HIGH TERMINAL OF DIGITAL POTENTIOMETER TO VCC                    |
| G  | H-W   | HIGH TERMINAL OF DIGITAL POTENTIOMETER SHORTED TO WIPER TERMINAL |
| O  | A-W   | ROFF_EXT TO DIGITAL POTENTIOMETER                                |
| O  | A-O1  | ROFF_EXT TO ANALOG POTENTIOMETER (O2 DIRECTLY GROUNDED)          |
| O  | L-G   | LOW TERMINAL OF DIGITAL POTENTIOMETER TO GROUND                  |
| O  | H-V   | HIGH TERMINAL OF DIGITAL POTENTIOMETER TO VCC                    |
| O  | H-W   | HIGH TERMINAL OF DIGITAL POTENTIOMETER SHORTED TO WIPER TERMINAL |
| T  | A-W   | RTR2 TO DIGITAL POTENTIOMETER                                    |
| T  | A-T1  | RTR2 TO ANALOG POTENTIOMETER (T2 DIRECTLY GROUNDED)              |
| T  | L-G   | LOW TERMINAL OF DIGITAL POTENTIOMETER TO GROUND                  |
| T  | H-V   | HIGH TERMINAL OF DIGITAL POTENTIOMETER TO VCC                    |
| T  | H-W   | HIGH TERMINAL OF DIGITAL POTENTIOMETER SHORTED TO WIPER TERMINAL |



SRL-194: RATIOMETRIC ASIC CHIP

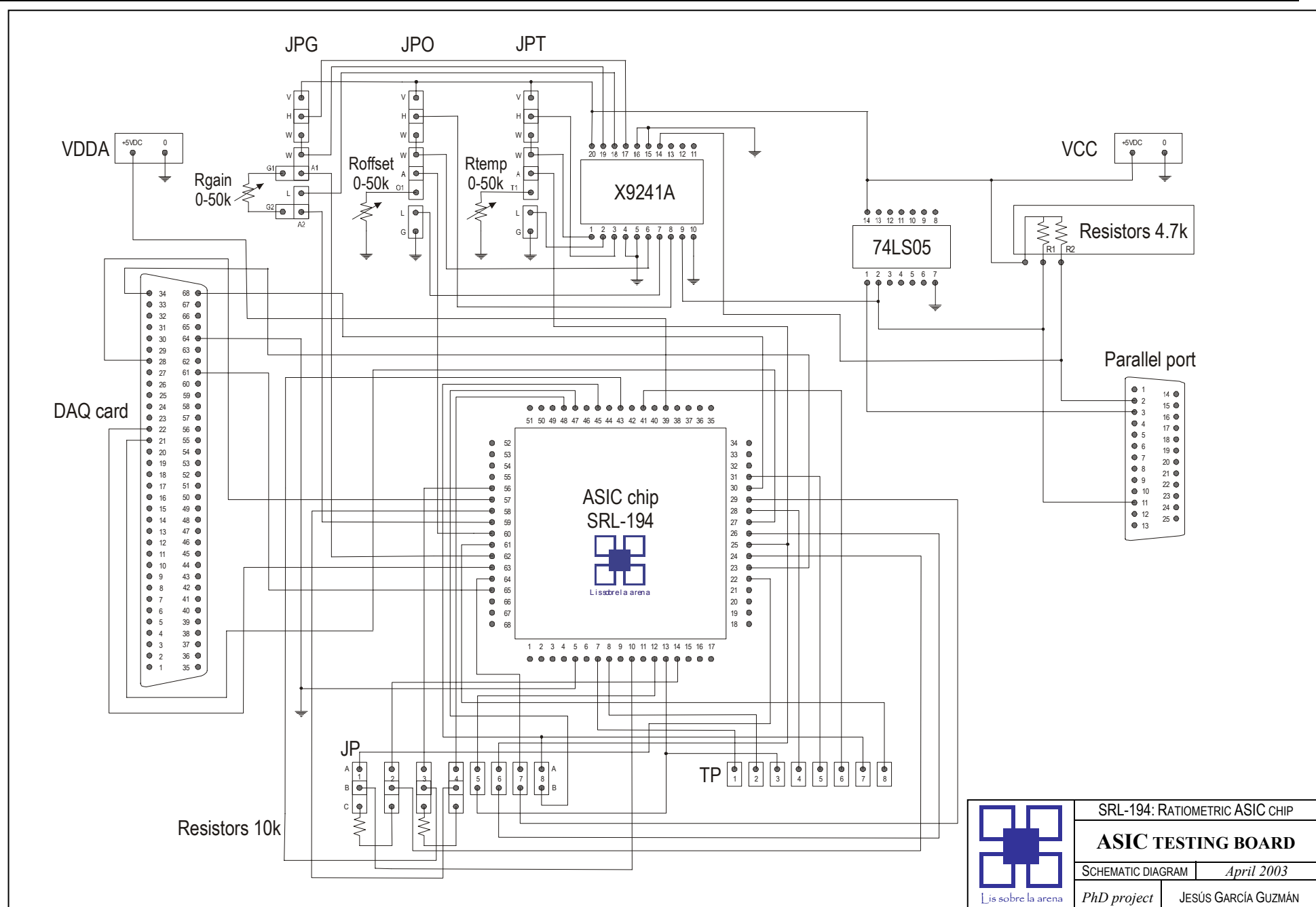
### ASIC TESTING BOARD

JUMPERS G-O-T

August 2002

PhD project

JESÚS GARCÍA GUZMÁN



|                                |                     |
|--------------------------------|---------------------|
| SRL-194: RATIOMETRIC ASIC CHIP |                     |
| <b>ASIC TESTING BOARD</b>      |                     |
| SCHMATIC DIAGRAM               | April 2003          |
| PhD project                    | JESÚS GARCÍA GUZMÁN |

---

**APPENDIX D**

**VIRTUAL INSTRUMENTATION**

---

## VIRTUAL INSTRUMENTATION

*LabView*<sup>TM</sup> software has been written for the automated control of the gas-exposure process that allow the characterisation of the response obtained with the ratiometric ASIC chip and several sets of sensors.

The software is going to be used together with the *Dual-chip test board* designed to fit into the test rig. Communication between the computer and the test board will be established both through the parallel port and through the National Instruments NI-6036E data acquisition card.

There are three main functions that the software performs:

- a) *Generation of the input pulses of voltage required for driving the ASIC chips.* A square waveform of 10 Hz and a duty cycle of 10% is used for energizing the voltage reference cell which produces the basic signal for the gas sensor circuit. A second square waveform of 5 Hz and duty cycle of 50% is required in order to alternately invert the polarity of the voltage applied to the sensing chemoresistors through the use of a set of FET-based switches. Both square waveforms are generated with *LabView*<sup>TM</sup> and are sent to the ASICs through the NI-DAQ card.
- b) *Calibration of the Xicor's digital potentiometers.* Three digital potentiometers are used with each ASIC chip for the adjustment of the following variables: the gain of the instrumentation amplifier, the offset voltage signal matching the output of the sensor circuit, and the voltage corresponding to the temperature set-point. The values of these potentiometers are set through a piece of *LabView*<sup>TM</sup> software that sends the proper resistance values using an I<sup>2</sup>C data stream via the parallel port of the computer.
- c) *Data acquisition of the output voltages from the ASIC chips.* The output of the ratiometric ASIC chips is monitored through the analog channels of the NI-DAQ card and the sampled response is saved to files in the computer by using *LabView*<sup>TM</sup> software.

A *LabView*<sup>TM</sup> virtual instrument has been written for each of these functions and the whole process is controlled from a main module that integrates the corresponding sub-programs. Some additional virtual instruments perform specific tasks inside the programs.

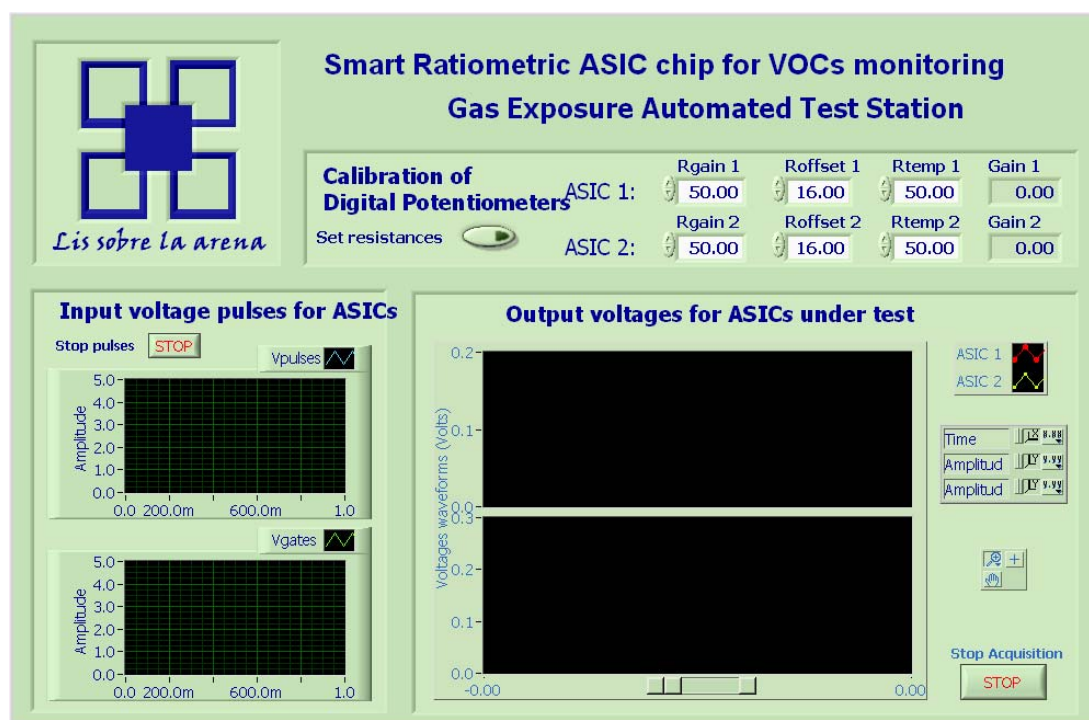
A folder containing the complete set of virtual instruments used in the project is included in the Appendix G (CD-ROM).

## MAIN MODULE FOR ASIC TEST

The front panel of the main module for ASIC test consists of three sub-panels that correspond to each of the main tasks described above. When the program is run, it starts immediately the virtual instrument that produces the input pulses for the two ASIC chips that are going to be under test. When the power supply is on, the input pulses produce in turn pulses in the voltage reference cell and from here all the corresponding parts of the circuit respond to the pulsed stimuli. The waveforms of the input pulses are shown in this sub-panel.

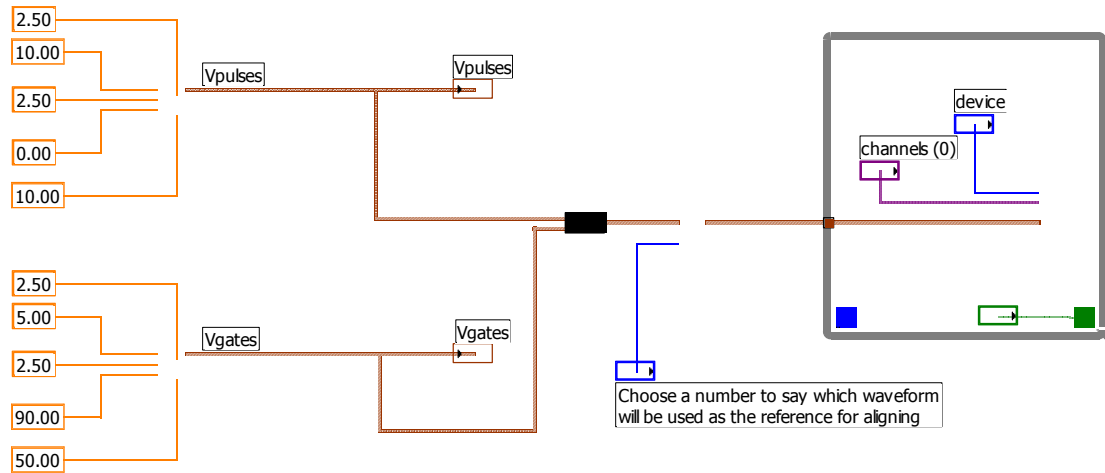
The calibration module is then available in order to set the required values for the resistances of the digital potentiometers. The resistance values in kilo-ohms can be varied from 0 to 50 through the controls in this sub-panel so the proper levels of gain, offset voltage and temperature set-point can be achieved.

The third sub-panel corresponds to the acquisition of data from the output of the ASIC chips. From this panel the actual acquisition of data can be started and finished, obtaining a file with the sampled values of voltages in a tabular form. The waveforms of the voltages are shown as they are obtained through the analogue channels of the NI-DAQ.



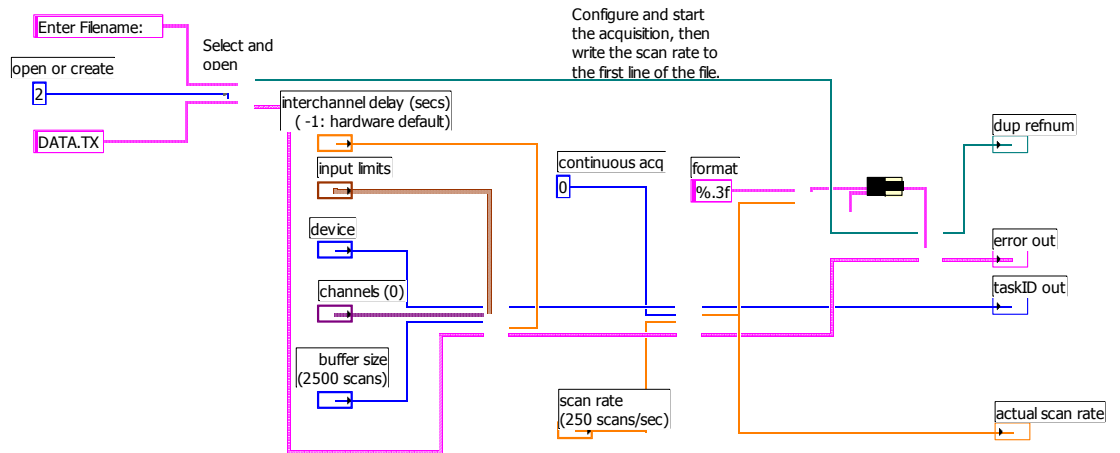
## SUB-PROGRAM FOR INPUT PULSES GENERATION

The sub-program for the generation of the input voltage pulses produces the two pulsed signals that are sent to the ASIC chips via the two output channels available in the NI-DAQ card.  $V_{pulses}$  appears in channel 0 whereas  $V_{gates}$  appears through channel 1. Both signals are previously aligned in order to make them appear at the times required for the proper ASIC functioning.

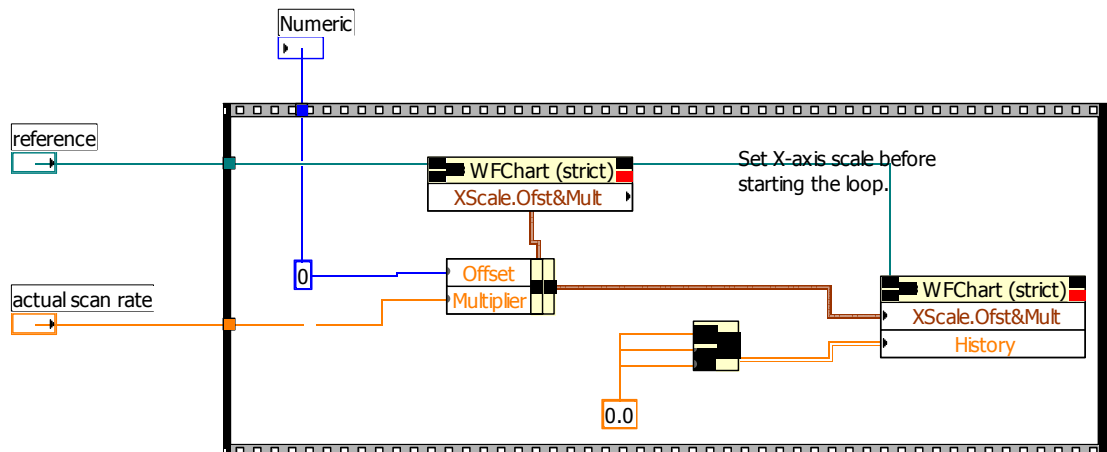


## SUB-PROGRAMS FOR DATA ACQUISITION

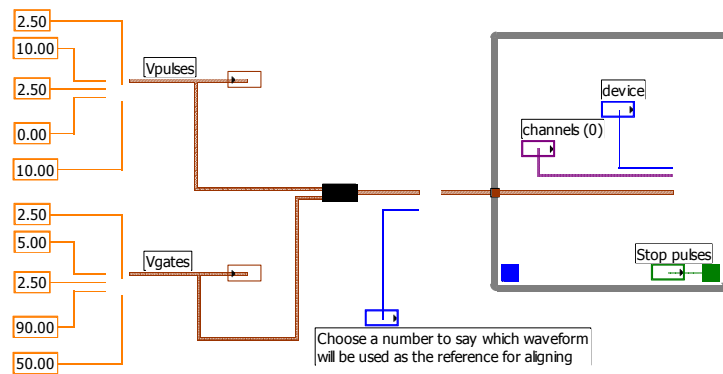
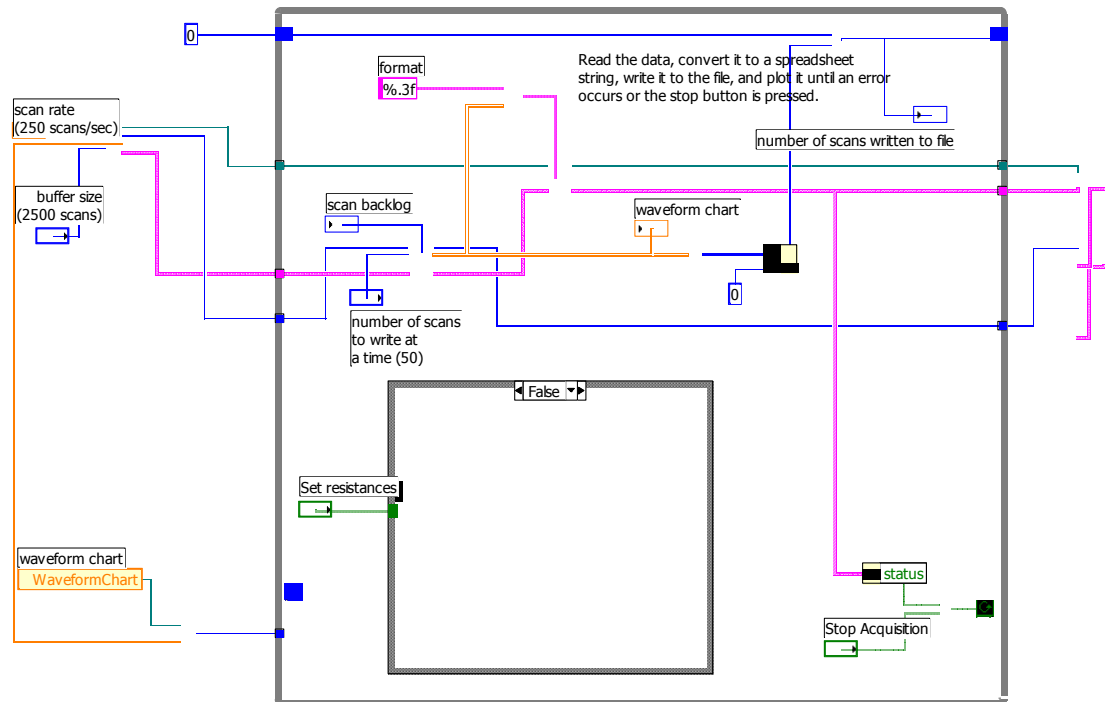
### Start.Vi



### SetX.vi

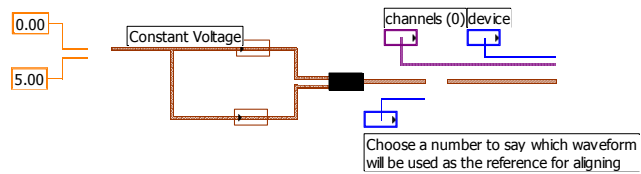
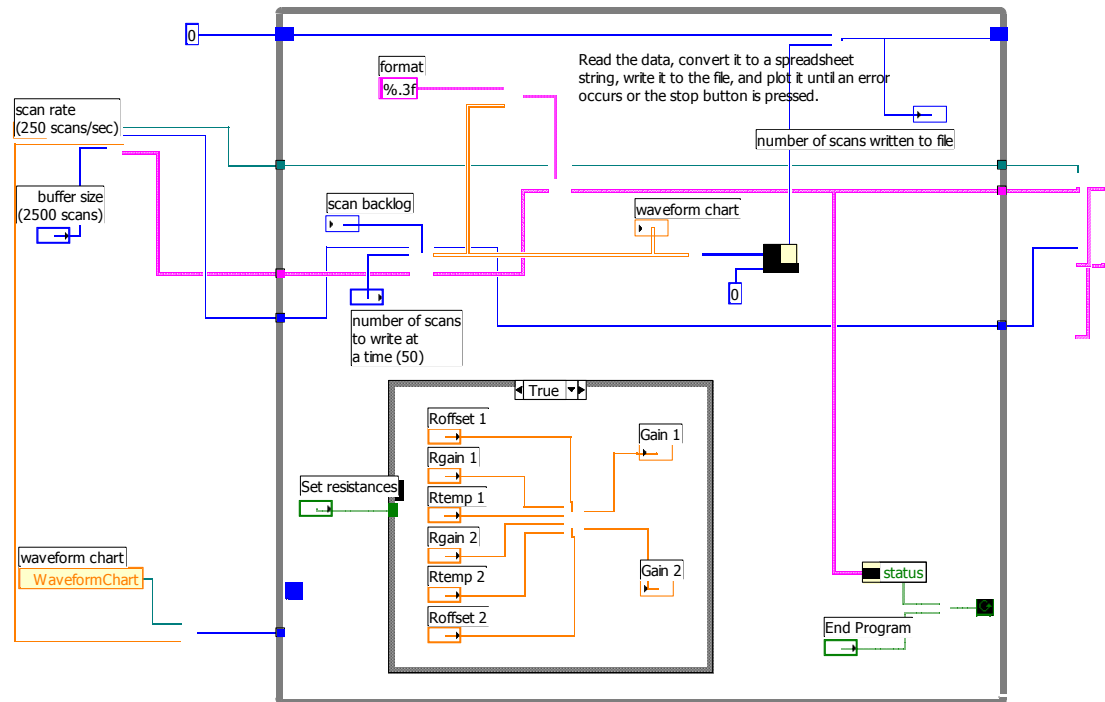


## PulsedTest.vi diagram





## ConstantTest.vi diagram

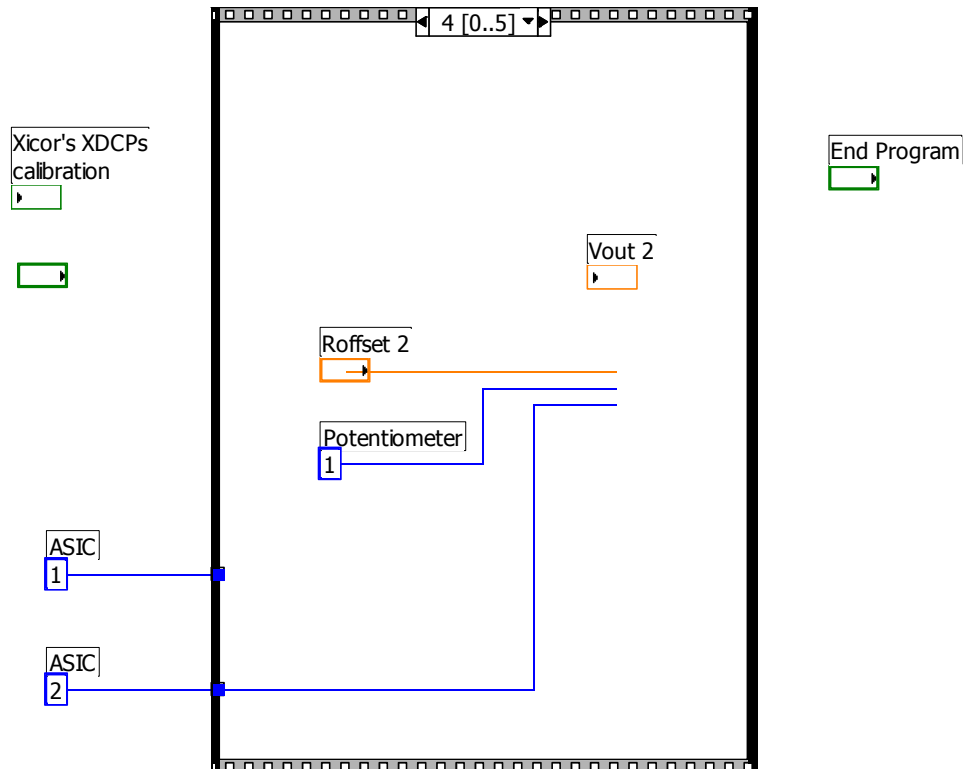


## SUB-PROGRAM FOR CALIBRATION OF DIGITAL POTENTIOMETERS

### Calibration.vi panel

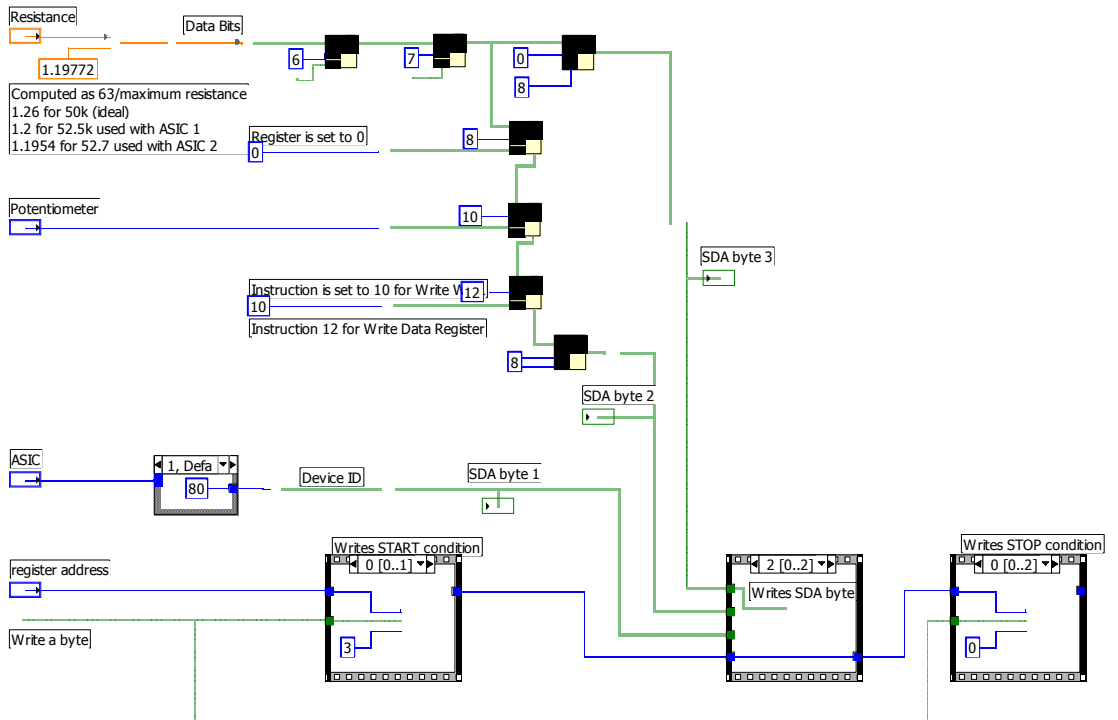


### Calibration.vi diagram

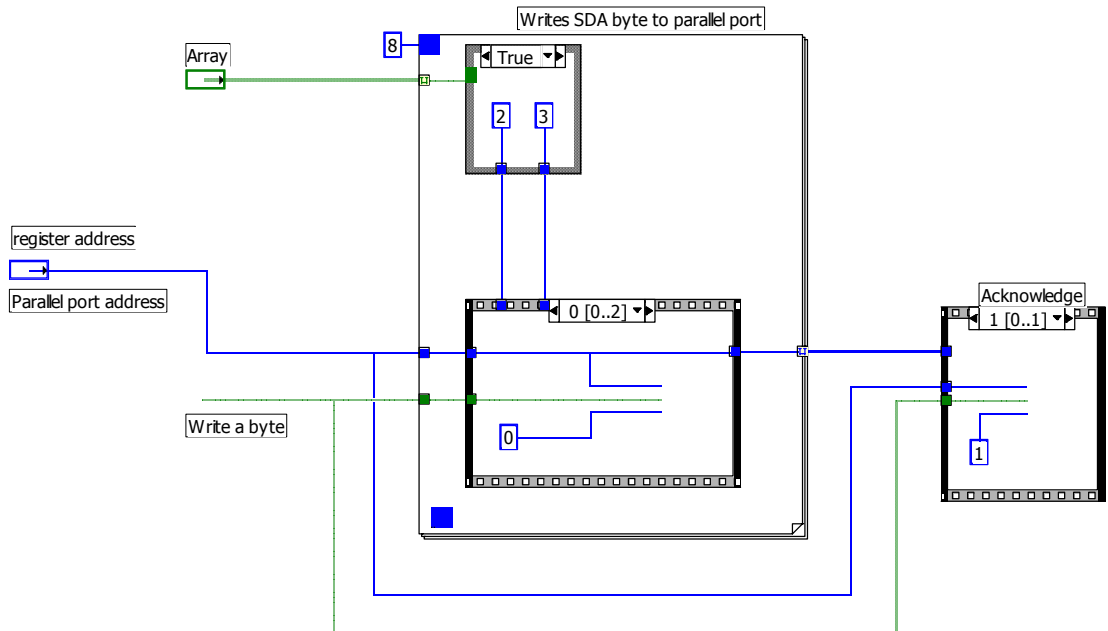


## SUB-PROGRAM FOR SETTING RESISTANCE VALUES

### SetResistance.vi



### Write SDA byte



---

**APPENDIX E**

**SPECIFICATIONS FOR THE  
MICRO-CONTROLLER UNIT**

## FUNCTIONS TO BE PERFORMED BY THE MICRO-CONTROLLER UNIT

| Signals and ranges  | Functions to perform in the micro-controller unit   |
|---|---|
| <i>V<sub>out</sub></i><br>Analogue input<br>0-4.5V  | A/D conversion <sup>2</sup><br><i>V<sub>out</sub></i> is an analogue signal that must be converted to digital before processing.<br>Offset (calibration mode)<br>Without gas exposition, while <i>V<sub>out</sub></i> is non-zero, the resistance of Pot1 must be adjusted, starting from 10kΩ, until the desired value is obtained. When the baseline <i>V<sub>out</sub></i> is set, the value in potentiometer Pot1 must be fixed. This will be the offset calibration point.<br>The offset point must be confirmed for the expected gain values of the Instrumentation Amplifier.<br>Gain adjusting (testing mode)<br>When the ASIC is exposed to VOC, <i>V<sub>out</sub></i> must be preferably between 2 and 3 volts. To obtain this, the potentiometer Pot2 must be automatically adjusted, giving the proper gain.<br>Display<br>The digital value of <i>V<sub>out</sub></i> must appear in the display unit |
| <i>Temp<sub>P</sub></i> and <i>Temp<sub>A</sub></i><br>Analogue input<br>0-800mV                    | A/D conversion<br>These analogue signals must be converted to digital before processing.<br>Temperature conversion<br>The diode voltage must be converted to temperature, for display purposes.<br>The signals will eventually reach the same temperature as the set-point.<br>Display<br>The digital values of the temperature equivalents for these signals must appear in the display unit   |
| <i>Temp<sub>ASIC</sub></i><br>Analogue input<br>3-4.5V  | A/D conversion<br>This analogue signal must be converted to digital before processing.<br>Temperature conversion<br>The diode voltage must be converted to temperature, for display purposes<br>Display<br>The digital value of the temperature equivalent of this signal must appear in the display unit   |
| Set-point temperature<br>20-100°C   | This temperature value must be entered to the micro-controller, ideally in Celsius degrees and converted by software to the required diode voltage or to the corresponding value of the potentiometer Pot3.   |
| <i>V<sub>pulses</sub></i><br>Digital output<br>0-5 VDC<br>Period 100ms<br>Width 10ms                | This digital pulsed signal must be applied to the <i>V<sub>pulses</sub></i> input of the ASIC chip.<br>This signal set the waveform of the voltage reference.   |
| <i>V<sub>gates</sub></i><br>Digital output<br>0-5 VDC<br>Period 200ms<br>Width 100ms<br>Delay -50ms | This digital pulsed signal must be applied to the corresponding input of the ASIC chip.<br>This signal controls the alternating switching process for the polymer resistors.  |

<sup>2</sup> Analogue to digital (A/D) conversion could be performed instead inside the ASIC chip, if a proper converter is integrated into the circuit.

---

**APPENDIX F**

**PUBLICATIONS RELATED  
TO THIS PROJECT**

---

**LIST OF PUBLICATIONS:**

- Cole, M., García Guzmán, J. and Gardner, J.W. (2002). “Smart ratiometric ASIC chip for a palm-top VOC monitor”, *Eurosensors XVI, the 16<sup>th</sup> European Conference on Solid-State Transducers*, Prague, Czech Republic, 509-512.
- García-Guzmán, J., Olivieri, N., Cole, M. and Gardner, J.W. (2003). “Design and simulation of a smart ratiometric ASIC chip for VOC monitoring”, *Sensors and Actuators B*, **95**, 232-243.
- Cole, M., Olivieri, N., García-Guzmán, J. and Gardner, J.W. (2003). “Parametric model of a polymeric chemoresistor for use in smart sensor design and simulation”, *Microelectronics Journal*, **34**, 865-875.
- Gardner, J.W., García-Guzmán, J. and Cole, M. (2004). “Smart ASIC chip for vapour detection based upon carbon black/polymer composite nanomaterials”, *Proceedings of SPIE*, **5389**, 344-354, in *Smart Structures and Materials 2004: Smart Electronics, MEMS, BioMEMS, and Nanotechnology*, Varadan, V.K., Ed. SPIE, Bellingham, WA.

---

**APPENDIX G**

**ADDITIONAL DETAILS  
AND RESULTS (CD-ROM)**



## Smart ratiometric ASIC chip for a palm-top VOC monitor

Marina Cole, Jesús García Guzmán, Julian W. Gardner

University of Warwick, School of Engineering, Coventry, CV4 7AL, UK

e-mail: mvc@eng.warwick.ac.uk <http://www.eng.warwick.ac.uk/SRL>

### SUMMARY

A novel ASIC chip has been designed for use in a hand-held instrument for the monitoring of volatile organic compounds (VOCs) or gases. The design integrates a ratiometric array of conducting polymer chemoresistors together with smart circuitry into a single chip fabricated through standard silicon CMOS process. The integrated circuit provides automatic compensation of variation in both supply voltage and ambient temperature, and permits control of sensor temperature. The ratiometric design principle also compensates for a large range in values of polymer resistance. It is believed that the circuit offers relevant smart capabilities at a very low cost and hence it can be used as the main component for the mass production of a self-calibrating programmable instrument.

**Keywords:** Smart sensor, gas sensor, ASIC.

**Subject category:** (6) Chemical sensors; (9) System architecture, intelligent sensor systems.

### INTRODUCTION

Further advances in the field of polymer resistors for the sensing of vapours require the development of

low-cost smart devices capable of addressing the problems in process variation and sensitivity to environmental conditions. The use of integrated circuits capable of self-calibration and compensation within a single chip unit can provide a good solution to these requirements. The adoption of a standard fabrication process allows the integration of smart interface circuitry and arrays of polymer-based sensors, leading to the development of novel intelligent sensor systems for gas or vapour monitoring.

This paper reports on the design of an Application Specific Integrated Circuit (ASIC) chip for gas monitoring that provides several smart features and incorporates polymer resistors and interface circuitry on a single unit. Cadence software and the Alcatel 0.7  $\mu\text{m}$  CMOS process were chosen for the design and low-cost fabrication of the chip through the Europractice scheme.

### DESCRIPTION OF THE DESIGN

Figure 1 shows the overall structure of the system. The main component is the ASIC chip, which performs two basic functions: (a) sensing the gas presence and concentration, and (b) controlling the operating temperature of the gas sensor. The top

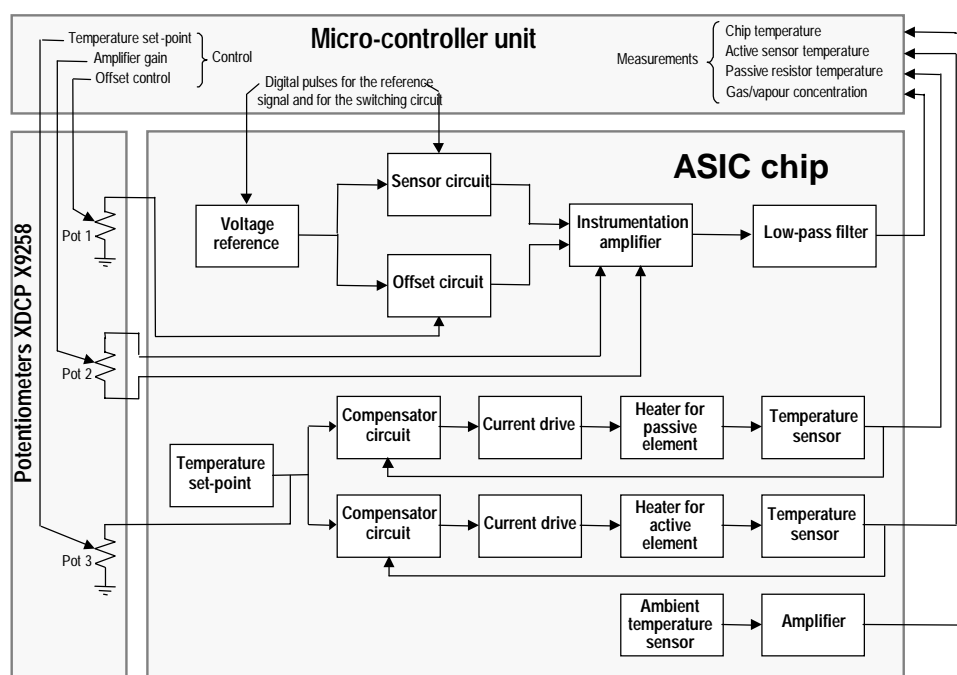


Fig. 1: Top representation of the sensor system.

section corresponds to the gas sensor circuit, whereas the bottom sections correspond to the temperature monitoring and control. A micro-controller unit is used for processing the inputs and outputs of the ASIC chip. Additionally, three digitally controlled potentiometers (available in the Xicor's X9258 integrated circuit) are used in order to accomplish some specific functions.

### Gas sensor section

The first section of the ASIC chip is the circuit that includes the polymeric sensors for the monitoring of gases or VOCs. These gas microsensors are constructed by depositing a polymer onto metal electrodes. One of the sensors is exposed to gases or VOCs whilst the second one is passivated with an inert material, such as Nafion, which offers common mode rejection of humidity signals, reduces the temperature sensitivity of the responses and produces an increase in response with an increase in temperature. When exposed to the presence of a gas, the electrical resistance of the active polymer element changes, giving an indication of the concentration of the gas. Only the metal electrodes are fabricated through the CMOS process, with the subsequent steps of polymer deposition and passive coating completing the fabrication of the sensing active and passive resistors.

The actual behaviour of these resistors cannot be precisely predicted. It is known from previous research [1-5] that the polymer resistance will vary in the presence of VOCs, but there are several factors which affect these variations, e.g. temperature, humidity, ageing and applied voltage. Even the actual resistance value of the devices is not easily controllable during the deposition process and significant differences appear between resistors fabricated through apparently identical steps.

Consequently, the structure of the gas sensor circuit was designed with the aim of overcome these problems. Firstly, a ratiometric array of polymer resistors is used in order to provide at least partial cancellation of the mentioned variations. Secondly, the polymeric sensors are excited through the use of circuitry that also reduces these effects. Finally, smart circuitry is added for the self-cancellation of some unwanted effects as well as for the calibration of the device.

As a result, the gas sensor circuit produces an amplified and filtered voltage signal proportional to the change in resistance experienced by one of the polymer resistors when exposed to the presence of organic vapours and gases while the other polymer resistor is used as a passive reference.

The blocks in the top section of the ASIC chip diagram in Figure 1 perform this sensing function. A reference pulsed voltage signal is sent to a pair of ratiometric circuits. The first of these is the sensor circuit, whose schematic view is shown in Figure 2. The polymer resistors  $R_p$  and  $R_{po}$  are connected to an

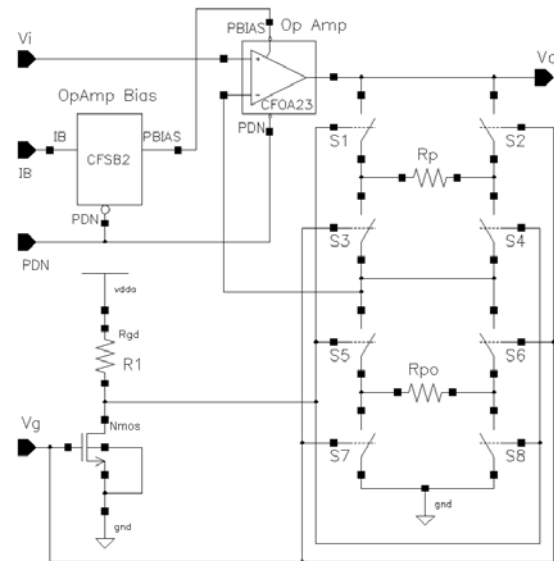


Fig. 2: Ratiometric sensor circuit.

operational amplifier in a non-inverting configuration, following basically the same ratiometric principle reported previously [6]. In this,  $R_p$  is the active sensor exposed to VOCs or gases, while  $R_{po}$  remains passive. The FET-based switches  $S1$  to  $S8$ , controlled through pulses applied to the input  $V_g$ , invert alternatively the voltage at the terminals of  $R_p$  and  $R_{po}$ , providing compensation against any polarisation effect and drifting associated with a constant DC voltage. The second ratiometric circuit is used to offset the output signal of the sensor ratiometric circuit under non-exposure circumstances, thus removing any variation in the polymer resistance ratio from unity. This offset signal is digitally adjusted through the external potentiometer *Pot 1* (Figure 1). The outputs of both ratiometric circuits are fed in to an instrumentation amplifier in which any difference between the input signals will cause an output approximately proportional to the concentration of a gas. The signal is adjusted with the aid of the potentiometer *Pot 2*, which sets the gain of the amplifier.

Finally, high-frequency components are removed from the amplified signal via a Bessel low-pass filter that was found to be the most suitable for the processing of the pulsed signals.

### Temperature control section

The second major task to be performed by the ASIC chip is the control of temperature, which is known to seriously affect the response of polymer sensors [1, 5]. The bottom sections on the ASIC chip diagram in Figure 1 correspond to this control and monitoring function. In order to maintain the proper operating conditions and to minimise variations, a controlled heater is placed underneath the electrodes of each polymer resistor. A temperature sensor closes the control loop by feeding back a signal to the compensator circuit, where it is compared with a

reference point that is set with the aid of a third external potentiometer. Here, a differential amplifier produces a compensating signal proportional to the difference of temperatures between the heater and the set-point. This compensating signal controls the current through the heaters thus in turn controlling the temperature of the polymer resistors. An additional temperature sensor, whose output is amplified, is used for monitoring the ambient temperature of the chip. The outputs of the temperature sensors are made externally available to the microcontroller unit.

### Simulations

The *Spectre* simulator was used to test every section of the design. Figure 3 shows the voltages obtained at the sensor circuit assuming equal resistances for  $R_p$  and  $R_{po}$  and disregarding any variations due to exposure to gases or vapours. The left plots correspond to the actual voltage waveforms at the terminals of the resistors, i.e. the differences in the corresponding positive voltages, plotted on the right, appearing at the *plus* and *minus* terminals of each resistor.

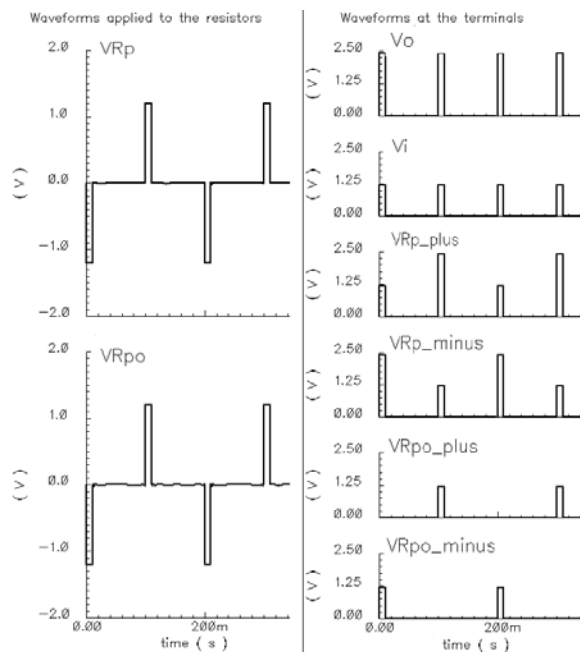


Fig. 3: Simulation of sensor voltages.

Figure 4 shows the voltage waveforms resulting at every stage of the gas sensor section. The reference signal  $V_{ref}$  produced by feeding pulses to a standard bandgap cell consists of pulses that are 10 ms width and have amplitude of 1.2 V. This signal produces the response that is registered at the output of the offset circuit, which is calibrated assuming the sensors unexposed to VOCs or gases. After calibration, exposure to VOCs and gases is simulated via the change in resistance  $\delta$  applied to the active sensor. The sensor output  $V_{sensor}$  differs from the offset

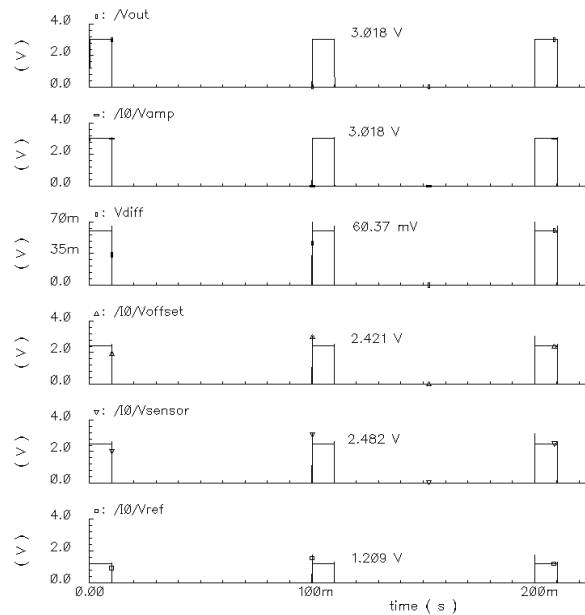


Fig. 4: Voltages simulation with  $\delta = 0.05$

signal  $V_{offset}$  and the difference in voltage is applied to the input of the instrumentation amplifier. This differential voltage  $V_{diff}$  was only 60.37 mV in the simulation when the change in resistance  $\delta$  was set to 0.05, i. e. 5% of  $R_{po}$ . With the gain of the amplifier adjusted to 50 the amplitude of the signal is raised to approximately 3 V in amplitude ( $V_{amp}$ ). Finally,  $V_{out}$  represents the filtered signal at the output of the circuit.

Further simulations also showed that the circuit is capable of dealing with the wide range in the actual resistance obtained for the different types of polymer sensors (e.g. three orders of magnitude).

### Layout view

The layout view for the chip, shown in Figure 5, was drawn with the *Virtuoso* layout editor according to the specifications and layout rules of the Alcatel Microelectronics 0.7  $\mu\text{m}$  CMOS technology. The dimensions of the ASIC chip are 3300  $\mu\text{m}$  x 3750  $\mu\text{m}$  and it contains all the components that are represented in the block diagram of Figure 1. The cells are placed along several rows in the layout, thus obtaining a symmetrical distribution with the two gas sensors located at opposite corners of the chip, to aid post-CMOS polymer deposition.

The cells *BIAS1* and *BIAS2* provide the bias current for the operational amplifiers according to the bias strategy required by the Alcatel analogue cells and they also supply the current for the driving of the temperature sensors.

Several test points are available at the bonding pads for testing purposes, allowing the realisation of measurements at different sections of the circuit.

A number of tests were performed with the *Diva* and *Dracula* software packages in order to check the

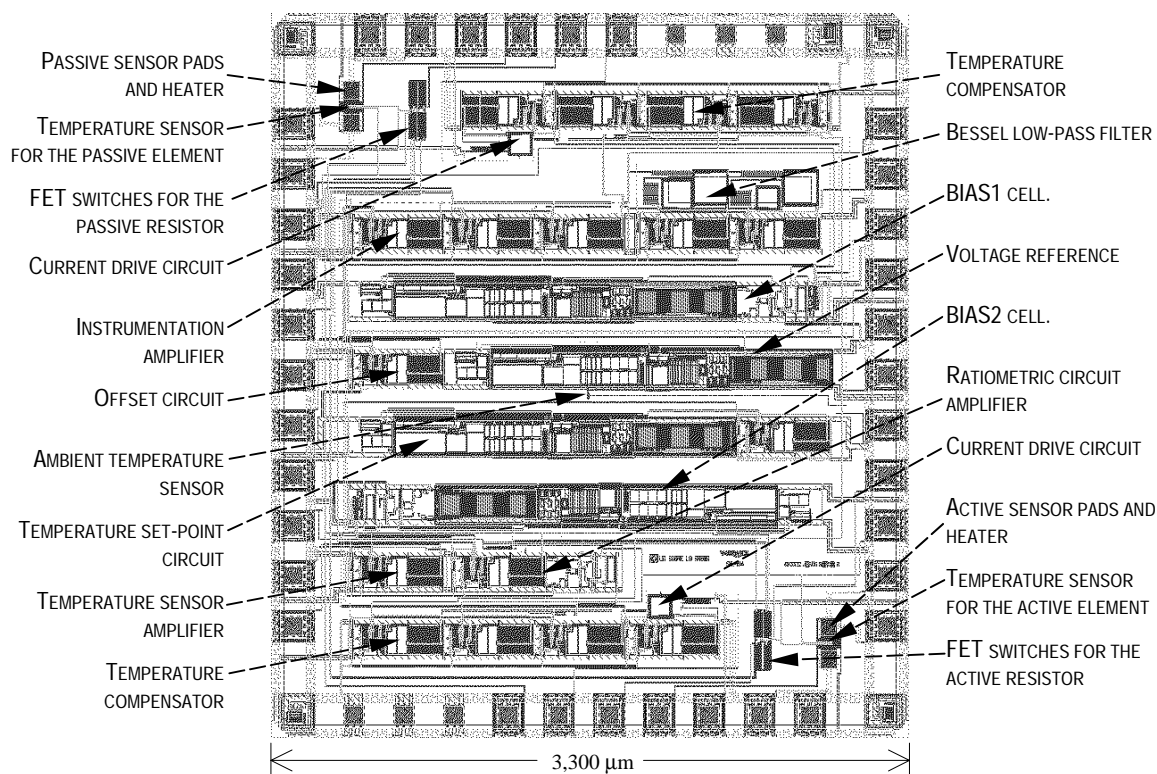


Fig. 5: Layout view of the ASIC chip.

consistence of the design with the layout rules, with the electrical rules and with the substrate requirements under the particular CMOS process selected for the fabrication of the ASIC chip. Nevertheless, in order to obtain the openings for the deposition of the polymers onto the sensor electrodes, it was necessary to violate some design rules and special modifications were introduced to the standard process.

## CONCLUSIONS

Our ASIC design offers the implementation of a gas microsensor with on-chip compensation of variation in ambient temperature. Features of self-calibration against voltage drift and other parameter correction are realisable through a microcontroller unit. Our design should permit the development of accurate low-cost palm-top gas monitors.

## ACKNOWLEDGMENTS

The authors express their gratitude to Steve Matheus and Greta Milczanowska, from IMEC, Belgium, for their valuable help and advice for the testing and verification of the design. The support provided through Europractice by Dr. Stephen Bell, from Rutherford Appleton Laboratory, is also appreciated.

## REFERENCES

- [1] Cole, M., Gardner, J. W., Covington, J. A., Fife, D., Kwok, C. Y., Brignell, J. E. and Bartlett, P. N.: "Active bridge polymeric resistive device for vapour sensing", *Euroensors XIV*, W2P41 (Bio)chemical sensors III (2000), 895-898.
- [2] Gardner, J. W., Vidic, M., Ingleby, P., Pike, A. C., Brignell, J. E., Scivier, P. Bartlett, P. N., Duke, A. J., Elliot, J. M.: "Response of a poly(pyrrole) resistive micro-bridge to ethanol vapour", *Sensors and Actuators*, B 48 (1998), 289-295.
- [3] P. Bruschi, A. Nannini, B. Neri: "Vapour and gas sensing by noise measurements on polymeric balanced bridge microstructures", *Sensors and actuators*, B 24-25 (1995), 429-432.
- [4] Hattfield, J. V., Neaves, P., Hicks, P. J., Persaud, K. and Travers, P.: "Towards an integrated electronic nose using conducting polymer sensors", *Sensors and Actuators*, B 18-19 (1994), 221-228.
- [5] Cole, M., Gardner, J. W., Lim, A. W. Y., Scivier, P. K. and Brignell, J. E.: "Polymeric resistive bridge gas sensor array driven by a standard cell CMOS current drive chip", *Sensors and Actuators*, B 58 (1999), 518-525.
- [6] M. Cole, J.W. Gardner, and P.N. Barlett: "Low-drift odour and vapour ratiometric resistive elements for analogue CMOS smart sensors", *ISOEN 2001*, Vol. 2001-15 (2001), 117-120.

# Design and simulation of a smart ratiometric ASIC chip for VOC monitoring

Jesús García-Guzmán<sup>a</sup>, Nicola Ulivieri<sup>b</sup>, Marina Cole<sup>a,\*</sup>, Julian W. Gardner<sup>a</sup>

<sup>a</sup> School of Engineering, University of Warwick, Coventry CV4 7AL, UK

<sup>b</sup> Department of Information Engineering, Università di Siena, 53100 Siena, Italy

## Abstract

This paper reports on the design and simulation of a novel ratiometric application specific integrated circuit (ASIC) chip for the monitoring of volatile organic compounds (VOCs) or gases. The design integrates two polymeric chemoresistors in a ratiometric configuration, together with smart circuitry, into a single chip fabricated through a standard silicon CMOS process. The circuit provides automatic compensation of signal from variations in both supply voltage and ambient temperature. On-chip control of the operating temperature of the sensors is also an option. The response of the ratiometric set of polymeric chemoresistors to different concentrations of gases at different temperatures and humidities was simulated with the aid of a novel parametric Cadence model. Simulations confirm that the ratiometric configuration is less sensitive to temperature variations and that it also has a better performance in terms of humidity dependence when compared to an individual chemoresistor. These features, together with its ability to compensate for a large range in values of polymer resistance, make us believe that the circuit offers relevant smart capabilities at a very low-cost and so it can be used as the main component for the mass production of a self-calibrating, programmable, palm-top instrument.

© 2003 Elsevier B.V. All rights reserved.

**Keywords:** Smart sensor; ASIC; Resistive gas sensor; Ratiometric sensor array; Behavioural models

## 1. Introduction

Further advances, in the field of polymer resistors for the sensing of vapours, require the development of low-cost smart devices capable of addressing the problems of both process variation and changes in environmental conditions. The use of integrated circuits capable of self-calibration and compensation within a single chip unit can provide a good solution. The adoption of a standard fabrication process allows the integration of smart interface circuitry and arrays of polymer-based sensors, leading to the development of novel intelligent sensor systems for gas or vapour monitoring.

Some of the problems associated with conducting polymers, such as temperature dependence, have already been addressed through the design of four-element and five-element microbridge devices [1–3] and a significant reduction in the values of temperature and humidity coefficients was achieved.

In this paper we describe an application specific integrated circuit (ASIC) chip for gas monitoring that provides several smart features and incorporates a pair of polymer resistors

in a ratiometric configuration [4]. In order to perform detailed analyses of the behaviour of this ratiometric chip, a parametric model was developed to simulate the polymer resistance on exposure to a given gas at different temperatures and humidities [5]. This model is particularly useful because it permits the response of polymeric chemoresistors to be predicted before CMOS processing. Cadence software was used for the design and simulation of the ASIC chip as well as for the implementation of the model. An Alcatel 0.7  $\mu\text{m}$  CMOS process was chosen for the design and fabrication of the chip through the low-cost Europractice scheme.

## 2. Description of the design

Fig. 1 shows the overall structure of the new smart gas sensor system. The main component is the ASIC chip, which performs two basic functions: (a) sensing the gas presence and concentration and (b) controlling the operating temperature of the gas sensor. Within the ASIC chip, the top section corresponds to the gas sensor circuit, whereas the bottom sections correspond to temperature control and monitoring. A microcontroller unit is used for processing the inputs and outputs of the ASIC chip. Additionally, three digitally controlled potentiometers (available in the Xicor's X9241A

\* Corresponding author. Fax: +44-1203-418922.  
E-mail address: [mvc@eng.warwick.ac.uk](mailto:mvc@eng.warwick.ac.uk) (M. Cole).  
URL: <http://www.eng.warwick.ac.uk/srl>.

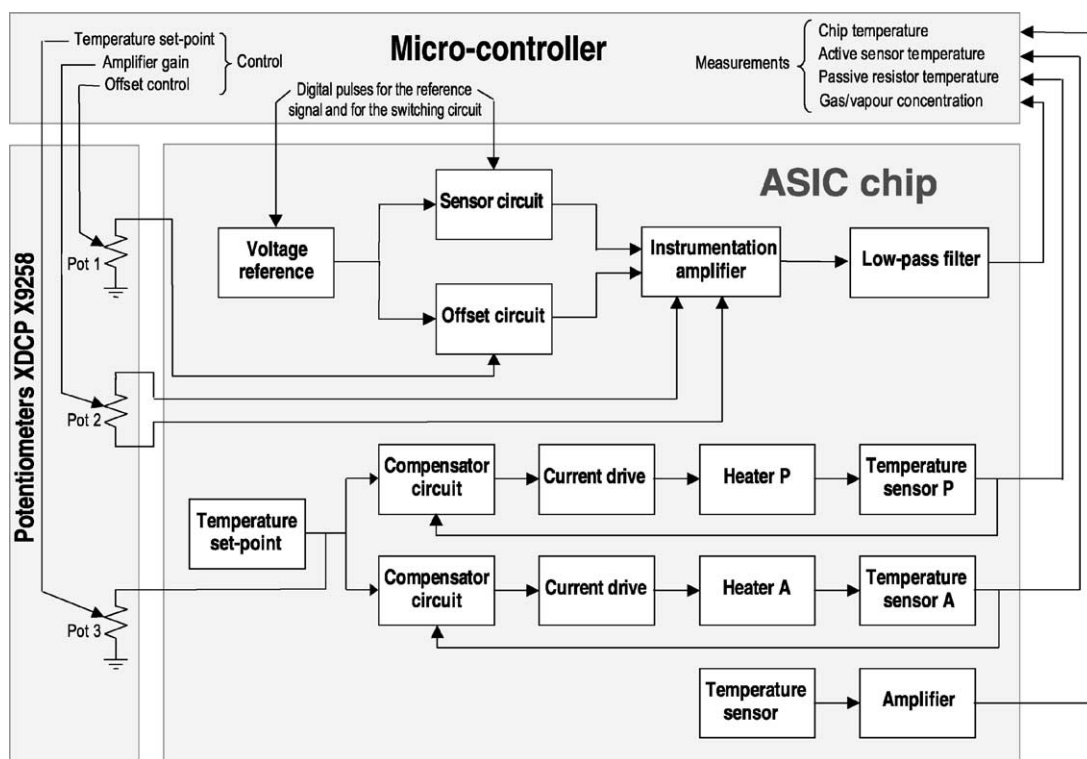


Fig. 1. Top representation of the ratiometric sensor system.

integrated circuit) are used in order to accomplish some specific trimming functions.

### 2.1. Gas sensor section

The first section of the ASIC chip is the circuit that includes two polymeric sensing resistors in a ratiometric configuration for the monitoring of gases. The basic operating principle of ratiometric configuration is shown in Fig. 2(a). In this, two sensors are connected in a non-inverting operational amplifier configuration. One of the sensors  $R_p$ , responds to gas whilst the second one  $R_{po}$ , is either passivated with an inert material, or placed in a separate flow path. When exposed to the presence of gases, the electrical resistance of the active polymer element changes, giving an indication of the concentration of the gas, whilst any common mode effects, such as aging, temperature dependence and humidity dependence, will cancel each other through the simple ratio  $R_p/R_{po}$ .

The gas microsensors are constructed by spray-coating a polymer across the aluminium electrodes following a plating process. The electrodes are fabricated in a CMOS process, with the subsequent steps of polymer deposition and passive coating completing the fabrication of the active and passive chemoresistors. The actual behaviour of these resistors cannot be precisely predicted. It is known from previous research [1–3,6,7] that the polymer resistance will vary in the presence of gases, but there are several factors which affect these variations, e.g. temperature, humidity,

ageing, and applied voltage. Even the actual resistance value of the devices is not easily controllable during the deposition process and significant differences appear between resistors fabricated through apparently identical batches.

Consequently, the structure of the gas sensor circuit was designed to overcome these problems. Firstly, a ratiometric pair of polymer resistors is used in order to provide at least partial cancellation of the above-mentioned variations. Secondly, the polymeric sensors are excited through the use of circuitry that also reduces these effects. Finally, smart circuitry is added for the self-cancellation of offset errors for the calibration of the device. As a result, the gas sensor circuit produces an amplified and filtered voltage signal proportional to the change in resistance experienced by one of the polymer resistors on gas exposure while the other resistor is used as a passive reference.

The blocks in the top section of the ASIC chip diagram in Fig. 1 perform this sensing function. A reference pulsed voltage signal is sent to a pair of ratiometric circuits. The first of these is the sensor circuit, whose schematic view is shown in Fig. 2(b). The polymer resistors  $R_p$  and  $R_{po}$  are connected, as described before, to an operational amplifier in a non-inverting configuration, following basically the same ratiometric principle reported previously [4]. In this,  $R_p$  is the active sensor exposed to the gas, while  $R_{po}$  remains passive. Apart from the elimination of temperature, humidity, and aging effects on the baseline resistance, the sensor circuit also incorporates polarity pulse switching in order to cancel long-term drift problems caused by a

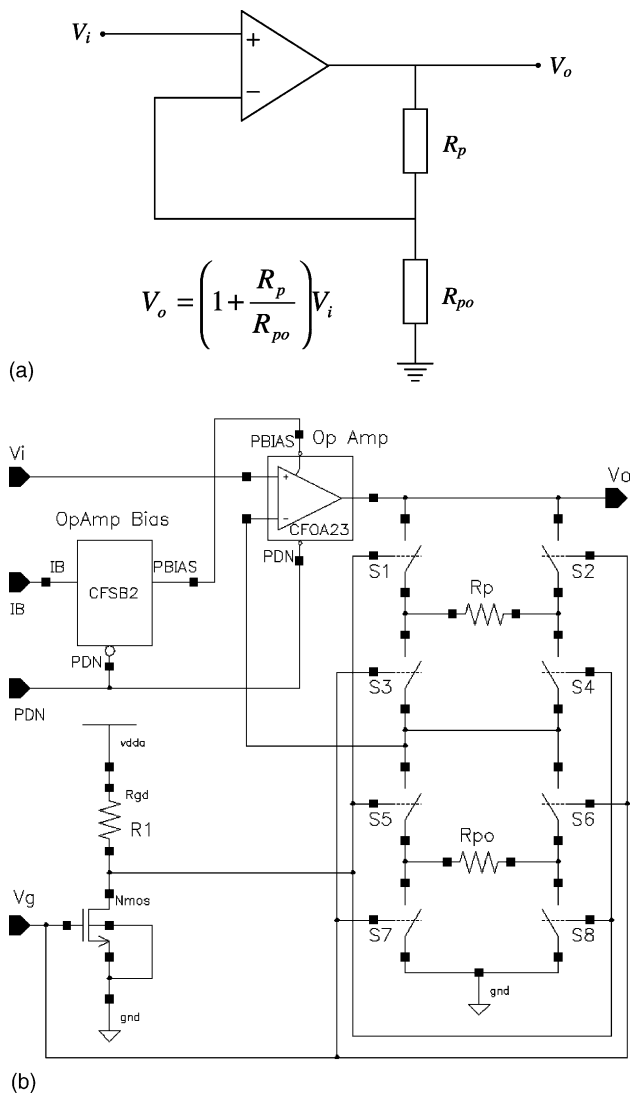


Fig. 2. Ratiometric sensor circuit: (a) basic principle; (b) Cadence implementation including analogue switching.

polarisation effect. The FET-based switches S1 to S8, controlled through pulses applied to the input  $V_g$ , invert alternately the voltage at the terminals of  $R_p$  and  $R_{po}$ , providing compensation against any polarisation effect or drifting associated with a constant dc voltage. The benefits obtained with the ratiometric configuration of the sensors were confirmed via simulations as described below.

The second ratiometric circuit is used to offset the output signal of the sensor ratiometric circuit under non-exposure circumstances, thus removing any variation in the polymer resistance ratio from unity. This offset signal is digitally adjusted through the external potentiometer *Pot 1* (Fig. 1). The outputs of both ratiometric circuits are fed into an instrumentation amplifier in which any difference between the input signals will cause an output approximately proportional to the concentration of the monitored gas. The signal is then adjusted with the aid of the potentiometer *Pot 2*, which sets the gain of the amplifier. Finally, a Bessel low-pass filter

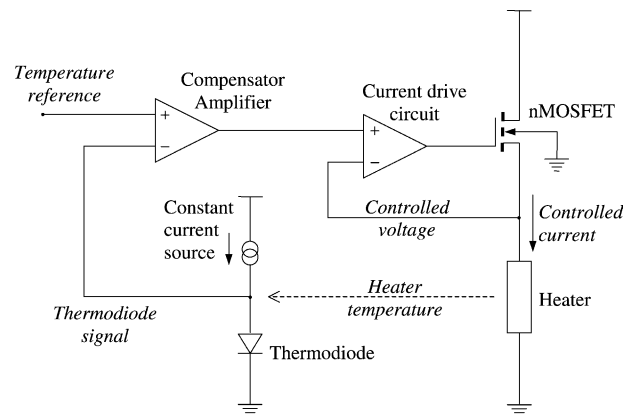


Fig. 3. Simplified schematic diagram of the temperature control circuit.

was found to be the most suitable to remove high frequency switching errors from the amplified signal.

## 2.2. Temperature control section

The second major task to be performed by the ASIC chip is the control of temperature, which is known to seriously affect the response of polymer sensors [1–3,6,7]. The bottom sections on the ASIC chip diagram in Fig. 1 correspond to this control and monitoring function. In order to maintain the proper operating conditions and to minimise variations, a controlled heater is placed underneath the electrodes of each polymer resistor. A temperature sensor closes the control loop by feeding back a signal to the compensator circuit, where it is compared with a reference point that is set with the aid of a third external potentiometer. Here, a differential amplifier produces a compensating signal proportional to the difference of temperatures between the heater and the set point. This compensating signal controls the current through the heaters thus in turn controlling the temperature of the polymer resistors. A simplified schematic diagram of the temperature control section is shown in Fig. 3. An additional temperature sensor, whose output is amplified, is used to monitor the ambient temperature of the chip. The outputs of the temperature sensors are made available to the microcontroller unit.

## 2.3. Layout view

The layout view for the chip, shown complete in Fig. 4(a), was drawn with the *Virtuoso* layout editor according to the specifications and layout rules of the Alcatel Microelectronics 0.7  $\mu\text{m}$  CMOS technology. The dimensions of the ASIC chip are 3300  $\mu\text{m}$   $\times$  3750  $\mu\text{m}$  and it contains all the components that are represented in the block diagram of Fig. 1. The cells are placed along several rows in the layout, thus obtaining a symmetrical distribution with the two gas sensors located at opposite corners of the chip, to aid post-CMOS polymer deposition.

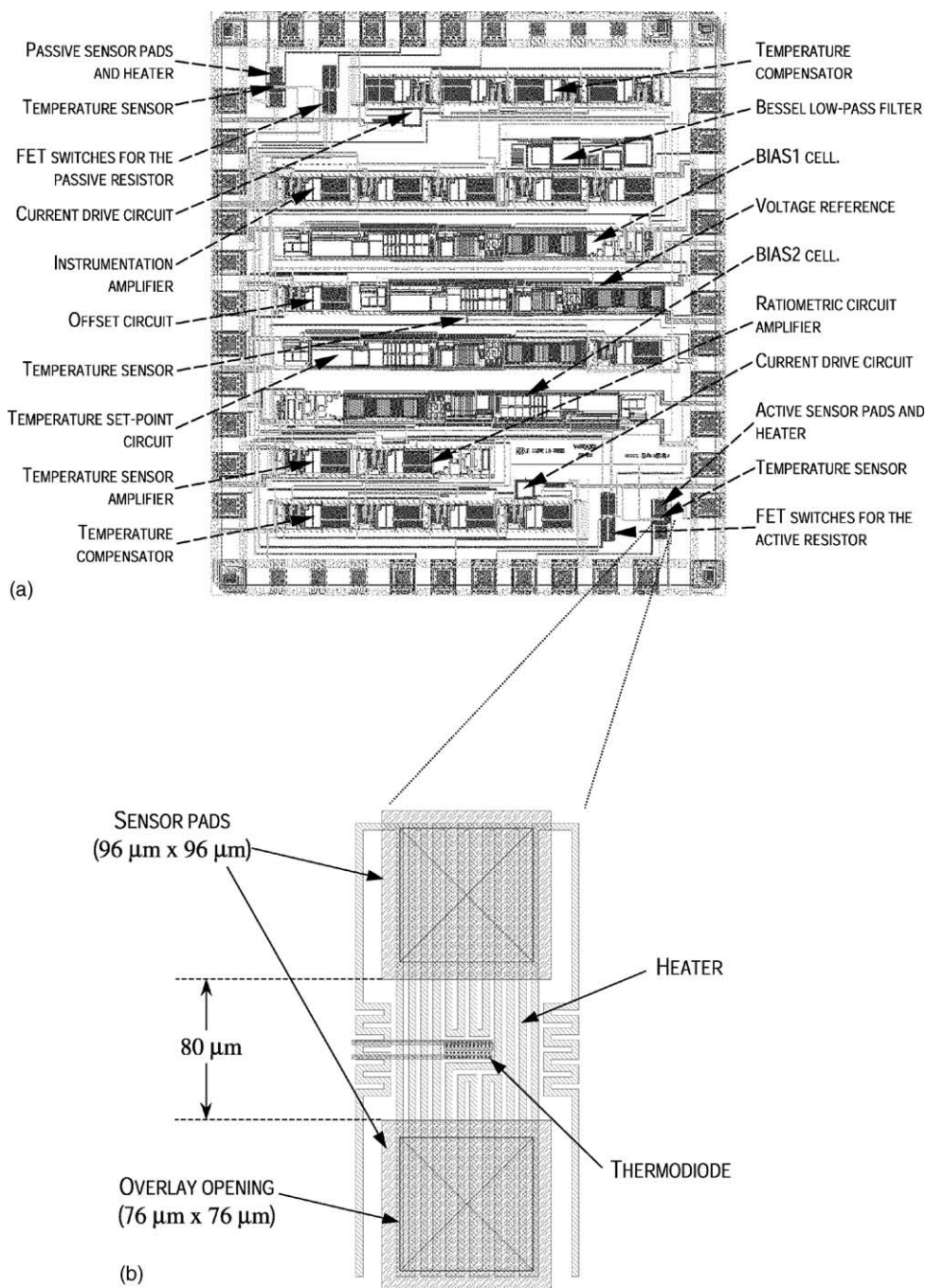


Fig. 4. Layout view of (a) the complete smart ratiometric ASIC chip and (b) the sensor area including heater and thermodiode.

The sensor area of the layout is shown in Fig. 4(b). The electrodes, in metal2 layer, are 96 μm × 96 μm in size, with 80 μm interelectrode gap, in order to achieve approximately 10 kΩ resistance when using carbon-black polymer composite films [8]. The heaters are constructed underneath the electrodes in the metal1 layer, which has a nominal sheet resistance of 50 mΩ/sq. Each heater has a nominal design resistance of 50 Ω. The thermodiodes are placed in the centre of the heater regions, just between the electrodes.

The cells *Bias1* and *Bias2* provide the bias current for the operational amplifiers according to the bias strategy required by the Alcatel analogue cells and they also supply the current for the driving of the temperature sensors. Several test points are available at the bonding pads for testing purposes, allowing the realisation of measurements at different sections of the circuit.

A number of tests were performed with the *Diva* and *Dracula* software packages in order to check the consistency of the design with the layout rules, with the electrical



rules and with the substrate requirements under the particular CMOS process selected for the fabrication of the ASIC chip. In order to obtain the openings down to metal2 layer for the deposition of the polymers onto the sensor electrodes, it was necessary to include some special modifications while still following the standard CMOS process.

### 3. Simulations

The *Spectre* simulator was used to test each part of the design. Fig. 5 shows the voltages obtained at the ratiometric sensor circuit when assuming initially equal resistances for  $R_p$  and  $R_{po}$  and hence disregarding any variations due to exposure to reactive gases. The left plots correspond to the actual voltage waveforms at the terminals of the resistors, i.e. the differences in the corresponding positive voltages, plotted on the right, appearing at the *plus* and *minus* terminals of each resistor. The simulation results confirm the advantage of using the switching circuitry in order to invert the sign of the voltages at the chemoresistors terminals and thus providing compensation against polarisation effects.

Fig. 6 shows the voltage waveforms appearing at every stage of the gas sensor section. The reference signal

$V_{ref}$  (Fig. 6(a)) produced by feeding pulses to a standard bandgap cell consists of pulses that are 10 ms in width and have an amplitude of 1.2 V. This signal produces the response that is registered at the output of the offset circuit (Fig. 6(c)), which is calibrated to the baseline signal, i.e. the sensors unexposed to gases. After calibration, exposure to gases is simulated via the change in resistance  $\delta$  applied to the active sensor. The sensor output  $V_{sensor}$  (Fig. 6(b)) differs from the offset signal  $V_{offset}$  and the difference in voltage is applied to the input of the instrumentation amplifier. This differential voltage  $V_{diff}$  (Fig. 6(d)) was only 60.37 mV in the simulation when the change in resistance  $\delta$  was set to 0.05, i.e. 5% of  $R_{po}$ . When the gain of the amplifier is set to 50, the amplitude of the signal is raised to approximately 3 V in amplitude ( $V_{amp}$ , Fig. 6(e)). Finally,  $V_{out}$  represents the filtered signal at the output of the circuit (Fig. 6(f)).

The performance of the temperature control section was also simulated. Fig. 7(a) shows the voltages obtained at 27 °C, whereas Fig. 7(b) shows the voltage waveforms resulting when temperature varies between 20 °C and a nominal setpoint at 35 °C.

Further simulations also showed that the circuit is capable of dealing with the wide range in the actual resistance

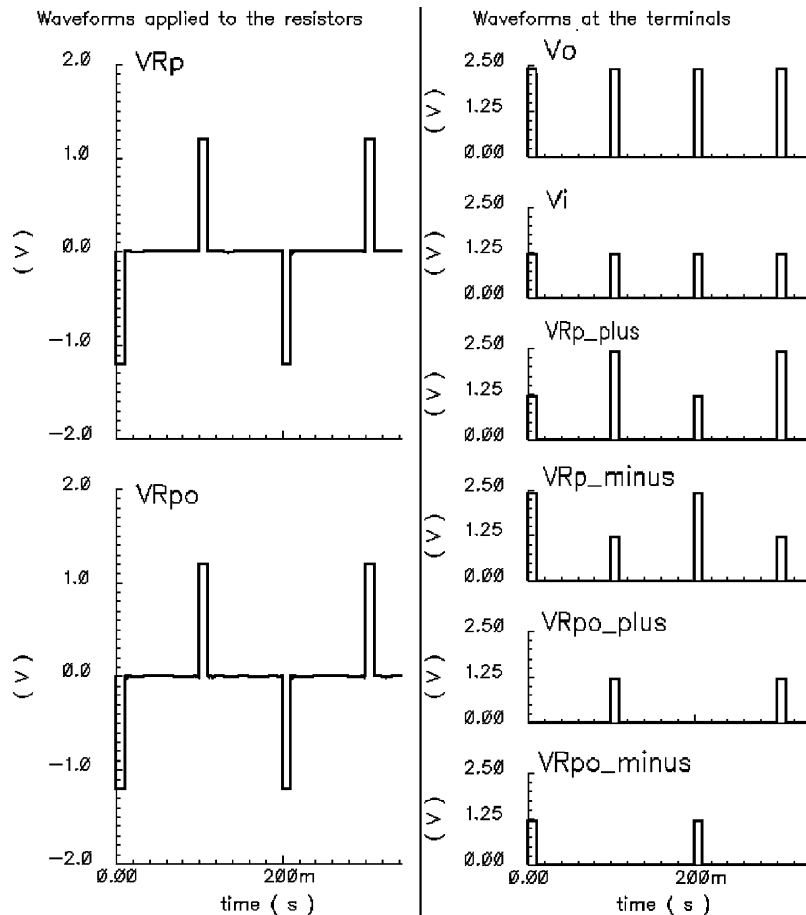


Fig. 5. Simulation of sensor voltages in the circuit.

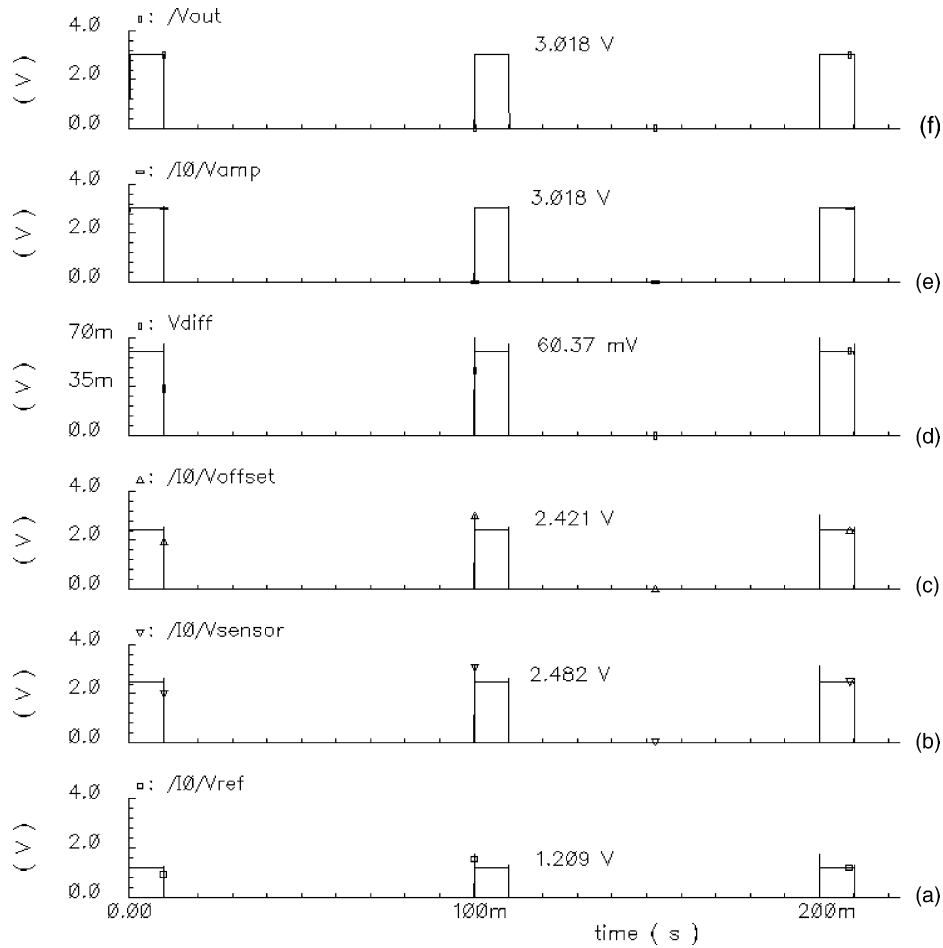


Fig. 6. Voltage simulation with a change in resistance equal to 5% of  $R_{po}$ : (a) reference voltage, (b) voltage at the output of the sensor circuit, (c) offset voltage, (d) differential input at the instrumentation amplifier, (e) amplified voltage, and (f) output of the low-pass filter.

obtained for the different types of polymer sensors (e.g. three orders of magnitude).

### 3.1. Application of the polymeric chemoresistor model

In order to compare performances of ratiometric configuration to discrete chemoresistors, the polymeric chemoresistor model was used. This model, implemented in Cadence and described thoroughly elsewhere [5], is able to simulate accurately the polymeric chemoresistor response to gas and humidity under different operating conditions. The model simulates the static and dynamic sensor response to gas or gas mixture exposure, and includes flicker and Johnson noise. It also takes account of the sensor sample delivery system. Fig. 8(a) shows the conceptual structure of the proposed model having three inputs ( $C_G$ ,  $C_H$ ,  $T$ ) for gas and humidity concentration and sensor temperature, and two pins ( $R_+$ ,  $R_-$ ) for sensor connection with the rest of the circuitry. The inputs are connected to voltage sources whose voltage level emulates both the gas and humidity concentrations ( $1\text{ V} \leftrightarrow 1\text{ ppm}$ ) and the sensor temperature ( $1\text{ V} \leftrightarrow 1\text{ }^\circ\text{C}$ ). The model has been implemented as a standard cell (SC) in Cadence software (Fig. 8(b)). The polymeric sen-

sor is represented as a complex impedance  $Z_{SC}$ , with two noise sources in series (flicker and Johnson noise [8]).  $Z_{SC}$  is the impedance resulting from the parallel combination of the sensor capacitance  $C_{SC}$  and the sensor resistance  $R_{SC}$ . Parasitic resistances and capacitances are neglected because they are insignificant when compared with  $R_{SC}$  and  $C_{SC}$  [5].

The sensor static response is a function of the gas concentration  $C_G$ , the sensor temperature  $T$  and the water vapour concentration  $C_H$ , while the dynamic response depends both on the gas transfer method and/or on the gas reaction kinetics. The static resistance of the SC,  $R_{SC}$ , is evaluated in the block ‘Sensor Static Response’ (see Fig. 8(a)) which implements the developed model, assuming that carbon-black composite polymer films are used as gas sensitive materials. The model developed for these materials in Ref. [5] has been expanded in order to include the temperature variations of the baseline resistance and the static resistance is given by

$$R_{SC} = R_{SC_0} \exp\left(\frac{B}{T}\right) \times \left[ 1 + k_G C_G^{1/G} \exp\left(\frac{K_{SG}}{T}\right) + k_H C_H^{1/H} \exp\left(\frac{K_{SH}}{T}\right) \right] \quad (1)$$

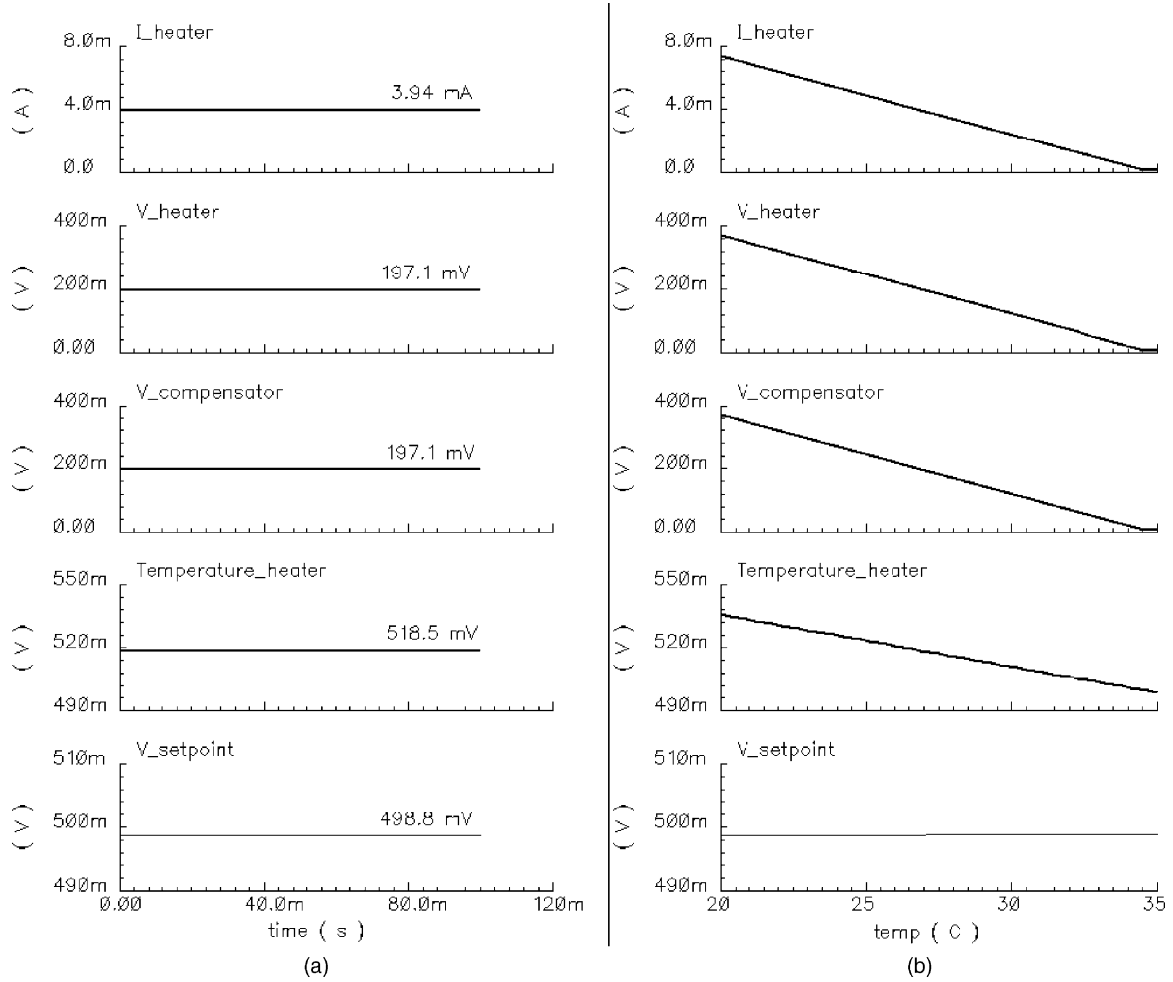


Fig. 7. Waveforms for the temperature control system: (a) results at 27 °C, (b) response between 20 and 35 °C.

where  $R_{SC0}$  is the baseline sensor resistance (measured in presence of a reference gas, generally synthetic air or nitrogen),  $k_G$  and  $k_H$  are sensitivity coefficients,  $C_G$  and  $C_H$  are the gas/vapour concentrations expressed in ppm,  $\gamma_G$  and  $\gamma_H$  are the power law exponents,  $B$ ,  $K_{sG}$  and  $K_{sH}$  are the temperature coefficients, and  $T$  the temperature in Kelvin. The subscripts G and H refer to the gas and the water vapour, respectively. The sensitivity coefficients can be positive or negative depending on the nature of the gas and the polymer, producing an increase or decrease of the sensor resistance after the gas injection. The transient behaviour of the polymeric gas sensor is simulated by a second-order multi-exponential model implemented through a second-order low-pass filter ('Sensor Dynamic Response' in Fig. 8(a)). Since the on-dynamics are generally faster than the off-dynamics, two filters with different poles have been used. The sample delivery system (SDS) is also modelled ('Sample Delivery System' in Fig. 8(a)) in order to include the real gas transfer [5].

The general parametric model described above and the values given in Table 1 were used to simulate the response of the polymeric chemoresistors in the ratiometric configura-

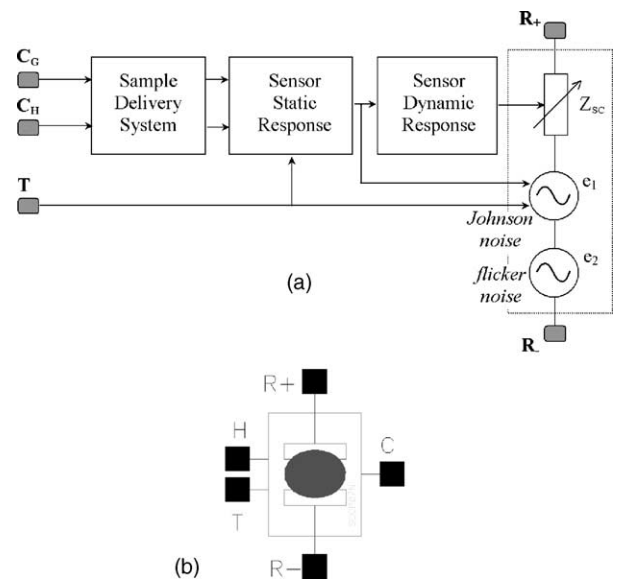


Fig. 8. (a) Model framework of the SC for a polymeric gas sensor. (b) symbol for the cell.

Table 1  
Model parameters used in the simulations

| Parameter used in the Cadence model | Value(s) <sup>a</sup> | Symbols used for Cadence parameters in the Eq. (1) | Description   |
|-------------------------------------|-----------------------|--|---|
| $C_{gas}$                           | 1 k                   | $C_G$  | Gas concentration (ppm)                                     |
| Humid                               | 0–30 k                | $C_H$  | Humidity concentration (ppm)                                |
| Temper                              | 40–100                | $T$  | Sensor temperature (°C)                                     |
| $K_{sH}$                            | 31.32                 | $K_{sH}$   | Temperature coefficient for the humidity (°C)               |
| $k_H$                               | $-94n$                | $k_H$  | Sensitivity coefficient for the humidity (1/ppm)            |
| $\gamma_{Hh}$                       | 1                     | $\gamma_H$   | Power low exponent for the humidity                         |
| Slope                               | 1                     | –  | Slope of the flicker noise ( $1/f^{slope}$ )                |
| Vol                                 | $30 \times 10^{-15}$  | –  | Polymer volume (m <sup>3</sup> )                            |
| X                                   | $300 \times 10^{-27}$ | –  | Polymer coefficient to evaluate flicker noise               |
| SDS.Ct                              | -1                    | –  | SDS control (positive → active, negative → inactive)        |
| w1SDS_off                           | –                     | –  | Pole for off-dynamics SDS                                   |
| w1SDS_on                            | –                     | –  | Pole for on-dynamics SDS                                    |
| w2_on                               | 10 k                  | –  | Second pole on-dynamics chemical transient                  |
| w2_off                              | 4 k                   | –  | Second pole off-dynamics chemical transient                 |
| w1_on                               | 10 m                  | –  | First pole on-dynamics chemical transient                   |
| w1_off                              | 4 m                   | –  | First pole off-dynamics chemical transient                  |
| $R_0$                               | 9512                  | $R_{SC0}$  | Sensor baseline resistance (Ω)                              |
| $B$                                 | 2                     | $B$  | Temperature coefficient for sensor baseline resistance (°C) |
| $K_s$                               | 88.42                 | $K_{sG}$   | Temperature coefficient for the gas (°C)                    |
| $k_1$                               | $3.2\mu$              | $k_G$  | Sensitivity coefficient for the gas (1/ppm)                 |
| gamma                               | 1.07                  | $\gamma_G$   | Power low exponent for the gas                              |

<sup>a</sup> The values of the parameters used for simulations are obtained from measurements on carbon-black polymer composite film performed at the Sensors Research Laboratory of the University of Warwick with exception of the noise measurements which were performed by the University of Torvegata (Rome).

ration. Fig. 9 shows how the cells  $SC_a$  and  $SC_p$  were used to represent the active and passive sensors.

Two passivation methods were tested in the simulations. In the first case, represented in Fig. 10(a), one of the polymeric sensors is coated with an inert material to avoid the

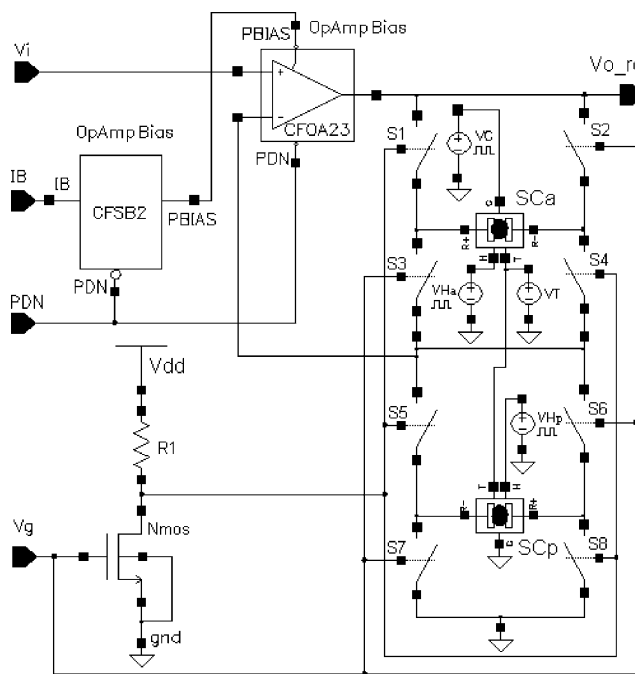


Fig. 9. Ratiometric sensor circuit. The sensor cell  $SC_a$  emulates the behaviour of the active polymeric sensor, while the cell  $SC_p$  emulates the passive sensor.

gas effect. In this way, the passive sensor is sensitive to temperature variation but it does not respond to the gas or ambient humidity. The water vapour concentration is fixed to the concentration present at the moment of the coat deposition (e.g. RH = 40% at 20 °C corresponding to 9214 ppm). The gas flow is split in two paths to expose both sensors. The passivation was simulated by connecting the input ‘C’ of the  $SC_p$  cell to gnd (gas concentration = 0 ppm) and the input ‘H’ to a voltage source (e.g.  $V_{Hp} = 9214 \text{ V} \rightarrow 9214 \text{ ppm}$ ).

The second method requires two separate inlets to carry the gas under test and a reference gas to the sensors  $SC_a$  and  $SC_p$  (Fig. 10(b)). In this case the sensor  $SC_p$  is not coated

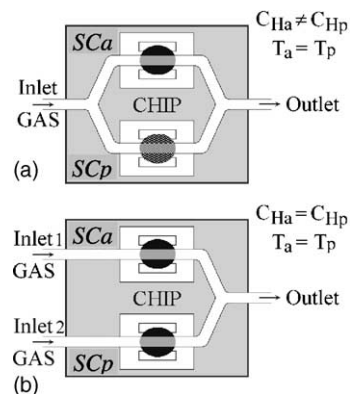


Fig. 10. The use of the reference sensor  $SC_p$  in the ASIC chip: (a) the polymer sensor  $SC_p$  is coated with an inert material to avoid the reaction with a gas which flow over sensors  $SC_a$  and  $SC_p$ ; (b) two separate flow paths are used to expose the two sensors to different gases but to the same water vapour concentration; this enables for humidity rejection.

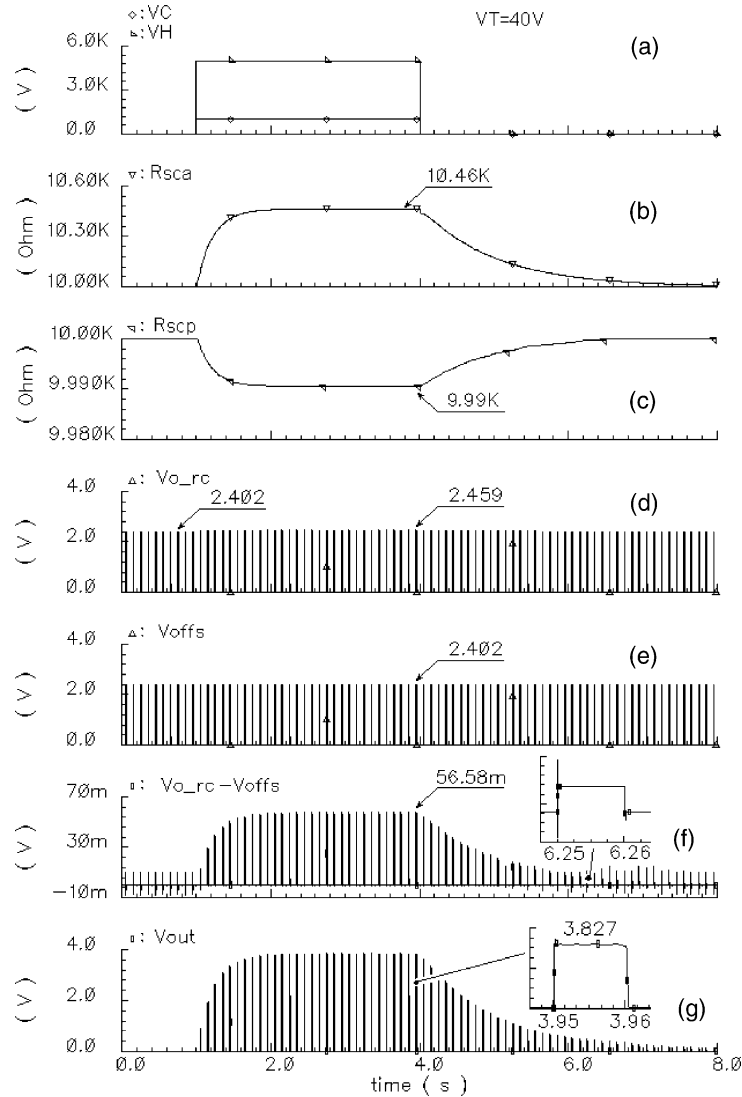


Fig. 11. Transient analysis of the ratiometric circuit for active and passive baseline resistances of  $10\text{ k}\Omega$  at  $40^\circ\text{C}$ , gas concentration =  $1000\text{ ppm}$ , water vapour mixed to the gas =  $5000\text{ ppm}$ : (a) voltage pulses applied to the sensor cell  $SC_a$  simulating the humidity and gas concentration ( $1\text{ V} \leftrightarrow 1\text{ ppm}$ ); (b) resistance of the active sensor; (c) resistance of the passive sensor; (d) output voltage of the ratiometric circuit; (e) output voltage of the offset circuit; (f) differential input of the instrumentation amplifier; (g) output of the gas sensor section.

but it acts as a reference device because the reference gas is injected in the second inlet ('Inlet 2 GAS'). This solution allows cancelling the humidity effect, when the reference gas has the same water vapour concentration as the gas under test injected in the 'Inlet 1 GAS'.

Fig. 11 shows the results of simulations performed using polymer resistors of  $10\text{ k}\Omega$  at  $40^\circ\text{C}$  under the second passivation method. Gas and humidity concentrations of  $1000$  and  $5000\text{ ppm}$ , respectively were applied to the sensors terminals. The changes in resistances of active and passive sensors are shown in Fig. 11(b) and (c). The output signals from ratiometric and offset sections are also shown. The differential input to the amplifier is depicted in Fig. 11(f) and the output signal of the gas sensor section is shown in Fig. 11(g).

The benefits of the ratiometric circuit structure are compared to the potential divider configuration (Fig. 12) already

discussed elsewhere [5]. In particular, the temperature and humidity dependencies of the circuits are explored.

Figs. 13 and 14 show the percentage variation of the circuit output voltage with varying sensor temperature and humidity. The two setups depicted in Fig. 10 are taken into account. The ratiometric configuration shows less sensitivity to temperature variation compared to the discrete circuit. In particular, the baseline output value is not sensitive to the temperature variation when the configuration with reference gas shown in Fig. 10(b) is adopted. These results can be observed in the curves for the ratiometric circuit with  $C_{Ha} = C_{Hp}$ , depicted in Fig. 13(a) and (b). This is expected, since the sensors are fabricated under the same conditions and they should respond to temperature changes with the same exponential law. The plots in Fig. 13(c) and (d) show that the ratiometric circuit has superior performance when

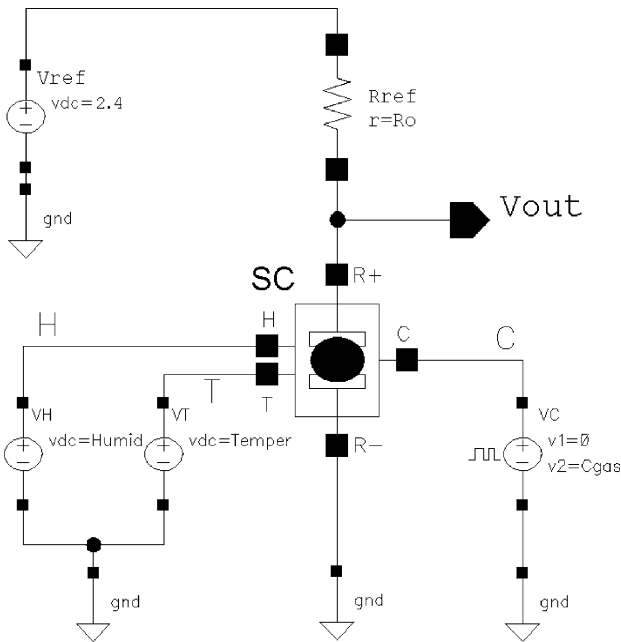


Fig. 12. Schematic view of the single chemosensor circuit.

compared to a single chemosensor circuit exposed to gas at varying temperature.

The ratiometric circuit shows better performance also in terms of linear humidity dependence (Fig. 14). The water vapour effect is cancelled by the reference sensor  $SC_p$  when this one is not coated and the configuration depicted in Fig. 10(b) is adopted ( $C_{Ha} = C_{Hp}$ ). If the reference sensor  $SC_p$  is coated with an inert material, as in Fig. 10(a), the humidity effect cannot be annulled (ratiometric curves for  $C_{Ha} \neq C_{Hp}$  in Fig. 14) but the ratiometric circuit is still less sensitive with respect to the potential divider configuration.

Noise simulation was also performed based on the model developed in Ref. [5]. Fig. 15 shows the simulated noise analysis of the ratiometric circuit. The operational amplifier CFOA23 (Fig. 9) gives the main contribution to the total output noise. The polymeric sensor noise is also shown and it is assumed to be dominated by flicker noise measured for carbon-black polymer composite films [8]. The RMS value of the noise voltage at the ASIC chip output is evaluated from the simulation results to be  $v_n = 33 \mu V$ . Considering a RMS signal output of 3.3 V the signal-to-noise ratio is

$$SNR = 20 \log \left( \frac{3.3}{33\mu} \right) = 100 \text{ dB}$$

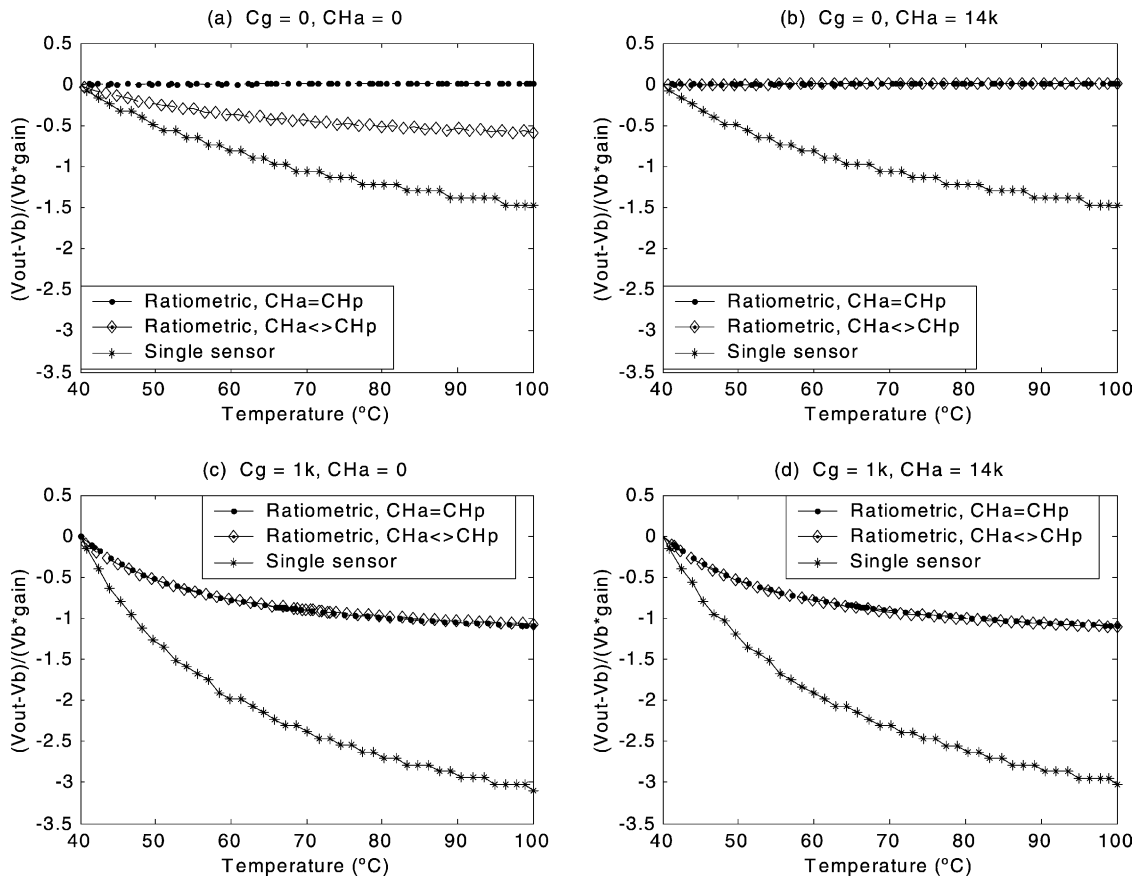


Fig. 13. Percentage variation of the output voltage for the ratiometric and potential divider circuits when the temperature of the sensors spans from 40 to 100 °C: (a) response to gas and water vapour concentrations equal to zero; (b) response with wet air and without gas exposure; (c) response to gas exposure with dry air; (d) response with gas exposure and wet air.

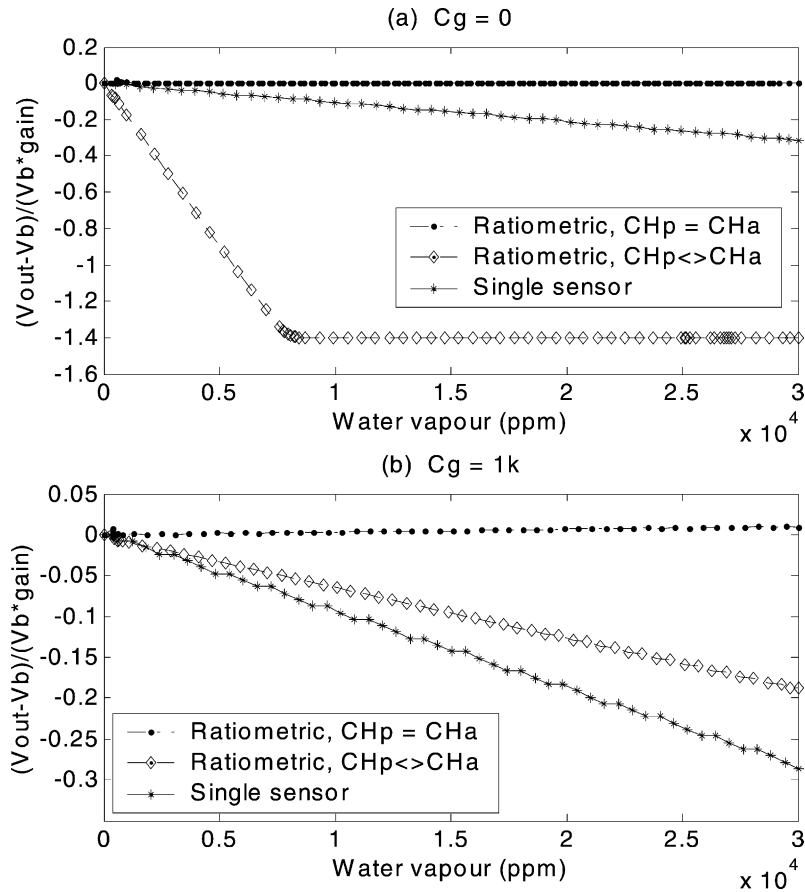


Fig. 14. Percentage variation of the output voltage for the ratiometric and potential divider circuits when the water vapour concentration spans from 0 to 30 ppt: (a) response without gas exposure; (b) response to gas exposure.

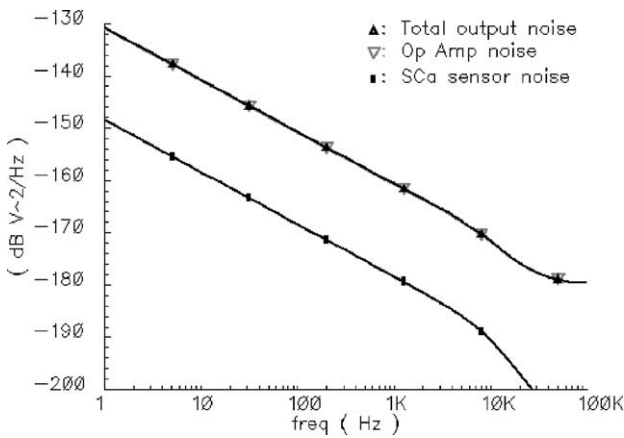


Fig. 15. Noise power spectral density at the ratiometric circuit output and noise contributions of the active sensor and the operational amplifier CFOA23.

**4. Conclusions**

A novel smart ratiometric ASIC chip has been designed for gas sensing applications and fabricated using a standard CMOS process. Simulations have shown that the ratiometric configuration shows superior performance when compared

to conventional resistive polymer devices. Its characteristics of pulsed-mode operation to prevent polarisation effects/voltage induced drifting, and on-chip compensation of temperature and humidity variations, are considered to be crucial features for the development of an accurate low-cost, palm-top gas monitor.

**Acknowledgements**

The authors express their gratitude to Steve Mattheus and Greta Milczanowska, from IMEC, Belgium, for their valuable help and advice for the testing and verification of the design. The support provided through Europractice by Dr. Stephen Bell, from Rutherford Appleton Laboratory, is also appreciated. Nicola Ulivieri acknowledges Exchange and Fellowship Programme of NOSE II (Second Network of Excellence on Artificial Olfactory Sensing) for financial support.

**References**

[1] M. Cole, J.W. Gardner, J.A. Covington, D. Fife, C.Y. Kwok, J.E. Brignell, P.N. Bartlett, Active bridge polymeric resistive device for

- vapour sensing, Eurosenors XIV, W2P41, (Bio)chem. Sens. III (2000) 895–898.
- [2] J.W. Gardner, M. Vidic, P. Ingleby, A.C. Pike, J.E. Brignell, P. Scivier, P.N. Bartlett, A.J. Duke, J.M. Elliot, Response of a poly(pyrrole) resistive micro-bridge to ethanol vapour, *Sens. Actuators B* 48 (1998) 289–295.
- [3] M. Cole, J.W. Gardner, A.W.Y. Lim, P.K. Scivier, J.E. Brignell, Polymeric resistive bridge gas sensor array driven by a standard cell CMOS current drive chip, *Sens. Actuators B* 58 (1999) 518–525.
- [4] M. Cole, J.W. Gardner, P.N. Bartlett, Low-drift odour and vapour ratiometric resistive elements for analogue CMOS smart sensors, in: J.R. Stetter, W.R. Penrose (Eds.), *Proceedings of the Artificial Chemical Sensing: Olfaction and the Electronic Nose (ISOEN 2001)*, vol. 15, The Electrochemical Society Inc., USA, 2001, pp. 117–120.
- [5] M. Cole, N. Ulivieri, J. García-Guzmán, J.W. Gardner, Parametric model of a polymeric chemoresistor for use in smart sensor design and simulation, submitted for publication. <http://www.eng.warwick.ac.uk/srl>.
- [6] P. Bruschi, A. Nannini, B. Neri, Vapour and gas sensing by noise measurements on polymeric balanced bridge microstructures, *Sens. Actuators B* 24–25 (1995) 429–432.
- [7] J.V. Hattfield, P. Neaves, P.J. Hicks, K. Persaud, P. Travers, Towards an integrated electronic nose using conducting polymer sensors, *Sens. Actuators B* 18–19 (1994) 221–228.
- [8] S.M. Briglin, M.S. Freund, P. Tokumaru, N.S. Lewis, Exploitation of spatiotemporal information and geometric optimisation of signal/noise performance using arrays of carbon black-polymer composite vapor detectors, *Sens. Actuators B* 82 (2002) 54–74.

## Biographies

*Jesús García-Guzmán* graduated in Mechanical and Electrical Engineering from the Universidad Veracruzana (Veracruz, Mexico) in 1978. He received his MSc degree in Higher Education, with honours, from the ICEST (Mexico) in 1997 and MSc degree in Advanced Engineering, with distinction, from the University of Warwick (UK) in 1999. He is a Lecturer in the Faculty of Engineering at the Universidad Veracruzana (Xalapa, Mexico). Currently he is completing work on a PhD project at

the Sensors Research Laboratory of the University of Warwick, where his main research interests are in the areas of analogue integrated circuit design, sensor interfacing and smart circuitry.

*Nicola Ulivieri* received his Laurea degree in Telecommunication Engineering at the University of Siena in 1999. He is currently a PhD student in Information Engineering (Electronics) at the University of Siena. In 2002 he spent a 6 months period at the School of Engineering of the University of Warwick to develop a Cadence model for chemoresistors gas sensors and to collaborate to an ASIC chip layout design. His main research activity is related to the development of laboratory electronic noses based on metal oxide sensors and QCM sensors. Recently, his interests were also devoted to integrated analogue and mixed signal electronics design and smart sensors development.

*Marina Cole* (BSc, PhD, MIEEE), received his BSc degree from the University of Montenegro (Yugoslavia) and the PhD from Coventry University (UK). She joined the School of Engineering at Warwick University in 1996 as a postdoctoral research assistant and in 1998 she was appointed to a lectureship in electronic engineering. Her main research interests are integrated silicon-based sensors, SAW-based sensors, analogue and mixed signal ASICs, smart sensors, actuators and microsystems.

*Julian W. Gardner* (BSc, PhD, DSc, CEng, FIEE, SMIEEE), joined the School of Engineering at Warwick in 1987. His research interests are microsensors, microsystems technology, electronic noses, intelligent sensors and multivariate data processing methods. He has previously spent 5 years in industry working first at AEA Technology Ltd. and later at Molins Advanced Technology Unit on Instrumentation. At Molins he developed a novel opto-electronic sensor that has been packaged in the UK and US for implementation on high speed packaging machinery. In 1989 he received the Esso Centenary Education Award sponsored by the Royal Society and Fellowship of Engineering to pursue his research interests. He has published over 300 technical papers and is an author of six books in Nanotechnology (1991), Electronic Noses (1992), Microsensors (1994), Electronic Noses (1999), MEMS (2001) Handbook of Machine Olfaction (2003). He was an Alexander von Humboldt Fellowship in Germany in 1994. He currently heads the Sensors Research Laboratory in the Centre for Nanotechnology and Microengineering at Warwick University, where he is Professor of Electronic Engineering.





ELSEVIER

Microelectronics Journal 34 (2003) 865–875

Microelectronics  
Journal

[www.elsevier.com/locate/mejo](http://www.elsevier.com/locate/mejo)

## Parametric model of a polymeric chemoresistor for use in smart sensor design and simulation

Marina Cole<sup>a,\*</sup>, Nicola Ulivieri<sup>b</sup>, Jesús García-Guzmán<sup>a</sup>, Julian W. Gardner<sup>a</sup>

<sup>a</sup>Smart Sensors and Devices Group, School of Engineering, University of Warwick, Coventry CV4 7AL, UK

<sup>b</sup>Department of Information Engineering, Università di Siena, Siena, Italy

Received 1 December 2002; revised 17 February 2003; accepted 25 February 2003

### Abstract

A novel parametric model of a polymeric chemoresistor is proposed for application in the design and simulation of smart gas sensors. The model has been implemented using Cadence™ software and enables the simulation of both the static and dynamic response of a chemoresistor to a mixture of different gases. It also takes into account parametrically the effects of ambient temperature, humidity and sensor noise. The layout design and a schematic symbol have also been generated in Cadence -thus creating a resistive polymeric cell that can be used in the general design of smart ASIC based systems. The top cell comprises several sub-cells allowing versatility and adaptability in implementation through its modular structure. By changing the values of the simulation parameters and/or the mathematical model of the sub-cell that evaluates the gas sensor response, it is possible to extend its application to the design and simulation of chemoresistors in *different* configurations and with different gas sensitive materials. Here we illustrate our model in the design and simulation of resistive sensors employing carbon-black polymer composite films as the class of gas sensitive material.

© 2003 Elsevier Science Ltd. All rights reserved.

**Keywords:** Resistive gas sensors; Smart sensors; ASICs; Carbon-black polymer composites; Parametric model

### 1. Introduction

Sensors, based on conducting polymer resistors, are very attractive for vapour/odour sensing applications because of the wide range of available polymer combinations and their ease of deposition, their ability to operate at room temperature (i.e. low device power consumption), and sensitivity to a broad range of volatile organic compounds [1–3]. The resistive principle, in which a change in the sensor resistance  $\Delta R_S$  is monitored while the sensor is exposed to the gas, is the most commonly used principle within the field of vapour/odour sensing [2,4–7,9]. However, there are some disadvantages commonly associated with polymeric chemoresistors, in particular the batch-to-batch variation in baseline resistance and its large temperature and humidity coefficients. There can also be a long-term drift effect, associated especially with conducting polymer resistors, when driven by constant d.c. voltage. A small signal-to-noise ratio, common for most types of gas

sensors, is another parameter that cannot be neglected. Different measurement techniques have been used to improve the resistive gas sensor performance. For instance, transient and dynamic sensor responses [1,10–13] can be monitored and used to extract information that can improve the gas recognition performance. Also high-frequency a.c. measurements can be employed to improve sensor sensitivity [14–16]. However, a fundamental understanding of the response of polymer film sensors to different gas species under different conditions and with different interferences is essential to ameliorate the undesirable features commonly associated with gas sensor signals as mentioned above.

Development of parametric models for polymeric chemoresistors can help in the design of new devices with improved characteristics and in the interpretation of experimental data. An absorption/desorption model for d.c. conducting polymer sensors consisting of a thin uniform polymer film deposited on a pair of finite coplanar electrodes supported by an insulating substrate was presented in Ref. [17]. The diffusion and adsorption equations were presented in terms of several fundamental dimensionless parameters describing the underlying

\* Corresponding author. Fax: +44-1203-418922.

E-mail address: [mvc@eng.warwick.ac.uk](mailto:mvc@eng.warwick.ac.uk) (M. Cole).

chemical and physical properties of the sensor. In another development electrical equivalent models for resistive gas and odour sensors have been developed using Pspice [18, 19]. Furthermore, the advances and benefits of the IC technology can be exploited in the development of integrated, low-cost, reliable devices capable of addressing problems associated with discrete chemoresistive sensors. This could be achieved through the design of smart sensors capable of self-testing, self-calibration and compensation within a single chip unit.

In this paper we present a parametric model of a polymeric chemoresistor developed for use in the design and simulation of smart gas/odour sensor systems. The model is implemented in Cadence software together with associated schematic, symbol and layout design; thus allowing both the implementation of resistive elements in smart sensor design and the simulation of the chemical static response and chemical step response of a polymeric chemoresistor to a mixture of different gases. The model takes into account temperature and humidity effects and simulates the noise present in polymer sensors, such as Johnson [20] and flicker or 1/f noise [21–23]. The new model also takes into account sample delivery system (SDS) parameters, such as the volumetric flow rate and volume of the sensor chamber that can be customised to specific experimental set-ups.

Polymer-carbon black composite films are used here as gas sensitive materials both to demonstrate the practical application of the new model in the design of polymeric chemoresistors and to simulate their behaviour. The films, firstly reported by Lewis at Caltech, consist of conducting carbon black nanospheres dispersed into a non-conducting base polymer films [4–7]. When exposed to gases, the polymer within the composite film absorbs the vapour and swells reversibly. This swelling causes the distances between the conductive carbon black particles to increase and thus, induces a resistance change in the composite film [4,6]. Carbon black polymer composite film-based sensors are not selective toward a specific gas but they show different sensitivities to different gases. However the pattern

response of an array of several sensors made up by different polymer composite films can be used as a ‘fingerprint’ to classify different gas or chemical mixture [1,8].

## 2. Architecture of the standard cell

Fig. 1 shows the basic structure of the proposed model, realised in Cadence, comprising four blocks that represent SDS, sensor’s static and dynamic responses and chemoresistor itself (dotted box). The model has two inputs for different gas concentrations and one input for temperature effect simulation ( $C_{\text{gas}_1}$ ,  $C_{\text{gas}_2}$ , and Temperature) as well as two external ports ( $R_+$ ,  $R_-$ ) for sensors connection within the complete test system. The sensor static response is a function of the input gas concentrations and temperature while the dynamic response depends both on the gas transfer method and the reaction process on, or within, the gas sensitive material. The chemoresistor itself is represented as a complex impedance  $Z_S$  element with two noise generators connected in series representing Johnson and flicker noise, which are dependant on the sensor temperature and sensor resistance [20] and the type of polymer, its volume and biasing voltage [21–23], respectively.

The schematic view for the model has also been designed in order to enable its application in the design of smart sensors and systems using commercial IC packages and it is shown in Fig. 2a with its associated symbol represented in Fig. 2b. One of the gas inputs,  $H$ , is assumed to be the water vapour concentration or humidity. More inputs can be added depending on the knowledge of the chemoresistive behaviour when exposed to the gas mixture. Each block (sub-cell) within the electrical model has been custom designed to perform a desired function or to emulate an electrical device and the graphical symbol has been edited, see Fig. 2b. In this, two main sections can be distinguished: the chain composed from the sub-cells *SDS02*, *eSR04*, *CT03*, *vcR01*, simulating the sensor’s response (i.e. change in resistance) and the noise generation section which comprises the sub-cells *eJN02*, *eFN02*, *WNS04* and

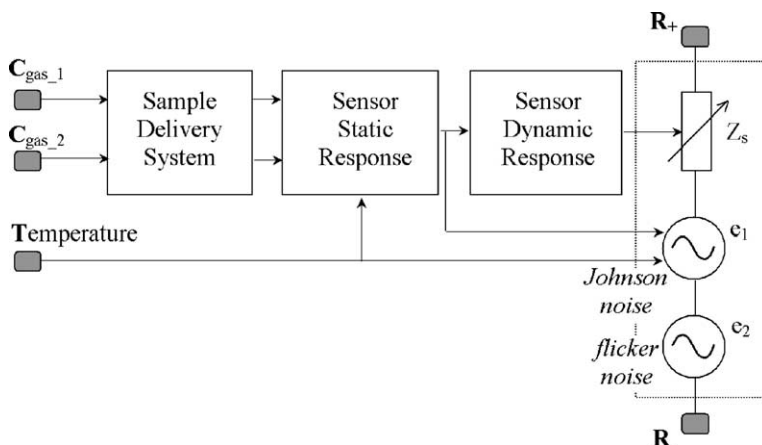


Fig. 1. Model framework.

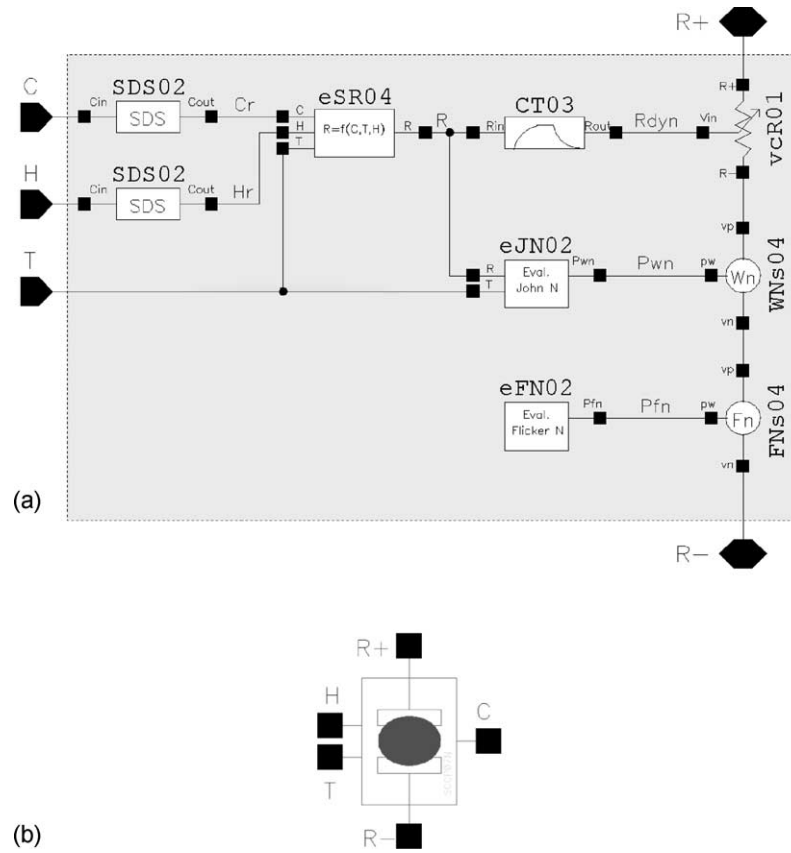


Fig. 2. Polymeric chemoresistor standard cell. (a) Schematic view. (b) Symbol.

*FNs04*. Functionality of the model, and all individual blocks within it, is explained in the following sections.

### 2.1. Modelling of chemoresistor's behaviour

The sub-cell *eSR04* (Fig. 2) evaluates the sensor static response as a function of the gas concentration **C**, the sensor's temperature **T** and the humidity **H**. For simulation purposes and simplicity reasons, a voltage source emulates the gas concentration where it is assumed that 1 V corresponds to 1 ppm of gas concentration. For instance, the injection of 100 ppm of carbon monoxide (CO) in air can be simulated by supplying a d.c. voltage of 100 V. *R* indicates the output voltage corresponding to the sensor resistance (1 V → 1 Ω).

The variation of the sensor resistance in the presence of a gas is modelled with the following generic power law function, which is suitable for carbon-black polymer composite films as well as other types [24]:

$$R = R_0 \cdot \left[ 1 + k C^\gamma \exp\left(\frac{K_S}{T}\right) \right] \quad (1)$$

where  $R_0$  is the baseline sensor resistance (measured in the presence of a reference gas, generally clean air),  $k$  is a sensitivity coefficient,  $C$  is the gas concentration expressed in ppm,  $\gamma$  is the power law exponent,  $K_S$  is a temperature coefficient and  $T$  is the temperature in degrees Kelvin.

The sensitivity coefficient can be positive or negative depending on the nature of the gas and the polymer used, producing an increase or decrease of the sensor resistance after the gas is introduced. It should be noticed that an increase in temperature results in a reduction of the sensor resistance when  $K_S$  is positive. The above resistance model can be extended to a gas mixture by adding the effect of the individual component as separate inputs assuming that there is no interaction between them. This assumption is valid for low concentrations of volatile organic compounds [24,25]. The resistance model can also be expanded to include the independent additive effect of humidity:

$$R = R_0 \cdot \left[ 1 + k_G C_G^{\gamma_G} \exp\left(\frac{K_{sG}}{T}\right) + k_H C_H^{\gamma_H} \exp\left(\frac{K_{sH}}{T}\right) \right] \quad (2)$$

where the subscripts G and H correspond to the gas and the water vapour, respectively.

The above model is implemented in Cadence through a combination of functional blocks, performing basic operations (e.g. adder block, exponential block). This is represented in the *schematic view* shown in Fig. 3. The same result could be achieved by the definition of the model using a *Verilog-A* or an *HDL* script [26,27].

The cell *CT03* emulates the dynamic sensor response to gas pulses (Fig. 4). The input to this cell is a voltage value corresponding to the steady-state sensor response  $R_{in}$  (1 V → 1 Ω) calculated by the *eSR04* block previously

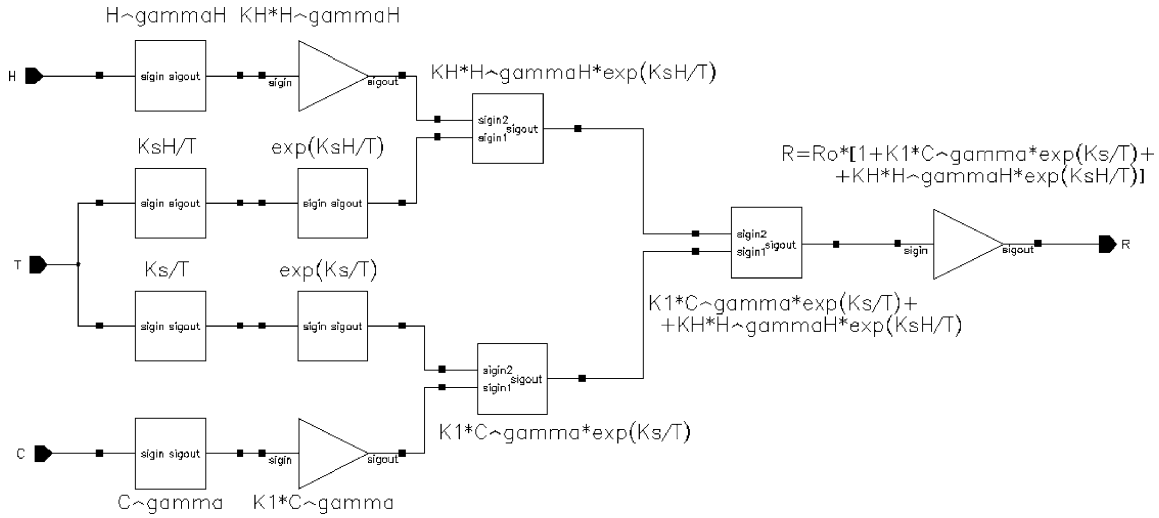


Fig. 3. Schematic view of the eSR04 cell evaluating the static sensor resistance.

described. The transient behaviour of a resistive gas sensor can often be approximated by a second-order multi-exponential model [11,18,19]. Two unity-gain second-order low-pass filters have been used to simulate the exposure (or on-dynamics) and recovery (or off-dynamics) of the sensor; the off-dynamics is generally slower [20,21]. The selection of the cell output ( $R_{out}$ ) is achieved using a switch sub-cell (*Swtc04*, in Fig. 4), which passes the higher out of the two filter outputs. This selection also avoids the occurrence of sharp changes in the output voltage when the simulation requires a gas switching before the steady-state condition is reached. The switch sub-cell acts as an ideal 2:1 multiplexer where the output voltage is equal to one of the two inputs  $in1$ ,  $in2$  depending on the voltage difference between the control signals  $sc_p$  and  $sc_n$ . In order to obtain a good portability of the model, the cell functionality is defined by both *ahdl* and *verilog-A* scripts. The filters are

realized with ideal passive components (independent of the temperature and noiseless) connected as shown in Fig. 4.

The transfer function of a second-order filter can be written in Laplace  $s$  notation as follows:

$$H_{lp2}(s) = \frac{1}{\left(1 + \frac{s}{\omega_1}\right)\left(1 + \frac{s}{\omega_2}\right)} = \frac{1}{\frac{s^2}{\omega_1\omega_2} + s\left(\frac{1}{\omega_1} + \frac{1}{\omega_2}\right) + 1} \quad (3)$$

The transfer function can also be written as a function of electrical elements  $L$ ,  $R$  and  $C$  :

$$H_{lp2}(s) = \frac{1}{s^2LC + s\frac{L}{R} + 1} \quad (4)$$

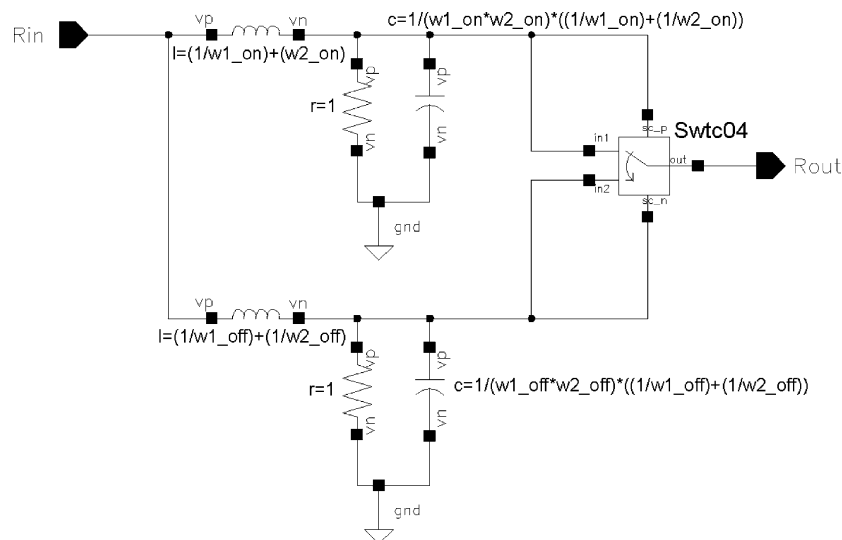


Fig. 4. Schematic view of the CT03 cell.

where

$$\frac{L}{R} = \left( \frac{1}{\omega_1} + \frac{1}{\omega_2} \right), \quad LC = \frac{1}{\omega_1 \omega_2} R = 1 \Omega \quad (5)$$

The cell acts as a functional block with no current flowing from the input to output terminal. The resistance  $R$  can have a value assigned to, e.g.  $1 \Omega$ , and the filter cut-off frequency can then be determined calculating the  $C$  and  $L$  values which are included in the model using following equations:

$$L = \left( \frac{1}{\omega_1} + \frac{1}{\omega_2} \right), \quad C = \frac{\frac{1}{\omega_1 \omega_2}}{\left( \frac{1}{\omega_1} + \frac{1}{\omega_2} \right)} R = 1 \Omega \quad (6)$$

Thus, the cell requires only the values of  $\omega_{1off}$ ,  $\omega_{2off}$ ,  $\omega_{1on}$ , and  $\omega_{2on}$  where *on* and *off* refer to on- and off-dynamics of the chemoresistor.

The sub-cell *vcROI* (Fig. 2) is a voltage-controlled resistance implemented in the model via the following formula,

$$I_{R_+R_-} = (V_{R_+} - V_{R_-})/V_{in} \quad (7)$$

where  $V_{in}$  is the input voltage corresponding to the simulated resistance value,  $I_{R_+R_-}$  is the current flowing from the terminal  $R_+$  to the terminal  $R_-$  and  $V_{R_+}$ ,  $V_{R_-}$  are, respectively the voltages at the terminals  $R_+$  and  $R_-$ .

Since the dynamic system is composed of the sensor itself and the SDS, a sub-cell *SDS02* (Fig. 2) simulating the gas transfer behaviour is also included in the model. Gas transfer methods can be divided into two main categories called headspace sampling and flow injection, but various other methods can also be used [1,28]. In the former case the headspace of an odorant material to be analysed is physically removed from a sample vessel and injected into a gas-tight chamber hosting gas sensors using either a manual or automated procedure. In the case of flow injection, a carrier gas can be used to carry the odorant from the sample vessel into the sensor chamber. It can be approximated that in the case of static headspace sampling the actual gas flow behaves like the output of a unity-gain first-order low pass filter where the input is an ideal voltage pulse. Therefore, the structure of the cell *SDS02* is very similar the one of the cell *CT03* where the two 2nd order filters are replaced by two 1st order filters with different poles to emulate different on-and off-dynamics. A further switch sub-cell (*Swtc04*) and a voltage source are included to allow the internal bypass of the *SDS02* cell by setting the voltage level to a negative value.

## 2.2. Noise model

Signals from gas sensors are often weak, noisy, and they exhibit parametric drift and contain undesirable components. The new model takes into account the presence of noise in terms of both Johnson noise and flicker noise. The noise factor is very important since the point at which the signal-to-noise ratio drops below an acceptable level

sets the limit or resolution of an electrical circuit and therefore the sensor system itself. Thermal (Johnson) noise, caused by the thermal agitation of charge carriers (electrons or holes) is present in all passive resistive elements [20]. The Johnson noise is spectrally flat and its root mean squared (rms) voltage density,  $V_{JN}$ , can be expressed as follows:

$$V_{JN} = (4kTRB)^{1/2} \quad (8)$$

where  $k$  is Boltzmann's constant ( $1.38 \times 10^{-23}$  J/K),  $T$  is the absolute temperature in Kelvin (K),  $R$  is the resistance of the conductor in ohms ( $\Omega$ ) and  $B$  is the bandwidth (Hz). The term  $4kTR$  is a voltage power density having units of  $V^2/Hz$ . Thermal noise is a fundamental lower limit on the noise of any device of resistance  $R$ , and its magnitude is independent of the volume or of other fabrication-dependent properties of the resistor.

In carbon-black polymer composite chemoresistors, additional noise is observed with a power spectral density that displays an inverse dependence on frequency of the form  $1/f^{exp}$  where the exponent *exp* is usually close to the unity but different slopes have been observed in different materials. Such noise is called flicker noise or  $1/f$  noise and is associated with the d.c. bias voltage applied to the resistor [20]. The power spectral density of the  $1/f$  noise scales with the square of the bias voltage. Further factors that affect the level of the  $1/f$  noise in carbon black-polymer composite resistors are the structure of the carbon black, its volume fraction in the composite, the type of insulator, the resistivity of the composite, and the method of resistor preparation [21–23]. The power density of the  $1/f$  noise in carbon-black polymer films is proportional to the resistor volume when the correlation length of the resistive particle network is small compared to the physical length scale of interest [22,23].

The Johnson and  $1/f$  noise effects are included in the polymeric chemoresistor model presented in this paper via series of noise sources (*WNS04*, *FNs04* in Fig. 2) created with both *verilog-A* and *ahdl* scripts. The scripts make use of the noise functions *white\_noise(pw)* and *flicker\_noise(pf,slope)*. The created noise sources accept as an input the voltage power density at 1 Hz (*pw*, *pf*), which is evaluated by other sub-cells (*eJN02* and *eFN02*). The flicker noise source has a further parameter, *slope*, which allows for the slope definition of the  $1/f^{slope}$  noise. The value of *slope* is stored in the *FNs04* cell and it depends on the type of chemoresistor implemented (usually is 1). The noise functions are active only during small-signal analysis and return 0 otherwise, and different noise models can be implemented by changing the *verilog-A* or *ahdl* scripts.

## 3. Layout the design and equivalent circuit

### 3.1. Layout design

The layout of the chemoresistive sensor, modelled in Section 2, was designed using the *Virtuoso* layout editor

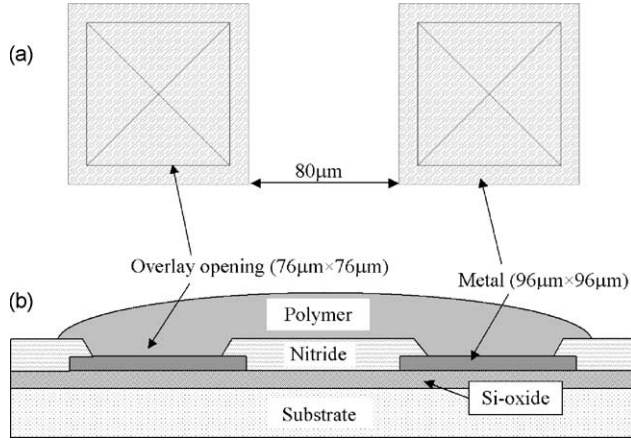


Fig. 5. Polymer chemoresistor layout. a) Layout view of the metal sensor pads; the two squares ( $96 \mu\text{m} \times 96 \mu\text{m}$ ) filled with dashed lines represents the metal pads and the crosses indicate the openings on the above insulator (Nitride) to allow the access to the metal pads. b) Cross-section view. The polymer is deposited across the two openings in a process subsequent to the standard CMOS process. All dimensions are in  $\mu\text{m}$ .

according to the specifications and layout rules of the Alcatel  $0.7 \mu\text{m}$  CMOS process. This process was chosen for possible implementation of our devices in smart sensor design and low-cost fabrication through the Europractice scheme. Fig. 5a shows the layout of the sensor electrodes consisting of two square metal pads, while the cross section of the carbon black polymer resistor is shown in Fig. 5b. Minimum size dimensions were chosen for the pads while the inter-electrode gap was chosen to be about  $100 \mu\text{m}$  in order to obtain a baseline sensor resistance of approximately  $10 \text{ k}\Omega$ , based on the typical sheet resistances of carbon-black polymers ( $R_{\square} = 1 - 10 \text{ k}\Omega$  per sq. depending on the polymer thickness and the carbon black volume fraction in the composite). There are two metal layers available within the Alcatel  $0.7 \mu\text{m}$  CMOS process. Both of these layers are aluminium, but the ‘METAL 2’ layer has a lower sheet resistance. It was decided to implement the metal electrodes using the ‘METAL 2’ layer, which requires an overlay opening to enable access for the polymer deposition. This also has the advantage that other layers can still be routed underneath this layer like a ‘METAL 1’ heater to ensure that the deposited polymer is

at the required temperature. Temperature control can be achieved using a temperature sensor within the device (i.e. temperature diode). Chemoresistors can also be constructed from poly-Si or  $\text{P}^+$  electrodes where a contact window again has to be opened for possible electrochemical deposition of electroactive polymers.

### 3.2. Equivalent circuit

Equivalent circuit of the chemoresistor layout is shown in Fig. 6. Circuit includes parasitic capacitances: metal pads capacitances  $C_p$ , metal tracks capacitances  $C_t$ , and polymeric sensor capacitance  $C_s$ . Capacitances are evaluated by the following formula given by Alcatel:

$$C_{\text{gnd}} = L \cdot (W \cdot C'_{\text{plane}} + 2 \cdot C'_{\text{side}}) \quad (9)$$

where

$$C'_{\text{plane}} = 1.15/H \left[ \frac{F}{\mu\text{m}^2} \right]$$

$$C'_{\text{side}} = 1.4 \cdot (T/H)^{0.222} \left[ \frac{F}{\mu\text{m}} \right]$$

$T$  is Poly, Metal1 or Metal2 line thickness,  $H$  is oxide thickness between Poly, Metal1, Metal2 and underlying layer,  $W$  is Poly, Metal1 or Metal2 line width and  $L$  is Poly, Metal1 or Metal2 line length. Hence the track capacitances  $C_{t1,2}$  were calculated to be  $320 \text{ fF}$ , while the pad capacitances  $C_{p1,2}$  were estimated to be  $210 \text{ fF}$ . The metal2 track resistance is  $R_t = 2.34 \Omega$  ( $R_{\square} = 35 \text{ m}\Omega$  per sq). Finally, the capacitance of the polymer sensor  $C_s$  can be calculated from the finite co-planar electrode geometry using the following equation based upon Jacobean elliptical integrals of the second kind:

$$C_s = \frac{b\epsilon_0}{2A^*} \epsilon_{\text{sub}} \left[ \int_{-\infty}^0 \frac{1}{\sqrt{(k^2x^2 + w^2/4)(x^2 + w^2/4)}} \right. \\ \left. + \epsilon_p \int_0^L \frac{1}{\sqrt{(k^2x^2 + w^2/4)(x^2 + w^2/4)}} \right. \\ \left. + \int_L^{+\infty} \frac{1}{\sqrt{(k^2x^2 + w^2/4)(x^2 + w^2/4)}} \right] \quad (10)$$

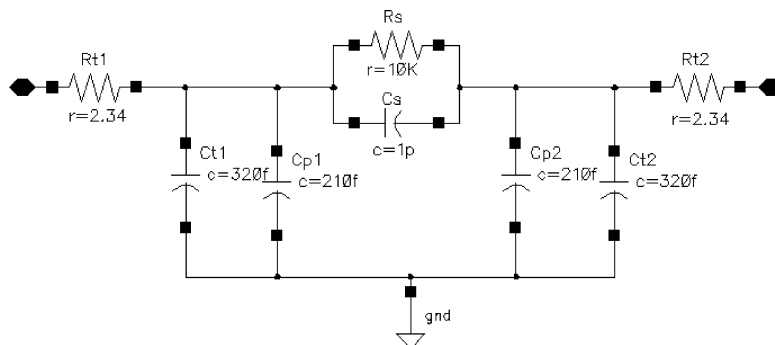


Fig. 6. Equivalent circuit of the polymeric sensor. Sensor capacitance  $C_s$ , pads capacitances  $C_p$ , metal tracks resistances  $R_t$ , and capacitances,  $C_t$ , are all taken into account. The sensor resistance  $R_s$  is represented with its baseline value.

where  $b$  is the breadth of the electrodes,  $w$  is the separation of the electrodes,  $L$  is the thickness of the polymer film,  $\epsilon_0$  is the dielectric permittivity of free space,  $\epsilon_{\text{sub}}$  and  $\epsilon_p$  are the dielectric constants of the substrate and polymer film,  $k$  is the geometric parameter equal to  $w/(w + 2d)$  where  $d$  is the depth of the electrodes, and finally  $A^*$  is another geometric constant computed from the following complete elliptical integral:

$$A^* = \int_0^{w/2} \frac{1}{\sqrt{(-k^2x^2 + w^2/4)(-x^2 + w^2/4)}} dx \quad (11)$$

The three integrals in Eq. (10) represent the capacitance associated with the substrate, film and air. The first and third terms will be largely the pad value provided above for Metall; the second term can be simplified when the electrode separation  $w$  is smaller than the electrode depth  $d$  and thus an approximate equation (excluding the pads) is given by:

$$C_s \approx \frac{b\epsilon_0\epsilon_p}{\pi} \ln \left[ \frac{1 + \sqrt{1 + w^2/4L^2}}{w/2L} \right]$$

For, say, an electrode breadth  $b = 100 \mu\text{m}$ , width  $w = 100 \mu\text{m}$ , film thickness  $L = 10 \mu\text{m}$  and dielectric constant  $\epsilon_p$  equal to 10, the capacitance associated with the film is only 0.70 fF. So the sensor capacitance is dominated by the parasitic capacitance of the two electrode pads, which is a total of 420 fF, rather than the inter-electrode capacitance.

#### 4. Simulation results

The model described in the above section was verified and used to simulate the behaviour of carbon-black polymer composite sensors when exposed to a single gas or mixture of gases. The complete cell comprising a chemoresistor model, schematic representation and a layout design, was used in a voltage divider configuration shown in Fig. 7. In this simulation a d.c. voltage of 2.4 V is applied to the input while the output signal is the voltage difference across the sensor terminal  $R_+$ ,  $R_-$ . A voltage divider configuration has been chosen here, as recommended by some gas sensor manufacturers, in order to convert the sensor resistance into a voltage that can be further processed, amplified or interfaced to other devices.

The variation in resistance of the gas-sensitive device (typically 1–50%), subsequent to exposure to a gas of concentration  $C$ , can then be measured through the change in the output voltage  $V_{\text{out}}$  which is function of the sensor resistance  $R_S$  :

$$V_{\text{out}} = V_{\text{ref}} \frac{R_S(C)}{R_{\text{ref}} + R_S(C)} \quad (12)$$

The sensitivity  $S$  of the potential divider is defined as

$$S = \frac{dV_{\text{out}}}{dR_S} = V_{\text{ref}} \frac{R_{\text{ref}}}{(R_{\text{ref}} + R_S(C))^2} \quad (13)$$

which has a maximum for  $R_{\text{ref}} = R_S$ . The reference resistance value was chosen to be equal to the sensor baseline value (10 k  $\Omega$ ) to maximize sensitivity for small

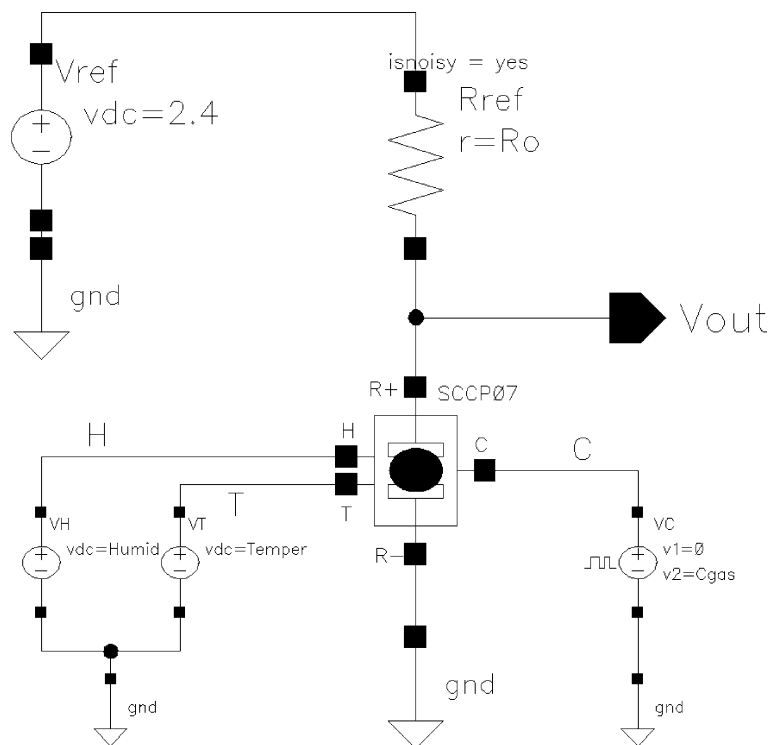


Fig. 7. Schematic view of the potential divider circuit used to test the cell.

changes of  $R_S$ . Gases injection and sensor temperature are simulated by voltage sources.

Fig. 8 shows the simulated behaviour of carbon-black polymer resistors while Table 1 summarizes the parameters used in the equations and Cadence sensor model. The coefficients are obtained from measurements on real polymeric gas-sensitive films made at the Sensor Research Laboratory at Warwick University [24]. The transient response to a gas pulse of 1000 ppm (Fig. 8a) is shown in Fig. 8c where it can be noticed that the gas presence causes a sensor resistance ( $R_S$ ) increase of about 5% with respect to the baseline value. Left-hand plots show the effect of temperature on the chemoresistor response and the right-hand plots show the effect of humidity variation. Plot labels are referred to nets in Fig. 7 and, for nets internal to the sensor model, to Fig. 2.  $C$  is the voltage input representing the gas concentration injected into the measurement chamber while  $R$  is the output voltage value of the *eSR04* cell (see Fig. 2) corresponding to the static sensor resistance.  $R_{dyn}$  is the dynamic sensor response, expressed in volts, evaluated by the *CT03* cell. It can be noticed that the return to the resistance baseline value is slower than the change after gas injection. In this, the block simulating the real SDS, *SDS02*, is bypassed and the dynamic response shown is due only to the gases interacting with the polymeric film. The temperature and humidity effects evaluated as the ratio

between the voltage across the sensor  $V_{out}$  and the current  $I_{R+R-}$  are shown in Figs. 8d and i. It can be observed that a temperature change of 10 °C causes a decrease in the sensor response of about 2% with respect to the baseline value. When low gas concentrations have to be recognised, the temperature effect *cannot* be neglected and an accurate temperature compensation/control system should be used. Humidity produces a slight decrease of the sensor resistance (Fig. 8i) because the carbon-black polymer here is weakly hydrophilic. Water vapour also affects the baseline resistance because it is present in the reference gas.

Fig. 9 shows the total electrical noise and the contribution of each noise source at the circuit output obtained by noise analysis. In the simulation the noise power density is evaluated considering a normalized bandwidth equal to 1. It should be noted that in carbon-black polymer resistors the total noise is dominated by the flicker noise; the thermal noise is much lower. The slight difference between the thermal noise of the sensor and the reference resistance  $R_{ref}$  is due to the different temperature. In fact, while the reference resistance is at ambient temperature, the polymer chemoresistor is heated and kept by a control system to a higher temperature than the ambient temperature (50 °C in the simulation). Recent measurements on thin films of carbon black-polymer composite resistors have shown an interesting

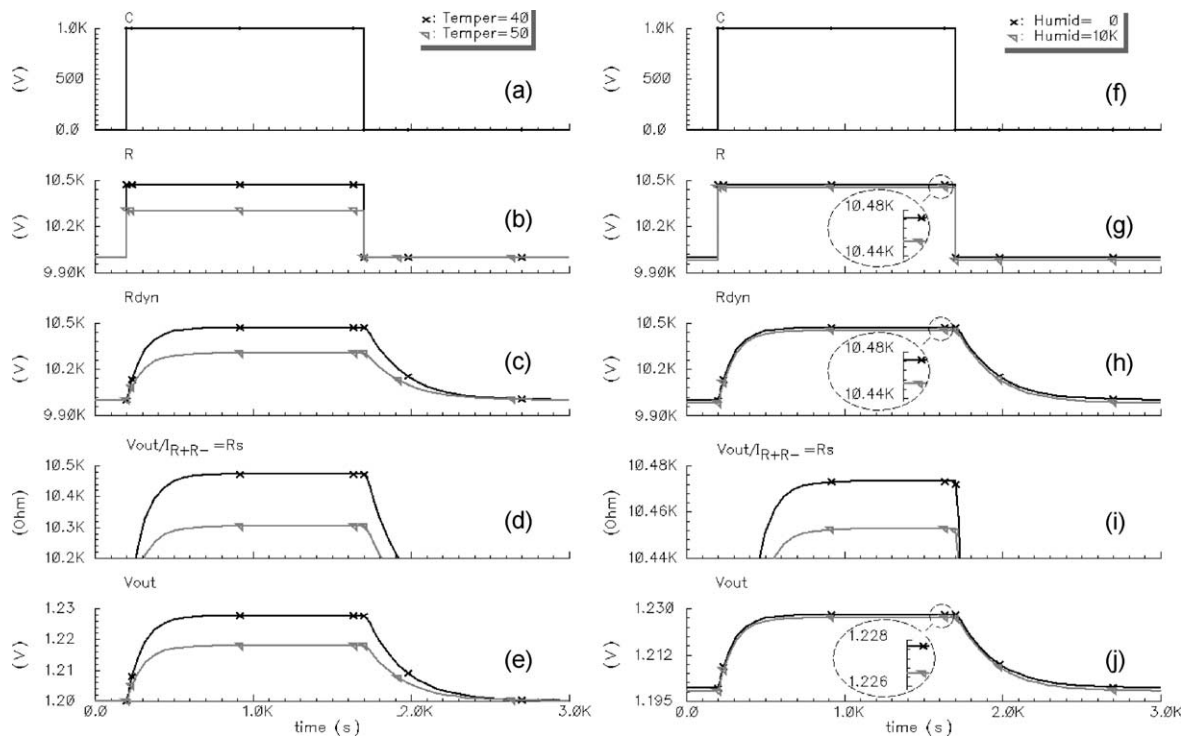


Fig. 8. Transient analysis responses during 1000 ppm gas injection for two different sensor temperatures (40 and 50 °C, absence of humidity, left-hand plots) and two different water vapour concentrations (0 and 10 kppm, temperature = 40 °C, right-hand plots). (a) and (f) show the simulated gas pulse, (b) and (g) the static sensor response, (c) and (h) the dynamic sensor response, (d) and (i) the sensor resistance evaluated as the ratio between the voltage across the sensor  $V_{out}$  and the current  $I_{R+R-}$ , (e) and (j) the output voltage.



Table 1  
Model parameters used in the simulations

| Parameter used in the Cadence model | Value(s) <sup>a</sup> | Symbols used for Cadence parameters in Eqs. (1–10) | Description  |
|-------------------------------------|-----------------------|--|--|
| Cgas                                | 1 k                   | $C_G$  | Gas concentration (ppm)                              |
| Humid                               | 0, 10 k               | $C_H$  | Humidity concentration (ppm)                         |
| Temper                              | 40, 50                | $T$  | Sensor temperature (°C)                              |
| KsH                                 | 31.32                 | $K_{sH}$   | Temperature coefficient for the humidity (°C)        |
| kH                                  | −94 n                 | $k_H$  | Sensitivity coefficient for the humidity (1/ppm)     |
| GammaH                              | 1                     | $\gamma_H$   | Power low exponent for the humidity                  |
| Slope                               | 1                     | –  | Slope of the flicker noise ( $1/f^{\text{slope}}$ )  |
| Vol                                 | $3.54 \cdot 10^{-15}$ | –  | Polymer volume (m <sup>3</sup> )                     |
| X                                   | $35.4 \cdot 10^{-27}$ | –  | Polymer coefficient to evaluate flicker noise.       |
| SDS_Ct                              | −1                    | –  | SDS control (positive → active, negative → inactive) |
| w1SDS_off                           | –                     | –  | Pole for off-dynamics SDS                            |
| w1SDS_on                            | –                     | –  | Pole for on-dynamics SDS                             |
| w2_on                               | 10 k                  | $\omega_{2on}$                                     | 2nd pole on-dynamics chemical transient              |
| w2_off                              | 4 k                   | $\omega_{2off}$                                    | 2nd pole off-dynamics chemical transient             |
| w1_on                               | 10 m                  | $\omega_{1on}$                                     | 1st pole on-dynamics chemical transient              |
| w1_off                              | 4 m                   | $\omega_{1off}$                                    | 1st pole off-dynamics chemical transient             |
| Ro                                  | 10 k                  | $R_0$  | Sensor baseline resistance (Ω)                       |
| Ks                                  | 88.42                 | $K_{sG}$   | Temperature coefficient for the gas (°C)             |
| k1                                  | 3.2 μ                 | $k_G$  | Sensitivity coefficient for the gas (1/ppm)          |
| Gamma                               | 1.07                  | $\gamma_G$   | Powder low exponent for the gas                      |

<sup>a</sup> The values of the parameters used for simulations are obtained from measurements on carbon-black polymer films performed at the School of Engineering of the University of Warwick with exception of the noise measurements which were performed by the University of Torvegata (Rome).

behaviour of their noise spectra, displaying different slopes ( $1/f$  and  $1/f^2$ ) in different frequency windows. Such kind of noise can also be implemented with Cadence by using the piecewise linear function *noise\_table*. However we cannot offer here an explanation for this unusual behaviour.

#### 4.1. A.C. simulation

An a.c. simulation was also performed in order to establish the circuit bandwidth. For this purpose, the developed model also includes parasitic elements calculated in Section 3.2. Fig. 10a shows the a.c. simulation

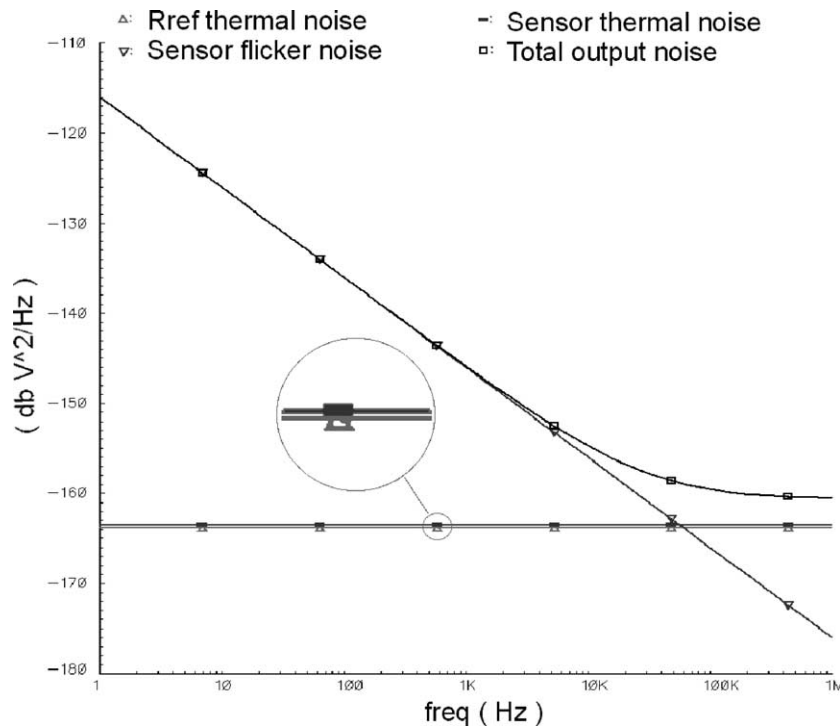


Fig. 9. Noise analysis responses for the polymeric chemoresistor model showed in Fig. 5; refer to Figs. 5 and 2 for symbols meaning.

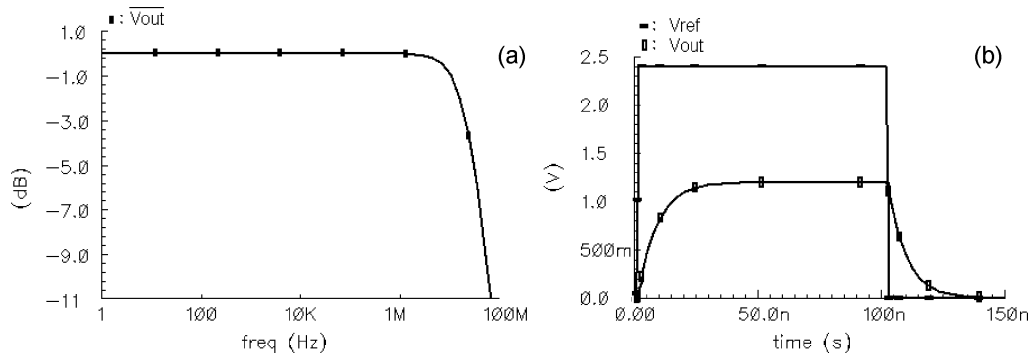


Fig. 10. A.c. analysis (a) and transient analysis (b) of the circuit shown in Fig. 7 where the sensor is modelled with the equivalent circuit shown in Fig. 6.  $V_{out}$  in (a) is normalised with respect to its d.c. value.

of the circuit shown in Fig. 7 where  $V_{out}$  is normalized with respect to its d.c. value. The evaluated bandwidth is less than 20 MHz and is mainly determined by the polymer capacitance and, actually, all the electrical parasitic elements can be neglected. In Fig. 10b the transient analysis of the circuit is also shown. From a comparison with the transient analysis in Fig. 8 it is clear that the dynamic response of the system is dominated by the chemical interaction rather than electrical properties. Furthermore, the electrical time-constant of the polymer chemoresistor may be estimated from the above calculations to be around 0.5 nF and this is several orders of magnitude smaller than the time-constants observed in practice. Thus, it is evident that the transient response of these sensors is associated with the chemical interaction between the gases and polymer film and typically lies in the range of 1–10 s. So the time-constants must be found experimentally for the precise choice of gas and polymer film.

## 5. Conclusions and future work

We have presented a newly developed model used for the design and simulation of a resistive polymeric cell that can be standardized and used in the design of smart gas or ASIC based systems. The model simulates the chemical static response and chemical step response to a gas or mixture of gases. It takes into account the temperature, humidity and sensor noise effects. The modular structure of the cell allows for versatility and adaptability. Changing values of the parameters it is possible to implement different polymeric chemoresistors with different sensing characteristics.

The new model was tested in a potential divider configuration, which is very simple to use but does possess some disadvantages. Firstly, it is not very sensitive to very small changes in  $R_S$ . Secondly, the output voltage  $V_{out}$  depends not only upon the input resistance of the next device but more importantly on the temperature-dependence of the sensor itself. The use of an active divider where the reference element is a duplicate of the sensing element (but does not sense the gas) can obviate this drawback [2].

The model will be extended to *ratiometric* circuit configurations in order to reduce temperature dependence and sensor drift. Noise reduction can be performed through dynamic offset-cancellation techniques like auto zero and chopper techniques. [29,30]. The model is complemented by the addition of the layout view and it also includes real parameters such as contacts' impedance and bulk capacitance. The advantage of the standard layout and the model is that it can be implemented in different technologies (e.g. Alcatel<sup>1</sup>, AMS<sup>2</sup>).

The cell SCCP07 is available from the website, <http://www.eng.warwick.ac.uk/SRL>.

## Acknowledgements

We would like to express our gratitude to Professor d'Amico of University Torvegata, Rome, for performing the noise measurements on carbon-black polymer composite sensors. Nicola Olivieri acknowledges the Exchange and Fellowship Programme of NOSE II (2nd Network of Excellence on Artificial Olfactory Sensing) for its financial support.

## References

- [1] J.W. Gardner, P.N. Bartlett, *Electronic Noses - Principles and Applications*, Oxford University Press, Oxford, 1999.
- [2] J.W. Gardner, *Microsensors: Principles and Applications*, Wiley, New York, 1994.
- [3] E.J. Samuelsen, W.R. Salaneck, D.T. Clark (Eds), *Science and Applications of Conducting Polymers*, Proceedings of the Sixth Europhysics Industrial Workshop held in Lofthus, Norway, 1990.
- [4] M.C. Lonergan, E.J. Severin, B.J. Doleman, S.A. Beaber, R.H. Grubbs, N.S. Lewis, Array-based vapor sensing using chemically sensitive carbon-black polymer resistors, *Chem. Mater.* 8 (1996) 2298–2313.
- [5] N. Tsubokawa, M. Tsuchida, J. Chen, Y. Nakalawa, A novel Contamination sensor in solution: the response of the electric

<sup>1</sup> <http://www.alcatelmicro.com/>

<sup>2</sup> <http://www.austriamicrosystems.com/>

- resistance of a composite based on crystalline polymer-grafted carbon black, *Sens. Actuators B* 79 (2001) 92–97.
- [6] J.A. Dickson, R.M. Goodman, Integrated chemical sensors based on carbon black and polymer films using a standard CMOS process and post-processing, *Circuits and Systems*, Proceedings of ISCAS Geneva, 2000.
- [7] F. Zee, J.W. Judy, Micromachined polymer-based chemical gas sensor array, *Sens. Actuators B* 72 (2001) 120–128.
- [8] J.W. Gardner, T.C. Pearce, S. Friel, P.N. Bartlett, N. Blair, A multisensor system for beer flavour monitoring using an array of conducting polymers and predictive classifiers, *Sens. Actuators B* 18 (1994) 240.
- [9] F. Zee, J. Judy, MEMS chemical gas sensor, *Industry Microelectronics Symposium*, 1999.
- [10] W. Rosenstiel, M. Schweizer-Berberich, A. Hierlemann, J. Mitrovics, U. Weimar, W. Göpel, J. Göppert, Application of neural-network systems to the dynamics response of polymer-based sensor arrays, *Sens. Actuators B*: 27 (1–3) (1995) 232–236.
- [11] J. Samitier, J.M. López-Villegas, S. Marco, L. Cámara, A. Pardo, O. Ruiz, J.R. Morante, A new method to analyse signal transients in chemical sensors, *Sens. Actuators B* 18/19 (1994) 308–312.
- [12] X. Vilanova, E. Llobet, X. Correig, R. Alcubilla, J.E. Sueiras, Analysis of the conductance transient in thick-film tin oxide gas sensors, *Sens. Actuators B*, 31 (1996) 175–180.
- [13] C. Di Nucci, A. Fort, S. Rocchi, L. Tondi, N. Ulivieri, V. Vignoli, F. Di Francesco, M.B. Serrano-Santos, Study of the dynamic response of QCM sensors by means of a fast and accurate all-digital frequency detector, *Proc. 19th IMTC*, Anchorage, USA (2002).
- [14] F. Musio, M.E.H. Amrani, K.C. Persaud, High-frequency a.c. investigation of conducting polymer gas sensors, *Sens. Actuators B*: 23 (2–3) (1995) 223–226.
- [15] M.E.H. Amrani, P.A. Payne, Multi-frequency interrogation technique applied to conducting polymer gas and odour sensors, *IEEE Proc.-Sci. Meas. Technol.* 146 (2) (1999) 95–101.
- [16] M.E. Hassan Amrani, R.M. Dowdeswell, P.A. Payne, K.C. Persaud, An intelligent gas sensing system, *Sens. Actuators B*: 44 (1–3) (1997) 512–516.
- [17] J.W. Gardner, P.N. Bartlett, K.F.E. Pratt, Modelling of gas-sensitive conducting polymer devices, *IEE Proc., Circuit Devices Syst.* 142 (5) (1995) 321–333.
- [18] J. Gardner, E. Llobet, E.L. Hines, PSPICE model for resistive gas and odour sensors, *IEE Proc., Circuit Devices Syst.* 146 (1999) 101–104.
- [19] E. Llobet, X. Vilanova, J. Brezmes, D. López, X. Correig, Electrical equivalent models of semiconductor gas sensor using PSPICE, *Sens. Actuators B*, 77 (2001) 275–280.
- [20] D.A. Bell, *Noise and the Solid State*, Pentech Press, London, 1985.
- [21] S.M. Briglin, M.S. Freund, P. Tokumaru, N.S. Lewis, Exploitation of spatio-temporal information and geometric optimisation of signal/noise performance using arrays of carbon black-polymer composite vapor detectors, *Sens. Actuators B* 82 (2002) 54–74.
- [22] A. Kolek, A. Dziedzic, Low-frequency noise of polymer thick-film resistors: analysis of volume and contact effects, *Proc. 22nd Intl Conf. Microelectron.* 2 (1999) 531–534.
- [23] A. Dziedzic, A. Kolek, 1/f noise in polymer thick-film resistors, *J. Phys. D: Appl. Phys.* 31 (1998) 2091–2097.
- [24] J.A. Covington, CMOS and SOI CMOS FET-based Gas Sensors, School of Engineering, PhD Thesis, University of Warwick, CV4 7AL, UK, 2001.
- [25] P.T. Moseley, A.M. Stoneham, D.E. Williams, *Techniques and Mechanisms in Gas Sensing*, The Adam Hilger Series on Sensors, Bristol, 1991.
- [26] Verilog-A reference Manual<sup>TM</sup>, Cadence Design System, Inc., Product Version 4.4.3, Dec., 1998.
- [27] Spectre<sup>®</sup> HDL Reference, Cadence Design System, Inc., Product Version 4.4.3, Dec. 1998.
- [28] P. Mielle, F. Marquis, An alternative way to improve the sensitivity of electronic olfactometers, *Sens. Actuators B*: 58 (1–3) (1999) 526–535.
- [29] P. Horowitz, W. Hill, *The Art of Electronics*, second ed., 1989. Cambridge University Press, Cambridge.
- [30] A. Bakker, *High-Accuracy CMOS Smart Temperature Sensors*, printed in The Netherlands, 2000.